Investigating the regulation of plant immunity by the N-degron pathway

Brian Críostóir Mooney

Thesis submitted to the
National University of Ireland
for the degree of
Doctor of Philosophy

December 2021

Department of Biology

Supervisor:
Dr. Emmanuelle Graciet

Head of Department:
Prof. Paul Moynagh

Declaration of Authorship

This thesis has not been submitted in whole or in part to this or any other university for any degree, and is original work of the author except where otherwise stated.

Date: 31.12.2021

Acknowledgements

I wish to extend my gratitude to everyone who has supported me during my PhD project. Firstly, my supervisor Dr. Emmanuelle Graciet - it has been a pleasure to work with you over these last six years and I am thankful for everything I learned from you as a scientist and a person. I will always be grateful for your guidance and for setting an example that I hope to follow.

I would like to thank all of my colleagues in the Plant Biochemistry laboratory, especially Dr. Kevin Goslin, Dr. Alexandra Miricescu, Dr. Maud Sorel, Kate Doorly and Leigh Landers Cribben for their support, friendship, and the many fun memories of working together in the lab. Thank you to the staff of the Biology Department at Maynooth University who foster a productive research environment, and particularly Dr. Jackie Nugent and Dr Martina Schroeder for their annual feedback. I would also like to acknowledge the many external collaborators who contributed to this project, including Prof. Pitter Huesgen, Prof. Frank Wellmer, Melissa Mantz, Andreas Perrar and Joseph Beegan. I also would like to acknowledge the Irish Research Council for funding this work.

To my parents Marie and Christopher – thank you for your constant encouragement and unwavering belief in me, and for always providing a welcoming home to return to after long days at the lab. My brother Seán, thank you for pioneering the path into science and always being someone that I can talk to. Thank you to my extended family, especially Nanny Mooney, all that Countdown paid off. Thank you to Lisa, Martin and family for their support and for letting us share the cabin with Honey. I would like to thank my friends from home including Peter, Emmet, Conor, Patrick, Ben and Stefan. I would also like to acknowledge my previous teachers at Trinity College Dublin where I was inspired to pursue scientific research as a profession, especially Dr. Michael Wride and Prof. Trevor Hodkinson.

To Hazel – Thank you for the unconditional support and for showing me the beauty of plants. This is only possible because of you. Thank you for making my PhD years my happiest years. Here's to the future…

Publications and Presentations

Research publications:

Mooney, B. C. & Graciet, E. (2020) A simple and efficient Agrobacterium-mediated transient expression system to dissect molecular processes in *Brassica rapa* and *Brassica napus*. *Plant Direct*, **4**, 1-12. https://doi.org/10.1002/pld3.237.

de Marchi, R.*, Sorel, M.*, **Mooney, B.**, Fudal, I., Goslin, K., Kwasniewska, K., Ryan, P. T., Pfalz, M., Kroymann, J., Pollmann, S., Feechan, A., Wellmer, F., Rivas, S. & Graciet, E. (2016) The N-end rule positively regulates pathogen responses in plants. *Scientific Reports*, **6**, 26020, doi: 10.1038/srep26020.

McDermott, N., Meunier, A., **Mooney, B.**, Nortey, G., Hernandez, C., Hurley, S., Lynam-Lennon, N., Barsoom, S. H., Bowman, K. J., Marples, B., Jones, G. D. D. & Marignol, L. (2016) Fractionated radiation exposure amplifies the radioresistant nature of prostate cancer cells. *Scientific Reports*, **6**, 34796, doi.org/10.1038/srep34796.

Review publications:

Mooney, B. C.*, Mantz, M.*, Graciet, E. & Huesgen, P. F. (2021) Cutting the line: manipulation of plant immunity by bacterial type III effector proteases. *Journal of Experimental Botany*, erab095. https://doi.org/10.1093/jxb/erab095.

Sorel, M.*, **Mooney, B.*,** de Marchi, R. & Graciet, E. (2019) Ubiquitin/Proteasome System in Plant Pathogen Responses. *Annual Plant Reviews*, 2, 1-52. doi:10.1002/9781119312994.apr0665

* denotes equal contribution.

Conference Presentations:

October 2019: Oral presentation at the International Society for Protein Termini meeting in Seoul, Republic of Korea, titled 'The role of the plant N-degron pathway in PTI'.

July 2019: Poster presentation at the New Phytologist Next Generation Scientists meeting in Dublin, Ireland: 'The role of the PRT1 E3 ligase in the regulation of plant-pathogen interactions'.

Table of contents

Abstract

Crop losses arising from plant diseases present a major obstacle for efforts to meet the food demands of a growing global population, and these impacts may be exacerbated by unprecedented rates of climate change. The Ubiquitin Proteasome System (UPS) contributes to the regulation of plant immunity and a greater understanding of its role in these processes could lead to the future development of disease-resistant crops. The N-degron pathway is a subset of the UPS that relates the stability of a protein to the identity of its N-terminal amino acid residue. Previous work has revealed distinct roles for the N-degron pathway as a regulator of plant defence responses (De Marchi *et al.*, 2016; Gravot *et al.*, 2016; Vicente *et al.*, 2018), although the molecular mechanisms underpinning this activity are not fully understood.

My project aims to elucidate the contribution of specific N-degron pathway enzymatic components to immunity through complementary approaches in *Arabidopsis thaliana.* These include (i) treatments with purified pathogen-associated molecular patterns (PAMPs) to unravel the role of the N-degron pathway in pattern triggered immunity (PTI) and (ii) inoculations with the model pathogen *Pseudomonas syringae* pv. tomato DC3000. Furthermore, this project aims to establish a foundation for N-degron pathway studies in the economically important crop *Brassica rapa* and transfer knowledge obtained via the experiments with its close relative *Arabidopsis*.

Together, this work has yielded novel insights into the role of the N-degron pathway in the PTI response of both the *Arabidopsis thaliana* model and *Brassica rapa*, and may indicate the molecular mechanisms underlying its contribution to the pathogen response. These findings should be considered during future efforts to engineer more resilient crops to ensure global food security.

1

Investigating the regulation of the plant immune system by the N-degron pathway: an introduction

1.1 Introduction

Homeostasis refers to the ability and tendency of organisms to maintain a relatively stable set of internal conditions optimal for biological function. The processes that uphold this state of equilibrium are subject to meticulous regulation at the intra- and inter-cellular levels to support survival in varying conditions. Protein homeostasis or 'proteostasis' describes the network of pathways that co-operate to achieve the concentration, conformation and subcellular localization of specific proteins as needed to execute cell functions. Protein concentration is largely a consequence of an ever-shifting balance between the rates of protein biosynthesis and degradation, both of which are constantly modulated according to the demands of the cell. In eukaryotes like animals and plants, the Ubiquitin Proteasome System (UPS) mediates the degradation of most proteins, thereby contributing to the regulation of almost all essential cell functions (Nakamura, 2018).

Physiological stress may be defined as the disruption of homeostasis by internal or external factors (Kagias *et al.*, 2012). Biological systems like the UPS that maintain and restore homeostasis are therefore inherently implicated in stress responses. Effective participation of proteolytic systems in these reactive physiological functions requires an ability to target specific proteins for destruction or stabilization as needed. To facilitate this process, proteins

relay signals known as 'degrons' that determine their rate of degradation through recognition by the UPS. An 'N-degron' is a degradation signal encoded by the identity of a protein's N-terminal amino-acid residue (Bachmair *et al.*, 1986). The N-degron pathway is the subset of the UPS that targets proteins for degradation based on N-degrons (reviewed by Varshavsky, 2019). Like other pathways of the UPS, the N-degron pathway has been implicated in numerous stress responses (Gibbs *et al.*, 2011; De Marchi *et al.*, 2016; Vicente *et al.,* 2017; Vicente *et al.*, 2018; Dissmeyer, 2019; Varshavsky, 2019).

Due to their sessile growth habit, plants are equipped with particularly sophisticated regulatory mechanisms that allow them to adapt to the persistent challenges encountered in the environment, including interactions with other organisms. These so-called 'biotic' stresses have severe impacts on society due to their capacity to trigger devastating crop losses. Occasionally, this can lead to catastrophe, exemplified by the Irish Potato Famine of 1845-1849 caused by the pathogenic oomycete *Phytophothora infestans.* Consequently, a major focus of plant science research throughout history has been to further our understanding of the strategies employed by plants to counteract biotic stresses. Recently, these enquiries have revealed that the UPS and the N-degron pathway specifically are involved in the plant immune response to certain pathogens (De Marchi *et al.*, 2016; Gravot *et al.*, 2016; Vicente *et al.*, 2018; Sorel & Mooney *et al.*, 2019; Till *et al.*, 2019).

This Ph.D. thesis aims to (i) investigate the molecular mechanisms underpinning the roles of the N-degron pathway in the regulation of the plant immune system using the model species *Arabidopsis thaliana* and translate these findings to the agriculturally important crop *Brassica rapa*. In the paragraphs that follow, I will provide an overview of foundational research in related fields to provide context for the aims of my project. This will include descriptions of the structure and known functions of the N-degron pathway in plants, the nature of the plant immune system and the societal significance of gaining improved understanding of these processes in *Brassica* crops. Finally, I will provide an introduction to the specific objectives of my project.

1.2 The N-degron pathway in plants

1.2.1 The Ubiquitin Proteasome System – Discovery and structure

Ubiquitin (Ub) is a 76-amino acid, 8.6 kDa protein that is exceptionally well conserved among eukaryotes. Many proteins are post-translationally modified by ubiquitin attachment in a process referred to as ubiquitylation. Ubiquitylation has varying consequences for substrate proteins, however the most common fate of ubiquitylated substrates is degradation by the 26S proteasome. This process constitutes the essential mechanism of the Ubiquitin Proteasome System (UPS).

Until the discovery of the UPS, most intracellular proteins were thought to be long-lived, and degradation was perceived as a relatively mundane process limited to the removal of damaged proteins (Varshavsky, 2006). This assumption persisted despite the earlier recognition of the pathway of lysosomal degradation (De Duve *et al.*, 1953), as researchers struggled to reconcile its mode-of-action with the system-specificity required to contribute to dynamic physiological responses (Ciechanover, 2010). This apparent incompatibility, coupled with prior observations hinting at the existence of an alternative and ATP-dependent proteolytic system (Etlinger and Goldberg, 1977), motivated the search that culminated in the discovery of the UPS. By the mid-1980s, the modern understanding of protein degradation as a major regulator of cell function had emerged as the prevailing viewpoint (Varshavsky, 2008). The scientific advances that provoked this re-evaluation are detailed below.

Ubiquitin was first described in 1975 as a universally expressed protein of unknown function (Goldstein *et al.*, 1975). In 1980, a team of researchers pioneered by Avram Hershko, Aaron Ciechanover and Irwin Rose observed that a small protein (soon identified as ubiquitin by Wilkinson *et al.* (1980)) became covalently conjugated to other proteins in a reticulocyte extract before their degradation by an ATP-dependent protease (Ciechanover *et al.*, 1980; Hershko *et al.*, 1980). This group proceeded to rapidly identify and characterize the key enzymatic components required for ubiquitylation - 'E1' ubiquitin-activating enzymes, 'E2' ubiquitin-conjugating enzymes and 'E3' ubiquitin ligases (Ciechanover *et al.*, 1982; Hershko *et al.*, 1983). Hershko, Ciechanover and Rose were later awarded the Nobel Prize for their discoveries, while Alexander Varshavsky has also been widely recognized for his substantial contributions that revealed the biological significance of the system.

The ubiquitylating enzymes act successively as a cascade to attach Ub to substrate proteins as follows: (i) E1 enzymes initiate the process by catalysing adenylation of Ub's C-terminal glycine and forming a thioester bond between Ub and the E1 active site (Haas *et al.*, 1982; Hann *et al.*, 2019); (ii) The E1 complex transfers the activated Ub to the catalytic cysteine of an E2 enzyme via transthioesterification (Hann *et al.*, 2019); (iii) E3 ligases bind to the E2 enzymes and facilitate the final transfer of Ub to lysine residues of select substrate proteins that they recognize via degrons. In some cases, 'E4' enzymes bind to these preformed Ub conjugates and catalyze the assembly of ubiquitin 'chains' (Koegl *et* al., 1999; Hoppe, 2005). As an additional layer of regulation, Ub conjugates can also be removed from substrates by the cleavage activity of the deubiquitylase (DUB) class of enzymes (Clague *et al.*, 2019).

Although primarily associated with degradation, ubiquitylation can have a range of distinct outcomes for substrate proteins depending on the specific nature of Ub attachment. The 'ubiquitin code' describes the different types of ubiquitylation signals and how they are deciphered by the cell (Komander and Rape, 2012; Yau and Rape, 2016). For example, a protein may be monoubiquitylated with a single Ub moiety or tagged with a poly-Ub chain with vastly different results. Polyubiquitylation occurs through the linkage of secondary Ub moieties to one of the seven lysine (K) residues of the existing Ub conjugate(s) (Swatek & Komander, 2016). UPS-mediated proteolysis usually requires K48-linked poly-Ub chains consisting of at least 4 Ub molecules on the substrate protein (Thrower *et al.*, 2000; Komander and Rape, 2012), although examples of atypical conjugates prompting proteasomal degradation have also been documented, (see review by Saeki, 2017). These entry requirements are enforced by the unique gated structure of the 26S proteasome.

The 26S proteasome is a large, ~2.5 MDa ATP-dependent protease complex consisting of two functionally distinct sub-complexes; the cylindrical 20S core protease (CP) capped at one or both ends by 19S regulatory particles (RP) (Kopp *et* al., 1986; Voges *et al.*, 1999; Adams, 2003; Livneh *et al.*, 2016). This self-compartmentalized barrel-like structure spatially limits off-target degradation (Book *et al.*, 2009). Upon arrival at the proteasome, certain subunits of the RP recognize, deubiquitylate and unfold proteins conjugated with K48-linked poly-Ub chains (van Nocker *et al.*, 1996; Lam *et al.*, 2002). The unfolded substrate is subsequently trafficked through the now-opened proteasome 'gate' into the proteolytic core where it is shredded to short peptides (Voges *et al.*, 1999). These typically inactive peptides may be reduced further by

cytosolic peptidases, yielding free amino acids that can be re-used for novel protein synthesis (Hershko & Ciechanover, 1998). The structure and mechanisms of the UPS are detailed further in Fig. 1.1.

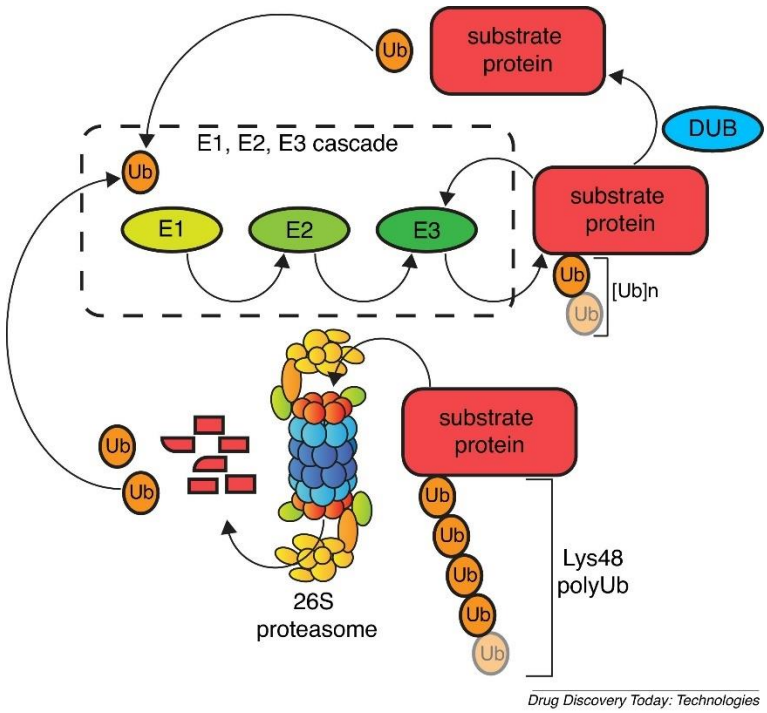

Figure 1.1. Structure of the Ubiquitin-Proteasome System. Ubiquitylation of the substrate protein is achieved by the successive activity of E1, E2 and E3 enzymes. Free Ub cleaved from substrate proteins by deubiquitylases (DUBS) is activated by the E1 Ub-activating enzyme and conjugated to the E2 Ub-conjugating enzyme. E3 Ub-ligases recognize degradation signals in substrate proteins and catalyze transfer of Ub from the E2 to the substrate. Substrate proteins bearing Lys48-linked polyUb chains of at least 4 moieties are bound by the proteasome and admitted to the proteolytic core where they are degraded to short peptides. Free amino acids and Ub molecules are recycled by the cell. This figure is taken from Leestemaker & Ovaa (2017).

1.2.2 Physiological roles of the UPS in plants

The model plant *Arabidopsis thaliana* contains approximately 27,000 genes. Over 1,600 of these are involved in the UPS, comprising 6% of the total genome (Sharma *et al.*, 2016). This proportion is several times larger than those of other model eukaryotes including yeast and humans (Vierstra, 2009). The sequential structure of the UPS and its reliance on E3 ligases for

substrate recognition is reflected in the representation of the individual enzymatic components in the genome. For example, *Arabidopsis* has only two E1 isoforms and 37 E2s but over 1300 loci for E3 Ub ligases (Vierstra, 2009). Various theories have been postulated to account for the remarkable complexity of the plant UPS. These include (i) a need for heightened cellular controls to sustain a sessile growth habit and (ii) that E3 ligases rapidly evolved to recognize substrate proteins from pathogenic microbes as an early, crude form of immunity (Gingerich *et al.*, 2007; Vierstra, 2009). In either case, genomic evidence indicates that plants are particularly reliant on the UPS for survival.

Indeed, experimental observations have confirmed many specific examples of UPS-mediated regulation of physiological functions essential for plants to succeed in their environment. These not only include the control of fundamental metabolic processes like hormone-signaling pathways required for growth, but also direct roles in the response to biotic or abiotic stress (Stone &Callis, 2007; Dreher & Callis, 2007; Vierstra, 2009; Sorel & Mooney *et al.*, 2019). In fact, the upregulation of Ub coding genes during the plant response to bacterial infection and extreme temperature was first described almost 30 years ago (Genschik *et al.*, 1992), while Ub overexpression has been shown to enhance tolerance to drought stress (Guo *et al.*, 2008).

A multitude of E2 and E3 ligase enzymatic components of the UPS across multiple plant families have also been shown to contribute to stress response (Lee & Kim, 2011; Stone, 2014; Cho *et al.*, 2017; Gao *et al.*, 2017; Adams & Spoel, 2018; Khan *et al.*, 2018; Sorel & Mooney *et al.*, 2019). Among these examples, there are two dominant recurring models of UPS activity: (i) direct regulation of the abundance of a protein actively involved in stress perception or tolerance (e.g. the immune receptor SNC1 - Cheng et al., 2011, Gou et al., 2012) and (ii) degradation of a transcriptional repressor/activator to upregulate/attenuate stress response genes as needed (e.g. the group VII ETHYLENE RESPONSE FACTORS (ERF-VII) transcription factors that control the hypoxia response (Gibbs *et al.*, 2011)). Within this framework, the UPS can influence a broad spectrum of distinct plant stress responses largely due to the immense diversity of E3 ligases. Detailed dissection of the contributions of the UPS to specific functions is therefore predicated on an understanding of the degron-recognition interactions between E3 ligases and their cognate substrates. In the case of ERF-VII transcription factors (TFs), the E3 ligase PROTEOLYSIS6 (PRT6) recognizes oxidation of their N-terminal cysteine (Cys) residue, triggering their destruction and thereby prohibiting hypoxia-responsive gene expression in

oxygen-rich environments (Gibbs *et al.*, 2011). The subset of the UPS that targets such 'N-degrons' participates in an array of plant stress responses, including the biotic stresses of particular interest to this study.

1.2.3 The N-degron pathway – a subset of the UPS

As mentioned earlier, E3 ubiquitin ligases recognize substrate proteins via degradation signals known as degrons. Certain subsystems of the UPS have been classified based on the specific type of degrons that are targeted. These include the N-degron and C-degron pathways (reviewed by Varshavsky, 2019). These pathways rely on the detection of specific amino acid residues or modifications at the N or C-termini of cellular proteins respectively. While much of the C-degron pathway has only been described in recent years (Koren *et al.*, 2018; Lin *et al.*, 2018), N-degrons were the first degradation signals to be discovered (Bachmair *et al.*, 1986). In the seminal study from the laboratory of Alexander Varshavsky, Ub-X-beta-galactosidase fusion proteins (with X representing any particular amino-acid) were expressed in the yeast *Saccharomyces cerevisiae*. Near post-translational *in vivo* de-ubiquitylation of the fusion protein exposed the modifiable residue X at the N-terminus of the beta-galactosidase reporter, and the stability conferred by the different N-terminal amino acids was assessed by quantifying the half-life of beta-galactosidase. The relationship between the identity of an N-terminal residue and the *in vivo* half-life of the protein was originally designated the 'N-end rule', although this has since been supplanted by the 'N-degron pathway' term (Bachmair *et al.*, 1986; Varshavsky, 2019).

In eukaryotes, the N-degron pathway is today considered as several distinct branches based on the exact nature of the targeted N-degrons. These are the Arg/N-degron pathway, the Ac/N-degron pathway, the Pro/N-degron pathway and the fMet/N-degron pathway (Varshavsky, 2019). Together, these pathways can recognize any of the 20 standard amino acids as N-degrons provided with an appropriate cellular environment, post-translational modification or sequence context. The Arg/N-degron pathway was the first branch described by Bachmair *et al.* (1986) and the understanding of its structure, mechanisms and functional scope in plants is the most comprehensively detailed thus far.

1.2.4 Structure and components of the plant Arg/N-degron pathway

According to the Arg/N-degron pathway (hereafter referred to as the N-degron pathway for simplicity), N-terminal (Nt) amino-acid residues that render proteins less stable than those with Nt-methionine (Met) are classified as 'destabilizing'. The destabilizing Nt residues follow a hierarchical structure and are categorized as primary, secondary, or tertiary based on the modifications that may be required prior to recognition by the N-degron pathway E3 ligases (referred to as 'N-recognins'). For example, in the case of the ERF-VII transcription factors that regulate hypoxia responses in plants, the initiating Met residue is cleaved by Met aminopeptidases (MAPs) to reveal the tertiary destabilizing Cys residue at the N-terminus. In the presence of O_2, Nt Cys is oxidized to Cys-sulfinic acid by PLANT CYSTEINE OXIDASEs (PCOs) (Gibbs *et al.*, 2011; Weits *et al.*, 2014; White *et al.*, 2017). Arginyl transfer RNA protein transferases (ATE1 and ATE2) can efficiently conjugate arginine (Arg) to the secondary destabilizing Cys-sulfinic acid residue, thus generating Nt-Arg substrates that are prime candidates for ubiquitylation by the PRT6 N-recognin, followed by proteasomal degradation (Garzon *et al.*, 2007; Graciet *et al.*, 2010). Refer to Fig. 1.2 for a schematic representation of the plant N-degron pathway.

Although the N-degron pathway is conserved in eukaryotes, the sets of destabilizing residues and individual enzymatic components vary slightly between yeast, mammals and plants (Varshavsky, 1996; Tasaki *et al.*, 2005; Graciet *et al.*, 2010; Varshavsky, 2019). For example, yeast encodes only one N-recognin, UBR1, while several are present in mammals (Varshavsky, 1996; Tasaki *et al.*, 2005). In *Arabidopsis thaliana*, two N-recognins have been identified, namely PRT1 and PRT6. Recently, due to the different specificities of the two N-recognins, it has been proposed that the Arg/N-degron pathway be reframed as two distinct pathways; the PRT1 N-degron pathway and the PRT6 N-degron pathway (Dissmeyer, 2019). PRT6 has affinity for basic Nt amino acids Arg, Lys and histidine (His), while PRT1 recognizes the bulky hydrophobic residues phenylalanine (Phe), tryptophan (Trp) and tyrosine (Tyr) at the N-terminus (Potuschak *et al.*, 1998; Garzon *et al.*, 2007). Considering the known set of destabilizing N-termini, it is likely that one or more N-recognin(s) capable of recognizing Nt aliphatic hydrophobic residues leucine (Leu) or isoleucine (Ile) remain undiscovered (Graciet *et al.*, 2010). While PRT6 contains the characteristic UBR domain present in UBR1, PRT1 bears no similarities to known N-recognins from yeast or mammals (Stary *et al.*, 2003; Graciet *et al.*, 2010).

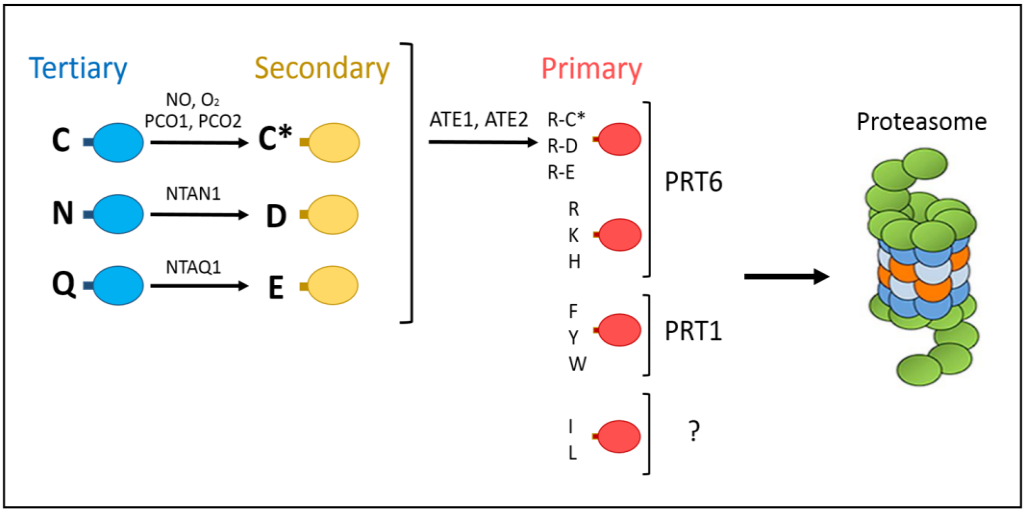

Figure 1.2. Structure of the plant Arg/N-degron pathway. Primary destabilizing N-t residues are recognized directly by N-recognins including PRT1 and PRT6. Secondary destabilizing residues require one modification prior to recognition, while tertiary destabilizing residues require 2 modifications. For example, Nt Cys is oxidized by PCOs in the presence of NO and O_2. Arginine (Arg, R) is then conjugated to the N-terminus of oxidized Cys (C*) by ATE1/2. N-t Arg is finally recognized by PRT6 and the substrate is ubiquitylated and directed to the 26S proteasome. (C = cysteine, N = asparagine, Q = glutamine, D = aspartic acid, E = glutamic acid, K = lysine, H = histidine, F = phenylalanine, Y = tyrosine, W = tryptophan, I = isoleucine, L= leucine. Pathway components are described in Bachmair *et al.*, 1986; Potuschak *et al.*, 1998; Worley *et al.*, 1998; Yoshida *et al.*, 2002; Stary *et* al., 2003; Hu *et al.*, 2005; Garzon *et al.*, 2007; Graciet *et al.*, 2010; Weits *et al.*, 2014 and White *et al.*, 2017).

The *Arabidopsis* genome also contains two closely related arginyl-transferases, ATE1 and ATE2 (Kwon *et al.*, 1999; Yoshida *et al.*, 2002). *In vitro* arginylation assays with combinations of *ate1* and *ate2* T-DNA insertion mutants has shown that both ATEs are active Arg-transferases, albeit with ATE1 contributing the majority of Arg-transferase activity (Graciet *et al.*, 2009). The *ATE1* and *ATE2* genes also have similar expression patterns and thus may be described as functionally redundant (Graciet *et al.*, 2009). The core functions of ATEs within the N-degron pathway have also been confirmed in the moss *Physcomitrella patens*, suggesting some degree of functional conservation across land plants (Schuessele *et al.*, 2015).

As shown in Fig. 1.2, the destabilizing Nt residues asparagine (Asn, N) and glutamine (Gln, Q) must be converted to the secondary destabilizing residues aspartic acid (Asp, D) and glutamic acid (Glu, E) prior to recognition by the Arg-transferases. In *Saccharomyces cerevisiae*, these

deamidation reactions are catalysed by a single dual-specificity Nt-amidase, NTA1 (Baker and Varshavsky, 1995). In contrast, *Arabidopsis* contains two Nt-amidases with distinct affinities; the Asn-specific NTAN1 and the Gln-specific NTAQ1 (Graciet *et al.*, 2010). These enzymes are also conserved in land plants (Graciet *et al.*, 2010).

Finally, *Arabidopsis* encodes a family of five PCOs (PCO1-5) that share the ability to oxidise Nt Cys in the presence of oxygen (O_2) (White *et al.*, 2017; White *et al.*, 2018). While double mutants of the hypoxia-inducible PCOs (*PCO1* and *PCO2*) display constitutive accumulation of ERF-VIIs, the non-inducible PCO4 is the most catalytically competent isoform (Weits *et al.*, 2004; White *et al.*, 2017; White *et al.*, 2018). As well as O_2, nitric oxide (NO) can cause N-degron pathway mediated degradation of ERF-VIIs (Gibbs *et al.*, 2014), but a direct role of PCOs in this process has not been established and the exact mechanism remains undescribed (White *et al.*, 2017).

1.2.5 Biological functions of the plant N-degron pathway

According to the current model of the Arg/N-degron pathway branch in plants, at least 13/20 amino acids can serve as destabilizing residues at the N-terminus (Graciet *et al.*, 2010) (Fig. 1.2). As the canonical start codon in eukaryotes encodes Met, exposure of these residues at the N-terminus of a substrate protein or peptide will almost always require a prior protease cleavage event. Nevertheless, this observation highlights the breadth of proteins (and associated physiological processes) potentially within the functional scope of the Arg/N-degron pathway. Due to the inherent difficulty of predicting protease cleavage sites among other challenges, only a handful of N-degron pathway substrates have been conclusively identified in plants. However, rigorous phenotypic analyses of mutants deficient for N-degron pathway components have greatly expanded our knowledge of its diverse physiological roles.

Notably, many functions of the N-degron pathway impact various aspects of plant development. For example, components of the PRT6 N-degron pathway regulate seed germination (Holman *et al.*, 2009; Gibbs *et al.*, 2014), leaf and shoot development (Graciet *et al.*, 2009) and plant growth (Weits *et al.*, 2014) in *Arabidopsis*. Abnormal growth and development have also been reported in *ate* deficient moss (Schuessele *et al.*, 2016). The PRT6 branch also directly targets the shoot apical meristem (SAM) regulator LITTLE ZIPPER 2 (ZPR2) via its position 2 Cys residue that becomes exposed at the N-terminus after removal of the

initiating Met by MAPs (Weits *et al.*, 2019). This regulatory mechanism elegantly avails of natural O_2 gradients across the SAM to restrict ZPR2 stability to a hypoxic niche that includes the organizing centre (Weits *et al.*, 2019). A similar mechanism has been described for PRT6-mediated degradation of VERNALIZATION 2 (VRN2), a subunit of the polycomb repressive complex 2 (PRC2) (Gibbs *et al.*, 2018; Labandera *et al.*, 2020). VRN2 is confined to endogenously hypoxic regions in the meristems and leaf primordia (where it exerts developmental roles) but can also be stabilized in a wider range of tissues in response to environmental cues like submergence and long-term cold (Gibbs *et al.*, 2018; Labandera *et al.*, 2020). Separately, the PRT1 N-degron pathway has been shown to contribute to the regulation of organ size by targeting the BIG BROTHER E3 ligase after its cleavage by the peptidase DA1 (Dong *et al.*, 2017).

However, the majority of plant N-degron pathway functions (and substrates) that have been documented thus far relate to roles in stress physiology (reviewed by Dissmeyer, 2019). In 2011, Gibbs *et al.* identified the aforementioned ERFVII transcription factors as substrates of the PRT6 N-degron pathway via the Cys-oxidation mechanism. The ERFVIIs govern the homeostatic response to hypoxia stress by regulating the transcription of core hypoxia-response genes (Mustroph *et al.*, 2009; Gibbs *et al.*, 2011). In the wild, plant tissues commonly experience oxygen deficiencies during waterlogging of the soil or foliage submergence caused by flooding (Klecker *et al.*, 2014). Concomitantly, barley (*Hordeum vulgare*) RNAi lines with impaired *HvPRT6* function show enhanced hypoxia gene induction and increased yield in response to waterlogging (Mendiondo *et al.*, 2015). *HvPRT6* mutants are also more tolerant to drought and salt-stress (Vicente *et al.,* 2017). Meanwhile, two mutant alleles of *AtPRT6*, *prt6-1* and *ged1,* display increased tolerance to other 'starvation'-associated environmental conditions, including prolonged darkness (Riber *et al.*, 2015). As a result of these observations, there is considerable interest in exploiting the N-degron pathway to facilitate the development of novel, more robust crop varieties.

Like the wider UPS (Adams & Spoel, 2018; Sorel & Mooney *et al.*, 2019), the N-degron pathway has also been directly implicated in the response of plants to biotic stresses by multiple studies (De Marchi *et al.*, 2016; Gravot *et al.*, 2016; Vicente *et al.*, 2018; Till *et al.*, 2019). Collectively, these experiments have indicated integral roles in the response to several bacterial and fungal pathogens of *Arabidopsis* and barley, and indicated potential immune signalling pathways that

may be subject to N-degron pathway mediated regulation. Recently, the PRT6 N-degron pathway was also shown to degrade fragments of several NOI (nitrate-induced) family proteins (Goslin *et al.*, 2019). Although the functions of these fragments remain elusive, these NOIs are also targets of the AvrRpt2 protease secreted by the bacterial pathogen *Pseudomonas syringae* (Chrisholm *et al.*, 2005; Kim *et al.*, 2005; Takemoto & Jones, 2005).

As stated previously, this thesis is specifically concerned with the roles of the N-degron pathway in the regulation of plant immunity. In order to interrogate the potential functional contribution of the N-degron pathway to immunity in more detail, it is first necessary to describe the features of the plant immune system.

1.3 The plant immune system

1.3.1 Structure of the plant immune system

Despite lacking the mobile cells and adaptive immunity found in vertebrates, plants are equipped with a sophisticated and robust innate immune system comprising two interconnected tiers (Jones & Dangl, 2006). This structure has been shaped by hundreds of millions of years of antagonistic interactions between plants and pathogenic microbes (Han, 2018). The first tier, known as Pattern-Triggered Immunity (PTI) relies on the detection of highly conserved pathogen molecules or 'PAMPs' (Pathogen Associated Molecular Patterns) (e.g. flagellin from bacteria or chitin from fungi) at the cell-surface by Pattern Recognition Receptors (PRRs) that subsequently activate the immune response. Some PRRs recognize 'DAMPs' (damage-associated molecular patterns), host-derived signals that commonly arise following pathogen attack, such as extracellular ATP (Yamaguci & Huffaker, 2011; Hou *et al.*, 2019). Thus, PTI provides protection against a broad spectrum of pathogens through the activity of relatively few PRRs. Common features of the PTI response include transcriptional reprogramming to activate defence-related genes, stomatal closure to limit pathogen invasion and the generation of reactive oxygen species (ROS) that are toxic to microbes.

To counteract these defences, pathogens may secrete repertoires of proteins known as 'effectors' directly into the plant cell to interfere with PTI and promote infection. In turn, plants have evolved resistance (R) proteins that recognize effectors and activate the second tier of

the immune system, Effector Triggered Immunity (ETI). ETI is an amplified form of PTI that can include a form of rapid cell-death known as the hypersensitive response (HR) and typically results in disease resistance (Jones & Dangl, 2006). Correspondingly, evolution of an R protein in a plant population can cause selection against the presence of the cognate effector in the associated pathogen, precipitating its eventual loss. This perpetual co-evolutionary conflict between plants and pathogens is an example of 'Red Queen' dynamics (reviewed by Han, 2018). Refer to Fig. 1.3 for a model of plant-pathogen interactions.

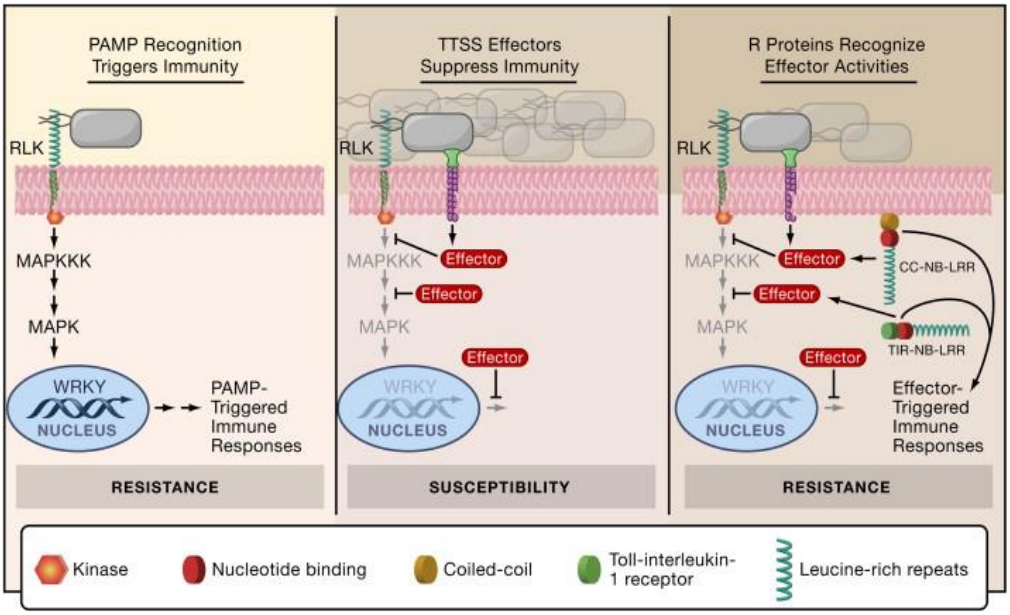

Figure 1.3. Model of plant-pathogen interactions. Plants recognize conserved pathogen molecules like bacterial flagellin via plasma membrane resident PRRs. This leads to PTI responses that can lead to resistance. Certain pathogens express effectors that can be secreted into plant cells to dampen PTI leading to a successful infection. In response, plants have evolved R proteins that recognize effectors and trigger ETI. ETI typically results in disease resistance. Figure taken from Chisholm *et al.* (2006).

1.3.2 Pattern-Triggered Immunity (PTI)

1.3.2.1 Pathogen-Associated Molecular Patterns (PAMPs)

As mentioned above, the plant immune system has evolved to activate PTI in response to highly conserved pathogen molecules. For example, one archetypal elicitor of PTI in plants is bacterial flagellin. Flagellin is the principal component of flagella, whip-like appendages

primarily used for cell locomotion. Flagellar motility is also a major virulence factor for bacterial pathogens of plants, and consequently flagellin is not easily lost from these populations (Ichinose *et al.*, 2003; Zipfel & Felix, 2005; Jones & Dangl, 2006; Rossez *et al.*, 2015). Plants have exploited this dependency by evolving extremely sensitive mechanisms to perceive flagellin. Indeed, many plant species can detect sub-nanomolar concentrations of 'flg22' (a peptide comprising 22 amino acids from the most conserved domain of eubacterial flagellins), leading to the onset of PTI (Felix *et al.*, 1999). Other well-characterized bacterial PAMPs include EF-Tu (elongation factor thermo unstable), an abundant and well conserved G protein that plays an essential role in protein synthesis in bacteria (Kunze *et al.*, 2004).

Similarly, plants may detect fungal pathogens through the perception of chitin. Chitin is a polymer composed of β-1,4-linked *N*-acetylglucosamine monomers that form an integral structural component of fungal cell walls (Chen *et al.*, 2011). During pathogenic infection, the cell wall naturally mediates the first physical contact with host tissues and thus chitin can play an important role in plant-pathogen interactions (Sánchez-Vallet *et al.*, 2015). For example, chitin synthase enzymes (CHSs) contribute positively to virulence in many fungi including *Botrytis cinerea*, a globally prevalent nectrotrophic pathogen of *Arabidopsis thaliana* and over 200 other plant species (Soulie *et al.*, 2003, 2006; Morcx *et al.*, 2013; Sánchez-Vallet *et al.*, 2015; Williamson *et al.*, 2007). However, like flg22, chitin and its de-acetylayed derivative 'chitosan' are potent elicitors of PTI responses in plants (Felix *et al.*, 1993; Igarashi *et al.*, 2013).

1.3.2.2 Pattern Recognition Receptors (PRRs)

PTI signaling is instigated by the recognition of PAMPs by PRRs, usually members of the receptor-like kinase (RLK) or receptor-like protein (RLP) families and reside at the plasma membrane (PM) (Monaghan and Zipfel, 2012). Both RLKs and RLPs comprise an N-terminal extracellular domain that putatively interacts with PAMPs and a single-pass transmembrane domain, while RLKs include an additional intracellular kinase domain that participates in downstream signalling (Macho & Zipfel, 2014). Notably, leucine rich repeat (LRR) motifs are found in the extracellular domains of most plant RLKs (Jones & Jones, 1997; Padmanabhan *et al.*, 2009).

Rather than acting alone, many PRRs feature as the central components in multi-protein receptor complexes that help to amplify and transduce early PTI signals (Monaghan & Zipfel, 2012). This is the case for most of the plant PRRs identified to date, including the LRR-RLK FLS2 (FLAGELLIN-SENSITIVE-2) which recognizes flg22 (Felix *et al.*, 1999; Gomez-Gomez & Boller, 2000) and the two highly similar chitin receptors CERK1 (CHITIN ELICITOR RECEPTOR KINASE-1) and LYK5 (LysM receptor kinase 5) (Kaku *et al.*, 2006; Miya *et al.*, 2007; Cao *et al.*, 2014).

The main features of PTI are described below with a particular focus on the flg22 response, as this pathway has been most extensively studied and has been the focus of my PhD. For a comprehensive account of signaling mechanisms during PTI, see the review by Bigeard *et al.* (2015).

1.3.2.3 PAMP perception by PRRs

In the absence of a pathogen threat, FLS2 constitutively associates with the receptor-like cytoplasmic kinase (RLCK) BIK1 (*BOTRYTIS*-INDUCED KINASE-1) at the PM (Lu *et al.*, 2010). Upon flg22 detection, FLS2 almost instantly forms a co-receptor complex with fellow LRR-RLK BAK1 (BRI1 ASSOCIATED RECEPTOR KINAS-1) (Bigeard *et al.*, 2015). BAK1 itself recognizes the C-terminus of FLS2-bound flg22 directly (Sun *et al.*, 2013). The close interaction between FLS2-BAK1 triggers a series of rapid auto- and trans-phosphorylation events. BIK1 is phosphorylated by BAK1 and in turn phosphorylates both FLS2 and BAK1 before dissociating from the receptor-complex (Macho & Zipfel, 2014). The phosphorylation of FLS2 and BAK1 can be detected within 15 seconds of stimulation with flg22 (Schulze *et al.*, 2010). The interaction of FLS2 with BAK1, as well as BAK1 kinase activity, are required to initiate flg22-responsive PTI signaling (Schulze *et al.*, 2010).

1.3.2.4 Ca^{2+} spike and ionic flux

Within minutes of flagellin sensing, BIK1 phosphorylates and activates a calcium channel comprising the two cyclic nucleotide-gated channel (CNGC) proteins CNGC2 and CNGC4, triggering an influx of Ca^{2+} from the apoplast to the cytosol (Tian *et al.*, 2019). During PTI, Ca^{2+} acts as a critical secondary messenger involved in the regulation of a variety of processes

including the induction of calcium-dependent protein kinases (CDPKs) and calmodulin-binding proteins (CBPs) (Seybold *et al.*, 2014). The elevated levels of intracellular Ca^{2+} also enable the opening of other ion channels, facilitating changes in ionic flux that are essential for the full activation of immune responses (Jabs *et al.*, 1997; Bigeard *et al.*, 2015; Moeder *et al.*, 2011). These changes profoundly alter the electrophysiological characteristics of the cell, causing membrane depolarization and a systemic increase in the pH of the apoplastic space (Jeworutzki *et al.*, 2010). It remains unclear whether this alkalinisation of the apoplast is an aspect of host plants' defensive efforts or merely a secondary effect of ionic flux (Gelifus, 2017). However, it should be noted that bacterial pathogens are typically limited to the apoplast during infection (Fatima & Senthil-Kumar, 2015) and alkalinisation appears to favour successful colonization in at least some cases (Geilfus *et al.*, 2020).

1.3.2.5 ROS burst

PTI is also characterized by a transient increase in apoplastic ROS primarily produced by the PM-localized NADPH oxidase RBOHD (RESPIRATORY BURST OXIDASE HOMOLOG D) (Qi *et al.*, 2017). Full activation of RBOHD requires phosphorylation at distinct sites by BIK1 and Ca^{2+}-induced CDPKs including CPK5 (Dubiella *et al.*, 2013; Kadota *et al.*, 2014). Once active, RBOHD produces the superoxide anion O_2^- which is converted by superoxide dismutase enzymes to H_2O_2, a more chemically stable ROS (Suzuki *et al.*, 2011). H_2O_2 is directly toxic to cells and effectively limits the growth of biotrophic and hemi-biotrophic pathogens during infection (Shetty *et al.*, 2007). In addition to these inhibitory effects, H_2O_2 molecules arising during PTI may be transported from the apoplast into the plant cell where they propagate immune signaling (Camejo *et* al., 2016; Qi *et al.*, 2017). The ROS burst can be detected within 2-4 minutes of elicitation by flg22, with a peak at 10-14 minutes and a return to baseline levels between 30-35 minutes (Smith & Heese, 2014).

1.3.2.6 MAPK cascade activation

Dynamic physiological processes like immune responses rely on post-translational modifications (PTMs) to modulate the activity of participating proteins. Phosphorylation is the

most common PTM used to transduce signals during PTI. Indeed, many of the components already described here including FLS2, BAK1 and BIK1 serve as phosphorylation substrates, while also exhibiting kinase activity of their own. Beyond PAMP perception, phosphorylation of a diverse range of downstream immunity-related substrates is directed by mitogen-activated protein kinases (MAPKs). MAPKs function as the final components of highly conserved signaling modules or 'cascades' that constitute three kinases acting in a sequential manner (Krysan & Colcombet, 2018). In essence, MAPKs are activated through phosphorylation by MAPK kinases (MAPKKs) which are themselves activated by a MAPKK kinase (MAPKKK) (Bigeard & Hirt, 2018).

Two *Arabidopsis* MAPK cascades are rapidly induced during the response to flg22 culminating in the peak activation of MPK3/MPK6 and MPK4 15 minutes post-elicitation (Meng & Zhang, 2013). Currently, the mechanisms connecting the FLS2-BAK1 receptor complex to the activation of the MPK3/MPK6 and MPK4 cascades are not known, although it has been suggested that RLCKs may play a role (Krysan & Colcombet, 2018). Notably, during the response to chitin, the CERK1-LYK5 receptor is connected to MAPK cascade activation via the RLCK PBL27 (Yamada *et al.*, 2016).

The MPK3/6 cascade is well-recognized as a positive regulator of multiple immune responses including stomatal closure and defence hormone synthesis (Meng & Shang, 2013). For example, *Arabidopsis* MPK3 and MPK6 phosphorylate ACS (ACC synthase), a key enzyme in the ethylene biosynthesis pathway (Han *et al.*, 2010). However, almost half of the immune-related MAPK substrates that have been identified are transcription factors that orchestrate the wholesale transcriptional reprogramming necessary to combat a pathogen challenge (Bigeard *et al.*, 2015).

1.3.2.7 Transcriptional Reprogramming

PTI signals originating at the PM and transduced by intracellular kinases and secondary messengers ultimately activate transcription factors (TFs) that regulate gene expression in the nucleus. Microarray experiments in *Arabidopsis* have identified over 2,500 genes that are significantly responsive to flg22-elicitation (Denoux *et al.*, 2008). Certain TF families such as the TGA-bZIPs, WRKYs, MYBs, C2H2 zinc fingers and APETALA2/ERF family are particularly

prominent mediators of these changes during the flagellin response (Tsuda & Somssich, 2015). The latter four families also account for 66/118 TF-encoding genes found to be differentially expressed during the *Arabidopsis* response to chitin, highlighting their central importance to the core features of PTI (Libault *et al.*, 2007). The activity of the WRKY33 TF is described below as a well-studied example of PTI-associated gene regulatory networks.

WRKY TFs target genes by binding to W-box motifs in promoters (Chen *et al.*, 2019). WRKY33 is a major transcriptional regulator of defence-response genes, including those responsible for the biosynthesis of camalexin like *PAD3*, and the jasmonic acid signaling pathway repressors JASMONATE ZIM DOMAIN-CONTAINING PROTEIN 1 (*JAZ1*) and *JAZ5* (Birkenbihl *et* al., 2012; Zhou *et al.*, 2020). Indeed, RNA-seq data has indicated that WRKY33 can bind to over 1,200 gene loci after flg22 treatment (Birkenbihl *et al.*, 2017). In the absence of a pathogen challenge, WRKY33 exists in nuclear complexes with MPK4 (Qiu *et al.*, 2008). Activation of MPK4 triggered by flg22 perception or following infection with the hemi-biotrophic bacterium *Pseudomonas syringae* releases WRKY33, allowing it to bind to the *PAD3* promoter (Qiu *et al.*, 2008). In an added layer of complexity, WRKY33 can be directly phosphorylated at distinct sites by MPK3, MPK6 and the CDPKs CPK5 and CPK6 during the response to the necrotrophic fungus *B. cinerea* (Mao *et al.*, 2011; Zhou *et al.*, 2020). MPK3/6 phosphorylation appears to activate a positive feedback loop where phosphorylated WRKY33 drives the expression of the *WRKY33* gene, allowing its rapid accumulation during infection (Mao *et al.*, 2011; Zhou *et al.*, 2020). Meanwhile, CPK5/6 phosphorylation at Thr-229 enhances WRKY33's DNA-binding ability (Zhou *et al.*, 2020).

As well as direct regulation by kinases or secondary messengers like Ca^{2+}, a sizable portion of transcriptional changes during PTI are mediated by phytohormone signaling pathways. The principal hormones involved in immune responses are ethylene, jasmonic acid (JA) and salicylic acid (SA) (Tsuda and Somssich, 2015). Each hormone controls an extensive network of response genes. For example, one large-scale study identified over 3,600 *Arabidopsis* genes responsive to JA (Hickman *et al.*, 2017). In general, the SA network is considered particularly effective against biotrophic or hemi-biotrophic pathogens, while JA and ET are associated with the response to necrotrophs (Glazebrook, 2005). The contrasting roles played by these hormones can lead to complex and often antagonistic signalling interactions, typified by the SA-mediated inhibition of JA-responsive genes (Bostock, 2005).

SA, JA and ET all accumulate in response to flg22 (Felix *et al.*, 1999; Tsuda *et al.*, 2008; Chang *et al.*, 2017). In many cases, the enzymes involved in the biosynthesis of these hormones are themselves activated via canonical PTI-signalling mechanisms. For example, SA production is partly controlled by the flg22-inducible TF CBP60g through transcriptional regulation of the key SA biosynthesis enzyme ISOCHORISMATE SYNTHASE1 (ICS1) (also known as SID2) (Zhang *et al.*, 2010; Wang *et al.*, 2011). CBP60g activation during PTI is likely a consequence of the Ca^{2+} influx, as its interaction with the Ca^{2+} sensor calmodulin is required for the promotion of SA synthesis (Wang *et al.*, 2011). The accumulation of SA triggers a renewed cascade of transcriptional reprogramming, largely controlled by the master regulator NPR1 (NONEXPRESSER OF PR GENES 1) (Seyfferth & Tsuda, 2014). NPR1 is a *bona fide* SA receptor and co-operates with TGA-bZIP transcription factors to upregulate the expression of most SA-responsive genes (Tsuda & Somssich, 2015; Ding *et al.*, 2018). An important subset of these are the *PR* (*PATHOGENESIS-RELATED*) genes that include the marker of SA signalling '*PR1*' (Seyfferth & Tsuda, 2014). Notably, *PR1* is strongly induced by flg22 as a 'late-response' gene, peaking 12 hours after elicitation (Denoux *et al.*, 2008).

1.3.2.8 Stomatal closure

Stomata are microscopic pores distributed on the epidermis of the aerial tissues of terrestrial plants and serve as an interface between plants and the atmospheric environment. In *Arabidopsis*, they are most abundant on the abaxial side of leaves (Pillitteri & Dong, 2013). Stomata mediate several essential physiological processes including gas exchange and transpiration. For foliar pathogens that otherwise struggle to penetrate the cuticle-protected epidermis, these pores also represent the principal route of entry into host tissues (Melotto *et al.*, 2017).

Each stomatal pore is surrounded by a pair of 'guard cells' that regulate aperture size by swelling or shrinking according to ionic fluxes that modulate the movement of water via osmosis (Aung *et al.*, 2018). This mechanism facilitates dynamic responses to environmental conditions. For example, during periods of drought, the accumulation of abscisic acid (ABA) in guard cells induces stomatal closure to improve water retention (Zhang & Outlaw, 2001). Similarly, during pathogen challenge, guard cells close stomata to limit pathogen access to

the inner tissues. This stomatal defence response diminishes the severity of plant disease (Melotto *et al.*, 2017). Flg22 elicits significant stomatal closure in an FLS2-dependent manner within 1 hour of the treatment (Melotto *et al.*, 2006). This response involves the activation of the PM-localized anion channels SLAC1 (slow anion channel-associated 1) and SLAH3 (SLAC1 homologue 3) that promote anion efflux thereby altering the osmotic potential of guard cells (Guzel Deger *et al.*, 2015). These anion channels can be activated by CDPKs as well as OST1 (OPEN STOMATA 1), a kinase also implicated in the ABA-triggered response (Melotto *et al.*, 2017). Chitin also induces stomatal closure via direct phosphorylation of the SLAH3 anion channel by the PBL27 RLCK (Liu *et al.*, 2019).

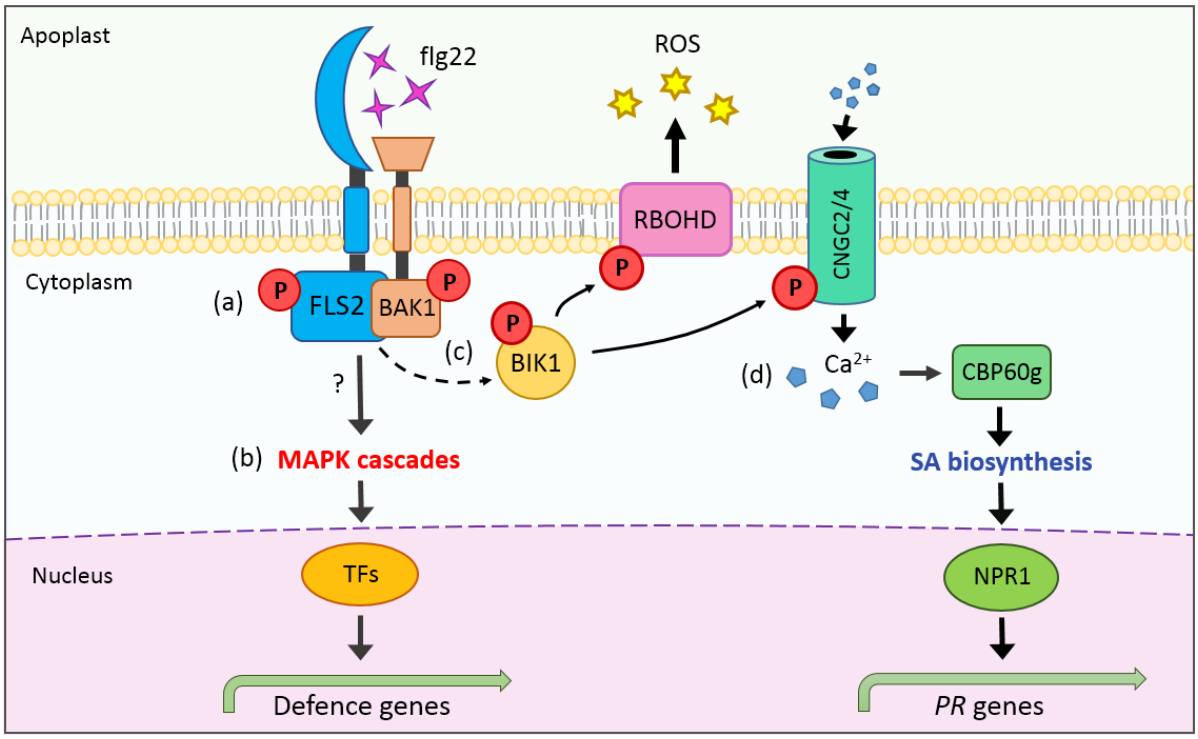

Figure 1.4. Molecular events during PTI. a. Flg22 is perceived at the PM by the FLS2-BAK1 co-receptor complex. A series of phosphorylation events result in the phosphorylation (P) of FLS2, BAK1 and BIK1, prompting its dissociation from the receptor complex. **b.** MAPK cascades transduce the PTI-signal intracellularly, ultimately activating transcription factors that drive the expression of defence genes. **c.** BIK1 phosphorylates RBOHD inducing ROS production and promoting an influx of extracellular Ca^{2+} by activating a calcium channel comprising CNGC2 and CNGC4. **d.** Ca2+ activates calcium-responsive proteins including CBP60g. This TF induces the biosynthesis of SA, allowing NPR1 to activate *PR* genes. This original figure is based on an image included in Sorel & Mooney *et al.* (2019) which I co-authored.

1.3.2.9 Other PTI responses

The physiological changes enacted during PTI extend beyond the responses detailed here. Examples of other notable features include the production of antimicrobial compounds such as phytoalexins (Mao *et al.*, 2011) and the deposition of the cell wall polymer callose at the infection site to reinforce the cell wall (Gomez-Gomez *et al.*, 1999; Ellinger & Voigt, 2014). The diversion of cellular resources towards defence during PTI has profound impacts for other fundamental metabolic and physiological processes, including growth. Indeed, treatment with 100 nM flg22 causes a striking half-maximal growth inhibition phenotype in *Arabidopsis* seedlings (Gomez-Gomez *et al.*, 1999). This relationship between growth and immunity is commonly referred to as the 'growth-defence trade-off' and provides an indication of the considerable energetic costs of PTI-associated responses (Huot *et al.*, 2014).

1.3.3 Effector-Triggered Immunity (ETI)

Some pathogens have evolved sophisticated mechanisms to subvert the PTI-associated resistance of plants. For example, the model pathogen *Pseudomonas syringae* secretes the phytotoxic molecule coronatine (a structural mimic of the phytohormone JA-Isoleucine) to re-open closed stomata and propagate infection (Melotto *et al.*, 2006). Many pathogens also deploy proteins known as 'effectors' to promote virulence (Jones & Dangl, 2006). Bacterial pathogens including *P. syringae* can deliver effectors directly into the cytoplasm of host plant cells via a needle-like appendage called the type three secretion system (T3SS) (Büttner & He, 2009). Over time, plant populations have acquired intracellular receptors (sometimes called R proteins) that can recognize specific effectors and activate a vigorous immune response known as ETI. A particularly important set of receptors are members of the polymorphic nucleotide binding/leucine-rich repeat (NLR) family (Cui *et al.*, 2014). The co-evolution of pathogen effectors and plant NLRs has resulted in a so-called 'gene-for-gene' model of disease resistance (proposed by Flor, 1942), whereby resistance or susceptibility to a pathogen harbouring a specific effector may be determined by the presence or absence of a particular NLR in the corresponding plant population (de Araújo *et al.*, 2020).

Several mechanisms of effector detection by NLRs have been described. These include direct binding interactions as well as 'indirect' surveillance of effector activities (Cui *et al.*, 2014). One well studied example of the latter is the activation of the coiled coil (CC)-type NLR RPM1 (Resistance to *Pseudomonas syringae* pv *maculicola* 1) by the *P. syringae* effector AvrB (Bisgrove *et al.*, 1994; Belkhadir *et al.*, 2004). RPM1 associates with RIN4 (RPM1-INTERACTING PROTEIN 4), a PM-localized protein that functions as a negative regulator of PTI and is targeted by numerous effectors (Mackey *et al.*, 2002; Ray *et al.*, 2019; Redditt *et al.*, 2019). Upon entry into the plant cell, AvrB associates with RIN4 and induces its phosphorylation by the host kinase RIPK (Mackey *et al.*, 2002; Liu *et al.*, 2011). Phosphorylation of RIN4 in turn triggers the activation of RPM1 and associated ETI responses (Liu *et al.*, 2011). Once active, ETI induces a reinforced and sustained application of the transcriptional changes initiated during PTI (Cui *et al.*, 2014). ETI can also provoke prolonged activation of MPK3/6, unlike the transient effects observed during PTI (Lang & Colcombet, 2020). In the case of RPM1 and many other NLRs, this sustained immune response culminates in a localized form of programmed cell death known as the 'hypersensitive response' (HR) which is associated with robust disease resistance (Russell *et al.*, 2015; Kurti, 2019).

Because of their divergent mechanisms of activation, ETI and PTI have long been considered as conceptually distinct. However, recent studies have demonstrated that these immune signalling pathways rely on shared molecular mechanisms and in fact co-operate to amplify defence outputs (Ngou *et al.*, 2021; Yuan *et al.*, 2021). For example, *Arabidopsis* mutants lacking PRRs associated with PTI also display impaired ETI responses, while NLR signalling during ETI augments transcript levels of known PTI components including *BAK1, BIK1* and *RBOHD* (Ngou *et al.*, 2021; Yuan *et al.*, 2021).

1.3.4 The N-degron pathway regulates immunity

The UPS is heavily involved in regulating the plant immune system at multiple levels (reviewed in Sorel & Mooney *et al.*, 2019). Genes encoding E3 ubiquitin ligases are rapidly upregulated in response to PAMPs such as flg22 (Navarro *et al.*, 2004) and chitin (Libault *et al.*, 2007). The roles of the UPS in plant immunity primarily adhere to the regulatory models described in section 1.1.2, i.e. direct regulation of essential immune components including FLS2 (Lu *et al.*,

2011), BIK1 (Ma *et al.*, 2020) and RBOHD (Lee *et al.*, 2020), as well as the control of downstream transcriptional changes through degradation of repressors (Adams & Spoel, 2018; Doroodian & Hua, 2021). Notably, recent observations have indicated that UPS-mediated regulation of immune function also involves the N-degron pathway.

In 2016, de Marchi *et al.* revealed that *Arabidopsis* N-degron pathway mutants are broadly more susceptible to bacterial and fungal pathogens with different lifestyles, including *Pseudomonas syringae* pv. tomato DC3000 (*Pst* DC3000) and *Sclerotinia sclerotiorum*. *Ate1ate2* mutant seedlings show reduced levels of defence hormones such as JA, which might contribute to the increased susceptibility phenotype of these double mutant plants to necrotrophic pathogens such as the fungus *Sclerotinia sclerotiorum* (de Marchi *et al.*, 2016). Additionally, the transcriptomic response of *ate1ate2* mutant plants to avirulent *P. syringae* carrying the AvrRpm1 effector appears to be dampened compared to wild-type plants (de Marchi *et al.*, 2016). *Ate1ate2* and *prt6-1* were also independently found to be more susceptible to clubroot gall caused by the protist pathogen *Plasmodiophora brassicae* (Gravot *et al.*, 2016).

In contrast, Vicente *et al.* (2018) found certain N-degron pathway mutants including *prt6-1* to be more resistant to *Pst* DC3000. The same study also showed that barley (*Hordeum vulgare*) plants containing mutations in Hv*PRT6* are more resistant to *P. syringae* pv *japonica*, but more susceptible to the fungal pathogens *Fusarium graminearum* and *F. culmorum* (Vicente *et al.*, 2018). Till *et al.* (2019) described negative regulation of immune responses by the PRT1 N-degron pathway and found that *prt1-1* mutants exhibit increased abundance of immune proteins encoded by *PR* genes.

Taken together, these findings strongly suggest that the N-degron pathway participates in the regulation of the plant immune system during pathogen challenge. On this basis, an important question is whether the pathway can be manipulated in crops to improve resilience to biotic and abiotic stresses. Using barley as a model species, Mendiondo *et al.* (2016) and Vicente *et al.* (2018) explored the potential exploitation of the N-degron pathway for crop improvement. These studies have shown that barley plants mutant for Hv*PRT6* were more tolerant of waterlogging stress and more resistant to some pathogens, respectively.

However, the somewhat conflicting nature of the observations regarding the disease susceptibility phenotypes of *ate1ate2* and *prt6* mutant plants to different pathogens complicate efforts to deploy knowledge of the N-degron pathway for improvement of crops in the *Brassicaceae* family, which are close relatives of *Arabidopsis*. Enhanced understanding of the molecular mechanisms underpinning these observations could thus pave new avenues for the development of disease-resistant crops.

1.4 *Brassica rapa* as a model crop

1.4.1 The economic and social importance of *Brassica* crops

As a member of the *Brassicaceae* family, *Arabidopsis thaliana* is related to a range of economically important crop species, many of which belong to the Brassica genus. These include *Brassica napus* (oilseed rape), *Brassica oleracea* (cabbage and broccoli) and *Brassica rapa* (with prominent cultivars including pak choi and turnip). The cultivation area of *B. napus* spans tens of thousands of kilohectares across the globe, while its economic value amounts to tens of billions of dollars per annum (Neik *et* al., 2017). *B. rapa* is also a highly valuable and extremely versatile crop whose seeds are used to produce vegetable oil, while the leaves and roots provide food for human and animal consumption (Cartea *et al.*, 2021). Seed oil from *B. rapa* can also have industrial applications depending on its fatty acid composition (Cartea *et al.*, 2019). Together, Brassica oilseed crops represent the second most important source of protein for animal fodder worldwide (McVetty *et al.*, 2016). Due to their significant economic and social utility, it is vital that *Brassica* crop yields can be sustainably increased to match projected population growth.

Phytopathogen infections cause the loss of approximately 15% of all crop yields per year (McDonald & Stukenbrock, 2016). *Brassica* crops are particularly vulnerable to diseases caused by *Hyaloperonospora parasitica* and the aforementioned pathogens *S. Sclerotiorum* and *P. brassicae*. Reducing these losses by augmenting the plant immune system is an attractive way to sustainably increase yields as needed to meet the demands of a growing global population. Considering the species-specific nature of plant-pathogen interactions, studying immune

responses directly in *Brassica* crops alongside traditional model organisms like *Arabidopsis* could accelerate these efforts.

1.4.2 Resources to study *Brassica rapa*

As scientific interest in *Brassica* crops has increased in recent decades, researchers have developed methods and genetic resources to facilitate their study. *B. rapa* may be considered as a more attractive representative model species for Brassica crops as its diploid genome is less complex than the allotetraploid *B. napus*. Indeed, the first *Brassica* genome to be sequenced was *B. rapa* (Chiffu-401-42 accession) in 2011 (The *Brassica rapa* Genome Sequencing Project Consortium, 2011). Since this original publication, the coverage and fidelity of the sequence has been incrementally improved, with the most updated version (v3.0) released in 2018 (Zhang *et al.*, 2018). These resources have enabled the use of sequencing-based approaches in *B. rapa*, including whole-transcriptome analysis of the response to *P. brassicae* by RNA-Seq (Chen *et al.*, 2016).

Another significant contribution to the *B. rapa* research community is the TILLING (Targeting Induced Local Lesions In Genomes) collection developed by Stephenson *et al.* (2010). Seeds of the *B. rapa* subsp. *trilocularis* genotype R-o-18 were randomly mutagenized with ethyl methane sulfonate (EMS) and DNA was isolated from over 9,000 plants in the M_2 population. Researchers can now request a screen of the collection for lines bearing SNP (single nucleotide polymorphism) mutations in their gene(s) of interest, thus permitting reverse genetics approaches in *B. rapa* (Stephenson *et al.*, 2010). To complement this resource, a project seeking to publish the genome sequence of *B. rapa* R-o-18 is currently ongoing (He *et al.*, 2021; King *et al.* unpublished).

Despite the substantial progress in the study of *Brassica* crops in recent years, a number of challenges remain. For example, prior to the present study, simple methods to rapidly transform *B. rapa* for transient expression experiments were lacking. However, as interest in these crops continues to grow, the repertoire of tools available to study *Brassica* crops will continue to expand.

1.5 Overview of project objectives

(i) Elucidate the roles of the N-degron pathway in the regulation of plant immunity using *Arabidopsis thaliana*.

As described above, numerous independent observations indicate that the N-degron pathway contributes to the regulation of immune responses (de Marchi et al., 2016; Gravot et al., 2016; Vicente et al., 2018; Till et al., 2019). In particular, data procured in my host laboratory indicates that *Arabidopsis thaliana* plants bearing mutations in N-degron pathway components are broadly more susceptible to a diverse range of pathogens (de Marchi et al., 2016). However, the molecular mechanisms have not been elucidated in detail and key questions remain unanswered. For example, it is not known whether this phenotype is the result of N-degron pathway mediated regulation of PTI or ETI, or perhaps an indirect role in the regulation of plant signal transduction pathways that contribute to mounting appropriate defence responses against pathogens. Considering that N-degron pathway mutants are defective in their response to diverse types of pathogens adhering to a range of different lifestyles, one hypothesis is that a core aspect of the plant immune response may be impaired in these lines, such as PTI.

This study aimed to elucidate the molecular mechanisms that underpin the role of the N-degron pathway in plant immunity by focusing on PTI. This is achieved through comprehensive assessment of the immune outputs of N-degron pathway mutants in response to the PAMP flg22, including ROS production and MAPK activation, coupled with global analysis of transcriptomic reprogramming by RNA-Seq.

(ii) Determine if N-degron pathway functions are conserved in *B. rapa*.

The second phase of this project sought to compare knowledge of N-degron pathway-mediated immune regulation gained in *Arabidopsis* to related *Brassica* crops of economic and social significance. As the N-degron pathway has not been studied previously in these species, the preliminary objective was to produce the biological reagents and molecular tools required. This work includes the first characterisation of the N-degron pathway in *B. rapa* using a newly

adapted transient expression method (Mooney and Graciet, 2020), followed by isolation of the *B. rapa* N-degron pathway mutants from the TILLING population generated by *Stephenson et al.* (2010). Equipped with these tools and the knowledge gained in the *Arabidopsis* experiments, the final aim of this project was to investigate the roles of the N-degron pathway in the *B. rapa* immune response. Significant outputs from this work include a dataset detailing the global transcriptomic response of *B. rapa* N-degron pathway mutants to flg22. The data obtained here facilitated comparison of the roles of the N-degron pathway in the regulation of plant immunity in a model plant and a related crop of economic importance.

2

Materials and Methods

2.1 Materials

2.1.1 Plant material

2.1.1.1 *Arabidopsis thaliana* lines

The *Arabidopsis thaliana* accession Columbia-0 (Col-0) was used for this study. Lines used containing mutations in N-degron pathway components and/or immune genes are listed in Table 2.1. The *Arabidopsis* ecotype Wassilewskija (Ws-0) is a natural *fls2* mutant and was used as a flg22-insensitive control when assessing PTI responses (Zipfel *et al.*, 2004). *Arabidopsis* lines were ordered from the *Arabidopsis* Biological Resource Centre (ABRC) or from the Nottingham Arabidopsis Stock Centre (NASC).

Table 2.1. List of *A. thaliana* lines used in this study.

Line	Description	Reference
Col-0	Wild-type Col-0 line	arabidopsis.info/CollectionInfo?id=94
ate1ate2	SALK_023492 x SALK_040788	Graciet *et al.*, 2009
prt6-1	SAIL_1278_H11	Graciet *et al.*, 2009
prt6-5	SALK_051088	Graciet *et al.*, 2009
ATE1 rescue in ate1ate2	*ATE1* gene restored in *ate1ate2* background	Graciet *et al.*, 2009

big-2	SALK_045560	Kasajima *et al.*, 2007
big-2 prt6-5	SALK_045560 x SALK_051088	Walter, 2010
rbohd-3	CS9555	Torres *et al.*, 2002
ate1ate2 rbohd	*ate1ate2* x *rbohd-3*	This study
cpk5-1	SAIL_657_C06	Dubiella *et al.*, 2013
ate1ate2 cpk5-1	*ate1ate2* x *cpk5-1*	This study
cpk28-1	GK-523B08	Matschi *et al.*, 2012. Seeds were donated by Prof. Cyril Zipfel (The Sainsbury Laboratory, UK).
ate1ate2 cpk28-1	*ate1ate2* x *cpk28-1*	This study
prt1-1	EMS mutant	Potuschak *et al.*, 1998
prt6-5 erf VII	Sextuple mutant	Abbas *et al.*, 2015
doc1-1	EMS mutant	Gil *et al.*, 1991
Ws-0	Wassilewskija ecotype	Zipfel *et al.*, 2004
WT R9-2	Col-0 wild-type expressing Arg-LUC reporter protein (line number R9-2)	Miricescu, 2019
prt6-5 R9-2	*prt6-5* expressing Arg-LUC reporter protein. Obtained after crossing *prt6-5* with WT R9-2.	Miricescu, 2019
big-2 R9-2	*big* expressing Arg-LUC. Obtained after crossing *big-2* with WT R9-2	Miricescu, 2019
big-2 prt6-5 R9-2	*big-2 prt6-5* expressing Arg-LUC. Obtained after crossing *big-2 prt6-5* double mutant with WT R9-2.	Miricescu, 2019

2.1.1.2 *Brassica rapa* lines

The *Brassica rapa* experiments in this study were performed using the *B. rapa* subsp. Trilocularis (Yellow Sarson) genotype R-o-18. This genotype was previously used to generate a TILLING (Targeting Induced Local Lesions In Genomes) population via EMS mutagenesis (Stephenson *et al.*, 2010). Several lines from this TILLING collection bearing mutations in N-degron pathway components were isolated and used for experiments in the present study (see Table 2.2). *B. rapa* TILLING lines were ordered from RevGen UK based at the John Innes Centre, Norwich.

Table 2.2. List of *B. rapa* lines used in this study.

Line	Description	Reference
R-o-18 'WT'	Wild-type R-o-18 seeds from John Innes Centre.	Stephenson *et al.*, (2010)
Brprt6.2-12	Contains early stop codon in *BrPRT6.2* (Bra009598).	This study
Brprt6.3-1	Contains early stop codon in *BrPRT6.3* (Bra028876)	This study
BrPrt6.2prt6.3 #68	Double mutant isolated from cross between *Brprt6.2-12* and *Brprt6.3-1*, line #68.	This study
Brprt6.2prt6.3 #80	Double mutant isolated from cross between *Brprt6.2-12* and *Brprt6.3-1*, line #80.	This study
#67 'WT'	'Wild-type' line isolated from F2 cross of *Brprt6.2-12* and *Brprt6.3-1* containing wild-type alleles of the *B. rapa* PRT6 orthologs. To serve as a control for remaining background SNPs caused by EMS mutagenesis.	This study

Brate1-2	Contains early stop codon in *BrATE1* (Bra009127).	This study
Brate2-2	Contains early stop codon in *BrATE2* (Bra034856).	This study
Brate1ate2	Double mutant isolated from cross between *Brate1-2* and *Brate2-2.*	This study

2.1.1.3 *Brassica napus* material

B. napus plants of the 'Westar' cultivar (Klassen *et al.*, 1987) were used for GUS staining following transient expression of N-degron pathway reporter constructs. These seeds were donated by Dr. Isabelle Fudal (INRA, France).

2.1.2 Bacterial strains

2.1.2.1 *Pseudomonas syringae*

Pseudomonas syringae pathovar tomato DC3000 was used for *Pseudomonas* infection assays. An avirulent strain of *Pst* DC3000 carrying the AvrRpm1 effector was used to infiltrate plants prior to RT-qPCR analysis of the transcriptomic response to infection.

2.1.2.2 *Agrobacterium tumefaciens*

Strains of *Agrobacterium tumefaciens* C58 pGV2260 carrying various N-degron pathway reporter constructs (section 2.1.3.1) were used for agroinfiltration assays to characterise the *B. rapa* N-degron pathway mutants and demonstrate transient expression in *Brassica napus*.

2.1.2.3 *Escherichia coli*

The *E. coli* strain Stbl2 (ThermoFisher) was used for cloning of plasmids used in this study (see section 2.1.3.).

2.1.3 Plasmid constructs

2.1.3.1 X-LUC N-degron pathway reporter constructs

All N-degron pathway reporter constructs used in this study have been previously published in Graciet *et al.* (2010). These constructs were generated from a vector produced by Worley *et al.* (1998) based on the ubiquitin-fusion technique pioneered in the laboratory of Alexander Varshavsky (Bachmair *et al.*, 1986). N-degron pathway reporters were stably expressed in *Arabidopsis thaliana* and used for transient expression in *B. rapa* and *B. napus* (Mooney & Graciet, 2020).

2.1.3.2 pCAMBIA2201

The pCAMBIA2201 plasmid containing the *β-glucuronidase* (*uidA) gene* with a cat1 intron was used to control for leaky expression of the GUS enzyme by *Agrobacteria*. pCAMBIA2201 was shared by Dr. Dheeraj Rathore and Dr. Ewen Mullins (Teagasc).

2.1.4 Oligonucleotides

The following tables list oligonucleotides used for genotyping (Table 2.3) and RT-qPCR analysis of gene expression (Table 2.4) respectively.

Table 2.3. List of oligonucleotides used to genotype *A. thaliana* and *B. rapa* lines.

Line	Primer name	Sequence
ate1-2	At1	GTGCAGCCCAGGGAACAAAGAGGTG
	At2-3	GAGAGGAGATCAATGATAAACTAAGGCATAG
ate2-1	At3	GCGAAGCCGAGTGAGCAGACAGA
	At4-2	CCACAAAGAGGAATCTTTTCTTCATCATCAT
Left border of SALK lines	LB2	CCAAACTGGAACAACACTCAACCCTATCTC
prt6-1	At120	AAAATTGATCCTTTCCATGCC
	At121	CAACATAAGAATCTGCGGGAG
Left border of SAIL lines	SAIL_LB	gcttcctattatatcttcccaaattaccaataca
cpk5-1	BM163_up	TGCTTGTGTACGTGGAGGTG
	BM164_lo	GTGTTCTTCATCAAAGGAACTGTTC
cpk28-1	BM168_up (from Monaghan et al. (2014)	GCGGCGGATTCTTTGACTAA
	BM169_lo (from Monaghan et al. (2014)	AGTACACAACGGCTCATTATGAA
rbohd-3	BM154_lo	GGTCAGGACCTTTCATGTTGTTGATG
	BM157_up (from Torres et al., 2002)	CTTATTTCAGTAAGAGTGTGGGGTTTTGG
prt1-1	FrWa4	AATGGCTTTCGTGAGTCTCATTGTCC
	FrWa5	GAGAATCTCCACTACACACAGACAAATCCAAAACAAGATCAACTT
Brate1-2	BM10_lo	CGAAGAGGACACAGAAGCTCAGACG
	BM22_up	GTCGAGTGTGTACTTGTTCTGGGA
Brate2-2	BM30_up	CGTAGTCTCTGAATGATAAACTTACTC
	BM31_lo	GATCTCTCTCTCAGAAATGAGAACAAG
Brate2-5	BM60_up	AGAGTTGATGGACATCTTATAGCTGTGGcA
	BM61_lo	AAGCTGGGAAGGACGATAAGTTGCT
Brprt6.2-12	BM97_up	TCTGACGGACATGTAAAGCACTCTTTGaTC
	BM98_lo	CCTCCTGGAACTTCTTTGCAGCC
Brprt6.2-12	qBM246_lo	ACCTTCACTTCCGAATATGCTGCT
	qBM247_up WT specific with 2 mismatches	TCTTATTACGAGTGGTACAGtGgACCC
	qBM248_up MUT specific with 2 mismatches	TCTTATTACGAGTGGTACAGtGgACCt
Brprt6.3-1	BM36_up	GCTCCCGATCTCCAGAGAATAAATGTTTCCTC
	BM37_lo	CATTGTATTCTTCCCACAACGAGTCAC
Brprt6.3-1	qBM235.2_up WT specific with 1 mismatch	TACTTTGCATAGGTTTCAAGATgTTC
	qBM236_up MUT specific with 1 mismatch	TACTTTGCATAGGTTTCAAGATgTTT
	qBM237_lo	AAGATAAATCCCATCACAGTCGG
Brprt1.1-5	qBM249_up WT specific with 1 mismatch fw	CGGTTTGTAAAGAAGCTCCaTGC
	qBM250_up MUT specific with 1 mismatch fw	CGGTTTGTAAAGAAGCTCCaTGt
	qBM251_lo	TTCACTGTTCAGACAAAGGAAGG
Brprt1.2-5	qBM252_up WT specific with 1 mismatch fw	AATTGGTTTGTAAAGAAGTTCCaTGC
	qBM253_up allele specific with 1 mismatch fw	AATTGGTTTGTAAAGAAGTTCCaTGt
	qBM254_lo	ATCTCCGATAAGTTTCTCTGCTG

Table 2.4. List of oligonucleotides used to monitor gene expression in RT-qPCR experiments.

Target	Primer name	Sequence
AOX1D (AT1G32350)	qBM259	AATGGTACGAACGAGCGATTGTGT
	qBM260	ACAGCCTCTTCTTCTAAGTATCCAGTGA
ATPI4Kγ3 (AT5G24240)	qBM257	AGATGGTCAGATGGTGCTTACTCCA
	qBM258	AGAGTATGGCTCTTTTGCTTGAGGC
bHLH093 (AT5G65640)	qBM327_up	GCTTCTTGTTCTGAGGGAGCTGAG
	qBM328_lo	GCTTCCACCATAACCTGCGTTTCT
BrGAPDH Reference gene. From Procko *et al*., 2014	qBM55_up	CACCACCGAGTACATGACGTACA
	qBM56_lo	TGCCCGTGAACACTGTCGTA
BrHb1 (Bra001958)	qBM234_up	TGTCGTTGATGAACACTTTGAGGTGAC
	qBM235_lo	CGGTGACCACATCTCTGGCAC
BrHRE2 (Bra021401)	qBM238_up	TGCTCAGGCTCAGTTGGTGG
	qBM239_lo	GCCTCTGCCTTATCCCTCTGTAC
BrMPK3 (Bra038281)	qBM225_up	GCTTATTGACAGAGTTGCTTGGCACA
	qBM226_lo	CAACAGTGATTCTTTTGCTGGGGTCA
BrPCO2 (Bra025636)	qBM229_up	GGTCGCTGATTCTCCCCAGC
	qBM230_lo	CCGTGAAGTCTGAATCCACTTTCACT
BrRBOHD (Bra020724)	qBM227_up	CGGTTAAGATTGTCAAGGTGGCTGT
	qBM228_lo	CGCTCACGTAGTCGTCTCCTG
ChiA (AT5G24090)	qBM265	CGCCAGGACTCTCTCAAAGTTTAGC
	qBM266	ATTACCTGAACTGTATGAACACGGTGG
Chitinase (At2G43620)	qBM121_up	TACACTCGCCAGGCTTTCATTGC
	qBM122_lo	GGTACGCAGTGCTCGGTGAG
FLS2 (AT5G46330)	qPCRBM25_up	GCCAGCTAATATACTCCTTGACAGTGACC
	qPCRBM26_lo	TTCCTCATATAAGCAAACTCTGGAGCTAAGT
FRK1 (AT2G19190)	qBM67_up	TGAGAACTTAGGAGACTATTTGGCAGGTAA
	qBM68_lo	ACCATTGTGAAGATACTCTAGTCCTTGCG
GSTU10 (AT1G74590)	qBM299_up	TCAACCAACAGGTGTTTGAGGTCAT
	qBM300_lo	GCCTCTTCTACAGACTTTGCTTGAGC
HRA1 (AT3G10040)	qBM207_up	GAAGCAGGGAAAATGGCGAGAATTG
	qBM208_lo	CCATCTCTGACTCCGAATCCTCCG
LAC7 (AT3G09220)	qBM305_up	CTGCTAATAATCCAGGTGCGTGGA
	qBM306_lo	TTGGGAAGATCTGGTGGTGGC
LBD41 (AT3G02550)	qBM317_up	ACCTTCGTCCTGGGATTTTCCG
	qBM318_lo	CGTCTTGACAAAGCTGCCAATTCC
LUC from firefly	KG59	GCGGTCGGTAAAGTTGTTCCAT
	At327_lo	GAAGTGTTCGTCTTCGTCCC
MON1 (Reference gene)	MON1_up	AACTCTATGCAGCATTTGATCCACT
	MON1_lo	TGATTGCATATCTTTATCGCCATC
MPK3 (AT3G45640)	qPCRBM5_up	CTGTTGAACAAGCTCTGAATCACCAGT
	qPCRBM6_lo	GTGCTATGGCTTCTTGGTAGATCATCTC
PR6 (AT2G38870)	qBM119_lo	CGGAGCTTACGGGAACAAATGGT
	qBM120_lo	CACCTGAAGTCTGCGGTCACC
RBOHD (AT5G47910)	qBM169_up	TGGATGTTGTGTCGGGTACACG
	qBM170_lo	TGGCATTCCACAGTAGAAGACTCCTA
WRKY33 (AT2G38470)	qPCRBM3_up	GGAGTGAACCTGAAGCAAAGAGATGGAA
	qPCRBM4_lo	CGTTGTCTGCACTACGATTCTCGGC

2.2 Methods

2.2.1 Plant cultivation

2.2.1.1 Plant growth media

A. thaliana, B. rapa and *B. napus* plants were grown in 4-cell pots on a soil mixture containing a 5:3:2 ratio of compost, vermiculite and perlite. The soil mixture was sterilized by autoclaving prior to use. Seedlings were also grown in petri-dishes or sterile plastic cups containing 0.5X Murashige and Skoog (MS) medium (pH 5.7) with 6 g/L agar with or without 0.5% sucrose (w/v). Trays or plates were incubated at 4°C for 3 days prior to transfer to growth rooms for stratification of seeds. 20 mg/L Basta (glufosinate) was added to media in cases where the bar gene was used as a selection marker.

2.2.1.2 Vapor-phase sterilization of seeds

Prior to growth on 0.5x MS medium, seeds were surface-sterilized using the vapor-phase sterilization method (Lindsey *et al.*, 2017). Seeds were aliquoted into 1.5 mL tubes and transferred to a desiccator chamber inside a fume hood. A beaker containing 100 mL of commercial bleach solution was placed in the chamber. 3 mL of concentrated hydrochloric acid (37%) was added to the beaker and the chamber was immediately sealed for 3-4 hours to permit sterilization of seeds by chlorine gas.

2.2.2 Microbiology methods

2.2.2.1 Microbiological culture

Agrobacterium tumefaciens strains were grown on LB media (10 g/L NaCl, 10 g/L tryptone, 5 g/L yeast extract) with appropriate antibiotics in an incubator set to 28°C. *E. coli* were grown on LB media at 37°C. *Pseudomonas syringae* DC3000 were grown on King's B media (20 g/L peptone, 10 mL/L glycerol, 1.5 g/L K_2HPO_4, 1.5 g/L $MgSO_4$ added after autoclaving, pH 7.2) containing rifampicin (50 mg/L) at 28°C.

2.2.2.2 Transformation of *Agrobacterium tumefaciens*

A. tumefaciens C58 pGV2260 were transformed with N-degron pathway reporter constructs, the pMLBART empty vector or pCAMBIA2201 prior to their use for agroinfiltration experiments. Miniprepped plasmid (2-5 µL) was added to 100 µL of thawed chemically competent *A. tumefaciens* cells and the tube was submerged in liquid nitrogen for 5 minutes. After thawing at room temperature, 1 mL of LB medium was added and the cells were incubated at 28°C for 4 hours. The culture was then centrifuged at 5,000 rpm for 5 minutes and 500 µL supernatant was removed to concentrate the cells. A 100 µL aliquot of the resuspended cells was plated out on LB agar media supplemented with rifampicin (50 µg/mL) (chromosomal marker), ampicillin (100 µg/mL) (Ti plasmid marker), with or without spectinomycin (100 µg/mL) (X-LUC reporter selection) and grown at 28°C. Glycerol stocks were prepared from overnight cultures (500 µL culture mixed with 500 µL 50% glycerol (v/v)) and stored at -80°C.

2.2.2.3 Transformation of *E. coli*

E. coli were transformed with plasmid DNA using the heat-shock method. 100 µL of frozen chemically competent cells were thawed on ice. 1-10 µL of plasmid DNA was added to the cells and the mixture was incubated on ice for 10 minutes. The tube was then transferred to a heat-block set to 42°C for 45 seconds and immediately returned to ice for 1 minute. 1 mL of LB medium was added and the cells were grown at 37°C with shaking for 1 hour. A 25 µL aliquot of cells was plated out on LB agar media supplemented with antibiotics to permit selective growth of transformed colonies.

2.2.2.4 Plasmid isolation

Transformed *E. coli* were cultured in 5 mL LB media with appropriate antibiotics at 37°C overnight with shaking and plasmids were isolated using the column-based E.Z.N.A. Plasmid Mini Kit (Omega Biotek).

2.2.3 Molecular biology techniques

2.2.3.1 Genomic DNA extraction from plants

Genomic DNA was extracted from plants using the method described by Edward's *et al.*, (1991). A small piece of detached leaf tissue was ground using a drill and pestle in 400 µL extraction buffer comprising 200 mM Tris-HCl pH7.5, 250 mM NaCl, 25 mM EDTA and 0.5% (w/v) SDS. Cellular debris was pelleted and removed. 300 µL of supernatant was mixed with 300 µL of isopropanol to precipitate DNA. After centrifugation, the DNA pellet was rinsed with 500 µL 70% ethanol. The supernatant was removed, and the pellet was dried. Isolated DNA was resuspended in 75 µL dH_2O and stored at -20°C.

2.2.3.2 RNA extraction from plants

Frozen plant material was ground to a powder using a drill and pestle dipped in liquid nitrogen. RNA was extracted using the column-based Spectrum Plant Total RNA Kit (Sigma Aldrich) according to the instruction manual provided. Briefly, tissue was mixed with a lysis buffer and incubated at 56°C for 3-5 minutes. A binding solution was added to the cell lysate that allows RNA to be retained in a column while genomic DNA and other cellular components flow through. The on-column RNA is then washed with a series of buffers and finally resuspended in 50 µL elution buffer. RNA yields and purity were quantified using a DS-11 microvolume spectrophotometer (DeNovix). RNA samples were catalogued and stored at -80°C.

2.2.3.3 Reverse transcription of RNA

Reverse transcription reactions were set up using 100-1000 ng of isolated RNA (see section 2.2.3.2). RNA was incubated with RevertAid Reverse Transcriptase (Thermo Fisher) and the associated buffer, RiboLock RNase inhibitor (Thermo Fisher), oligo(dT)18 and 1 mM dNTP mixture at 42°C for 45 minutes. Synthesized cDNA was used directly for qPCR analysis or diluted 1:1 with nuclease-free water prior to use. cDNA was stored at -20°C.

2.2.3.4 Oligonucleotide primer design

DNA sequences were viewed and edited using the ApE plasmid editor software. Oligonucleotide primers were designed manually and their properties (including melt temperature, self-dimerization, hairpin formation and hetero-dimerization) were assessed using the OligoAnalyzer online tool (IDT Integrated DNA Technologies). Custom DNA oligos were ordered from IDT and diluted to 100 µM in nuclease-free H_2O prior to storage at -20°C.

2.2.3.5 Reverse transcription quantitative PCR (RT-qPCR)

cDNA was synthesized as described in section 2.2.3.3. qPCR reaction mixtures were prepared in LightCycler 480 96-well plates (Roche). 1 µL of cDNA was mixed with 1 µL of a primer pair mixture (1 µM final concentration each) and 5 µL 2X SYBR green master mix (Roche), with nuclease-free water added to a final volume of 10 µL per well. qPCR reactions were carried out in a LightCycler 480 instrument (Roche). The second derivative maximum method was used to determine crossing point (Cp) values. Gene expression was calculated relative to a reference gene with the comparative Ct method ($Cp_{reference\ gene} - Cp_{gene\ of\ interest}$ = deltaCp). Assuming a PCR efficiency value of 2, relative expression was calculated as $2^{deltaCp}$. *MON1* (AT2G28390) was used as a reference gene for RT-qPCRs in *Arabidopsis thaliana* (de Marchi et al., 2016). *BrGAPDH* (GLYCERALDEHYDE 3-PHOSPHATE DEHYDROGENASE; Bra016729) was used as a reference gene for RT-qPCRs in *Brassica rapa* (previously used in Procko et al., 2014). Primers used to target genes of interest for RT-qPCR analysis are listed in Table 2.4. Relative expression values were calculated and analysed using Microsoft Excel and GraphPad Prism. The qPCR instrumentation was funded by Science Foundation Ireland (Grant No.: SFI/07/RFP/GEN/F571/ECO7).

2.2.4 Biochemistry techniques

2.2.4.1 Protein extraction for immunoblot

Frozen plant material was ground in liquid nitrogen using a drill and pestle. Prior to immunoblot, proteins were extracted in SDS loading buffer (Laemmli buffer) with 13.33 µL β-

mercaptoethanol added fresh per 1 mL. After mixing, samples were boiled at 95°C for 5 minutes to denature proteins. Cellular debris was pelleted by centrifugation at 14,000 rpm for 10 minutes and removed. Protein extracts were loaded directly on acrylamide gels for SDS-PAGE or concentrations were measured first using the amido-black assay (Schaffner & Weissmann, 1973) (see section 2.2.4.2).

2.2.4.2 Amido-black assay for protein concentration

Protein concentrations of samples extracted in buffers containing SDS were quantified using the amido-black assay (Schaffner & Weissmann, 1973). 10 µL of protein extract was diluted in 190 µL H_2O and added to 800 µL amido-black stain solution (10% v/v acetic acid, 90% v/v methanol, a small quantity of amido lack 10B powder). Samples were mixed well and centrifuged 10,000 x g at 25°C for 20 minutes. Supernatant was discarded and 1 mL of wash solution (10% acetic acid, 90% methanol) was added before centrifugation at 10,000 x g at 25°C for 20 minutes. The wash step was repeated twice. After removal of the supernatant, the pellet was air-dried under a chemical fume hood before resuspension in 1 mL 200 mM NaOH. Sample absorbance at 600 nm was measured and values were compared to a standard curve of prepared concentrations of BSA ranging from 1-10 mg/mL.

2.2.4.3 SDS-PAGE and immunoblot

Protein extracts were loaded on SDS-PAGE gels consisting of a stacking gel and a lower separating gel containing 10 or 12% acrylamide/bis-acrylamide (40% solution; Sigma-Aldrich). 10 µL of PageRuler pre-stained protein ladder (ThermoFisher) was loaded alongside the samples for comparison of molecular weights. Gels were run at 60 V through the stacking gel and 110 V through the separating gel. Separated proteins were transferred to a PVDF membrane (Amersham) for 2 hours at 80 mA. Equal protein transfer was assessed using Ponceau S staining (0.4% (w/v) Ponceau S, 10% (v/v) acetic acid in water) for 5 minutes. After imaging, Ponceau S stain was removed using 200 mM Tris pH8.8. Membranes were then blocked with 5% milk powder (w/v) in PBS-T or TBS-T (containing 0.05% (v/v) Tween-20) for 3 x 10 minutes at room temperature.

5 mL of primary antibody diluted in blocking solution was prepared and added to a 50 mL centrifuge tube. The membrane was placed into the tube and probed overnight at 4°C while mixing gently on a tube roller (Stuart). After removal of the primary antibody, the membrane was washed 3 x 5 minutes with PBS-T or TBS-T (0.05%). The membrane was then incubated with a dilution of the secondary antibody (conjugated to horseradish peroxidase) for 2 hours at room temperature with mild shaking. After rinsing in PBS-T / TBS-T (0.05% Tween-20), 1 mL of WesternBright ECL substrate (Advansta) for HRP was applied to the membrane for 2 minutes. Chemiluminescence was detected using the G:BOX gel documentation system and the GeneSys software.

2.2.4.4 Protein extraction for LUC and GUS enzymatic assays

To test the enzymatic activity of transiently expressed LUC and GUS in planta, proteins were extracted from frozen ground tissue using 1X Luciferase Cell Culture Lysis Reagent (CCLR) (Promega), supplemented with 1 mM phenylmethylsulfonyl fluoride (PMSF) and 1:100 plant Protease Inhibitor Cocktail (Sigma-Aldrich). Samples were centrifuged 12,000 x g for 10 minutes at 4°C to pellet cellular debris. Supernatant was retained on ice and the protein concentration was determined using the Bradford protein assay (see section 2.2.4.5) prior to use in LUC and GUS enzymatic assays (sections 2.2.4.6 and 2.2.4.7 respectively).

2.2.4.5 Bradford protein assay

The concentrations of protein samples extracted in CCLR reagent (see section 2.2.4.4) were measured using the Bradford protein assay (Bradford, 1976). 1.5 µL of protein extract was added to 500 µL Bradford reagent (Thermo Fisher) and incubated at room temperature for 5 minutes. Samples were transferred to 1 mL cuvettes and absorbance values at 595 nm were measured using a spectrophotometer (Eppendorf BioPhotometer). Measurements were compared to values obtained for BSA standards prepared at known concentrations ranging from 1-10 mg/mL.

2.2.4.6 LUC enzymatic assays (adapted from Mooney & Graciet, 2020)

LUC activity was measured as described in (Luehrsen *et al.*, 1992, Graciet *et al.*, 2010). CCLR protein extract (1-2 µL) was added to 100 µL LAR buffer (20 mM tricine, pH7.8, 1.07 mM $(MgCO_3)_4$, $Mg(OH)_2.5H_2O$, 2.67 mM $MgSO_4$, 0.1 mM ethylenediaminetetraacetic acid (EDTA), 33.3 mM dithiothreitol (DTT), 270 µM coenzyme A, 470 µM luciferin, 530 µM ATP) in a 96-well plate (Sterilin). Luminescence was measured using a POLARstar Omega microplate reader (BMG LABTECH) for 10 seconds.

2.2.4.7 GUS enzymatic assays (adapted from Mooney & Graciet, 2021)

GUS activity was quantified using 4-methylumbelliferyl-β-D-glucuronide (MUG) as described in (Weigel and Glazebrook, 2002, Graciet *et al.*, 2010). Protein extract in CCLR buffer was added to the GUS reaction mixture (50 mM sodium phosphate buffer pH 7.0, 10 µM, EDTA, 0.1% (v/v) sodium dodecyl sulfate (SDS), 0.1% (v/v) Triton X100). The fluorescent product 4-methylumbelliferone (4-MU) was measured 10, 20, 30 and 40 min after the initiation of the reaction using the POLARstar Omega instrument (BMG LABTECH). These values were calibrated against a standard curve prepared with known concentrations of 4-MU ranging from 12.5 µM to 400 µM.

2.2.4.8 R-LUC reporter assays in *Arabidopsis thaliana*

Wild-type and mutant *Arabidopsis thaliana* plants stably expressing LUCIFERASE with an N-terminal arginine residue (R-LUC) (see section 2.1.3.1) were used to investigate the role of BIG (AT3G02260) in the N-degron pathway. Seedlings were grown vertically on 0.5X MS + 0.5% sucrose plates containing 20 mg/L Basta to select for the presence of the reporter. Plates were incubated in continuous light at 19.5℃ for 7 days. Forty seedlings per genotype were harvested directly in liquid nitrogen. Frozen tissue was ground using a drill and pestle and the powder was split equally between two tubes (i) for LUC enzymatic assays (see section 2.2.4.6) and (ii) RNA extraction followed by RT-qPCR to test expression of the LUC gene (see section 2.2.3.5).

2.2.5 Plant genotyping

2.2.5.1 Genotyping of *Arabidopsis thaliana* T-DNA mutants by PCR

Arabidopsis thaliana mutants segregating T-DNA insertions in genes of interest were genotyped with dual PCR reactions containing 'wild-type only' or 'T-DNA only' allele-specific primer combinations (O'Malley et al., 2017). Genomic DNA was extracted using the procedure described by Edwards *et al.* (1991) (see section 2.2.3.1). Following extraction, 2-3 µL of DNA was used as template for PCR with 0.2 µM each of a primer pair, 0.2 mM dNTP mixture and Taq polymerase. Denaturation was carried out at 94°C, primer annealing between 50-60 ℃ (depending on primer melt temperatures) and extension at 72 ℃ for 1 minute per 1 kb of DNA. PCR products were subject to agarose gel electrophoresis and visualized with SYBR safe DNA stain (ThermoFisher).

2.2.5.2 dCAPS genotyping of *Brassica rapa* TILLING lines

SNPs present in N-degron pathway genes of interest in B. rapa TILLING lines were genotyped using the tailored dCAPS assays as described by Neff *et al.* (1998). PCR primers were designed to contain mismatches that permit the introduction of a restriction enzyme recognition site contingent on the presence or absence of a given mutant SNP allele.

Up to 3 µL of *B. rapa* genomic DNA was used as template for PCR with 0.2 µM each of the dCAPS primer and reverse primer, 0.2 mM dNTP mixture and Taq polymerase. The amplified PCR product was subjected to restriction digest and the products were visualized after agarose gel electrophoresis using SYBR safe DNA stain (ThermoFisher). Digestion and the genotype of the sample can be inferred from the size (base pairs) of the DNA fragments compared against the GeneRuler 100bp Plus DNA ladder (ThermoFisher).

2.2.5.3 DMAS qPCR-based genotyping of *Brassica rapa* TILLING lines

SNPs in *B. rapa* TILLING lines were also genotyped using a recently published double mismatch allele-specific (DMAS) quantitative PCR method (Lefever *et al.*, 2019). This approach relies on

the use of primers specific for the wild-type or mutant variant of the SNP with intentional mismatches placed several nucleotides upstream of the SNP site to moderate primer specificity as required. *B. rapa* genomic DNA was used as a template for wild-type-specific and mutant-specific qPCR reactions (comprising 1 µL DNA, 1 µL primer-mix at a final concentration of 1 µM each, 5 µL 2X SYBR green master mix and 3 µL nuclease-free water) and the Cp values obtained from each qPCR were compared using Microsoft Excel. Initial genotyping experiments using this method were validated by Sanger sequencing of the SNP site and surrounding genomic region with Eurofins Genomics.

2.2.6 Assessment of immune responses

2.2.6.1 Seedling growth inhibition assays in *Arabidopsis*

Seeds were sterilized using vapor-phase sterilization procedure and plated on 0.5X MS + 0.5% sucrose plates before being stratified at 4°C for 3 days. Plates were subsequently transferred to a growth room set to 19.5°C with continuous light. After 4 days of growth, individual seedlings were placed in 1 mL of 0.5X MS + 0.5% sucrose liquid medium per well of a 48-well plate. The medium was supplemented with either 100 nM flg22 or an equivalent volume of water for mock treatment). Plates were incubated with gentle shaking in continuous light conditions for a further 4 days. Seedlings were then weighed and the average mass of 8 seedlings per genotype was calculated.

2.2.6.2 MAPK activation immunoblots

Seedlings were grown in continuous light on 0.5X MS agar containing 0.5% sucrose. After 10 days, seedlings were transferred to 0.5X MS + 0.5% sucrose liquid medium (10 seedlings per 6 mL medium per well in 6-well plates) and incubated overnight. On day 11, seedlings were treated with either 100 nM flg22 or an equal volume of water (mock) for 15 minutes. Tissue was harvested on liquid nitrogen and stored at -80°C.

Proteins were extracted in 2X SDS buffer. Protein concentrations were measured using the amido-black assay (Schaffner & Weissmann, 1973) against prepared standard solutions of BSA

(bovine serum albumin). 50 µg of each protein extract was loaded on 12% acrylamide SDS-PAGE gels. Separated proteins were transferred to a PVDF membrane (Amersham) for 2 hours at 80 mA. Equal protein transfer was assessed using Ponceau staining for 5 minutes. Membranes were blocked with 5% milk powder (w/v) in TBS-T (containing 0.05% Tween-20 (v/v)) for 30 minutes at room temperature.

Membranes were probed overnight at 4°C with a 1:1,000 dilution of anti-phospho-p44/42 MAPK antibody (Cell Signaling #4370) in 5% milk TBS-T, which can detect phosphorylated MPK3, MPK4 and MPK6 in *Arabidopsis* (Yamada *et al.*, 2016). After washing with TBS-T, the membrane was incubated with a 1:30,000 dilution of the secondary antibody (anti-rabbit IgG conjugated to horseradish peroxidase; Sigma-Aldrich) for 2 hours at room temperature. After rinsing in TBS-T, 1 mL of WesternBright ECL substrate (Advansta) was added to the membrane for 2 minutes. Chemiluminescence was detected using the G:BOX gel documentation system and the GeneSys software.

2.2.6.3 Detection of reactive oxygen species

Flg22-induced ROS were detected using a luminol-based approach that has been established previously with some minor changes (Smith & Heese, 2014; Gigli-Bisceglia *et al.*, 2015, Yuan *et al.*, 2015). Seeds were sown on 0.5X MS plates containing 0.5% sucrose, and stratified at 4°C for 3 days. Plates were transferred to a growth chamber at 19.5°C with 9 hours of light per day. After 7 days of growth, individual seedlings were carefully moved to expanded Jiffy-7 (44 mm) pellets for a further 3 weeks. Discs were taken from leaves of 4-week-old plants with a cork borer (1 cm diameter). Leaf discs were then carefully divided into 4 quarters with a razor blade. Each quarter-disc was placed into a separate well of a white Sterilin 96-well plate (ThermoScientific) containing 200 µL dH_2O with the abaxial leaf surface facing upwards. The plate was then returned to the growth room for a recovery period of at least 3 hours to reduce the effects of the wounding response.

100X stock solutions of luminol (Sigma) (17.7 mg/mL in 200 mM KOH) and horseradish peroxidase (HRP) (Fisher Scientific) (10 mg/mL in dH_2O) were prepared fresh. 60 µL of a luminescence solution containing 2.8 µL 100X luminol, 2.8 µL 100X HRP and 54.4 µL dH_2O was added to each well using a multichannel pipette. The plate was then transferred to a POLARstar

Omega microplate reader (BMG LABTECH) and luminescence was detected for 15 minutes to establish a baseline measurement. During this time, a 1.4 µM stock solution of flg22 was prepared in dH_2O. 20 µL of flg22 solution was added to each well, bringing the total volume to 280 µL, resulting in final concentrations of 100 nM flg22, 1X luminol and 1X HRP. Luminescence was detected every 120 seconds for a 60-minute period after addition of flg22. Data was analysed using Microsoft Excel and graphs were prepared using GraphPad Prism.

2.2.6.4 *Arabidopsis thaliana* flg22 RNA-Seq experiments

Seedlings were grown on 0.5X MS + 0.5% sucrose plates in continuous light conditions at 19.5°C. After 9 days of growth, 50 seedlings per genotype per treatment were moved to 2 wells of a 6-well plate, each containing 6 mL of 0.5X MS + 0.5% sucrose liquid medium and returned to the growth room with gentle agitation. On day 10, 1 µM flg22 or an equivalent volume of water (mock) were added to each well. After 1 hour, 50 seedlings per sample were harvested in liquid nitrogen and stored at -80°C. After grinding, frozen tissue was divided equally for RNA extraction and protein isolation for proteomics. RNA was isolated using the Spectrum Total RNA kit and the yield was quantified. RNA integrity was assessed using the Tapestation system (Agilent). RNA samples were frozen at -80 °C prior to shipping to BGI Genomics (Hong Kong) for transcriptome sequencing using the DNBseq sequencing technology.

2.2.6.5 *Brassica rapa* flg22 RNA-Seq experiment

B. rapa seedlings were grown in cups on 0.5X MS + 0.5% sucrose agar medium in continuous light conditions at 19.5°C. After 3 days, 4 seedlings per genotype per treatment were transferred to a well of a 6-well plate containing 6 mL of 0.5X MS + 0.5% sucrose (liquid medium) and returned to the growth room for incubation overnight with mild shaking. On day 4, seedlings were treated with 1 µM flg22 or an equivalent volume of water (mock) for 1 hour. Seedlings were collected and frozen immediately in liquid nitrogen. RNA was extracted and the yield was quantified. *B. rapa* RNA samples were shipped to BGI for transcriptome sequencing as described for the *Arabidopsis* samples in the previous section 2.2.6.4.

2.2.6.6 *Pseudomonas syringae* DC3000 infection assays (adapted from de Marchi *et al*., 2016)

Seedlings were grown for 7 days on 0.5X MS + 0.5% sucrose plates with a 9-hour light period. After one week, individual seedlings were transferred to expanded jiffy pots for a further 3 weeks of growth. Plants were covered with plastic tray lids overnight prior to inoculation. Using a blunt 1 mL syringe, a bacterial suspension at 5×10^5 cfu/mL *Pst* DC3000 in 10 mM $MgCl_2$ was infiltrated into the abaxial side of 3 leaves per plant. For determination of *in planta* bacterial growth, leaf disc samples were harvested at 3 dpi, combined and ground in 10 mM $MgCl_2$ before dilutions were plated out on King's B supplemented with rifampicin (50 mg/L). Plates were incubated at 28°C and colonies were counted after 2-4 days.

2.2.6.7 Chitosan treatment of seedlings for RT-qPCR

Arabidopsis seedlings were grown on 0.5X MS agar plates for 11 days in continuous light conditions before transfer to a 0.5X MS liquid culture. On day 12, media was supplemented with a final concentration of 100 µg/mL chitosan (dissolved in 1% acetic acid) or an equivalent volume of mock solution (1% acetic acid). Tissue was harvested 0, 1, 3, 6 and 24 hours after treatment and stored at -80°C prior to RT-qPCR analysis.

2.2.7 Transient expression in *B. rapa* and *B. napus*

2.2.7.1 Co-cultivation transformation of *B. rapa* seedlings (adapted from Mooney & Graciet, 2020)

B. rapa seeds were planted on 15 mL 0.5x MS agar medium in 50 mL centrifuge tubes and seedlings were grown in constant light at 19.5°C for 3 days. A previously published co-cultivation protocol known as the Fast Agro-mediated Seedling Transformation or 'FAST' technique (Li *et al*., 2009) was modified for *B. rapa*, as indicated below. *Agrobacterium tumefaciens* C58 pGV2260 (McBride & Summerfelt, 1990) transformed with the N-degron pathway reporter construct pML-BART $UBQ3_{pro}$:Ub-Gly-LUC $35S_{pro}$:GUS (pEG378; (Graciet *et*

al., 2010)) was streaked from glycerol stock on LB medium supplemented with 50 mg/L rifampicin and 100 mg/L spectinomycin and grown for 2-3 days at 28°C before being suspended in washing solution (10 mM $MgCl_2$, 100 µM acetosyringone). Seven individual 3-day-old *B. rapa* seedlings were transferred to a 50 mL centrifuge tube containing 30 mL co-cultivation medium (1.13 g/L MS medium, 1% sucrose (w/v), 100 µM acetosyringone, 0.001% Silwet (v/v), pH6.0) and *Agrobacteria* transformed with the indicated plasmids were added to a final OD_{600} of 0.5. Samples were then vacuum infiltrated at 80 kPa for 10-20 min. Tubes were wrapped in aluminium foil and incubated at 19.5°C for 30-48 hours of co-cultivation. Seedlings were washed with autoclaved dH_2O three times and placed on 0.5x MS agar plates for 24 hours before GUS staining procedure (section 2.2.7.3).

2.2.7.2 Agroinfiltration of *B. rapa* and *B. napus* (from Mooney & Graciet, 2020)

A. tumefaciens C58 pGV2260 (McBride & Summerfelt, 1990) transformed with the indicated N-degron pathway reporters, a pMLBART empty vector or pCAMBIA2201 were grown for 3-4 days at 28°C on LB agar supplemented with 50 mg/L rifampicin and 100 mg/L spectinomycin. After 3-4 days growth, bacteria were suspended from plates in 2 mL infiltration medium (10 mM MES pH5.5, 10 mM $MgCl_2$, 150 µM acetosyringone) and diluted to OD_{600} of 0.75. Four to 5-week-old *B. rapa* or *B. napus* were covered with plastic lids overnight prior to infiltration to increase humidity and encourage stomatal opening. A ~2 cm diameter area was marked on the abaxial side of the first and second true leaves. Using a blunt 1 mL syringe, the bacterial suspension was infiltrated into the marked areas. Excess liquid was removed with tissue paper and plants were returned to the growth room. Unless otherwise stated, tissue was harvested 3-days post agroinfiltration for GUS staining or protein extraction.

2.2.7.3 GUS staining (adapted from Mooney & Graciet, 2020)

Agroinfiltrated leaf-discs were harvested in 90% acetone and incubated at room temperature with mild shaking for 15-20 minutes to remove chlorophyll. GUS staining was performed as described in Jefferson et al., (1987) using 2 mM X-Gluc (5-bromo-4-chloro-3-indolyl-beta-D-

glucuronic acid, cyclohexylammonium salt; Thermo Scientific) as a substrate. *B. rapa* and *B. napus* leaf-disc samples were incubated in the X-gluc solution for 3 days at 37°C. Samples were stored in 70-90% ethanol at 4°C**.**

2.2.7.4 Determining GUS and LUC activity in *Brassica rapa* (adapted from Mooney & Graciet, 2020)

For LUC and GUS assays, 4 agroinfiltrated leaf discs (diameter: 1 cm) per construct were pooled and proteins were extracted in 450 µL 1x CCLR buffer (Promega) supplemented with 1 mM phenylmethylsulfonyl fluoride (PMSF; Sigma-Aldrich) and 1% (v/v) plant protease inhibitor cocktail (Sigma-Aldrich). Protein concentration of CCLR extracts was measured using Bradford protein assay (see section 2.2.3.10). Absorbance values were compared to a standard curve of absorbance readings for BSA solutions of known concentration ranging from 1-10 mg/mL. LUC activity was measured as described in section 2.2.4.6. Values were normalized to either GUS activity (see section 2.2.4.7) or the relative expression of the *LUC* gene as determined by RT-qPCR (section 2.2.3.5)

2.2.7.5 LUC and GUS immunoblots (adapated from Mooney & Graciet, 2020)

Agroinfiltrated *Brassica rapa* leaf tissue was harvested and frozen immediately in liquid nitrogen. Proteins were extracted using 6x SDS loading buffer (Laemmli buffer), with 80 µL of buffer used per 1.5 cm diameter leaf disc. Proteins were separated on a 10% acrylamide SDS-PAGE gel before being transferred to a PVDF membrane for 2 hours at 80 mA. LUC was detected using a goat antibody against firefly luciferase (AB3256, Merck) diluted 1:2,000 in PBS-T (1x PBS with 0.05% Tween 20 (v/v)) containing 5% milk (w/v). After imaging the immunoblot, the antibodies were removed from the membrane by incubating in a stripping buffer (50 mM Tris pH 6.8, 2% SDS, 100 mM β-mercaptoethanol) at 50°C for 15 minutes. The stripping buffer was removed by washing 3 x 5 minutes in PBS-T.

The same membranes were then probed with the rabbit anti-GUS antibody (A5790, Invitrogen) at a 1:1,000 dilution in PBS-T with 5% milk. To observe LUC expression in samples with approximately equal GUS levels, the protein quantity loaded was adjusted based on previous immunoblots with replicate samples.

2.2.8 RNA-Seq analysis performed by BGI

The following section is adapted from documents provided by BGI detailing the RNA-Seq procedure and preliminary analysis of raw data.

2.2.8.1 Experimental procedure

The experimental procedure performed by BGI on the isolated RNA samples were as follows: 1) mRNA enrichment and purification from total RNA samples using Oligo dT Selection; 2) RNA fragmentation and cDNA synthesis; 3) End repair and adaptor ligation; 4) PCR; 5) Circularization to form DNA nanoballs (DNBs); and 6) Sequencing on DNBSEQ platform.

2.2.8.2 BGI analysis pipeline

Quality control (QC) was performed on raw reads obtained from sequencing to determine whether the data is suitable for subsequent analysis. After quality control, the filtered clean reads were aligned to the reference sequence. After the alignment, the statistics of the mapping rate and the distribution of reads on the reference sequence were used to determine whether the alignment result passes the second QC of alignment.

Following this, gene quantification analysis and other analysis based on gene expression (principal component, correlation, differential gene screening, etc.) was carried out, alongside significant enrichment analysis of GO function on differentially expressed genes among the screened samples.

2.2.8.3 Sequencing data filtering

This project employed the filtering software SOAPnuke developed by BGI independently for filtering. The specific steps are as follows:

1) Remove the reads containing the adaptor (adaptor pollution).

2) Remove reads whose N content is greater than 5%.

3) Remove low-quality reads (we define reads with bases with a quality score less than 10 as the proportion of total bases in the reads that are greater than 20% as low-quality reads).

The filtered "Clean Reads" are saved in FASTQ format.

2.2.8.4 Reference genome alignment

The Hierarchical Indexing for Spliced Alignment of Transcripts (HISTAT) software was used for mapping RNA-seq reads. Compared with other software, HISAT has the advantages of high speed, high sensitivity and accuracy, and low memory consumption.

2.2.9 Identification of homologous genes in *Arabidopsis* and *B. rapa*

This analysis was performed in collaboration with Prof. Frank Wellmer and Joseph Beegan (Trinity College Dublin, Ireland). CDS sequences from the *B. rapa* (Chiffu-401-42) v3.01 genome (GCF_000309985.2) were queried against the *Arabidopsis thaliana* TAIR10.1 genome (GCF_000001735.4) using the following nucleotide BLAST settings: E.value threshold: 1e-6; Max number of target sequences: 6 (to account for genome triplication/duplication). BLASTn queries were automated using a Python script written by Joseph Beegan.

3

Investigating the roles of the N-degron pathway in the regulation of immunity in *Arabidopsis*

3.1 Introduction and aims

Multiple previous studies have implicated the plant N-degron pathway in the regulation of immunity (detailed in section 1.3.4). Of particular interest to the present study is the observation by de Marchi *et al.* (2016) that *Arabidopsis* N-degron pathway mutants are broadly more susceptible to a wide range of pathogens. As PTI mediates basal resistance following recognition of highly conserved pathogen molecules, we hypothesized that N-degron pathway mutants may be impaired in PTI. In a laboratory setting, PTI can be activated independently from ETI by exposing plants to commercially available purified PAMP molecules. These are typically pathogen-derived peptides (e.g. the flg22 peptide derivative of bacterial flagellin or the elf18 peptide from bacterial EF-Tu) or complex polysaccharides (e.g. chitin oligosaccharides) that are released during pathogen challenge. The experiments detailed here aim to characterise the contribution of the N-degron pathway to the PTI response, primarily via treatments with flg22 followed by assessment of various PTI-related signaling outputs. These include the transcriptional changes elicited during PTI, PAMP-induced ROS production, MAPK cascade activation and seedling growth inhibition. Following this,

inoculations with the model pathogen *Pst* DC3000 reveal novel insights into the roles of the N-degron pathway during pathogen infection.

3.2 The transcriptomic response of N-degron pathway mutants to flg22

3.2.1 Experimental details

Global transcriptomic reprogramming is a key hallmark of the PTI response (see section 1.3.2.7). I aimed to characterise the transcriptional response of N-degron pathway mutants to flg22, to determine whether this aspect of PTI could be N-degron pathway regulated. A pilot experiment was conducted over a 6-hour time-course to assess the activation of PTI-associated marker genes after flg22 treatment in wild-type *Arabidopsis* plants. Seedlings of Col-0 and the flg22-insensitive ecotype Ws-0 were treated with dH_2O (mock) or 1 µM flg22, a dose commonly used to assess PTI as it is saturating for medium alkalinization (Felix-Felix *et al.*, 1999; Denoux *et al.*, 2008) caused by immunity-associated ion efflux (section 1.3.2.4).

RT-qPCR analysis confirmed robust increases in the expression of *MPK3* and *WRKY33* in Col-0 wild-type seedlings treated with 1 µM flg22, peaking 1 hour after elicitation (Fig.3.1). Notably, expression of these genes was not elevated in the flg22-insensitive Ws-0, strongly indicating the flg22-induced activation of PTI in Col-0 in these experimental conditions.

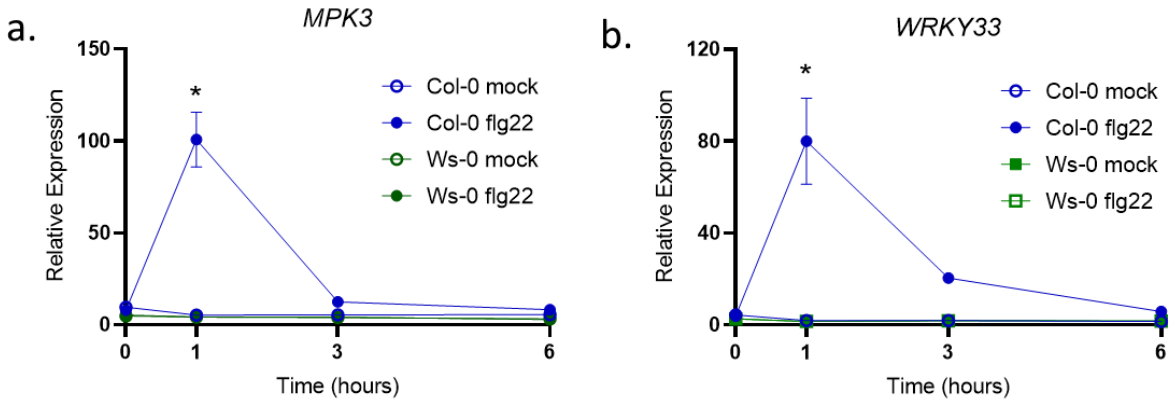

Figure 3.1. Time-course of PTI-marker gene expression after flg22 treatment. Relative expression of PTI marker genes **a.** *MPK3* and **b.** *WRKY33* at 0, 1, 3 and 6 hours after treatment with flg22 or dH_2O (mock). Expression was calculated relative to the *MON1* reference gene. Datapoints indicate means +/-

SEM error bars. 3 independent replicates were performed for 0 and 1 hour timepoints and 2 replicates for 3 and 6 hour timepoints. One-way ANOVA comparison to Col-0 mock-treated control at 1 hour revealed statistically significant difference in Col-0 flg22 treated samples ($p<0.001$), denoted by asterisk.

Similar experimental conditions were used to investigate the early transcriptomic response of various N-degron pathway mutants to flg22 via RNA sequencing (RNA-Seq) and accompanying RT-qPCR assays. Specifically, seedlings of wild-type (Col-0), N-degron pathway mutants (*ate1ate2* and *prt6-1*), an ATE1 rescue line in the *ate1ate2* background and the flg22-insensitive ecotype (Ws-0) were treated with 1 µM flg22 or an equivalent volume of dH_2O (mock) for 1 hour. Three independent replicate experiments were performed.

As previous data indicated that *ate1ate2* exhibits dampened transcriptional responses to *Pst* DC3000 AvrRpm1, as well as a consistently increased susceptibility to bacterial pathogens (de Marchi *et al.*, 2016), this line was selected for comparison with Col-0 by RNA-Seq to explore the contribution of the N-degron pathway to global flg22-triggered transcriptional reprogramming. RNA samples generated from other genotypes mentioned were stored in order to validate hypotheses arising from the RNA-Seq datasets at a later stage of the project.

3.2.2 RNA-Seq data summary

RNA isolated from mock and flg22-treated Col-0 and *ate1ate2* seedlings was subjected to RNA-Seq using the DNBseq platform at BGI (Hong Kong). Identification of uniquely mapped reads was carried out by BGI. The proportion of reads uniquely mapped to the genome ranged from 93.64 - 94.55%, indicating that the data were of sufficient quality for further analysis. In all samples combined, 24,195 genes were detected. Principal component analysis (PCA) of sample similarity revealed clustering of samples primarily according to treatment received (i.e. mock or flg22) (Fig. 3.2), as opposed to differences based on genotype.

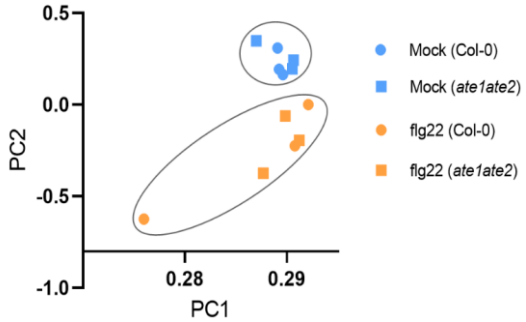

Fig.3.2. PCA plot of samples following RNA-Seq. Datapoints represent individual RNA samples. PCA analysis was performed by BGI and plot was generated using GraphPad Prism.

An analysis plan was established to investigate differential gene expression among the samples, consisting of four main comparisons:

(a) Col-0 mock-treated seedlings compared to Col-0 flg22-treated seedlings to assess PTI in wild-type plants.

(b) *ate1ate2* mock-treated seedlings compared to *ate1ate2* flg22-treated seedlings to assess PTI in N-degron pathway deficient plants.

(c) Direct comparison of wild-type and *ate1ate2* transcriptomes upon mock treatment to determine genotype-specific differences in the absence of PTI.

(d) Direct comparison of wild-type and *ate1ate2* seedlings following flg22 treatment to determine genotype-specific differences during PTI activation.

These analyses were performed using the Dr. Tom analysis software developed by BGI (Ye *et al.*, 2019). Volcano plots showing gene expression differences (fold-change) and statistical significance (q-value) for each of the four comparison groups are shown in Fig. 3.3. A maximum q-value threshold of 0.05 was applied for the determination of statistically significant differences in gene expression as is the convention in biological research. Additionally, a moderate fold-change cut-off of ≥ 1.5 (equivalent to |log2(fold change)| ≥ 0.585) was implemented for the classification of differentially expressed genes (DEGs) following visual inspection of volcano plots, to balance stringency with retention of legitimate differences between treatment groups.

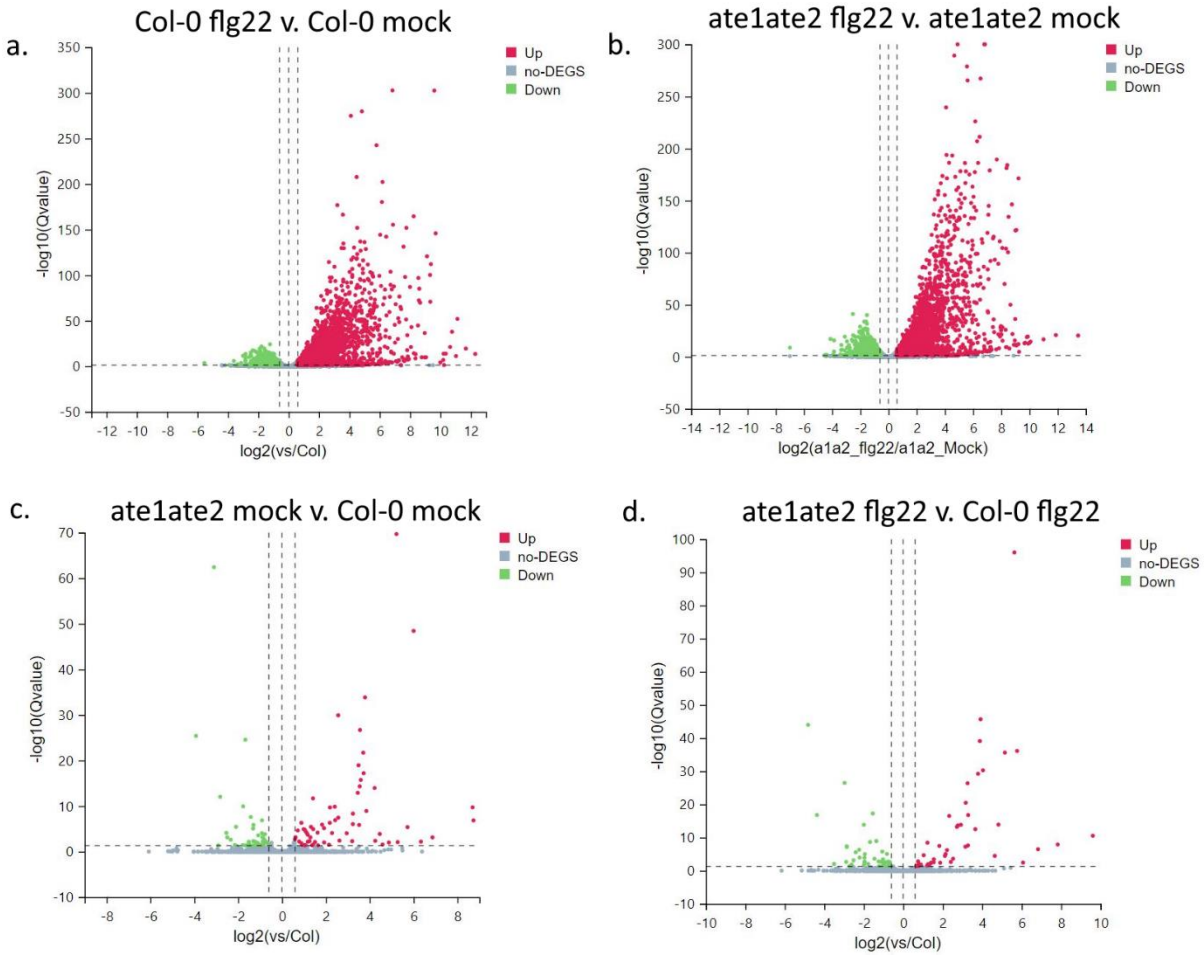

Figure 3.3. Volcano plot of comparison groups following RNA-Seq. Volcano plots of comparison groups following RNA-Seq indicating statistical significance on the x-axis (q-value) and magnitude of change (log2 of fold-change) on the y-axis. Cut-off thresholds (q-value ≤ 0.05, log2 fold-change ≥ 0.585) are indicated by dashed lines. Upregulated genes are shown in red, downregulated genes are shown in green and genes outside the cut-off values are shown in grey. Comparisons are shown as follows: **a.** Col-0 flg22-treated samples v. Col-0 mock, **b.** *ate1ate2* flg22-treated samples v. *ate1ate2* mock, **c.** *ate1ate2* mock-treated samples vs. Col-0 mock and **d.** *ate1ate2* flg22-treated samples vs. Col-0 flg22. Plots were generated on the Dr. Tom software developed by BGI.

3.2.3 Flg22-responsive genes in Col-0 and *ate1ate2*

To investigate flg22-responsive genes in each genotype, I investigated the DEG datasets retrieved from comparison groups (a) and (b) (see section 3.2.2). After application of the cut-off values described above (q-value ≤ 0.05, $|\log_2$ fold-change$|$ ≥ 0.585), 2,792 genes were found to be upregulated in Col-0 after flg22 treatment, while 1,458 were downregulated (Fig

3.4a). A similar number of genes were differentially expressed in *ate1ate2* seedlings, with 2,861 showing increased expression and 1,582 genes downregulated after flg22 treatment (Fig. 3.4a). Importantly, genes upregulated in Col-0 samples showed substantial overlap with a previously published list generated by microarray analysis following a similar experimental procedure by Denoux *et al*. (2008), serving as external validation of this dataset (Fig. 3.4b).

Gene ontology (GO) enrichment analysis was performed to compare the biological pathways involved in the flg22 response of Col-0 and *ate1ate2* seedlings (Fig. 3.4c). As could be expected, immunity-related GO categories including defence response to bacterium, response to chitin, protein phosphorylation and response to salicylic acid were among the most significantly enriched in both genotypes, strongly indicating that PTI was indeed activated by flg22 treatment. Overall, GO pathway enrichment was very similar in both genotypes, with some notable differences (e.g. the inclusion of 'response to jasmonic acid' in *ate1ate2*). Combined with the similar number of flg22-responsive genes (Fig. 3.4a), this data suggests that the *ate1ate2* mutant is not severely compromised in its overall ability to alter global gene expression in response to flg22.

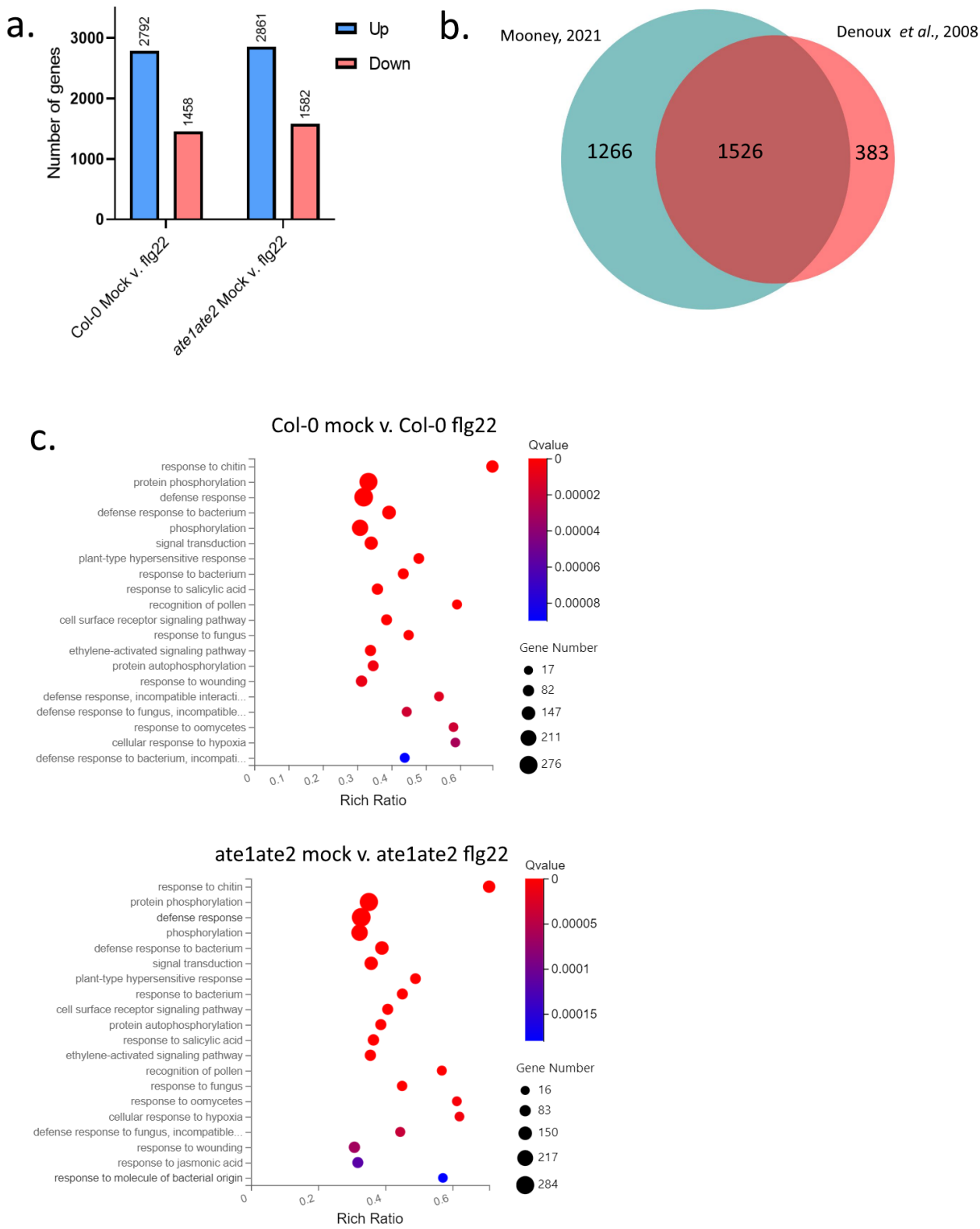

Figure 3.4. Flg22-responsive genes in Col-0 and *ate1ate2*. a. Summary of the number of differentially expressed genes (DEGs) and the directionality of expression changes in Col-0 and *ate1ate2* seedlings in response to 1 µM flg22. **b.** Comparison of flg22-induced genes in Col-0 identified in this study with previously published datasets with identical cut-offs applied (fold-change > 1.5, q-value/p-value < 0.05). Denoux *et al.* (2008) treated Col-0 seedlings with 1 µM flg22 for 1 hour and assessed transcriptional

response using microarrays. Area-proportional Venn diagram was created using BioVenn (Hulsen et al., 2008). **c.** GO pathway enrichment of differentially expressed genes in Col-0 (upper) and *ate1ate2* (lower) in response to flg22. Figure was generated using the Dr. Tom analysis platform (BGI).

In agreement with this overall similarity, Venn diagram comparison of the flg22-responsive genes in Col-0 and *ate1ate2* revealed that a sizable majority (3,743 / 4,950 total genes, ~76%) were commonly found in both datasets (Fig. 3.5). Of the remaining genes, 507 responded to flg22 treatment exclusively in Col-0 (218 induced, 289 repressed), with 700 exclusively detected in the *ate1ate2* dataset (287 induced, 413 repressed) (Fig. 3.5). Although no GO categories are significantly over-represented among the 507 genes exclusively detected in wild type seedlings, this dataset does include several genes with known functions in immunity, including *WRKY54* (Chen *et al.*, 2021) and *WRKY19/MEKK4* (Warmerdam *et al.*, 2020) (Fig 3.5b). This indicates that *ate1ate2* may indeed be impaired in the expression of specific immune genes after flg22 treatment, despite the overall similarity in the sets of flg22-responsive genes.

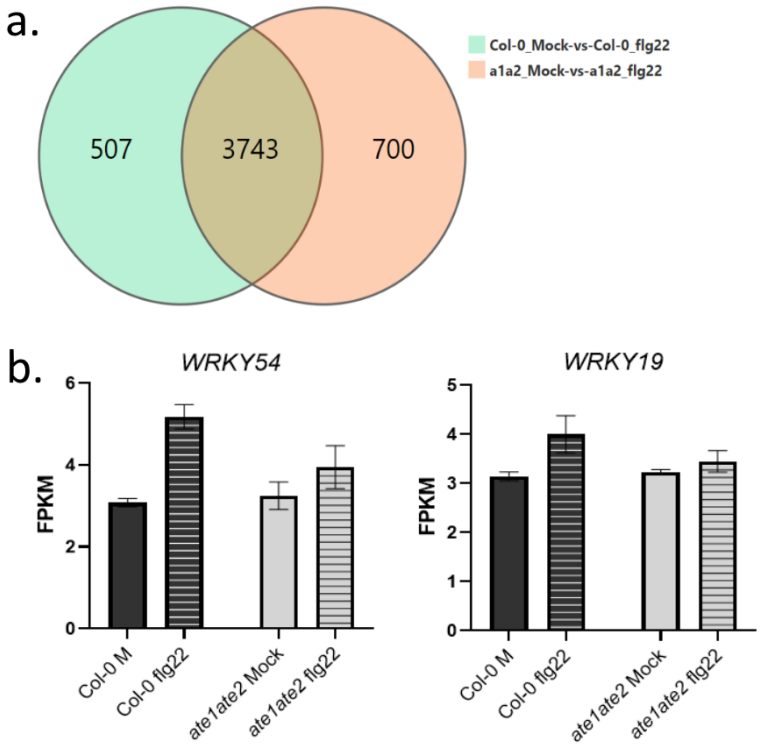

Figure 3.5. Differences in flg22-responsive genes in Col-0 and *ate1ate2*. a. Overlap of flg22-responsive genes in Col-0 and *ate1ate2* (fold-change > 1.5, q-value < 0.05). *ate1ate2* denoted as 'a1a2'.

b. Transcript abundance of selected immune genes *WRKY54* and *WRKY19*. FPKM = Fragments Per Kilobase of transcript per Million detected by RNA-Seq. Columns represent means of 3 independent replicates +/- SEM error bars.

3.2.4 Direct comparison of Col-0 and *ate1ate2* datasets

To further explore differences between the genotypes, gene expression in Col-0 and *ate1ate2* was compared directly after mock and flg22-treatment (comparisons (c) and (d) as outlined in the analysis plan in section 3.2.2).

104 genes were identified as differentially expressed in *ate1ate2* compared to Col-0 after mock treatment (Fig. 3.6a). These genes are listed in full in Tables B1 (down in *ate1ate2* mock) and B2 (up in *ate1ate2* mock) in Appendix B. GO analysis of the 104 genes revealed significant enrichment in categories including 'response to hypoxia', 'detection of hypoxia' and 'protein arginylation' (Fig. 3.6b). This observation is consistent with the previously described role of the N-degron pathway as an important regulator of hypoxia (see section 1.2.2 – 1.2.5), and the molecular function of the *ATE1* and *ATE2* enzymes as arginyl-tRNA transferases. Indeed, as may be expected, *ATE1* and *ATE2* were recovered as the two genes with the most strongly reduced expression in *ate1ate2* seedlings (Table B1).

Direct comparison of Col-0 flg22 and *ate1ate2* flg22-treated samples revealed 87 DEGs, including 59 also found in the mock treatment comparison of the two genotypes (Fig. 3.6a). These 87 genes are listed in Tables B3 (down in *ate1ate2* flg22) and B4 (up in *ate1ate2* flg22) in Appendix B.

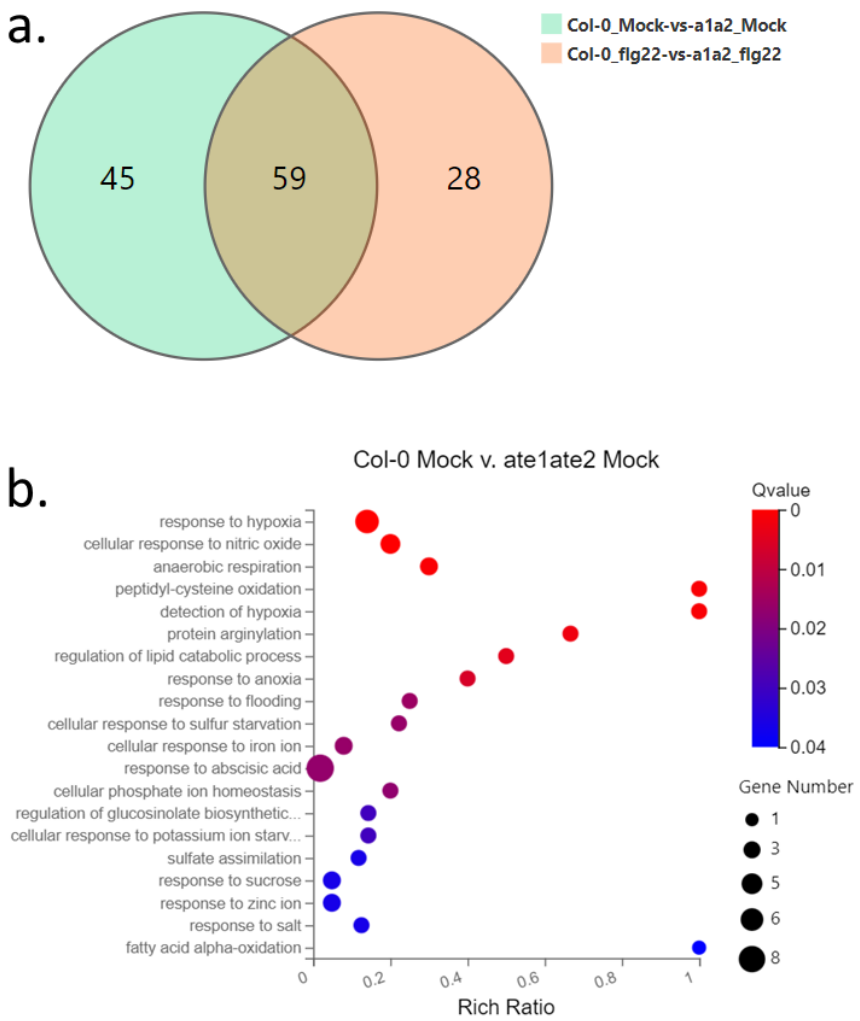

Figure 3.6. Col-0 vs. *ate1ate2* comparison after mock or flg22 treatment. a. Overlap of DEGs between Col-0 and *ate1ate2* in mock and flg22-treated conditions (fold change >1.5, q-value < 0.05). **b.** GO enrichment of genes misregulated in *ate1ate2* mock-treated seedlings compared to Col-0.

3.2.5 Regulation of flg22-responsive genes by the N-degron pathway

To identify flg22-responsive genes regulated by the N-degron pathway, I compared the 87 genes differentially expressed between Col-0 flg22 and *ate1ate2* flg22-treated samples (Fig. 3.6a) with the 4,250 DEGs (Fig. 3.5a) retrieved in the Col-0 mock vs. Col-0 flg22 comparison. In total, 17 of the 87 genes were present in this dataset, indicating that their altered expression is a feature of the wild-type PTI response. Hence, their differential expression in flg22-treated *ate1ate2* plants may be relevant in the context of the pathogen defence-related phenotypes of the *ate1ate2* mutant. These 17 genes are listed in Fig. 3.7b.

a.

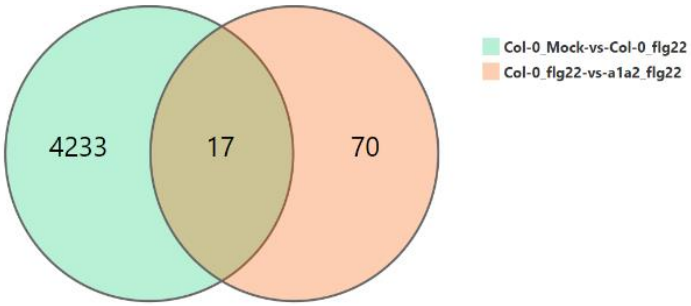

b.

AGI number	Gene name	Description (TAIR / UniProt)	LOG2 fold change	
			Col-0 flg22/Col-0 Mock	a1a2 flg22/Col-0 flg22
AT5G46295	*AT5G46295*	Transmembrane protein	7.270685732	3.883192019
AT1G32350	*AOX1D*	Alternative oxidase 1D	4.442368884	-1.959224987
AT5G45340	*CYP707A3*	involved in ABA catabolism.	3.362808928	0.666184568
AT3G02550	*LBD41*	LOB-domain containing	3.284727212	2.109948032
AT5G24240	*ATPI4Kγ3*	Phosphatidylinositol 4-kinase gamma 3	2.971448345	-4.820507733
AT3G21080	*AT3G21080*	ABC transporter-like protein	2.860668084	0.682353082
AT2G28270	*AT2G28270*	Cys/His-rich C1 domain family	1.727399255	-1.987411983
AT2G47520	*ERF71/HRE2*	Hypoxia responsive ERF	1.572451127	2.147084771
AT1G31290	*AGO3*	ARGONAUTE 3	1.382194495	0.77838912
AT1G74590	*GSTU10*	glutathione transferase	0.986834591	-1.203769886
AT5G24090	*CHIA*	Chitinase A	0.888096053	-0.860897468
AT2G46750	*GulLO2*	L-ascorbic acid biosynthesis	0.812722241	-1.059878351
AT2G16060	*HB1*	Hemoglobin induced by low oxygen levels	0.759842425	3.260100996
AT3G09220	*LAC7*	Laccase-like enzyme	0.609716081	-0.753053251
AT5G65640	*bHLH093*	bHLH transcription factor	-0.778242682	1.22686921
AT4G33560	*WIP5*	Wound-induced polypeptide 5	-0.87716056	2.923568494
AT3G10040	*HRA1*	Hypoxia response attenuator 1	-0.94105679	2.720694407

Figure 3.7. Flg22-responsive genes misregulated in *ate1ate2*. a. Overlap of DEGs found in the Col-0 Mock v. Col-0 flg22 and Col-0 flg22 v. *ate1ate2* flg22 comparisons (fold-change > 1.5, q-value <0.05). **b.** Table listing the 17 genes found in the overlap from **a.** Gene descriptions were adapted from The Arabidopsis Information Resource (TAIR) and UniProt websites.

3.2.5.1 Regulation of CIR genes by the N-degron pathway

Notably, two genes on this list, *ATPI4Kγ3* and *ChiA* (Fig. 3.7b), have recently been implicated as members of the so-called 'core immunity response' (CIR) genes (Bjornson *et al.*, 2021). *ChiA* (also known as *LYS1*) encodes a plant lysozyme-like hydrolase capable of cleaving peptidoglycan fragments from the cell walls of invading bacteria (Liu *et al.*, 2014). *ATPI4Kγ3* is involved in the generation of phosphoinositide metabolites that mediate responses to various environmental stimuli (Akhter *et al.*, 2015). To assemble the CIR dataset, Bjornson *et al.* (2021) conducted comparative RNA-Seq experiments on *Arabidopsis* seedlings following PTI

elicitation with a range of PAMPs including flg22, elf18, nlp20 and chitooctaose. The resulting group of commonly induced genes was then compared with datasets of genes involved in the response to abiotic stresses. 38 CIR genes were defined as those that were commonly induced in response to all PAMPs tested but not in response to abiotic stresses. Following the identification of CIR genes *ATPI4Kγ3* and *ChiA* as differentially expressed in the *ate1ate2* mutant, the expression of all 38 CIR genes in *ate1ate2* flg22-treated samples was assessed relative to flg22-treated Col-0 samples (Fig. 3.8).

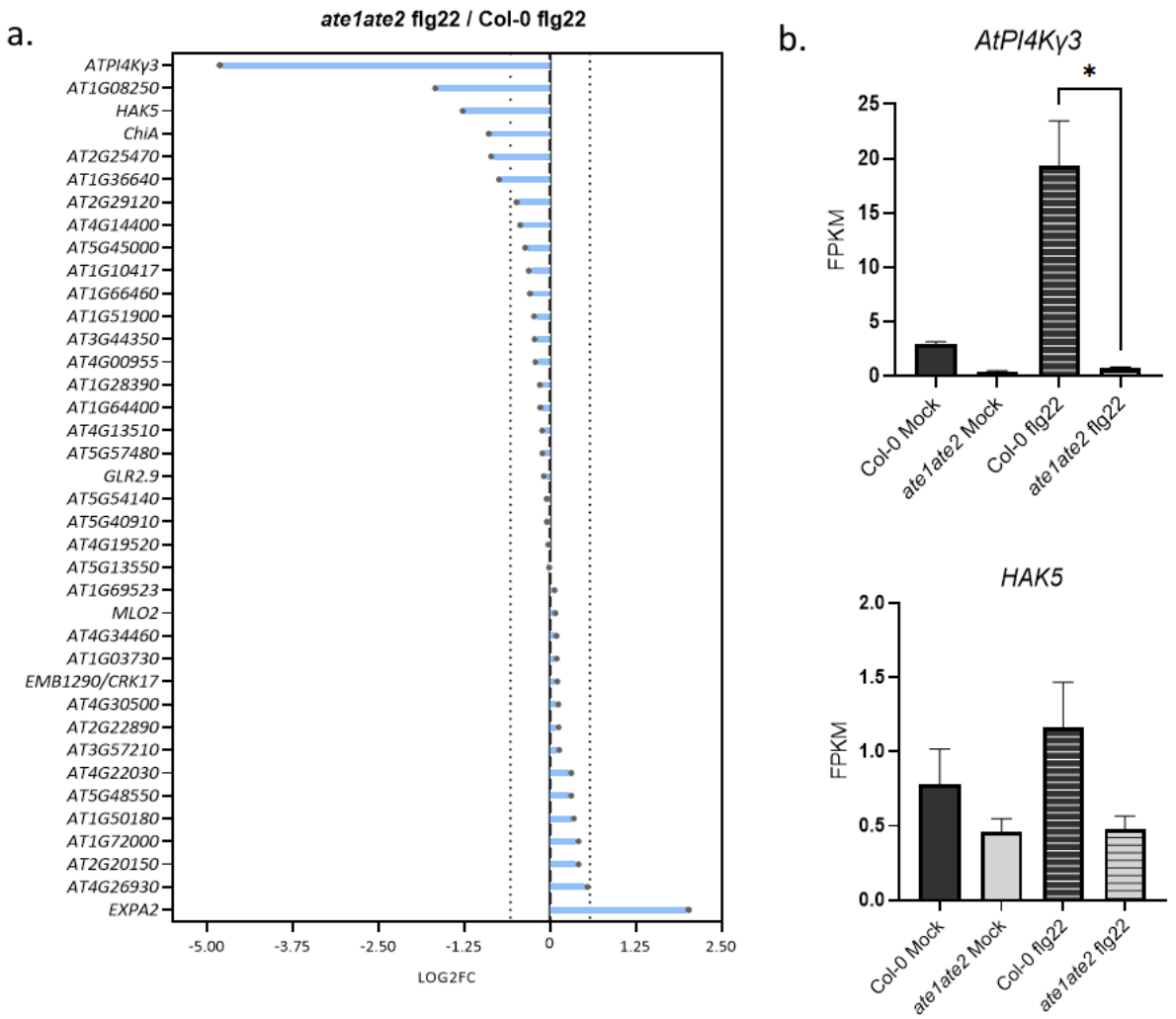

Figure 3.8. CIR gene expression. a. Differential expression of 38 CIR genes in flg22-treated *ate1ate2* relative to Col-0 treated with flg22. A |$\log_2$ of the fold change| of 0.585 (equivalent to a fold-change of 1.5) is indicated by dotted lines. **b.** Mean FPKM values for selected CIR genes. Means from 3 independent replicates + SEM error bars. Asterisk denotes statistical significance after t-test ($p<0.05$).

Six CIR genes exhibit a greater than 1.5-fold reduction in expression in *ate1ate2* compared to Col-0 after flg22 treatment, namely: *ATPI4Kγ3* (AT5G24240), *ADT6* (AT1G08250), *HAK5* (AT4G13420), *ChiA* (AT5G24090), *RLP21* (AT2G25470) and AT1G36640, while a single CIR gene - *EXPA2* (AT5G0290) - showed a greater than 1.5-fold increase in expression in *ate1ate2* (Fig. 3.8). However, it should be noted that *ChiA* and *ATPI4Kγ3* were the only CIR genes whose altered expression in *ate1ate2* after flg22-treatment was statistically significant ($q \leq 0.05$).

The expression of *ChiA* and *ATPI4Kγ3* were analysed further by RT-qPCR assays in *prt6-1*, the flg22-insensitive Ws-0 and an ATE1 rescue line (Fig. 3.9). The ATE1 rescue line is an *ate1ate2* mutant in which the *ATE1* genomic locus was re-introduced (Graciet *et al.*, 2009). ATE1 contributes about 90% of Arg-transferase activity in *Arabidopsis* and its restored expression is sufficient to rescue developmental defects of *ate1ate2* mutant plants (Graciet *et al.*, 2009). However, the possibility that *ATE2* expression is specifically required for some functions cannot be ruled out, and could explain the failure of the ATE1 rescue line to rescue some phenotypes.

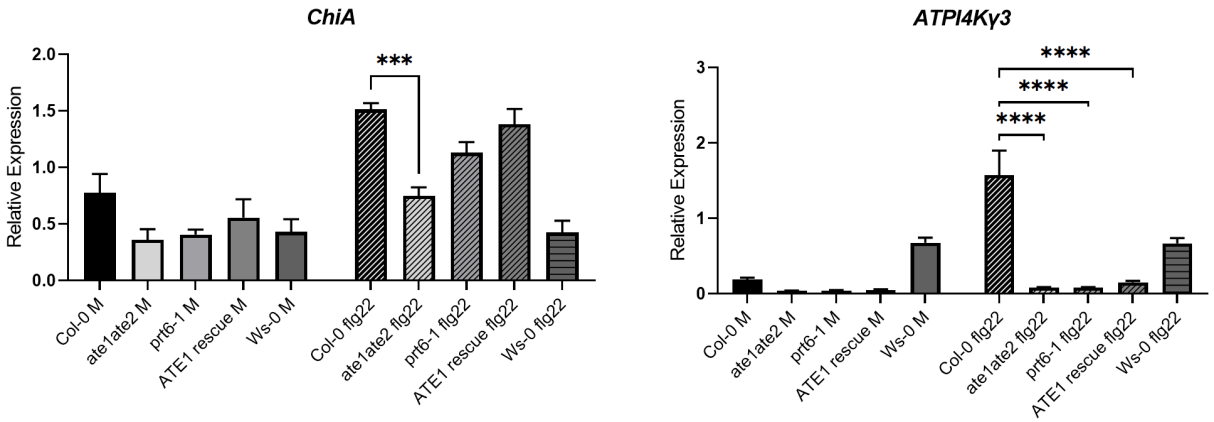

Figure 3.9. CIR gene expression in N-degron pathway mutants. Relative expression of *ChiA* and *ATPI4Kγ3* detected by RT-qPCR. Error bars represent SEM values. Asterisks denote statistical significance determined by one-way ANOVA comparisons with Col-0 flg22 control group (*** = $p \leq 0.001$). Ws-0 is included as a flg22 insensitive control. *MON1* was used a reference gene.

These experiments confirmed that *ChiA* exhibits significantly reduced expression in *ate1ate2* compared to wild-type seedlings after flg22 treatment (Fig. 3.9). A similar reduction is evident in *prt6-1*, a null allele of the PRT6 N-recognin that acts downstream of ATE1 and ATE2,

although this difference was not statistically significant. Furthermore, the ATE1 rescue line shows near wild-type levels of *ChiA* expression after flg22 treatment, indicating that this gene is indeed likely positively regulated by ATE1 and the Arg/N-degron pathway.

ATPI4Kγ3 also showed significantly weaker expression in *ate1ate2* and *prt6-1* after flg22 treatment compared to wild-type seedlings, but this expression was not restored in the ATE1 rescue line. This suggests that the N-degron pathway may not be a *bona fide* regulator of *ATPI4Kγ3* expression. Interestingly, *ATPI4Kγ3* transcription is primarily regulated by methylation of its promoter region (Akhter *et al.*, 2015). In fact, the *ATPI4Kγ3* locus has been designated as a 'differentially methylated region' (DMR) (Schmitz *et al.*, 2011), genomic regions whose methylation status is subject to metastable spontaneous variations (Havecker *et al.*, 2012). Such epiallelic variation at the *ATPI4Kγ3* locus has been specifically associated with considerable differences in transcript abundance, even among plants of the same genotype (Schmitz *et al.*, 2011). Thus, the observed differences in the expression of *ATPI4Kγ3* could be attributable to spontaneous epigenetic variation. Another flg22-responsive gene with altered expression in *ate1ate2* after flg22 treatment, AT5G46295 (Fig. 3.7b), is also a known DMR (Rudolf *et al.*, 2021).

3.2.5.2 Regulation of flg22-inducible genes by the N-degron pathway

A number of additional flg22-responsive genes of interest (*AOX1D*, *GSTU10* and*LAC7*) identified as misregulated in *ate1ate2* after flg22 treatment (Fig. 3.7b) were also selected for analysis by RT-qPCR. Previously, *AOX1D* has been described as a positive regulator of plant defences, likely by limiting oxidative damage during biotic interactions (Gupta, 2013), while *GSTU10* encodes a pathogen-inducible glutathione-S-transferase (Gullner *et al.*, 2018). *LAC7* is involved in drought responses (Pegler *et al.*, 2019) and encodes a laccase enzyme, whose primary functions are related to the polymerization of lignin to reinforce plant cell walls (Zhao *et al.*, 2013).

These experiments validated the reduced expression of the flg22-inducible genes *GSTU10*, *AOX1D* and *LAC7* in the *ate1ate2* mutant (Fig. 3.10a-c). Notably, *ate1ate2* seedlings showed this reduced expression of these genes compared to Col-0 after mock treatment, indicating that the N-degron pathway may regulate these genes under basal conditions in the absence

of immune elicitation. However, the differences between *ate1ate2* and Col-0 become more pronounced after flg22 treatment (Fig. 3.1a-c). Similar, albeit less prominent, defects in the expression of these genes were observed in the *prt6-1* mutant. Expression of these genes was also partially or fully restored to wild-type levels in the ATE1 rescue line. Together, this data indicates that the arginylation branch of the N-degron pathway, which relies on the activity of the Arg-transferases and PRT6, plays a role in the positive regulation of certain flg22-inducible genes.

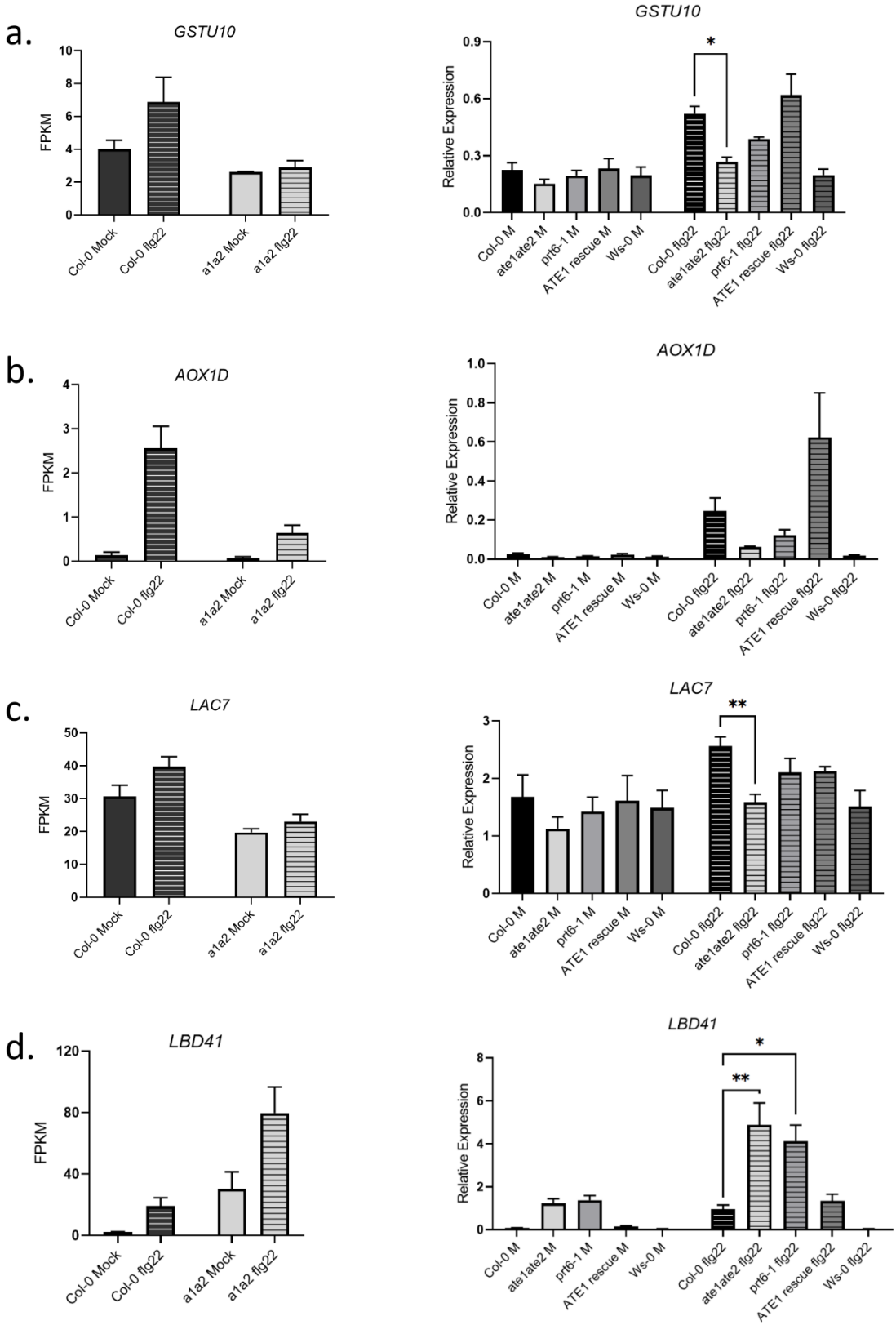

Figure 3.10. N-degron pathway regulation of flg22-inducible genes. Left = FPKM values from RNA-Seq. Right = Relative expression of flg22-inducible genes detected by RT-qPCR. Error bars represent SEM values. Asterisks denote statistical significance determined by one-way ANOVA comparisons with Col-0 flg22 control group (* = $p \leq 0.05$, ** = $p \leq 0.01$). Ws-0 is included as a flg22 insensitive control.

In contrast, RNA-Seq revealed *LBD41* as a flg22-inducible gene that is highly over-expressed in the *ate1ate2* mutant (Fig. 3.7b). RT-qPCR analysis supported the assertion that this gene is induced by flg22 and is negatively regulated by the N-degron pathway (Fig. 3.10d). Notably, *LBD41* has been previously implicated in the hypoxia response (Licausi *et al.*, 2010). Indeed, 5 out of 10 flg22-responsive genes with increased expression in the *ate1ate2* mutant (Fig 3.7b) were previously identified as members of an anaerobic cluster (*LBD41*, *HRA1*, *Hb1, HRE2*, *WIP5*) regulated by the ERF-VII transcription factors (Licausi *et al.*, 2010). This finding suggests that the N-degron pathway's regulation of hypoxia responses via the ERF-VIIs may contribute to its roles in immunity.

3.2.6 The N-degron pathway regulates flg22-responsive genes during pathogen infection

To investigate whether the regulation of flg22-responsive genes by the N-degron pathway is relevant in the context of plant-pathogen interactions, RT-qPCRs were conducted on Col-0 and *ate1ate2* mutant plants following infection with the model pathogen *Pst* DC3000 carrying the AvrRpm1 effector (Fig. 3.11). AvrRpm1 suppresses PTI but is perceived by the *Arabidopsis thaliana* receptor RPM1, leading to the onset of ETI (Mackey *et al.*, 2002; Kim *et al.*, 2005; section 1.3.3).

The expression of two genes with reduced expression in *ate1ate2* compared to wild-type after flg22 treatment (*AOX1D* and *LAC7*), and two genes with elevated expression in *ate1ate2* (*LBD41* and *bHLH093*) (Fig. 3.7b) was monitored over a 24-hour time course following infection with *Pst* AvrRpm1. Similarly to the results obtained after flg22 elicitation, *AOX1D* and *LAC7* showed a lower induction in the *ate1ate2* mutant compared to wild type plants after *Pst* inoculation (Fig. 3.11). In contrast, *bHLH093* and *LBD41* were more strongly induced in *ate1ate2* compared to the wild type (Fig. 3.11), again in agreement with the data obtained after flg22 exposure. *Arabidopsis bHLH093* encodes a basic helix-loop-helix transcription factor that has been previously implicated in gibberellin biosynthesis (Poirier *et al.*, 2018), but has not been implicated in immunity previously. However, *bHLH093* from *Nicotiana benthamiana* has recently been shown to interact with the RipI effector from *Ralstonia solanacearum* to induce host defences (Zhuo *et al.*, 2020).

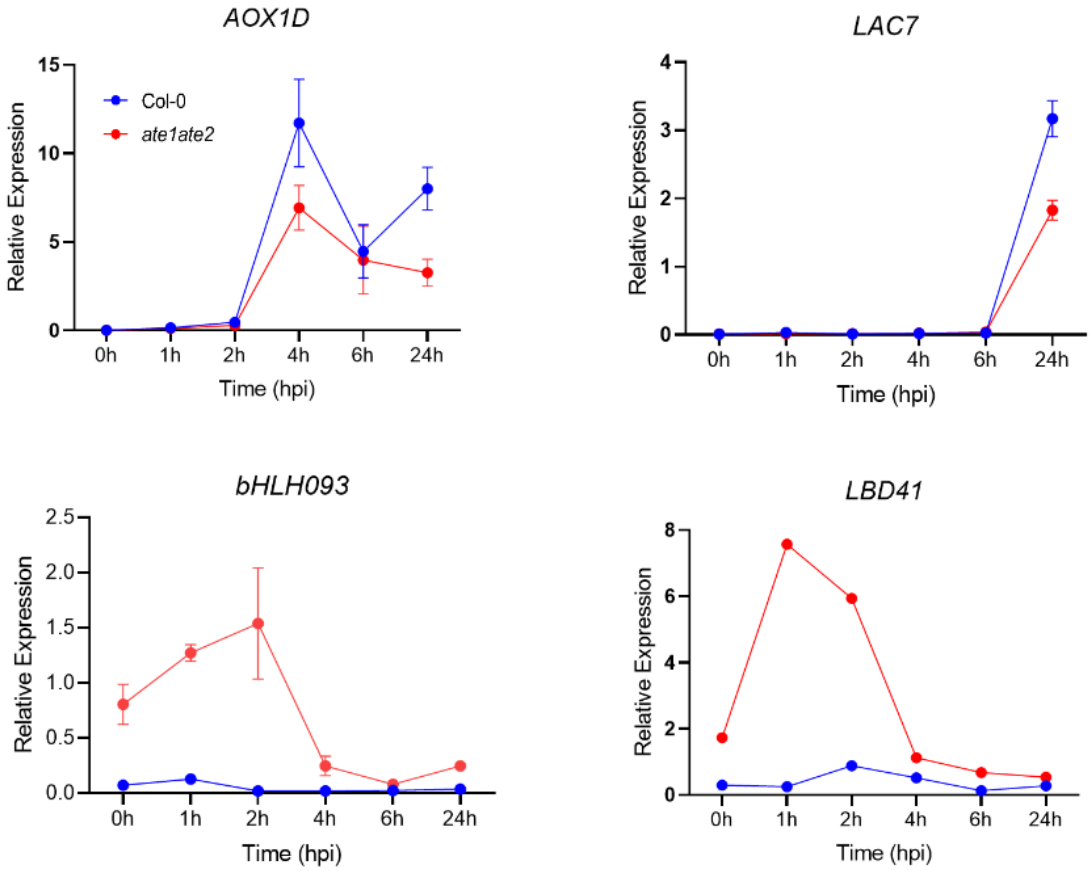

Figure 3.11. N-degron pathway regulation of flg22-responsive genes during *Pst* AvrRpm1 infection. RT-qPCR analysis of gene expression during 24 hours of infection with *Pst* DC3000 AvrRpm1 (5×10^7 cfu/m) in 4-week-old Col-0 and *ate1ate2* plants. Points represent means with SEM error bars. Three independent replicates are shown for *AOX1D*, 2 replicates for *LAC7* / *bHLH093* and one replicate for *LBD41*. 'hpi' = hours post inoculation.

3.2.7 Genetic basis of N-degron pathway regulation of immune genes

To investigate the molecular mechanisms underpinning N-degron pathway mediated regulation of transcriptional changes during PTI, I examined the expression of selected genes of interest in the *prt6-1 erfVII* sextuple mutant (Abbas *et al.*, 2015) after flg22 treatment (Fig. 3.12). In addition to the T-DNA insertion in *PRT6*, this line contains mutations in the five ERF-VII transcription factors (*RAP2.2*, *RAP2.3*, *RAP2.12*, *HRE1* and *HRE2*), which are known substrates of the Arg/N-degron pathway. The expression of three flg22-responsive genes overexpressed in N-degron pathway mutants, *HRA1*, *LBD41* and *bHLH093,* (Figs. 3.7b, 3.10, 3.11) was restored to wild-type levels in the *prt6 erfVII* line, while *AOX1D* showed increased

expression in the *prt6 erfVII* mutant (Fig. 3.12). This data indicates that the misregulation of some flg22-responsive genes in N-degron pathway mutants is a consequence of the stabilization of ERF-VII transcription factors, likely, in some cases, as a result of their additional involvement in the hypoxia response (e.g. *HRA1* and *LBD41*) (Licausi *et al.*, 2010).

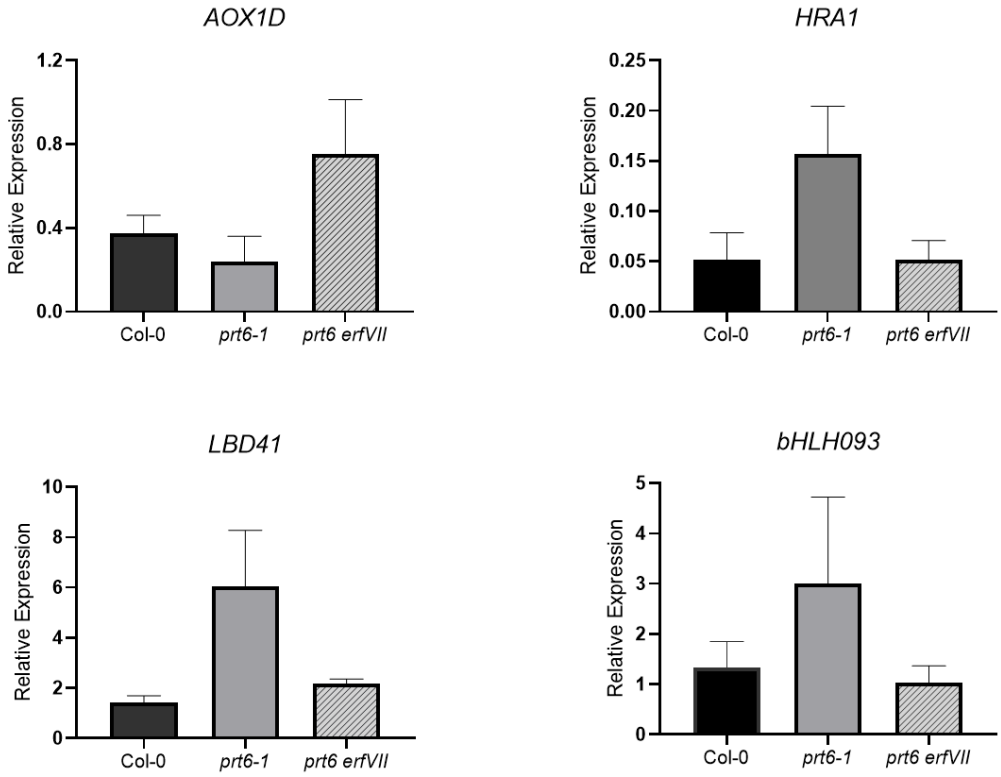

Figure 3.12. N-degron pathway regulation of immune genes can be ERF-VII dependent. Expression of N-degron pathway regulated PTI-responsive genes in *prt6-1* and *prt6 erfVII* mutants compared to wild-type seedlings after treatment with 1 µM flg22 for 1 hour. Columns represent means of 2 independent replicates consisting of 10 individual seedlings each + SEM error bars.

3.3 The N-degron pathway may regulate flg22-induced ROS

3.3.1 Introduction

Reactive oxygen species (ROS) are critical for the activation of immune responses (described in section 1.3.2.5). These highly reactive molecules, such as hydrogen peroxide and nitric oxide, directly exert anti-microbial effects and also serve as important secondary messengers to

regulate immune signaling pathways (Lee *et al.*, 2020). Several genes identified during the transcriptomic analysis as misregulated in N-degron pathway mutants versus wild-type after flg22-treatment have been implicated in ROS homeostasis, e.g. *AOX1D* (Strodtkötter *et al.*, 2009) and *GSTU10* (Gullner *et al.*, 2018). Additionally, the N-degron pathway substrate and ERF-VII transcription factor RAP2.12 has been previously shown to positively regulate the expression of *RBOHD* – the primary source of apoplastic ROS produced during PTI (Licausi *et al.*, 2010; Yao *et al.*, 2017; Lee *et al.*, 2020). Consequently, I sought to investigate whether the production of flg22-induced ROS was altered in *ate1ate2* plants. PAMP-induced ROS can be detected using a luminol-based approach (Smith & Heese, 2014) (section 2.2.5.3). Briefly, extracellular ROS generated in response to an immune stimulus triggers the oxidation of luminol catalysed by horseradish peroxidase included in the reaction mixture. Oxidised luminol emits a chemiluminescent signal which can then be quantified using a luminometer or microplate reader.

3.3.2 ROS production in *ate1ate2*

ROS produced by leaf discs taken from 4-week-old Col-0, *ate1ate2* and ATE1-rescue plants treated with 100 nM flg22 were measured every 2 minutes for 1 hour. In each genotype, ROS production peaked at 14 minutes after the addition of flg22 to the medium, consistent with previous reported peaks at 10-15 minutes after flg22 elicitation (Boutrot *et al.*, 2010; Smith & Heese, 2014). PTI-induced ROS production appears to be diminished in the *ate1ate2* mutant compared with Col-0 and ATE1-rescue plants. This is particularly evident between 12-22 minutes (Fig. 3.13a). Peak ROS production values (measured at 14 minutes) were significantly reduced in *ate1ate2* compared to the ATE1-rescue ($p = 0.0001$) as determined by Welch's t-test (Fig. 3.13b). The difference between peak ROS in Col-0 and *ate1ate2* plants was marginally outside the threshold of statistical significance ($p = 0.099$). However, overall the data appears to suggest that *ATE1/2* and the N-degron pathway may positively regulate PTI-induced ROS.

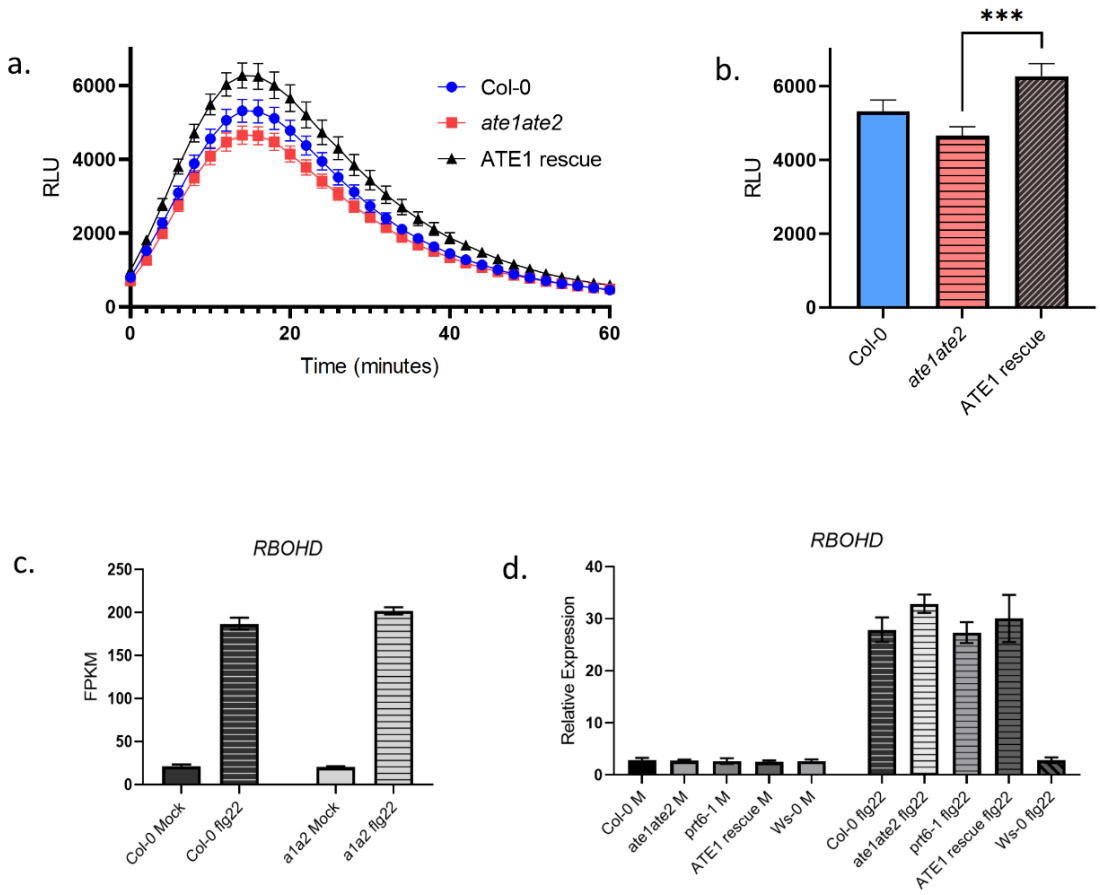

Figure 3.13. ROS production in *ate1ate2* mutant. a. XY plot showing ROS production in 4-week-old Col-0, *ate1ate2* and ATE1-rescue plants after elicitation with 100 nM flg22. ROS were detected every 2 minutes for 1 hour using a luminol-based assay. Col-0 and *ate1ate2* points each represent mean values of 192 readings (leaf-disc quarters) taken from 48 leaf discs over 8 independent replicates. ATE1-rescue points represent means of 120 readings from 30 leaf discs over 4 independent replicates. Error bars indicate SEM at each timepoint. RLU = Relative Light Units. **b.** RLU detected at 14 minutes (peak ROS production). Data is taken from 14-minute timepoint shown in Fig. 3.9a. Error bars indicate SEM. Asterisks indicate statistically significant difference detected after Welch's t-test ($p = 0.001$). **c.** FPKM values indicating mean *RBOHD* transcript abundance as detected by RNA-Seq in Col-0 and *ate1ate2* (a1a2) seedlings after mock and flg22 treatment. **d.** Results of RT-qPCR experiments indicating relative expression of *RBOHD* in N-degron pathway seedlings and Ws-0 +/- 1 µM flg22 treatment for 1 hour. Data indicates means of 3 independent replicates. Error bars indicate SEM. Differences between Col-0, *ate1ate2*, *prt6-1* and ATE1-rescue lines are not statistically significant.

Apoplastic ROS generated during immunity are chiefly produced by the NADPH oxidase RBOHD (Qi *et al.*, 2017; section 1.3.2.5). Due to its central importance, the activity of RBOHD is

tightly regulated at both the transcriptional and post-translational levels. Notably, the RNA-Seq experiment did not detect significantly altered expression of the *RBOHD* transcript in *ate1ate2* seedlings compared to wild-type before or after flg22 treatment (Fig 3.13c). Furthermore, RT-qPCR analysis indicated that expression of *RBOHD* was not significantly altered in *prt6-1* or the ATE1 rescue line compared to wild-type plants (Fig. 3.9d). Therefore, it appears unlikely that transcriptional repression of *RBOHD* is responsible for any of ROS production phenotypes observed here (although it should be noted that the ROS measurements are carried out using 4-week-old plants versus the seedlings used in the transcriptomics experiments). The absence of any significant overexpression of *RBOHD* in *ate1ate2* and *prt6-1* is also noteworthy, in light of previous reports that this transcript is positively regulated by the ERF-VII transcription factor RAP2.12, which is expected to be stabilized in N-degron pathway mutants (Licausi et al., 2010; Yao et al., 2017).

To investigate mechanisms underlying the proposed role of the N-degron pathway in the regulation of ROS production, I generated higher-order mutant lines combining *ate1ate2* with mutations in two established post-translational regulators of RBOHD – *CPK5* (a positive regulator) and *CPK28* (a negative regulator). Genotyping assays from these crosses are shown in Fig. A1 (Appendix A).

CPK5 (CALCIUM-DEPENDENT PROTEIN KINASE-5) has been previously identified as a positive regulator of ROS production and acts by directly phosphorylating serine residues in RBOHD upon flg22 treatment (Dubiella *et al.*, 2013). The same study revealed that the *cpk5-1* mutant line accumulates less ROS than wild-type plants after elicitation with 200 nM flg22, although no statistical significance was indicated in this case (Dubiella *et al.*, 2013).

By contrast, CPK28 (CALCIUM-DEPENDENT PROTEIN KINASE-28) functions as a negative regulator of the PTI-induced ROS burst (Monaghan *et al.*, 2014). Specifically, CPK28 phosphorylates BIK1, prompting its turnover (Monaghan *et al.*, 2014). As BIK1 positively regulates RBOHD via phosphorylation (Fig. 1.4), CPK28 effectively inhibits the PTI-associated ROS burst indirectly. Consistent with this, the *cpk28-1* mutant line was also shown previously to exhibit an enhanced ROS burst in response to treatment with 100 nM flg22 (Monaghan *et al.*, 2014).

Here, I generated *ate1ate2 cpk5-1* and *ate1ate2 cpk28-1* triple mutants and measured the PTI-induced ROS burst as described earlier following treatment with 100 nM flg22. I also generated an *ate1ate2 rbohd* triple mutant, to investigate any potential direct genetic interaction between *RBOHD* and *ATE1* / *ATE2*. The ROS burst of the single mutant parental lines was also measured in these assays.

The *rbohd* and *ate1ate2 rbohd* lines exhibited almost complete elimination of flg22-induced ROS (Figs. 3.14a & 3.14d), strongly indicating that the ROS being detected in these experimental conditions are almost entirely produced by the NADPH oxidase activity of RBOHD, consistent with previous reports.

As mentioned above, the *cpk5-1* line has been reported to produce less ROS than wild-type plants in response to 200 nM flg22 (Dubiella *et al.*, 2013). Here, in the presence of 100 nM flg22, the *cpk5-1* line showed only marginally lower ROS production than Col-0 (Figs. 3.14b & 3.14d). The *ate1ate2 cpk5-1* triple mutant showed a more robust reduction in ROS accumulation compared to Col-0, and lower than either of the parental lines. This phenotype reflects an additive genetic effect of the *ate1ate2* and *cpk5-1* mutations and suggests that the mechanisms underlying potential positive regulatory roles of *CPK5* and *ATE1/2* are likely independent.

The *cpk28-1* mutant has been reported previously to display an enhanced ROS burst (Monaghan *et al.*, 2013). The *cpk28-1* mutant also displayed increased ROS production in the experimental conditions employed here (Figs. 3.14c & 3.14d). Strikingly, the *ate1ate2 cpk28-1* triple mutant obscured the diminished ROS phenotype of the *ate1ate2* parent and in fact displayed an elevated ROS production compared to Col-0 and the *cpk28-1* single mutant parent (Figs. 3.14c & 3.14d). The impact of the *ate1ate2* mutations on plants also harbouring the *cpk28-1* mutation is particularly notable as it stands in contrast to effect observed in either the Col-0 or *cpk5-1* genetic backgrounds. This epistatic effect may indicate a genetic interaction between *CPK28* and *ATE1/ATE2* (this is discussed in more detail in section 3.8.2).

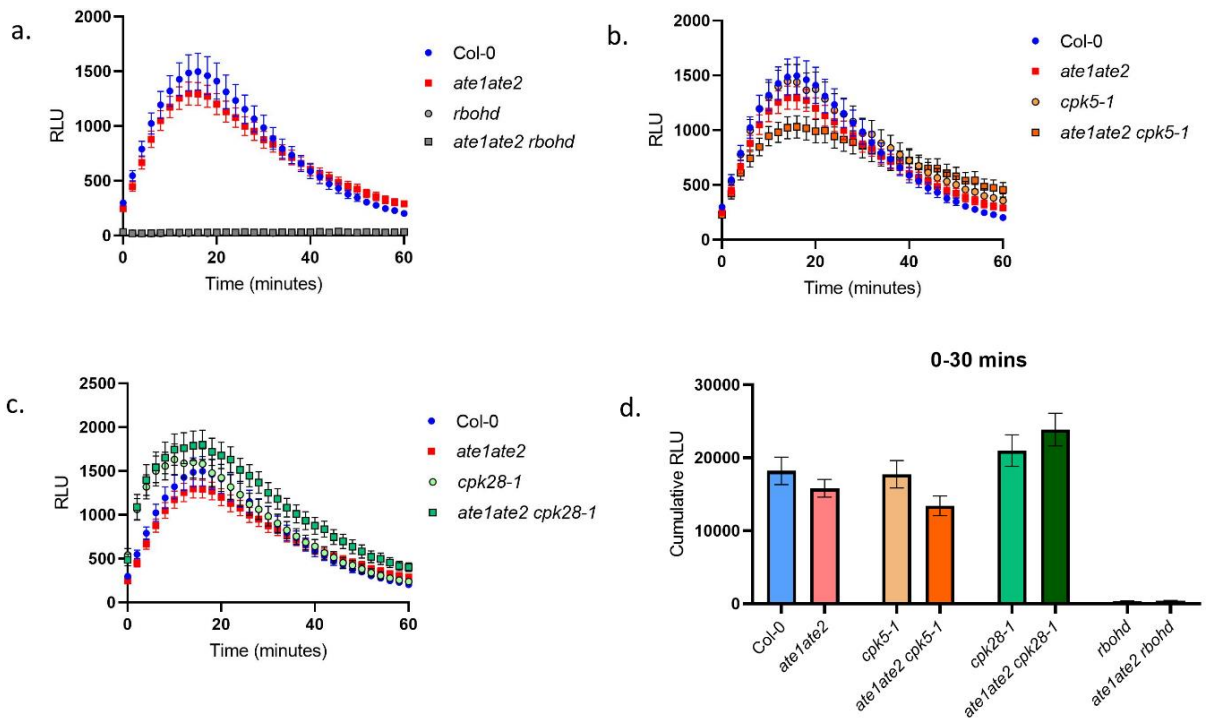

Figure 3.14. ROS production in higher-order mutants. a-c. ROS production in 4-week-old plants up to 60 minutes after elicitation with 100 nM flg22. Genotypes are presented separately for visibility, except for Col-0 and *ate1ate2* which are presented on each graph to facilitate comparison. Each datapoint represents mean value +/- SEM. For Col-0, *ate1ate2*, *cpk28-1* and *ate1ate2 cpk28-1*, n = 48 wells from 12 leaf disks over 3 independent replicates; *cpk5-1* and *ate1ate2 cpk5-1*, n = 32 wells from 8 disks over 2 independent replicates; *rbohd* and *ate1ate2 rbohd* = 16 wells from 4 disks from a single replicate. **d.** Column chart of cumulative RLU representing the sum of ROS production from 0-30 minutes shown in a-c. Mean values +/- SEM error bars are shown.

3.4 Other features of PTI in N-degron pathway mutants

3.4.1 Flg22-induced growth inhibition

Flg22 treatment of seedlings induces a pronounced growth inhibition due to the diversion of cellular resources towards immunity and away from development (see section 1.3.2.9; Gomez-Gomez *et al.*, 1999). This phenomenon is sometimes referred to as the growth-defence trade-off (Figueroa-Macías *et al.*, 2021). Seedlings of Col-0, *ate1ate2*, *prt6-1* and the flagellin-insensitive Ws-0 were grown in the presence of 100 nM flg22 or mock solution (dH_2O). Growth

inhibition was assessed by measuring the mass of flg22-treated seedlings relative to mock-treated seedlings (Fig. 3.15).

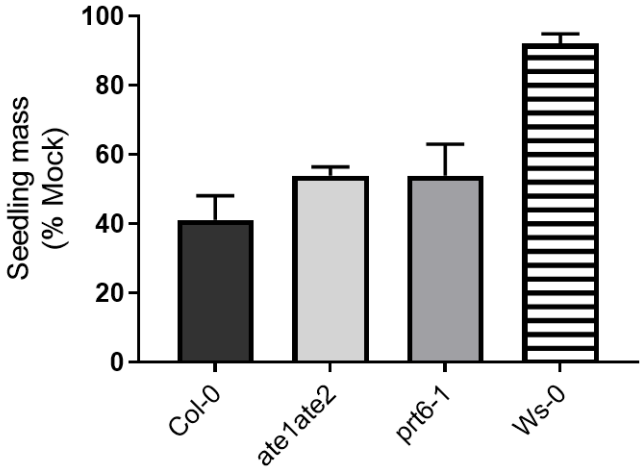

Figure 3.15. Flg22-induced growth inhibition in seedlings. Seedlings were grown for 4 days on agar plates before transfer to liquid media containing 100 nM flg22 or mock solution (dH_2O) for a further 4 days of growth. Columns indicate means +/- SEM of 3 independent replicates with the masses of 8 seedlings measured per replicate (n=24). No significant differences were observed between genotypes after mock-treatment.

Col-0 seedlings treated with flg22 grew to just 41% of the mass of mock-treated seedlings (Fig. 3.15). Meanwhile, flg22-treatment of *ate1ate2* and *prt6-1* seedlings resulted in 54% growth relative to the respective mock-treated seedlings. These differences suggest a reduction in the amplitude of general PAMP-responsiveness in N-degron pathway mutants. As expected, flg22-treatment had a negligible effect on growth of Ws-0 seedlings (92% mass relative to mock). This phenotype is indicative of a mild but consistently impaired PTI signaling in the N-degron pathway mutants, similar to prior observations concerning the misregulation of PTI-responsive genes and flg22-induced ROS production.

3.4.2 MAPK phosphorylation

Mitogen-activated protein kinase (MAPK) cascades are rapidly activated in response to flg22 treatment, typically peaking 15 minutes after elicitation (see section 1.3.2.6; Meng & Zhang, 2013). Nine-day-old seedlings of Col-0 and various N-degron pathway mutants were treated with 1 µM flg22 for 15 minutes and protein extracts were probed with a rabbit antibody that detects phosphorylated MAPKs.

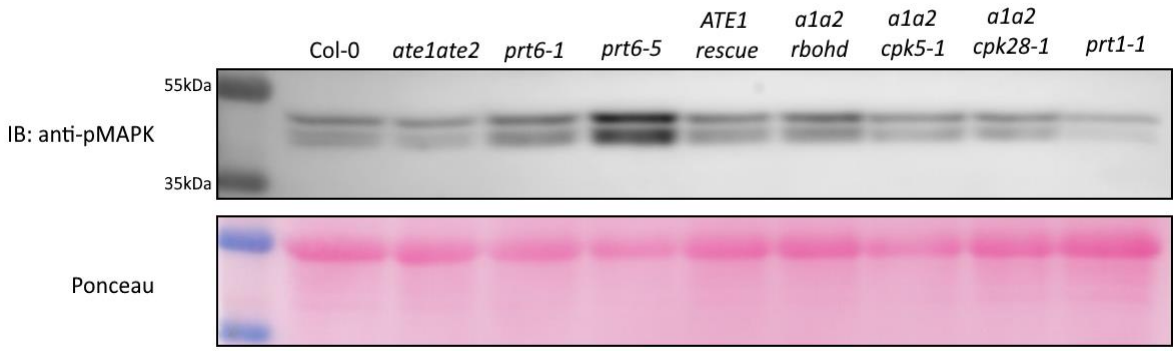

Figure 3.16. Flg22-induced MAPK phosphorylation in N-degron pathway mutants. Seedlings were treated with 1 µM flg22 for 15 minutes. 50 µg of protein extract from each genotype was loaded. Phosphorylated MAPK proteins were detected with 1:1,000 dilution of anti-Phospho-p44/42 MAPK antibody. Ponceau staining of PVDF membrane indicates equal protein transfer. The full images are included in Fig. A3 (Appendix A). This immunoblot was repeated with mostly similar results (Fig. A4).

Phosphorylated MPK6 (upper band) and MPK3 (lower band) were detected in each sample (Fig. 3.16). No obvious differences were detected between Col-0, *ate1ate2* or *prt6-1* seedlings. Notably, *prt6-5* displayed enhanced MAPK cascade activation compared with Col-0 and *prt6-1.* Both *prt6-1* and *prt6-5* are null alleles of *PRT6* and have been considered functionally interchangeable so far (Zhang *et al.*, 2018). However, previous reports have also described conflicting susceptibility / resistance phenotypes in response to *P. syringae* in each of these lines (De Marchi *et al.*, 2016; Vicente *et al.*, 2019). The ATE1 rescue line exhibited a slightly elevated MAPK activation signal compared with the *ate1ate2* mutant in replicate immunoblots (Figs. 3.16 and A4 – Appendix A). Overall, the Arg/N-degron pathway does not appear to function as a major regulator of flg22-induced MAPK activation, indicating that its contribution

to the regulation of PTI occurs independently (or downstream) of this cascade. Consistent differences in the levels of MAPK phosphorylation were not evident in the cases of the higher-order mutants (i.e. *ate1ate2 rbohd*, *ate1ate2 cpk28-1* and *ate1ate2 cpk5-1*) or the *prt1-1* mutant, (deficient in the PRT1 branch of the N-degron pathway) across both replicate experiments (Figs 3.16 and A4 – Appendix A).

3.4.3 Infection with *Pst* after PTI induction

Another key indicator of the strength of an induced PTI response is the increased pathogen resistance conferred by pre-treatment with a PAMP (Winkelmuller *et al.*, 2021). For example, growth of *P. syringae* is dramatically reduced on plants that have been exposed to flg22 prior to bacterial inoculation (Zipfel *et al.*, 2004; Winkelmuller *et al.*, 2021). To investigate whether the N-degron pathway contributes to the regulation of this phenomenon, I tested the flg22-induced resistance against the model pathogen *Pst* DC3000 in Col-0, *ate1ate2* and ATE1 rescue plants (Fig. 3.17).

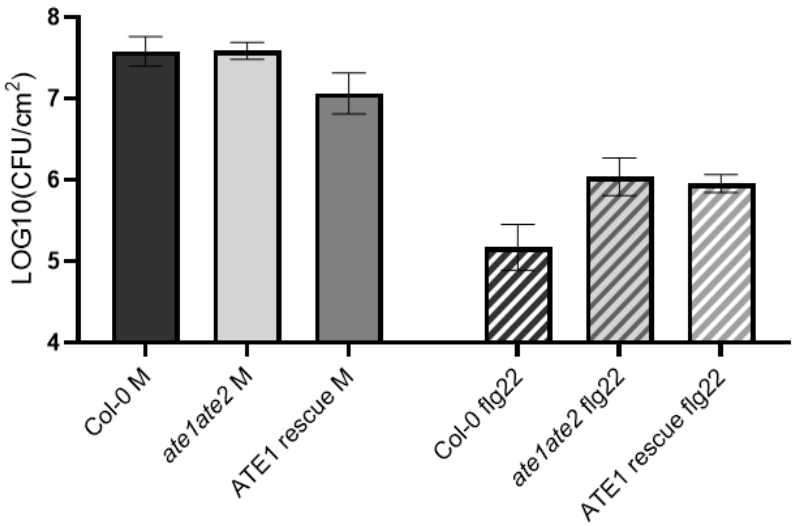

Figure 3.17. Flg22-induced resistance to *Pst* DC3000. Growth of *Pst* DC3000 on Col-0, *ate1ate2* and ATE1-rescue plants following pre-treatment with 1 µM flg22 or a dH_2O (mock) 24h prior to inoculation. Columns represent means +/- SEM from 3 plants per genotype per treatment from a single experiment. CFU = colony forming units. Bacterial counts from each genotype after the respective treatments were compared using ANOVA and no statistically significant differences were identified.

Pst DC3000 proliferated to similar levels in Col-0 and *ate1ate2* plants subjected to pre-treatment with dH_2O (mock), while the ATE1 rescue line appeared to be more resistant (Fig. 3.17). Consistent with previous reports, pre-treatment with 1µM flg22 24 hours prior to inoculation led to a considerable increase in resistance to *Pst* across all genotypes. However, this resistance was less pronounced in *ate1ate2* and the ATE1 rescue line compared to Col-0. Considering the preliminary nature of this data (only one biological replicate was carried out), it is not possible to draw meaningful conclusions.

3.5 The response of *ate1ate2* to *Pst* DC3000 is age-dependent

As described earlier, there have been conflicting reports regarding the contribution of the N-degron pathway to the regulation of the immune response to *P. syringae* (see section 1.3.4) and one aim of the present study was to address this. Specifically, de Marchi *et al.* (2016) observed that *ate1ate2* mutants are more susceptible to infection caused by *Pst* DC3000, while Vicente *et al.* (2019) found that *prt6-1* plants are more resistant to this pathogen. Detailed comparison of the methods used in each of these studies revealed several key experimental differences that may contribute to this disparity. These included varied growth conditions (e.g. 9 hour vs. 12 hour light cycles respectively), bacterial density of the inoculum (5×10^5 or 10^6 cfu/mL) and age of the plants at the time of inoculation (4 weeks or 3 weeks post-germination). Plant age in particular has long been considered a critical factor in determining resistance to disease (Griffey and Leach, 1965; Kus *et al.*, 2002; Hu and Yang, 2019). In general, plants become increasingly resistant to pathogens as they mature due to a phenomenon known as 'age-related resistance' or ARR (Kus *et al.*, 2002) To investigate whether plant age could influence the roles of the N-degron pathway in plant immunity, I evaluated ARR in *ate1ate2.*

Col-0 and *ate1ate2* plants at 3.5 and 4 weeks old were simultaneously inoculated with the same inoculum of *Pst* DC3000, and bacterial growth was quantified 3 days post-inoculation (dpi) (Fig. 3.18). Despite this seemingly minor difference in plant age, a statistically significant increase in resistance was visible in 4-week-old wild-type plants ($p = 0.0486$). By contrast, no ARR was detected in the *ate1ate2* mutant. Interestingly, direct comparison of *ate1ate2* plants to wild-type plants revealed a mild resistance phenotype at 3.5 weeks (mean $\log_{10}(cfu/cm^2)$ = 6.34 for *ate1ate2* vs. 6.72 for Col-0) and a mild susceptibility phenotype at 4 weeks (mean

$log_{10}(cfu/cm^2)$ = 6.48 for *ate1ate2* vs. 6.21 for Col-0). In this case, these differences between genotypes were not statistically significant. Nevertheless, this data suggests that the N-degron pathway plays particular roles in the regulation of immune responses depending on plant age and may partially explain the different outcomes described by de Marchi *et al* (2016) and Vicente *et al*. (2019). Notably, the activity of ERF-VII transcription factors is reduced as plants age, although this change appears to occur via an N-degron pathway independent mechanism (Giuntoli *et al*., 2017). An open question would be whether the age-dependent regulation of ERF-VII activity could contribute to the age-dependent nature of the susceptibility phenotype of *ate1ate2*, potentially as the relative impact of non-ERF-VII substrates may become increasingly prominent.

Further experiments will be required to understand these processes in greater detail. For example, could the N-degron pathway be directly involved in the activation of ARR? To date, there have been no explicit links between N-degron pathway components and genes specifically implicated in ARR. Potential developmental regulation of the roles of the N-degron pathway in PTI outlined here may also be of interest to future studies. For example, is the positive regulation of ROS production by ATE1/2 at 4 weeks old (Fig. 3.13) also present in younger plants? Interestingly, *ate1ate2* exhibits general defects in development, including delayed leaf senescence (Yoshida *et al*., 2002; Graciet *et al*., 2009). Therefore, it could be considered that an accumulation of secondary effects arising from problems with the development of *ate1ate2* could contribute to increasingly dysfunctional immune responses as the plants age. Another possibility is that ARR may itself be specifically 'delayed' in N-degron pathway mutants. To this end, future experiments incorporating a wider range of developmental stages could determine whether ARR is indeed absent or merely delayed in *ate1ate2*. In either case, the apparent age-dependency of the disease-susceptibility phenotype of an N-degron pathway mutant may help to resolve previous conflicting observations.

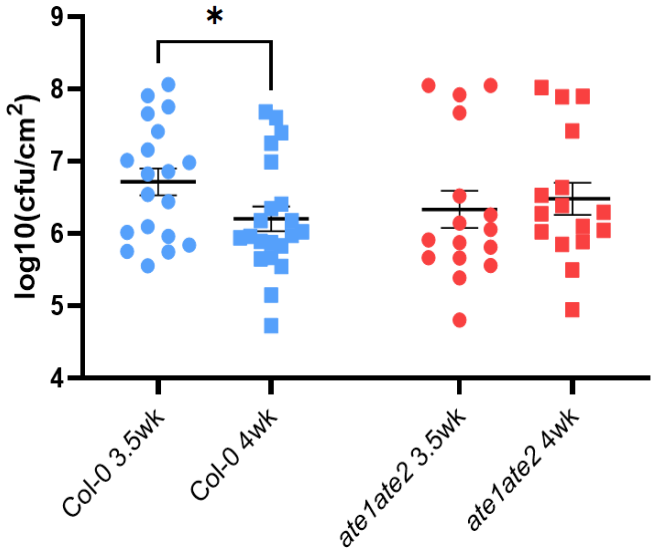

Figure 3.18. The N-degron pathway regulates ARR. *Pst* DC3000 growth 3 days post inoculation in 3.5 or 4-week old Col-0 and *ate1ate2* plants. Each datapoint represent bacterial growth from a single plant, with 3 leaves inoculated per plant (n > 16 for each group, with data from 4 independent experiments). Means +/- SEM are indicated. Asterisk indicates statistically significant difference after t-test ($p<0.05$). Cfu/cm^2 refers to bacterial colony forming units per unit area of leaf tissue. See Fig. A5 in Appendix A for images of infected plants.

3.6 BIG contributes to the Arg/N-degron pathway

As understanding of the physiological roles of the N-degron pathway continues to improve, an important avenue demanding further investigation concerns the potential identification of novel N-degron pathway components and/or co-factors. Candidate N-degron pathway components could be identified based on the presence of structural features that may indicate N-degron pathway related functions. For example, the 567 kDa *Arabidopsis* protein BIG (AT3G02260) contains a UBR domain which is characteristic of N-recognins like PRT1 and PRT6 (Kim *et al.*, 2021). BIG has previously been implicated in multiple biological processes including a range of hormone and light responses (Kanyuka *et al.*, 2003) as well as auxin-mediated organ growth (Guo *et al.*, 2013), but direct evidence of its role in the N-degron pathway has remained elusive. Previous researchers in my host laboratory have generated reagents to investigate whether BIG contributes to the N-degron pathway (Walter, 2010; Miricescu, 2019). Here, I tested whether the absence of BIG in a wild-type or *prt6-5* mutant background leads to an

enhanced accumulation of a model N-degron pathway substrate – a LUCIFERASE reporter protein containing an N-terminal arginine residue (Fig. 3.19a).

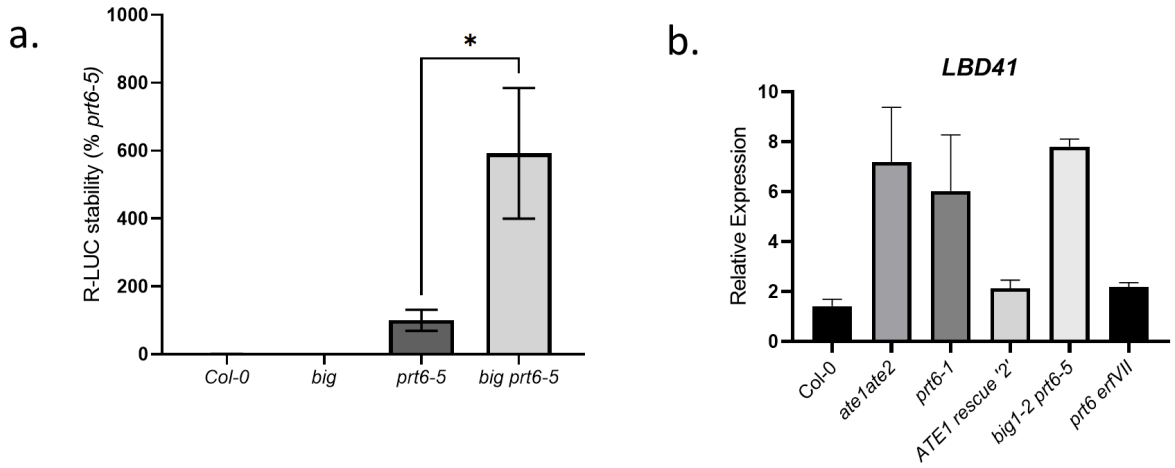

Fig. 3.19. BIG and PRT6 co-operate to degrade N-terminal Arg. a. 7-day-old seedlings of Col-0, *big*, *prt6-5* and *big prt6-5* were harvested. To calculate Arg-LUC stability, Arg-LUC enzymatic activity was determined and normalized to relative expression of the *LUC* gene (RT-qPCR). Columns indicate means +/- SEM of 4 independent replicates expressed as a percentage of *prt6-5*. Asterisk indicates significant difference after one-way ANOVA (p = 0.0175). **b.** Relative expression of *LBD41* in seedlings after treatment with 1 µM flg22 for 1 hour. Columns indicate means +/- SEM from 2 independent replicates.

As expected, the *prt6-5* mutant exhibited strong stabilization of the Arg-LUC protein compared with Col-0, while no Arg-LUC stabilization was observed in the *big* single mutant. This data indicates that BIG is not required for the almost complete degradation of Arg-LUC when PRT6 is present. However, the *big prt6-5* double mutant exhibited a substantial >5-fold increase in the stability of Arg-LUC (Fig. 3.19a) compared to the *prt6-5* parental line. This implies that BIG contributes to the destabilization of N-terminal Arg in the absence of PRT6. Further experiments are required to explore the mechanisms underlying this observation, for example the potential physical interactions of BIG with PRT6 or Nt-Arg substrates. Notably, the *big prt6-5* double mutant did not display enhanced expression of the N-degron pathway regulated flg22-inducible gene *LBD41* when compared to the *prt6-5* single mutant (Fig. 3.19b). However, whether a putative interaction of the known repertoire of N-degron pathway

components with BIG or other as-yet-unidentified proteins could influence other immune phenotypes detailed here remains to be determined.

3.7 The roles of the PRT1 N-degron pathway in PTI

The PRT1 N-degron pathway targets peptides bearing the aromatic residues Phe, Trp and Tyr at the N-terminus (Fig.1.2). As described earlier in section 1.3.4, various roles for the PRT1 N-degron pathway in plant immunity have been described, primarily through phenotypic characterisation of the *prt1-1* mutant. De Marchi *et al.* (2016) observed increased susceptibility of *prt1-1* to multiple pathogens including *Pst* DC3000. By contrast, Till *et al.* (2019) described increased resistance of *prt1-1* to *Pst* DC3000, and this was attributed to an increased abundance of immunity-related proteins. Here, the response of *prt1-1* to flg22 was assessed to investigate whether PRT1 or its substrates may play a role in the regulation of PTI.

An RT-qPCR time-course experiment was conducted assessing the response of *prt1-1* mutants to treatment with flg22 (Fig. 3.20a). Strong induction of the flg22-PTI associated genes *FLS2* and *FRK1* was observed in both genotypes. At their respective peak levels of expression, *FLS2* expression was slightly lower in *prt1-1* compared to wild-type seedlings, while *FRK1* (FLG22-INDUCED RECEPTOR-LIKE KINASE 1) induction was slightly higher. However, these differences were not statistically significant. Detection of phosphorylated MAPKs after flg22 treatment revealed reduced activation of MPK3 and MPK6 in *prt1-1* (Fig. 3.20b). This may indicate impairment of flg22-PTI signaling in *prt1-1*, but as this data was obtained in a single experiment, additional replicates will be required before this can be concluded with certainty. Seedling growth inhibition triggered by flg22 was not impaired in *prt1-1* (Fig. 3.20c).

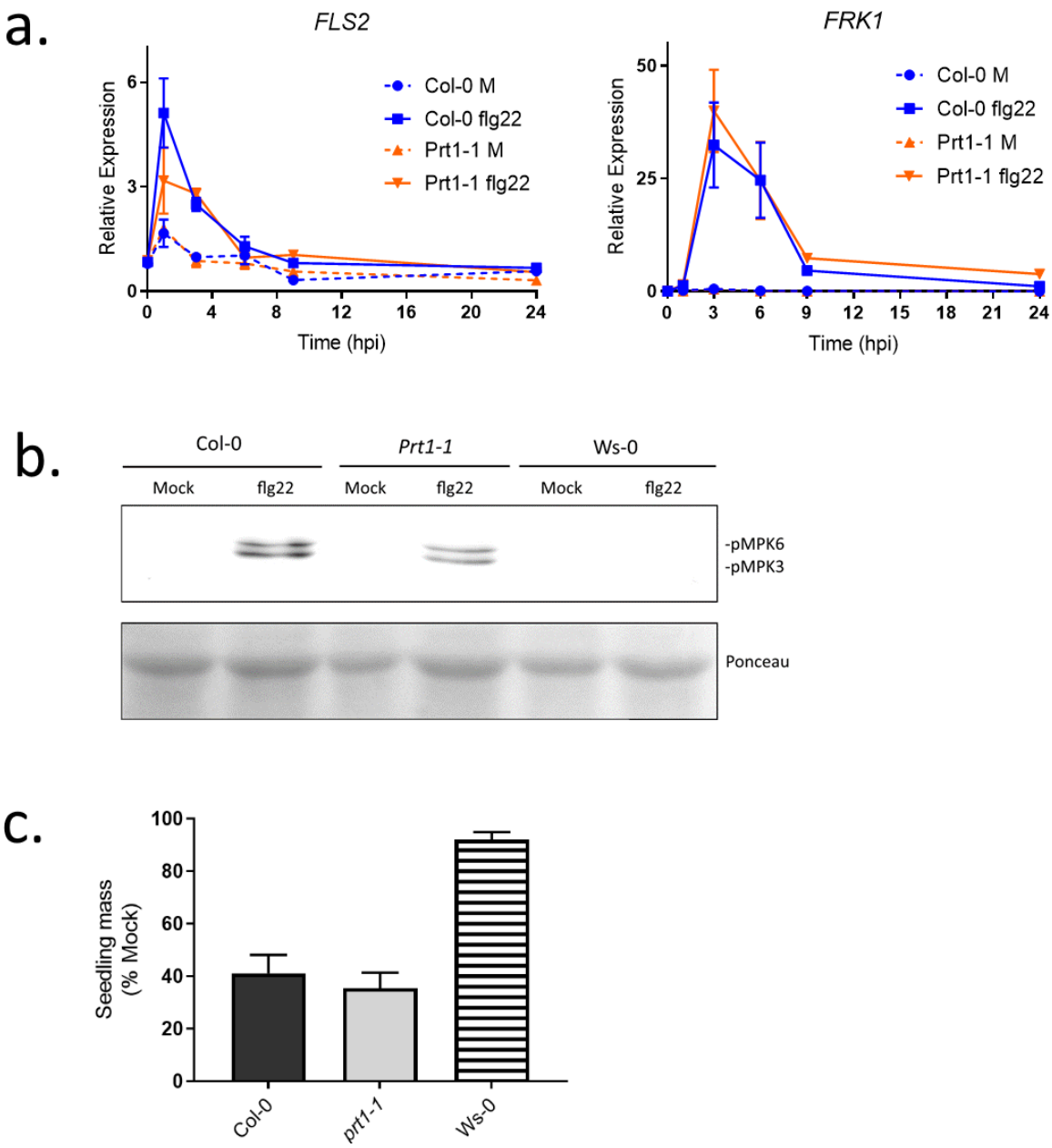

Figure 3.20. The flg22 response of *prt1-1*. a. RT-qPCR analysis of the relative expression of genes associated with flg22-PTI – *FLS2* and *FRK1* in wild-type and *prt1-1* mutant seedlings over a 24-hour time course after treatment with 1 µM flg22 or water (mock). Datapoints represent means of 3 replicates +/- SEM. Three replicates are shown for 0, 1, 3 and 6-hour timepoints, a single replicate is shown for the 9 and 24-hour timepoints. **b.** MAPK activation in Col-0, *prt1-1* and Ws-0 15 minutes after treatment with water or 1 µM flg22. Ponceau indicates equal loading (lower panel). Uncropped blot and Ponceau images are shown in Fig. A6 (Appendix A). **c.** Flg22-induced seedling growth inhibition in *prt1-1*. Seedlings were grown for 4 days on agar plates before transfer to liquid media containing 100 nM flg22 or mock solution (dH_2O) for a further 4 days of growth. Columns indicate means + SEM of 3 independent replicates with the masses of 8 seedlings measured per replicate (n=24). The data displayed for Col-0 and Ws-0 is also shown in Fig. 3.15.

The study by de Marchi *et al.* (2016) also described an increased susceptibility of *prt1-1* to the fungal pathogens *S. sclerotiorum* (necrotroph) and *E. cruciferarum* (a biotroph which causes powdery mildew). PTI can be triggered in response to fungal infection by the perception of chitin, a component of the fungal cell wall which is perceived by CERK1 and LYK5 (Kaku *et al.*, 2006; Miya *et al.*, 2007; Cao *et al.*, 2014; section 1.3.2.2). Chitosan is a water-soluble derivative of chitin, and elicits a very similar PTI response (Igarashi *et al*, 2013). The chitin-PTI marker genes *Chitinase* (AT2G43620) and *PR6* (AT2G38870) have been shown to be induced by chitosan (Igarashi *et al.*, 2013), and were assessed in the *prt1-1* mutant compared with wild-type plants over a 24-hour time course (Fig. 3.21). Interestingly, both genes showed a significantly reduced induction in *prt1-1* at the peak of expression at 3 hours post-elicitation with 100 µg/mL chitosan compared to Col-0 (Fig. 3.21).

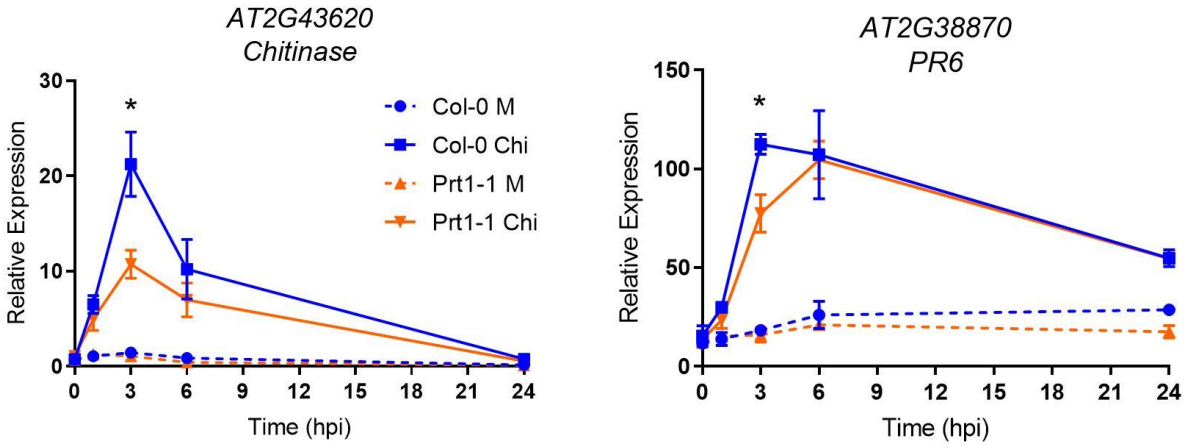

Figure. 3.21. Induction of chitosan-responsive genes in *prt1-1*. RT-qPCR analysis of the relative expression of chitin-PTI marker genes *Chitinase* and *PR6* in wild-type and *prt1-1* mutant seedlings over a 24-hour time course. Datapoints represent means of 3 replicates +/- SEM. Asterisks indicate statistical significance ($p \leq 0.05$) after t-test comparison of chitosan-treated *prt1-1* and Col-0 samples.

This finding suggests that PRT1 may contribute to chitin induced PTI signaling, which may correlate with the increased susceptibility of *prt1-1* to diverse fungal pathogens. Future experiments assessing other features of chitin-PTI in *prt1-1* (e.g. ROS production, MAPK cascade activation) could elucidate the molecular mechanisms underpinning this observation.

3.8 Discussion

3.8.1 The N-degron pathway regulates transcription during PTI

RNA-Seq analysis of the global transcriptomic changes in the *ate1ate2* mutant following flg22 treatment revealed the misregulation of numerous flg22-responsive genes. This includes the reduced induction of genes with previously established roles in immunity (e.g. *WRKY54*; Chen *et al.*, 2021) (Fig. 3.5) and several members of a recently described 'core immunity response' gene cluster (e.g. *ChiA;* Bjornson *et al.*, 2021) (Figs. 3.8 and 3.9). RT-qPCR experiments indicated that multiple differentially expressed genes of interest identified in the *ate1ate2* RNA-Seq experiment may also be misregulated in *prt6-1* and exhibited wild-type-like expression in an *ATE1* rescue line, strongly supporting that these genes are indeed regulated by the N-degron pathway (Figs. 3.9 and 3.10). Subsequent analysis of *ate1ate2* plants inoculated with a *P. syringae* DC3000 strain carrying the AvrRpm1 effector revealed that the misregulation of certain flg22-responsive genes remains relevant in the wider context of plant interactions with whole pathogens, including those that elicit ETI (Fig. 3.11). Notably, de Marchi *et al.* (2016) reported that *ate1ate2* is significantly more susceptible to *Pst* DC3000 AvrRpm1, which could correlate with the observed reduced induction of flg22-responsive genes. One avenue for further investigation is whether this susceptibility phenotype could be partly attributed to the misregulation of specific genes – for example, would the restored expression of *AOX1D* or knockout of *bHLH093* in the *ate1ate2* background enhance resistance to *P. syringae*?

At least some of the misregulation of PTI-responsive genes in N-degron pathway mutants appears to be a result of the stabilisation of ERF-VII transcription factors in these lines (Fig. 3.12; Gibbs *et al.*, 2011). Indeed, several of the ERF-VII regulated genes identified as flg22-responsive in this study have been specifically identified as members of a hypoxia-inducible gene cluster (e.g. *LBD41*, *HRA1*, *Hb1, HRE2*, *WIP5;* Licausi *et al.*, 2010; Fig. 3.7b). Hence, some genes appear to participate in the responses to both pathogen infection and hypoxia/flooding. Some perspectives on the common transcriptomic responses to these two seemingly distinct stresses include the increased likelihood that plants encounter pathogen attack while flooded (Hsu & Shi, 2013), and the recent findings that hypoxic niches may form during pathogen infection (Valeri *et al.*, 2021). The finding that some genes induced as an aspect of the flg22-response are negatively regulated by the ERF-VIIs (e.g. *AOX1D*; Fig. 3.12) may have implications

for efforts to develop flood-tolerant crops without compromising immunity. Resolving the specific target genes of the individual transcription factors of the ERF-VII group may be important to uncouple the regulation of hypoxia and immune responses.

Importantly, these experiments also highlighted that the N-degron pathway participates in both the positive and negative regulation of flg22-responsive genes. For example, the flg22-triggered induction of *LAC7* and *ChiA* appears to be reduced in *ate1ate2*, while *LBD41* was over-expressed (Figs. 3.9 & 3.10). The bilateral nature of the misregulation of immune genes in N-degron pathway mutants may contribute to the somewhat conflicting pathogen susceptibility / resistance phenotypes that have been described previously for these mutants (detailed in section 1.3.4; de Marchi *et al.*, 2016; Gravot *et al.*, 2016; Vicente *et al.*, 2018). In certain plant-pathogen species contexts, potential advantages conferred by the hyper-expression of some immune genes may outweigh the detrimental impacts arising from diminished expression of others, or *vice-versa*. Additionally, the impacts of hyper-expression of immunity-induced genes for disease susceptibility are not easily predictable. For example, the enhanced activation of hypoxia-associated genes in N-degron pathway mutants has been associated with increased virulence of *P. brassicae* (Gravot *et al.*, 2016). In this case, the targeting of components downstream of the N-degron pathway that regulate immune genes particularly relevant for specific pathogen interactions may be more fruitful for the genetic engineering of disease-resistant crops.

3.8.2 The N-degron pathway may regulate flg22-induced ROS

The PTI-induced ROS burst appears to be mildly diminished in *ate1ate2* mutants (Fig. 3.13a). Restoration of a functional *ATE1* to the *ate1ate2* genetic background leads to a significant increase in the peak ROS produced in response to flg22 (Fig. 3.13b). This data suggests that N-degron pathway component ATE1 (and likely ATE2 as well) may contribute to the positive regulation of ROS production during PTI. However, it should be noted that the observed differences between Col-0 and *ate1ate2* (Figs. 3.13a & 3.13b) were not statistically significant.

PTI-induced ROS are primarily generated by RBOHD (Lee *et al.*, 2020). Indeed, no observable ROS burst was detected after 100 nM flg22 treatment in an *rbohd* mutant line (Fig. 3.14a). However, it appears that the role of the N-degron pathway in the regulation of the PTI-induced

ROS burst is not due to altered transcription of *RBOHD* (Fig. 3.13c & 3.13d). This is particularly notable as the N-degron pathway substrate and ERF-VII transcription factor RAP2.12 positively regulates this gene (Licausi *et al.*, 2010; Yao *et al.*, 2017) (Fig. 3.22). The absence of *RBOHD* over-expression coupled with reduced ROS production in *ate1ate2* therefore suggests that another as-yet unidentified N-degron pathway substrate stabilized in this line may function oppositely as a negative regulator of RBOHD and the flg22-induced ROS burst.

As well as regulation at the transcriptional level, the PTI-induced ROS burst and the activity of RBOHD specifically are tightly regulated by post-translational modifications including phosphorylation and ubiquitylation (Lee *et al.*, 2020). To explore the potential involvement of these mechanisms in any regulatory role of the N-degron pathway, I analysed the ROS burst of triple mutants of *ate1ate2* combined with mutation of known regulators of RBOHD – CPK5 and CPK28 (Figs. 3.14b-d). The diminished ROS phenotype of *ate1ate2* was apparent in the *cpk5-1* background, indicating that these genes likely contribute independently to the regulation of the ROS burst.

In contrast, the effect of the *ate1ate2* mutation on the flg22-induced ROS burst was seemingly altered in the *cpk28-1* background, with marginally higher ROS production detected in the *ate1ate2 cpk28-1* line compared to the *cpk28-1* parental line (Figs. 3.14c & 3.14d).

One explanation consistent with these complex observations is that positive regulation of the PTI-induced ROS burst by ATE1/2 may involve inhibition of CPK28, thus alleviating its buffering effect on BIK1 (Fig. 3.22). In this case, CPK28 would be inhibited by ATE1/2 in wild-type plants by an as-yet-unknown mechanism, resulting in increased stability of BIK1 and permitting full activation of RBOHD (Fig. 3.22). Meanwhile, an *ate1ate2* mutant would accumulate CPK28, resulting in increased turnover of BIK1 and reduced activation of RBOHD. This model thus explains both the reduced ROS phenotype evident in the *ate1ate2* mutant and the absence of this effect in the *ate1ate2 cpk28-1*.

CPK28 transcript abundance was not altered in *ate1ate2* (Fig. A2 – Appendix A), but other (post-translational) mechanisms of inhibition could be speculated upon (e.g. suppression of kinase activity). However, further experiments would be required to validate the proposed model, including investigating potential physical interactions between ATE1/2 and CPK28, the

effect of *ate1ate2* mutation on CPK28 kinase activity and protein levels, or the phosphorylation status of BIK1.

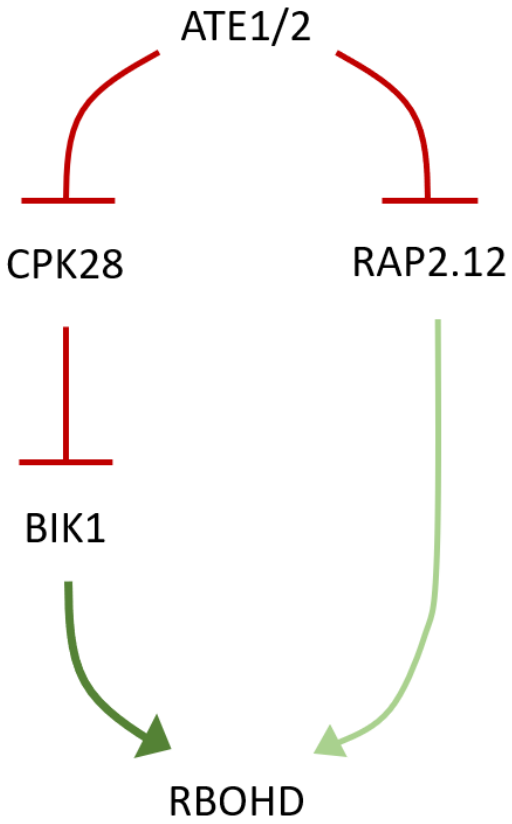

Figure 3.22. Proposed model of the role of ATE1/2 in the regulation of PTI-induced ROS. ATE1/2 exerts positive and negative regulation of the flg22-induced ROS burst via dual inhibition of a negative regulator (CPK28) and a positive regulator (RAP2.12), respectively. CPK28 promotes the turnover of BIK1, whose interaction with RBOHD is required for the full activation of ROS production. RAP2.12 is a known substrate of the N-degron pathway that positively regulates transcription of *RBOHD*. In *ate1ate2* mutants, relieved inhibition of CPK28 outweighs the effects of RAP2.12 stabilization resulting in a diminished ROS phenotype. In the *ate1ate2 cpk28-1* triple mutant, this mechanism is obscured, and ROS production is elevated compared to the *cpk28-1* parental line due to the positive regulation of *RBOHD* by the extant RAP2.12.

3.8.3 Growth inhibition, MAPK activation and flg22-induced pathogen resistance

Growth inhibition prompted by exposure to flg22 was reduced in *ate1ate2* and *prt6-1* seedlings compared to wild-type (Fig. 3.15). Although the N-degron pathway seems to play multifaceted roles in the regulation of immunity, this finding suggests that the N-degron pathway functions as a net positive regulator of PTI overall. This data is also in accordance with the reduced expression of certain immune genes and diminished ROS production observed in *ate1ate2* (Figs. 3.10 and 3.13 respectively).

The activation of MAPK cascades during PTI was not significantly altered in *ate1ate2* or *prt6-1* (Fig. 3.16). This implies that the roles of the N-degron pathway in the regulation of PTI are independent from MPK3/6 phosphorylation or occur downstream (see Fig 1.4). Notably, the *prt6-5* line displayed elevated abundance of phosphorylated MPK3 and MPK6 compared to *prt6-1* in replicate immunoblots (Figs. 3.16 and A4 – Appendix A) and compared to Col-0 in one experiment. Interestingly, varied phenotypes between these two null alleles of *PRT6* in response to *Pst* DC3000 have also been observed separately (de Marchi *et al.*, 2016; Vicente *et al.*, 2019) but as yet have not been addressed directly. It is essential that the reasons underpinning these differences are investigated in future studies to determine whether the *prt6-1* and *prt6-5* mutant alleles may indeed be considered equivalent, as has been assumed so far within the research community. In the meantime, inclusion of both *prt6* alleles and/or other mutant lines compromised in the PRT6 N-degron pathway (such as *ate1ate2* together with the ATE1 rescue line) can bolster confidence in conclusions drawn from reverse genetics studies. In this case, as *ate1ate2* and *prt6-1* exhibit similar levels of MAPK phosphorylation (Fig. 3.16 and A4), it is perhaps less likely that the phenotype observed in *prt6-5* reflects *bona fide* negative regulation of this PTI cascade by the N-degron pathway.

The flg22-induced resistance to *Pst* DC3000 was assessed in Col-0, *ate1ate2* and ATE1 rescue plants in a preliminary experiment (Fig. 3.17). Among mock pre-treated plants, the ATE1 rescue line appeared to exhibit enhanced resistance, while Col-0 and *ate1ate2* behaved similarly. Although the latter observation is different from the increased susceptibility identified in the previous study by de Marchi *et al.* (2016), definitive conclusions cannot be drawn from a single replicate, particularly as even the mock pre-treatment could influence pathogen susceptibility

(e.g. via activation of wounding responses by infiltration). After flg22 pre-treatment, a striking reduction in *Pst* growth was evident across all genotypes. Notably, the magnitude of the flg22-induced increase was lower in *ate1ate2* compared to Col-0. This could suggest that flg22-induced resistance is disrupted in *ate1ate2*. However, a similar level of *Pst* DC3000 growth was also observed in the flg22 pre-treated ATE1 rescue line. In sum, these preliminary data warrant future replicate experiments to investigate the role of the N-degron pathway in flg22-induced pathogen resistance.

3.8.4 Conclusions and future directions

The experiments detailed in this chapter reveal specific immune signaling pathways that appear to be partly regulated by the N-degron pathway. These include the induction of important defence-associated genes (Figs. 3.9 and 3.10), the production of ROS during PTI (Fig. 3.13) and age-related resistance (Fig. 3.18). In addition, the N-degron pathway may be involved in the regulation of flg22-induced seedling growth inhibition (Fig. 3.15), and the elevated resistance to *Pst* after a flg22 pre-treatment (Fig. 3.17). These apparent phenotypes could also be a consequence of the roles of the N-degron pathway in the regulation of PTI-associated genes and ROS production. The phosphorylation of MAPK cascades does not appear to be strongly affected in N-degron pathway mutants (Fig. 3.16).

Importantly, the N-degron pathway regulation of immune responses appears to be multifaceted, with some defence outputs promoted by the activity of the pathway and others inhibited. These dual-roles are perhaps most clearly illustrated here in the results of the RNA-Seq experiment where both positive and negative regulatory roles of ATE1 and ATE2 are evident, and in the varying susceptibility of *ate1ate2* to *Pst* DC3000 in 3.5 and 4 week-old plants. Additionally, while ATE1 and ATE2 appear to positively regulate ROS production during PTI, previous reports have indicated that RAP2.12, which is targeted for degradation by the N-degron pathway, promotes transcription of *RBOHD* (Licausi *et al.*, 2010; Yao *et al.*, 2017). Taken together, these findings have revealed potential the molecular mechanisms underpinning the roles of the N-degron pathway in immunity and clarified previous observations.

Notably, many flg22-responsive genes that are more strongly up-regulated in the *ate1ate2* mutant were previously known to be regulated by the ERF-VII transcription factors (discussed

in section 3.8.1). Meanwhile, the reduced expression of *AOX1D* in *ate1ate2* and *prt6-1* also appears to be a result of repression by the stabilised ERF-VIIs (Figs. 3.10 – 3.12). As ERF-VIIs are primarily responsible for the enhanced hypoxia tolerance of N-degron pathway mutants, the misregulation of immune responses by these same factors may prove problematic for efforts to develop flood-tolerant crops. It remains to be studied whether the other immunity-related phenotypes of N-degron pathway mutants described here are dependent on stabilization of the ERF-VIIs.

In conclusion, the N-degron pathway appears to be involved in the positive and negative regulation of multiple immune outputs. The roles detailed here may partially explain the conflicting pathogen susceptibility / resistance phenotypes of N-degron pathway mutants observed previously (e.g. De Marchi *et al.*, 2016; Vicente *et al.*, 2019). At least some of the contributions of the N-degron pathway to the regulation of immunity may be attributed to the activity of stabilized ERF-VII transcription factors. It is imperative that the regulation of immune responses by the N-degron pathway is considered extremely carefully when exploiting the pathway for the development of novel crop varieties.

4

Developing tools to study the N-degron pathway in *Brassica rapa*

4.1 Introduction and aims

Phenotypic analyses of *Arabidopsis thaliana* mutants revealed novel roles of the N-degron pathway in the regulation of plant immunity (Chapter 3). The *Arabidopsis* model is convenient for these reverse genetics approaches due to its relative genetic simplicity and the abundance of molecular and bioinformatic resources that have been generated over decades of plant science research. Knowledge gained in *Arabidopsis* can subsequently be exploited to direct crop improvement strategies, particularly as it is closely related to important crops in the *Brassicaceae* family (discussed in section 1.4). However, an essential component of such 'model-to-crop' translation is ultimate validation in the crop species of interest (Stephenson *et al.*, 2019). *Brassica rapa* and *B. napus* are oilseed crops of considerable social and economic value (introduced in section 1.4.1). Despite its widely acknowledged contributions to various stress responses, the N-degron pathway has not been directly studied in these species and efforts to do so are impeded by the scarcity of molecular tools presently available, as well as the increased complexity of their genomes.

The experiments detailed in the following chapter seek to establish a framework for the study of the N-degron pathway in *Brassica rapa*. Firstly, I describe the adaptation of a transient expression system to permit characterisation of the *B. rapa* N-degron pathway for the first

time. Secondly, I will present isolation of the first *B. rapa* N-degron pathway mutants and a preliminary molecular characterisation of their loss-of-function. Certain figures and modified excerpts of this chapter are published in Mooney & Graciet (2020).

4.2 The structure of the *B. rapa* N-degron pathway

4.2.1 Introduction

In order to study the physiological roles of the *B. rapa* N-degron pathway, it is first necessary to characterise its structure and components. The sets of stabilizing and destabilizing N-terminal amino-acid residues were initially discovered in yeast via expression of so-called N-degron pathway reporter proteins (Bachmair *et al.*, 1986). Such constructs are based on the 'Ubiquitin fusion technique' pioneered by the group of Alexander Varshavsky. In brief, a reporter protein (e.g. β-galactosidase or firefly luciferase) is modified to contain a variable amino-acid residue X at the N-terminus, which is also preceded by a single ubiquitin moiety. When expressed *in vivo*, the Ub fusion is cleaved near co-translationally by deubiquitylating enzymes, exposing residue X at the N-terminus of the reporter protein. By measuring the relative abundance (or activity) of the reporter protein, the stability conferred by the N-terminal residue X can be inferred. Using Ub fusion constructs developed by Worley *et al.* (1998), Graciet *et al.* (2010) transiently expressed X-luciferase (X-LUC) N-degron pathway reporter proteins in tobacco and utilized stable expression in *Arabidopsis thaliana* to characterise the plant N-degron pathway. Considering the success of these experiments, I resolved to employ a similar approach in *Brassica rapa*.

Various protocols for the stable transformation of *Brassica* crops have been developed previously. However, the majority of these involve *Agrobacterium* co-cultivation followed by plant regeneration from callus (De Block *et al.*, 1989, Sparrow *et al.*, 2006, Sanimah *et al.*, 2010), which makes them difficult to implement because of their labour intensiveness and the need for tissue culture. In contrast, transient expression methods enable rapid experiments, thus accelerating the characterisation of biological mechanisms. However, the development of transient expression approaches in *Brassica* crop species to-date has been hindered by low transformation efficiency or the need for biolistic equipment (although sparse examples of

Agrobacterium-based methods have begun to emerge in recent years (Zhong *et al.*, 2016; Das *et al.*, 2019)). The initial experiments described here focus on the optimisation of an efficient and reliable agroinfiltration-based transient expression system tailored for use in *B. rapa* to permit interrogation of the structure of the *B. rapa* N-degron pathway.

4.2.2 Developing a transient expression system for *Brassica rapa*

4.2.2.1 *Agrobacterium* co-cultivation for transient expression in *B. rapa*

Co-cultivation of *A. tumefaciens* transformed with a plasmid coding for a T-DNA of interest has been shown to allow transient expression of transgenes in *Arabidopsis thaliana*, although with variable efficiency depending on the genotype used (Li *et al.*, 2009, Wu *et al.*, 2014). Essentially, these transient expression methods rely on the co-cultivation of young seedlings with *Agrobacterium* for several days. After washing the seedlings to remove *Agrobacterium* cells, seedlings are transferred to MS agar medium for a 'recovery period' during which the transgene(s) may be transiently expressed.

To test if a co-cultivation method could lead to successful transient expression in *Brassica*, I used 3-day-old *B. rapa* seedlings as a model to express a GUS reporter gene under the control of the constitutive Cauliflower Mosaic Virus 35S promoter. We tested the effects of varying concentrations of Silwet in the co-cultivation medium (0.001% - 0.005% (v/v)), different co-cultivation (30-48 hrs) times, as well as the use of vacuum infiltration or not. Recovery time was kept constant at 24 h. Overall, the use of a lower Silwet concentration (0.001%) and a shorter co-cultivation period improved seedling survival, with higher doses resulting in limp seedlings that senesced during the 24-h recovery period (Fig. A7 in Appendix A). Despite these improvements, only small patches of cells expressing the GUS reporter could be observed in the cotyledons of co-cultivated seedlings (Figure 4.1b-d). In order to establish a more efficient protocol that would yield widespread transgene expression, I next investigated the feasibility of an agroinfiltration-based assay using adult *Brassica* leaves.

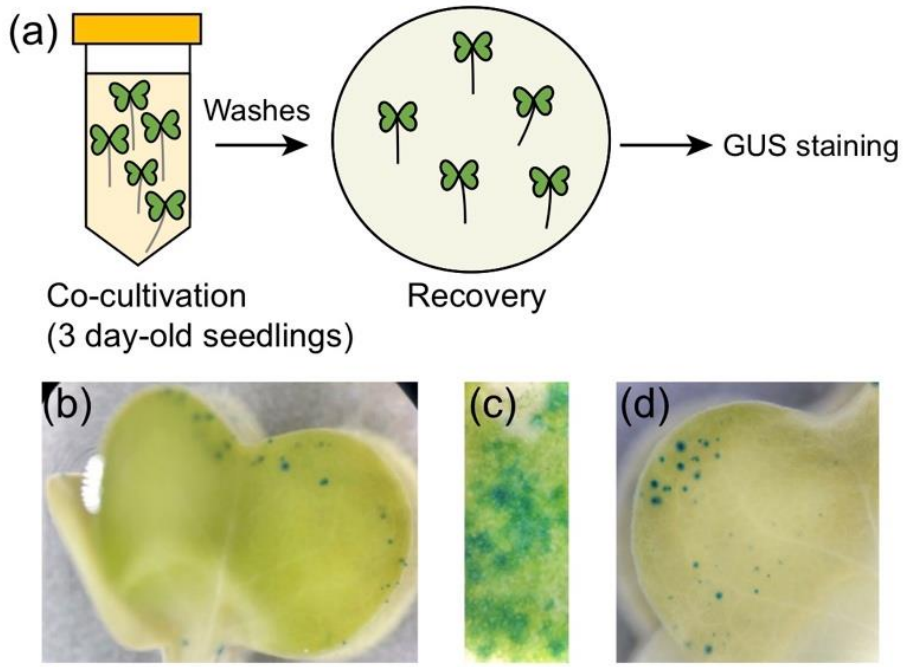

Figure 4.1. Agrobacterium-mediated co-cultivation in *B. rapa* seedlings. a. Schematic illustrating a summary of the protocol used for transient expression by agrobacterium-mediated co-cultivation in *B. rapa*. **b - d.** GUS staining images taken under stereomicroscope after co-cultivation and recovery period.

4.2.2.2 Agroinfiltration-based protocol for transient expression in *Brassicas*

Agroinfiltration experiments were conducted using *B. rapa* plants grown in walk-in growth chambers in short-day conditions (10 h light/14 h dark; 22°C) using leaves number 1 and 2 of 3 to 4-week-old plants that had formed 5-6 leaves in average (Fig. A8 in Appendix A). The results showed that the transient expression of the GUS reporter worked well under these conditions (Fig. 4.2). I also tested the expression of a GUS reporter that carried the cat1 intron inserted after the first 15 bases of the GUS coding sequence ($35S_{pro}$:GUS^{intron}) and confirmed that the GUS signal indeed originated from transient expression *in planta*, as opposed to potential leaky expression in the *Agrobacterium* strains used to infiltrate the plants (Fig. 4.2b). Additionally, we validated the use of our protocol in *B. napus* (variety: Westar) using leaves 1 and 2 (i.e. the first and second true leaves to emerge) of 4-5week-old plants grown under short-day conditions (10 h light/ 14 h dark; 22°C) (Figure 4.2b), thus extending the potential applications for this transient expression protocol to the study of biological processes in oilseed rape.

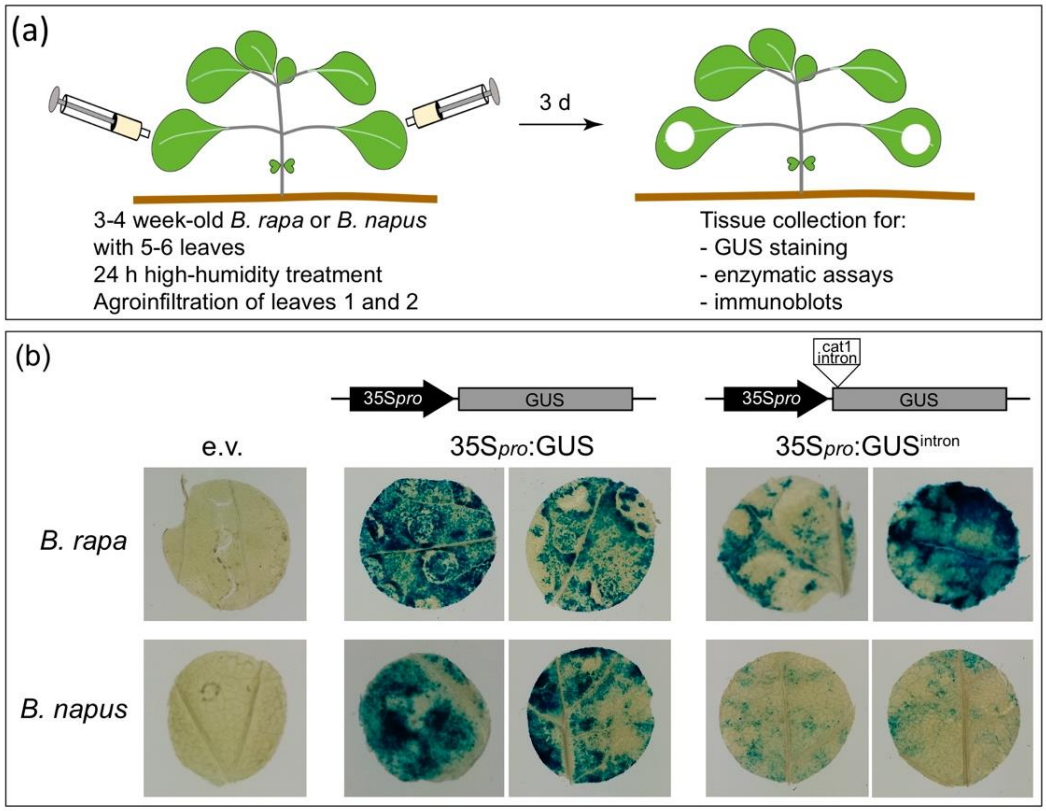

Figure 4.2. Transient expression of GUS in *Brassicas* by agroinfiltration. a. Schematic illustration summarising the method used for agroinfiltration of *B. rapa* leaves. A suspension of *Agrobacterium* at an OD_{600} of 0.75 was infiltrated into leaves 1 and 2 of 4-5 week-old plants grown in short-day conditions. Leaf tissue was harvested for analysis of transgene expression by GUS staining, LUC enzymatic assays and immunoblots. **b.** Representative GUS stains of *B. rapa* and *B. napus* leaf discs 3 days after agroinfiltration with a pMLBART empty vector (e.v.), $35S_{pro}$:GUS or 35S:GUS^{intron} (pCAMBIA2201).

Next, we conducted a time course experiment to determine the onset and duration of GUS expression after agroinfiltration. Our results show that in *B. rapa*, expression may be detected as soon as 24h post agro-infiltration, although in most cases, it took up to 2 days to detect GUS activity (Fig. 4.3a). Notably, peak GUS levels were observed at 3 days post agroinfiltration. GUS activity was sustained for at least 4 days after agroinfiltration. Similar results were observed with *B. napus* (Fig. 4.3b), further validating the transient expression method for use in this crop.

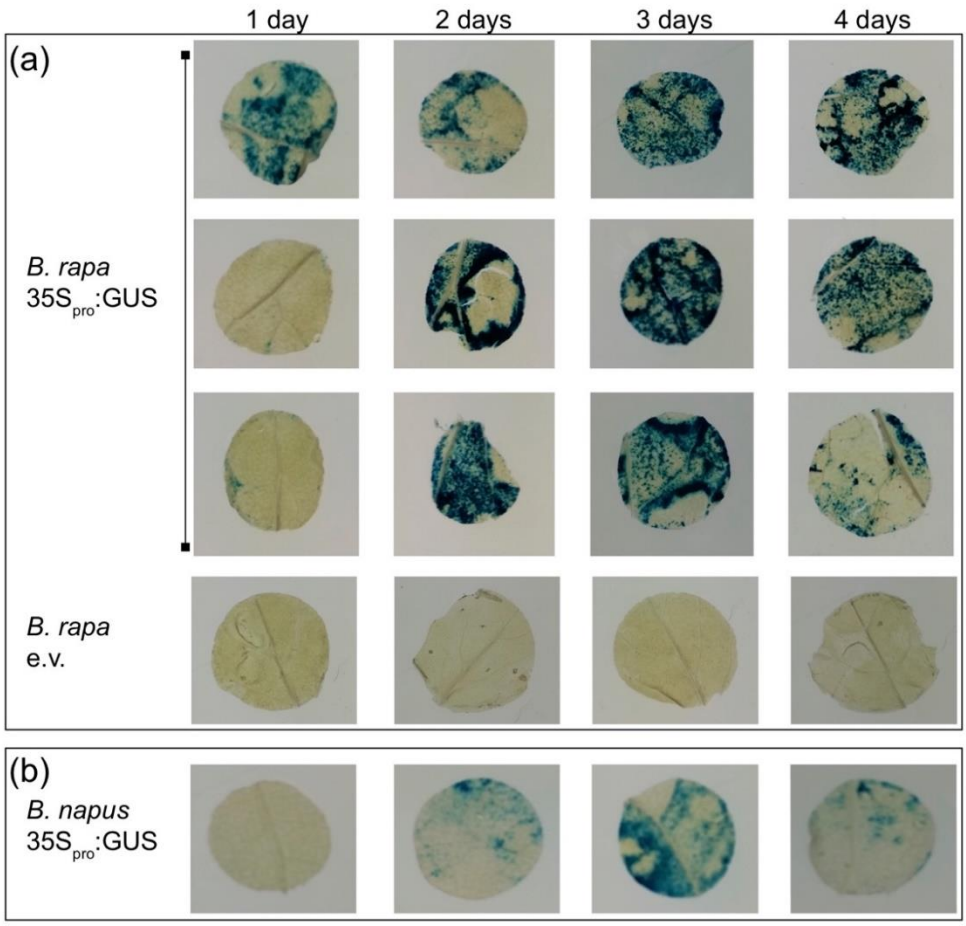

Figure 4.3. Time course of GUS expression in *Brassicas* by agroinfiltration. a. GUS staining of *B. rapa* tissue collected 1-4 days after agroinfiltration of *B. rapa* with either 35S$_{pro}$:GUS or the pMLBART empty vector control (e.v.). **b.** GUS of *B. napus* tissue 1-4 days after agroinfiltration with 35S$_{pro}$:GUS.

4.2.3 Revealing the structure of the *B. rapa* N-degron pathway

Considering the strong expression of the GUS reporter obtained using the agroinfiltration-based protocol, I employed this method to express X-LUC N-degron pathway reporter constructs in *B. rapa*. These constructs consist of a Ub-X-LUC N-degron pathway reporter fused to the constitutively expressed 35S$_{pro}$:GUS reference protein which can be used for normalization of LUC activity (Fig. 4.4a). To validate the successful transient expression of LUC and GUS in *B. rapa*, I performed immunoblot analysis on protein samples extracted from plants agroinfiltrated with *Agrobacteria* carrying a plasmid encoding the canonically stable Met-LUC / 35S$_{pro}$:GUS N-degron pathway reporter construct (Worley *et al.*, 1998; Graciet *et al.*, 2010) or the pMLBART empty vector (Fig. 4.4b).

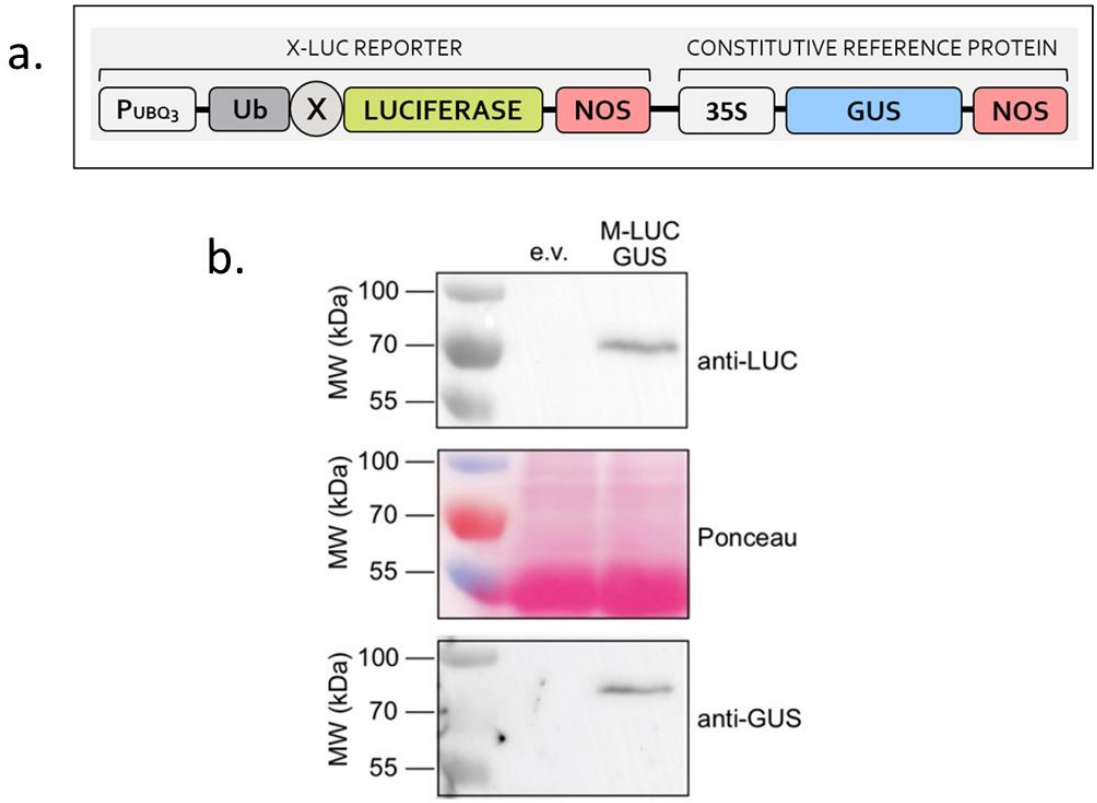

Figure 4.4. Immunoblot detection of LUC and GUS protein expression in *B. rapa*. a. The structure of the N-degron pathway reporter constructs. The N-degron pathway reporters rely on the differential stability of LUCIFERASE with varying N-terminal amino-acid residues (denoted by X), preceded by a single ubiquitin moiety. Upon expression *in planta*, near co-translational deubiquitylation reveals the residue of interest at the N-terminus (Worley *et al.*, 1998). A GUS enzyme under the control of the 35S promoter serves as a constitutively expressed reference protein. P_{UBQ3} = UBQ3 promoter. NOS = NOS terminator. **b.** Proteins were extracted from *B. rapa* plants 3 days after agroinfiltration with *Agrobacterium* harbouring either the plasmid pEG356 (coding for $UBQ3_{pro}$:Ub-Met-LUC $35S_{pro}$:GUS in the pMLBART plasmid) or a pMLBART empty vector (e.v.) and analysed by immunoblot. LUC was detected using a goat antibody against firefly LUC (AB3256, Merck). After stripping, the same membrane was re-probed with rabbit anti-GUS antibody (A5790, Invitrogen). Molecular weight standards are included in the first lane. Expected molecular weight (Mw) for LUC = 62 kDa, GUS = 68.5k Da. Uncropped blot image is presented in Fig. A9b.

While no bands were observed in the sample infiltrated with the empty vector construct as expected, robust accumulation of LUC and GUS proteins were detected in *B. rapa* infiltrated with the Met-LUC N-degron pathway reporter construct (Fig. 4.4b). This finding serves as a proof-of-concept for the transient expression of N-degron pathway reporter constructs in

Brassica rapa. To confirm *in planta* deubiquitylation of the LUC reporter, I compared the molecular weight of M-LUC expressed in *B. rapa* with Ub-M-LUC in *E. coli*, which lacks deubiquitinating enzymes and thus retains the 8.6kDa Ub conjugate (Fig. 4.5). The molecular mass of each protein can be inferred from their respective migration patterns through an SDS-PAGE gel and comparison with the molecular weight standards in lane 1 (Fig. 4.5). The relative size difference observed verified that the X-LUC N-degron pathway reporters are indeed deubiquitylated efficiently in *B. rapa*, and that the junctional residue X will be exposed at the N-terminus as required to characterise N-degron pathway mediated instability.

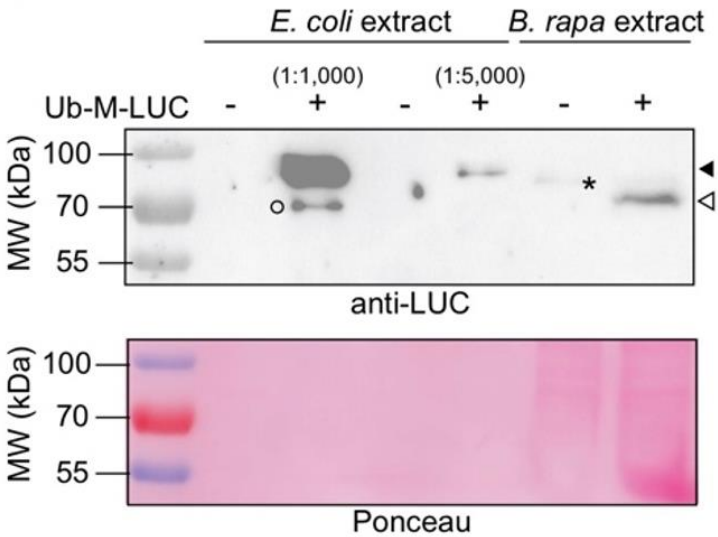

Figure 4.5. Deubiquitylation of the X-LUC N-degron pathway reporter in *B. rapa*. *In vivo* deubiquitylation of Ub-Met-LUC in *B. rapa*. A polyhistidine-tagged His_6-Ub-Met-LUC was expressed in *E. coli*, as a molecular weight control for a non-deubiquitylated N-degron reporter. Different dilutions of the crude *E. coli* protein extracts were loaded (1:1,000 and 1:5,000) to ensure that the signal was comparable to that obtained after expression of Ub-Met-LUC in *B. rapa*. Similar dilutions of a protein extract generated from untransformed *E. coli* were used as a negative control for potential antibody cross-reactivity. The absence of proteins on the Ponceau staining with the *E. coli* samples is due to the low amount of protein loaded for these extracts. Ub-Met-LUC was transiently expressed in *B. rapa* and tissue was harvested 3 days after agroinfiltration. *B. rapa* agroinfiltrated with the pMLBART empty vector was used as a background control. Expected Mw for His_6-Ub-Met-LUC = 72kDa, Ub-Met-LUC = 71kDa, Met-LUC = 62kDa. Black arrowhead: His_6-Ub-Met-LUC; open arrowhead: Met-LUC; asterisk: cross-reacting protein; open circle: potential degradation product of Ub-Met-LUC in *E. coli*. Uncropped blot image is presented in Fig. A9a.

Subsequently, I agroinfiltrated *B. rapa* plants with a subset of 10 N-degron pathway reporter constructs bearing one of methionine (Met), serine (Ser), alanine (Ala), threonine (Thr), cysteine (Cys), glutamine (Gln), asparagine (Asn), aspartic acid (Asp), arginine (Arg) or tryptophan (Trp) at the N-terminus. These amino-acids are representative of the different types of destabilizing N-terminal residues found in plants previously, including a basic primary destabilizing residue (Arg; recognized by AtPRT6 (Garzon *et al.*, 2007)), a hydrophobic primary destabilizing residue (Trp; bound by AtPRT1 (Potuschak *et al.*, 1998, Stary *et al.*, 2003)), a secondary destabilizing residue (Asp; modified by Arg-transferases) and tertiary destabilizing residues (Asn and Gln, which are deamidated by AtNTAN1 and AtNTAQ1 respectively (Graciet *et al.*, 2010), as well as Cys, which is oxidized by AtPCO enzymes (Weits *et al.*, 2014, White *et al.*, 2017)). The enzymatic activity of the associated LUC enzyme was quantified in each case and normalized to the activity of the constitutively expressed GUS reference protein (Fig. 4.6).

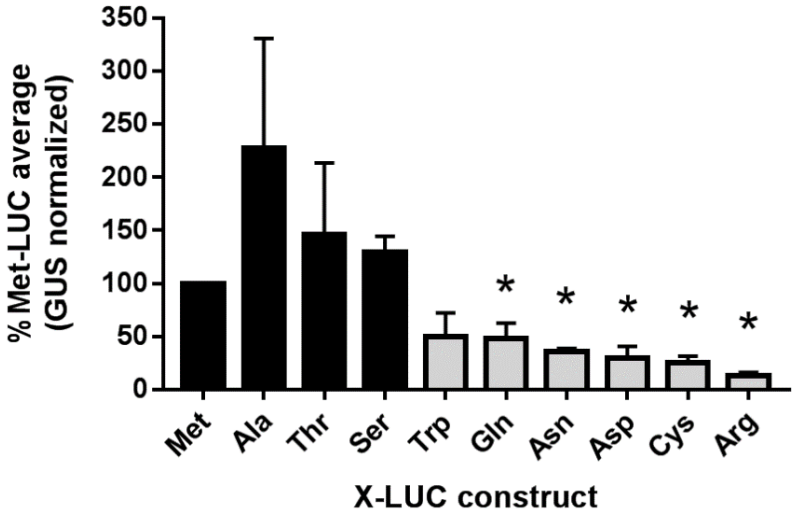

Figure 4.6. Structure of the *B. rapa* N-degron pathway. LUC activities for each N-degron pathway reporter construct were normalized against the corresponding GUS activities and expressed relative to that of Met-LUC for each of the replicates. Columns represent means + SEM of 4 independent replicates, except for Asn, for which two independent replicates were conducted. Black and grey bars correspond to stabilizing and destabilizing N-terminal residues, respectively. Un-normalized measurements for LUC and GUS enzymatic activity are included in Fig. A10 (Appendix A). Asterisks indicate significant difference ($p \leq 0.05$) after Welch's t-test comparison with Met-LUC.

Relative to Nt Met, 3 of the 9 additional amino-acids tested – Ala, Thr and Ser - conferred stability to the X-LUC reporter. The remaining 6 residues (Trp, Gln, Asn, Asp, Cys, Arg) appeared to be destabilizing at the N-terminus. Indeed, each of these destabilizing residues (except for Trp) displayed a statistically significant reduction in the stability of the X-LUC reporter when compared directly to Nt Met. Strikingly, for all of the amino acids tested here, the effect on protein stability matches that which was previously observed in tobacco by Graciet *et al.* (2010), indicating strong conservation of the N-degron pathway structure in *B. rapa*.

To validate the findings of these enzymatic assays, the abundance of transiently expressed Met-LUC (the canonical 'stabilizing' N-terminal residue) and Arg-LUC (which exhibited the lowest LUC activity; Fig. 4.6) were also assessed by immunoblot (Fig. 4.7). While Met-LUC was readily visible under these conditions, the Arg-LUC reporter was not detected. Importantly, the transiently expressed GUS reference protein was similarly abundant in each sample, strongly suggesting that the absence of the Arg-LUC protein is a consequence of its N-degron pathway mediated instability rather than comparatively poor expression of this reporter construct.

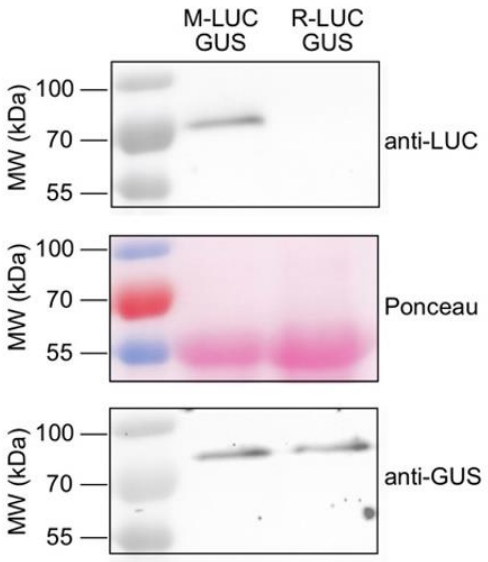

Figure 4.7. Arg is a destabilizing N-terminus in *B. rapa*. Comparison of Met-LUC and Arg-LUC signal intensities for equal GUS levels after infiltration with *Agrobacterium* transformed with pEG356 ($UBQ3_{pro}$:Ub-Met-LUC $35S_{pro}$:GUS) or pEG368 ($UBQ3_{pro}$:Ub-Met-LUC $35S_{pro}$:GUS). Ponceau staining was performed before immunoblotting with anti-LUC. The membrane was then stripped and re-probed with rabbit anti-GUS antibody (A5790, Invitrogen). Molecular weight standards are indicated in the first lane. Uncropped blot images are shown in Fig. A9c.

4.2.4 Components of the *B. rapa* N-degron pathway

The apparent conservation of the N-degron pathway structure in *B. rapa* suggests that N-degron pathway enzymatic components may also be conserved. To investigate this, the amino-acid sequences of the *Arabidopsis* N-degron pathway protein components were queried against the *B. rapa* proteome using BLASTp (the Basic Local Alignment Search Tool for protein sequences). *B. rapa* orthologs were identified for each of the N-degron pathway components encoded in *Arabidopsis* (Fig. 4.8a).

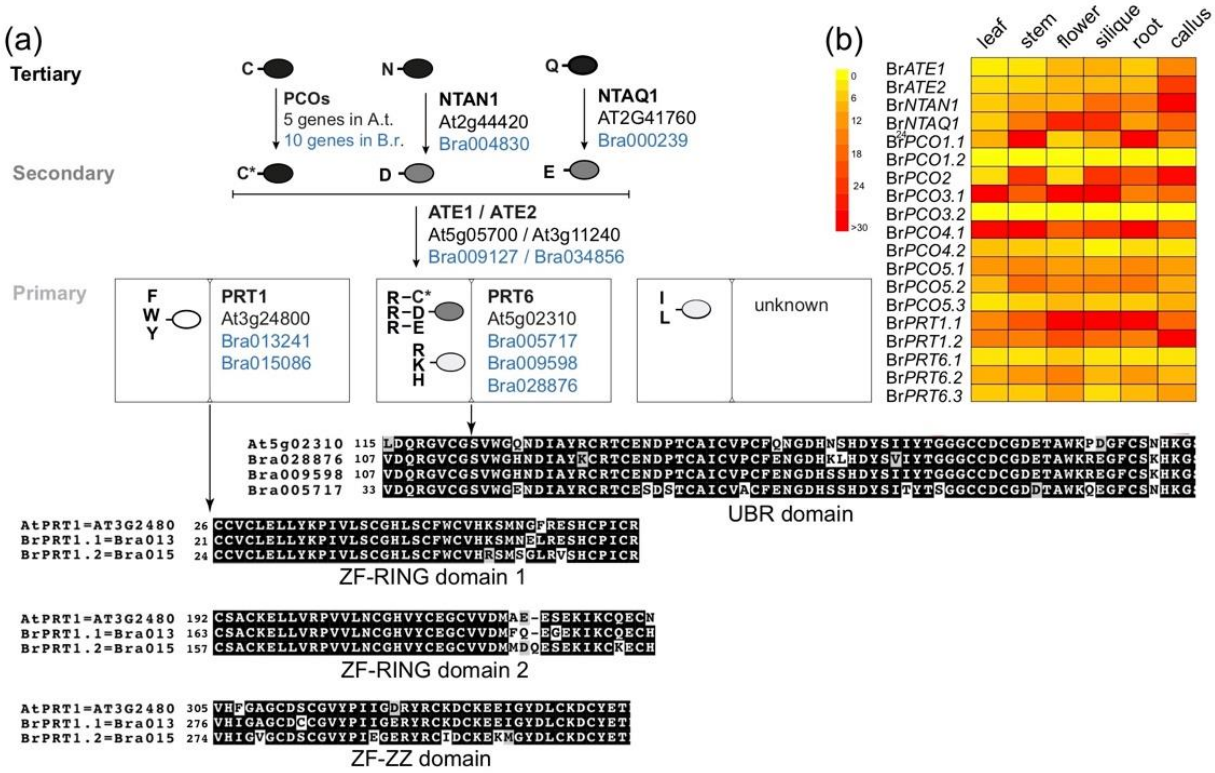

Figure 4.8. N-degron pathway components in *B. rapa*. a. Protein sequences from *Arabidopsis thaliana* N-degron pathway enzymatic components were used as query in a BLASTp search to identify *B. rapa* orthologs. Filled ovals denote proteins, with single letters indicating the N-terminal destabilizing residue. The abbreviated names of the enzymatic components are specified, as well as the genome identifier numbers in *A. thaliana* (black) and in *B. rapa* (blue). C*: oxidized cysteine; PCOs: PLANT CYSTEINE OXIDASEs; NTAN1: N-terminal Asn amidohydrolase; NTAQ1: N-terminal Gln amidohydrolase; ATE1/ATE2: Arg-transferases 1 and 2, respectively; PRT1: PROTEOLYSIS1; PRT6: PROTEOLYSIS6. The genome identifiers for the 10 *B. rapa PCO* orthologs are as follows: *BrPCO1.1* = Bra006280; Br*PCO1.2* = Bra008720, Br*PCO2* = Bra025636, Br*PCO3.1* = Bra025900, Br*PCO3.2* = Bra038171, Br*PCO4.1* =

Bra004726, Br*PCO4.2* = Bra000271, Br*PCO5.1* = Bra00741; Br*PCO5.2* = Bra01456; Br*PCO5.3* = Bra030926. Alignment of the functional domains of PRT1 (ZF-RING domain 1, ZF-RING domain 2 and ZF-ZZ domain) and PRT6 (UBR domain) orthologs. **b.** Heatmap showing the expression atlas of N-degron pathway components in *B. rapa*. The tissue-specific gene expression of the N-degron pathway-related genes in *B. rapa* (accession Chiifu-401-42) was obtained from a previously published dataset (GEO43245) (Tong *et al.*, 2013). Scale: fragments per kilobase of exon model per million reads mapped (FPKM) values for each indicated gene.

Interestingly, there appears to be more diversity among the N-degron pathway E3 ligases (N-recognins) in *B. rapa* compared to *Arabidopsis*. While the *Arabidopsis* genome codes for one N-recognin specific for hydrophobic aromatic residues (AtPRT1) and one for basic residues (AtPRT6), the *B. rapa* genome encodes 2 orthologs of At*PRT1* and 3 orthologs of At*PRT6* (Fig. 4.8a). Alignment of the known functional domains of these N-recognins indicates that they are extremely well conserved within *Brassicaceae* and are likely to execute the same functions in *B. rapa* as in *Arabidopsis* (Fig. 4.8a). The diversification at the N-recognin level may instead be relevant in the context of their spatial expression patterns, or in response to specific environmental cues. Hence, we used publicly available transcriptomics datasets (Tong *et al.*, 2013) to determine the expression atlas of N-degron pathway-related genes in *B. rapa* (Fig. 4.8b). In general, all *B. rapa* N-degron pathway-related genes except for Br*PCO1.2* and Br*PCO3.2* are expressed broadly in a variety of tissues, albeit with some differences (Fig 4.7b). For example, Br*PRT6.2* and Br*PRT6.3* exhibit generally higher expression in most tissues than Br*PRT6.1*.

4.2.5 Discussion

These experiments revealed that co-cultivation with *Agrobacterium* and leaf agroinfiltration permit transient expression of transgenes in *B. rapa*. While seedling co-cultivation remained inefficient with only few cells in cotyledons expressing the GUS reporter gene (Fig. 4.1), agroinfiltration of leaves resulted in robust and sustained transgene expression throughout the infiltrated area (Figs. 4.2 & 4.3). The primary advantage of this agroinfiltration protocol compared to stable transformation methods of *B. rapa* or *B. napus* are its ease of use and the

rapidity with which results can be obtained without the need for tissue culture and regeneration. Developing an efficient and simple transient expression protocol that is practicable in *Brassica* crops also facilitates the study of molecular mechanisms in a homologous system, as opposed to relying on heterologous transient expression in *N. benthamiana*, for example, which may lack *Brassica*-specific proteins or cofactors needed to study certain proteins of interest. Notably, the agroinfiltration protocol described here is also applicable to *B. napus*, which can greatly facilitate potential applications in this essential oilseed crop.

The utility of this protocol is exemplified by its use to identify destabilizing N-terminal residues of the N-degron pathway in *B. rapa* for the first time (Fig. 4.6). The stability of 10 N-terminal amino acids was determined by quantification of the enzymatic activity of transiently expressed X-LUC reporters normalized to a constitutively expressed GUS protein, and validated further by immunoblot analysis of the model destabilizing N-degron reporter Arg-LUC and the canonically stable Met-LUC (Fig. 4.7). Notably, the destabilizing (or stabilizing) effect conferred by each N-terminal amino acid tested matched those that have been identified previously by transient expression of N-degron pathway reporters in tobacco (Graciet *et al.*, 2010). Additionally, the 5 N-degron pathway reporters found to be significantly less stable than Met in *B. rapa* (Gln, Asn, Cys, Asp, Arg) have each been shown to be destabilizing in *Arabidopsis* upon stable expression of the same X-LUC reporter constructs (Graciet *et al.*, 2010). Together, this data strongly indicates that the destabilizing residues of the plant N-degron pathway are well conserved between *B. rapa, Arabidopsis* and the more distantly related *N. benthamiana*. More broadly, this set of 5 amino acids have also been implicated as destabilizing N-termini in mammals (Graciet *et al.*, 2010) and all except Cys are also considered destabilizing in yeast (Varshavsky, 2019). Thus, this finding further illustrates the conservation of destabilizing N-terminal amino acid residues in diverse eukaryotes (discussed in section 1.2.4).

In agreement with this, *in silico* analysis of protein sequence similarities revealed *B. rapa* proteins homologous to every known N-degron pathway component in *Arabidopsis* (Fig. 4.8a). Functional domains of N-recognins such as the PRT6 UBR domain responsible for the recognition of Arg/N-degrons show high levels of conservation (Fig. 4.8a). In most cases, a single *B. rapa* homolog was identified for each *Arabidopsis* component, i.e. NTAQ1, NTAN1,

ATE1 and ATE2. However, 2 *B. rapa* orthologs of PRT1 and 3 *B. rapa* PRT6 orthologs were identified alongside 10 *B. rapa* PCOs compared to the 5 present in *Arabidopsis*. This increased diversity in *B. rapa* correlates with whole genome comparisons indicating that *B. rapa* contains approximately twice as many genes as *Arabidopsis* (Mun *et al.*, 2009). Indeed, *Brassica* crops may be expected to exhibit more genetic redundancy than *Arabidopsis* as a result of an ancient genome triplication event (Lysak *et al.*, 2005; Stephenson *et al.*, 2010). Interestingly, analysis of the expression patterns of *B. rapa* genes encoding N-degron pathway components suggests that most are well expressed in a variety of tissues, including those which may be expected to be functionally redundant e.g. Br*PRT1.1* and *PRT1.2* (Fig. 4.8b).

Taken together, these experiments have resulted in a novel tool for the expression of transgenes in *B. rapa* and established a foundation for the study of the N-degron pathway in *Brassica* crop species. Considering the critical physiological roles of the N-degron pathway as an integrator of various environmental signals (Miricescu *et al.*, 2018), these findings could facilitate efforts to improve the resilience of *Brassica* crops to environmental stresses, including flood-tolerance and pathogen challenge.

4.3 Isolation of *B. rapa* N-degron pathway mutants

4.3.1 Introduction

Having revealed the destabilizing residues of the *B. rapa* N-degron pathway and identified its enzymatic components, I next sought to explore its physiological functions in more detail. Reverse genetics approaches to investigate gene function in *B. rapa* have been expedited by the development of the first *B. rapa* EMS TILLING collection in 2010 (Stephenson *et al.*, 2010). Briefly, seeds of the *B. rapa* subsp. *trilocularis* (R-o-18 genotype) were mutagenized with EMS (ethyl methanesulfonate), which typically causes G:C to A:T point mutations (Sega, 1984; Stephenson *et al.*, 2010). At the time this project started, scientists from the *B. rapa* research community could avail of this resource by requesting a TILL screen of pooled DNA from 9,216 M_2 plants for mutations in a ~1.2 kb genomic region of interest from RevGenUK (based at the John Innes Centre; revgenuk.jic.ac.uk/). As this TILLING population contains a particularly dense rate of ~1 mutation per 60kb of genomic sequence, each screen has a high likelihood

of recovering a line harbouring a nonsense mutation in the gene of interest (Stephenson *et al.*, 2010). However, this density also increases the incidence of background mutations in these lines and specific considerations are required to mitigate their impact. The following section describes the isolation of *B. rapa* N-degron pathway mutants from the TILLING collection.

4.3.2 TILLING screens of *B. rapa* N-degron pathway genes

Initially, we requested TILLING screens of 5 *B. rapa* Arg/N-degron pathway genes – the 3 orthologs of the At*PRT6* N-recognin: Br*PRT6.1* (Bra005717) Br*PRT6.2* (Bra009598), Br*PRT6.3* (Bra028876) and the 2 arginyl-transferase components: *BrATE1* (Bra009127) and Br*ATE2* (Bra034856). At least 20 lines containing SNP mutations in the TILLed region were available for each of the genes screened. In total, over 50 TILLING lines were purchased from RevGenUK (listed in Table B1 – Appendix B). Each mutation was categorised as either missense, truncation (i.e. the introduction of an early stop codon or mutation occurring at a splice site) or silent (i.e. synonymous amino-acid substitutions or occurring in non-coding regions). Truncation mutants are of particular interest as these are the most likely to severely impair protein function. Fortunately, the TILLING screens of M_2 parent plants revealed multiple truncation mutants in each of the 5 N-degron pathway genes of interest. Accordingly, my primary aim was to use selected early stop codon lines (Table 4.1) to generate a *Brate1ate2* double mutant and a *Brprt6.1prt6.2prt6.3* triple mutant to overcome genetic redundancy and investigate the physiological functions of the *B. rapa* N-degron pathway.

Table 4.1. Summary of truncation mutants for *B. rapa* N-degron pathway genes. Gene IDs correspond to identifiers used in the Brapa_1.0 genome sequence of the *B. rapa* Chiifu-401-42 accession (The Brassica rapa Genome Sequencing Project Consortium *et al.*, 2011). Line numbers as labelled by RevGen UK. Line names originate from the present study. Gene coding sequences (CDS) were downloaded from the Brassicaceae Database (BRAD) and analysed on the ApE plasmid editor.

Gene name	Gene ID	Line number	Line name	Type	CDS length	SNP site
Br*ATE1*	Bra009127	JI31799-B	*Ate1-2*	Stop codon	1878 bp	1223 G>A
Br*ATE2*	Bra034856	JI31089-B	*Ate2-2*	Stop codon	1680 bp	1239 G>A
Br*PRT6.1*	Bra005717	JI30884-A	*Prt6.1-11*	Stop codon	5550 bp	42 G>A
Br*PRT6.2*	Bra009598	JI40184-A	*Prt6.2-12*	Stop codon	5958 bp	4735 C>T
Br*PRT6.3*	Bra028876	JI32812-B	*Prt6.3-1*	Stop codon	5904 bp	3985 C>T

4.3.3 Genotyping and breeding of TILLING lines – general introduction

4.3.3.1 Genotyping methods

M_3 seeds of the early stop-codon lines listed in Table 4.1 were obtained from RevGenUK. Each of these lines originated from a heterozygotic M_2 parent. Several methods were employed to permit genotyping of the SNPs – initially, the derived cleaved amplified polymorphic sequence or 'dCAPS' technique (Neff *et al.*, 1998), and later, double mismatch allele-specific quantitative PCR or 'DMAS-qPCR' (Lefever *et al.*, 2019). In cases where a suitable assay could not be designed or an inconclusive result was obtained, genotypes were confirmed by Sanger sequencing of the genomic region after PCR amplification.

The dCAPS technique utilizes PCR primers containing intentional mismatches positioned adjacent to the mutation site that introduce or abolish a restriction enzyme recognition site based on the presence (or absence) of the SNP. The genotype can thus be inferred by gel electrophoresis of the products of a restriction digest performed on the PCR-amplified DNA. An example of a dCAPS assay for the *ate2-5* missense line is provided in Fig. 4.9. Although simple and inexpensive, dCAPS genotyping of multiple lines can be quite labour-intensive as each SNP requires a customized assay and unique set of primers. However, tools like the dCAPS Finder 2.0 (available online at helix.wustl.edu/dcaps/dcaps.html) have been developed to automate this process. Additionally, distinguishing heterozygotes from homozygotes can be challenging, particularly where only partial digestion of homozygous samples occurs.

In the later years of my project, I increasingly used the DMAS-qPCR method (Lefever *et al.*, 2019) to genotype *B. rapa* TILLING lines, which may be considered a higher-throughput approach. This technique combines the familiar principles of allele-specific PCR genotyping and quantitative PCR. Essentially, two parallel qPCR reactions are performed on a genomic DNA sample each using either a wild-type or mutant specific forward primer and a common reverse primer. Naturally, the wild-type or mutant specific reaction will strongly favour amplification of the wild-type or mutant sequence respectively, and this difference can be observed by comparison of the quantification cycle (Cq) values obtained from each qPCR. The inclusion of intentional mismatches in the allele specific primers upstream of the SNP site can increase the discriminating power of this approach (Lefever *et al.*, 2019). All assays developed using DMAS-qPCR were validated using Sanger sequencing to ensure validity and robustness.

a. **WT genomic sequence:**
AGAGTTGATGGACGTCTTATAGCTGTGGGAGTGAT

***Ate2-5* mutant sequence:**
AGAGTTGATGGACGTCTTATAGCTGTGGGAATGAT

dCAPS primer:
AGAGTTGATGGACATCTTATAGCTGTGGcA

WT sequence after dCAPS PCR:
AGAGTTGATGGACGTCTTATAGCTGTGGcAGTGAT

***Ate2-5* mutant after dCAPS PCR:**
AGAGTTGATGGACGTCTTATAGCTGTGGcAATGAT

BseMI (BsrDI) recognition site GCAATGNN is present in *Ate2-5* mutant sample.

b.

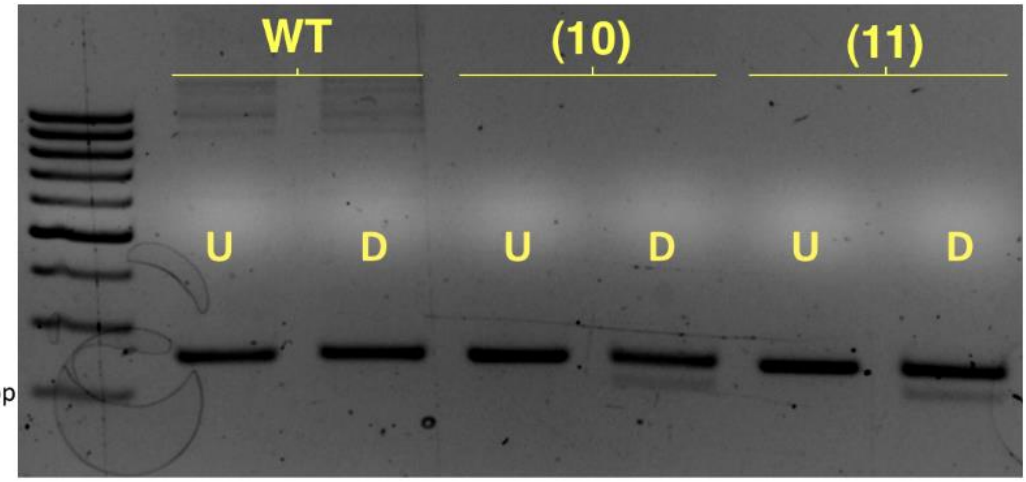

Figure. 4.9. dCAPS assay to genotype *ate2-5* line. a. dCAPS assay designed to genotype the *ate2-5* G>A point mutation (underlined red text). The dCAPS primer contains a mismatched nucleotide upstream of the SNP site (shown in lower case). After PCR amplification, products bearing the *ate2-5* mutation will be susceptible to digestion by the BseMI (BsrDI) restriction enzyme based on the presence of the GCAATGNN sequence. **b.** Agarose gel electrophoresis of the products of BseMI (BsrDI) digestion after dCAPS PCR. A wild-type control sample is indicated as 'WT', while TILLING mutants segregating the *ate2-5* mutation are numbered. U = Undigested control, D = Digested. No digestion of the wild-type sample is observed, while partial digestion of samples 10 and 11 is evident indicating the presence of the *ate2-5* SNP. In this case, the expected size of the undigested PCR amplicon is 249 bp, while digested samples are expected to be 214 bp + a 35 bp fragment (not visible). The GeneRuler 100 bp DNA ladder (Thermo) is loaded in the first lane, ranging from 200-1000 bp in 100 bp increments.

4.3.3.2 Background mutations

Each line from this *B. rapa* TILLING collection is expected to contain approximately 10,000 point mutations in total as a result of EMS mutagenesis (Stephenson *et al.*, 2010). However, as only 11% of the *B. rapa* genome comprises coding sequences (Trick *et al.*, 2009), Stephenson *et al.* (2010) estimated that an average of only 1,100 of these SNPs occur in exon regions, with 700 predicted to cause amino acid substitutions and ~50 which could introduce premature stop codons. In some cases when growing the N-degron pathway TILLING lines, the cumulative burden of mutations in M_3 plants appeared to cause problems for development and reproduction, manifesting in unusual phenotypes (Fig. A11 – Appendix A) and occasionally hindering the breeding process (e.g. via the production of non-viable seeds or male sterility etc.). To reduce the impact of background mutations, backcrossing of TILLING lines to wild-type plants is advisable (Stephenson *et al.*, 2010; Ó Lochlainn *et al.*, 2011). For example, one recent study that characterised a *B. rapa HRA4a* mutant originating from this collection mentioned backcrossing M_3 plants once to wild-type R-o-18 prior to phenotypic analysis (Navarro-Leon *et al.*, 2019). On this basis, I aimed to backcross each individual line at least once prior to the generation of the higher-order N-degron pathway mutants. Comparison of mutants with 'wild-type' plants re-isolated from the TILLING population can also serve as useful controls for the presence of remaining background mutations.

4.3.4 Isolation of *B. rapa* ATE mutants

As the *Arabidopsis ate1ate2* mutant was of particular interest in Chapter 3, I initially focused on the isolation of a *Brate1ate2* double mutant. Typically, the *ate1-2* and *ate2-2* SNPs were genotyped using Sanger sequencing after PCR amplification and clean-up using the E.Z.N.A Cycle Pure kit (Omega Biotek) (Fig. 4.10). To reduce the mutation load of background SNPs, the *ate1-2* line was backcrossed twice to a wild-type R-o-18 parent and *ate2-2* was backcrossed once prior to double crossing the two mutant lines.

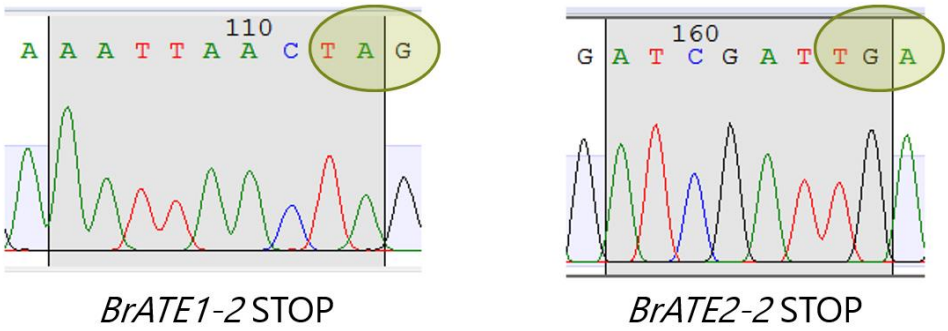

Figure 4.10. Sequencing of *Brate1ate2* lines. Sanger sequencing chromatograms showing the identification of the *Brate1-2* and *Brate2-2* SNPs (left and right respectively). The *Brate1-2* mutation substitutes a TAG stop codon (circled) for a tryptophan residue (TGG). *Brate2-2* substitutes a TGA stop codon (circled) for tryptophan (TGG). The *Brate1-2* genomic region was amplified using primers BM10 + BM22. The *Brate2-2* region was amplified using BM30 + BM31.

After crossing the *ate1-2* and *ate2-2* lines together, seeds were obtained from a self-fertilized F1 plant heterozygous for both mutations after self-fertilization. As no homozygous double mutants could be identified after initial screening in the first F2 population, seeds were instead collected from *Brate1-2* +/- *ate2-2* -/- and *Brate1-2* -/- *Brate2-2* +/- plants. The likelihood of recovering a homozygous double mutant in the offspring of these plants after self-fertilization is 25% based on expected segregation ratios. However, I again failed to detect a homozygous double mutant in the offspring of either parent. For example, despite sequencing 20 plants resulting from the selfing of the *Brate1-2* +/- *ate2-2* -/- parent, I identified 10 heterozygotes for the *ate1-2* SNP, with the remaining 10 all wild-type for *BrATE1*. As the likelihood of this occurring by random chance is extremely low (0.75^20 = 0.00032 or 0.32%), I began to consider that the *B. rapa ate1ate2* double mutant may cause early lethality. Although this would contrast starkly with the comparatively milder phenotypes of the *Arabidopsis ate1ate2* mutant (Graciet *et al.*, 2009), deletion of *ate1* in mice is in fact embryonic lethal (Brower and Varshavsky, 2009), highlighting the essential roles of Arg-transferases in some eukaryotes. Subsequent phenotypic analyses accompanied by DMAS-qPCR genotyping indicated that the combination of the homozygous *ate1-2* and *ate2-2* mutations in *B. rapa* leads to severely disrupted morphological development (Fig. 4.11), culminating in seedling lethality. In particular, cotyledon formation appears to be delayed or absent and hypocotyl length is reduced in the *Brate1-2ate2-2* double mutant, while single mutants or heterozygotes develop

normally overall (Fig. 4.11b), with some mild leaf morphology defects identified sometimes in *Brate1-2 -/- Brate2-2* +/- plants. Together, this data indicates that the Arg-transferases play redundant, essential roles in the early developmental stages of *B. rapa*.

a.

Plant #	WT Cp	MUT Cp	WT-MUT	*Ate2-2* genotype
1	30.61	23.61	7	MUT
2	30.19	23.82	6.37	MUT
3	24.03	24.05	-0.02	HET
4	30.62	23.89	6.73	MUT
5	26.24	32.2	-5.96	WT
6	23.63	23.58	0.05	HET
7	24.07	23.99	0.08	HET
8	22.83	32.63	-9.8	WT

b.

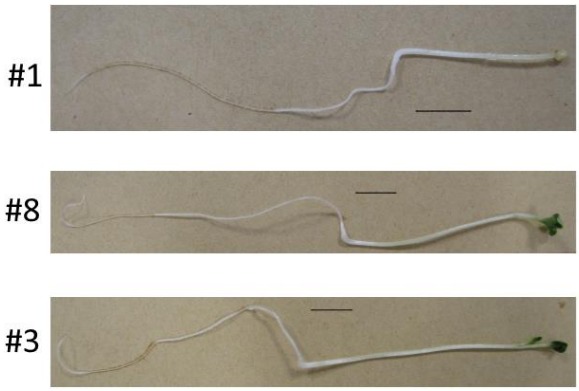

Figure 4.11. Genotype to phenotype assessment of *Brate1ate2* seedlings. a. DMAS-qPCR genotyping of the offspring from a *Brate1-2 -/- ate2-2* +/- parent after self-fertilization. Numbers indicate Cp (crossing point) values obtained after each allele-specific qPCR. *Brate2-2* genotype predictions are indicated in the last column. **b.** Representative images of plants DMAS-qPCR genotyped plants highlighted in '**a**'. Each seedling is homozygous for the *Brate1-2* SNP and segregating the *ate2-2* mutation as indicated. Seedlings were grown under continuous light (20°C) on 0.5xMS agar medium supplemented with 1% (w/v) sucrose. Pictures were taken after 4 days of growth. Scale bar = 1cm.

4.3.5 Isolation of *B. rapa* PRT6 mutants

The early lethality and consequent infertility of the *Brate1ate2* mutant severely limits its utility for many experimental protocols, including the transient expression of X-LUC reporters to confirm N-degron pathway loss-of-function. Considering there are three homologs of *PRT6* in

B. rapa (noted *BrPRT6.1*, *BrPRT6.2* and *BrPRT6.3*), I investigated whether the deletion of the two most strongly expressed *PRT6* orthologs would be sufficient to permit interrogation of the functions of the *B. rapa* N-degron pathway without severely compromising early plant development. To this end, I focused on the generation of a *Brprt6.2prt6.3* double mutant, retaining the function of the lesser-expressed *BrPRT6.1* ortholog (Fig. 4.8b). The *Brprt6.2-12* and *Brprt6.3-1* lines (see table 4.1) were each backcrossed twice to a wild-type R-o-18 parent prior to the initial double cross. Genotyping results of the parent plants used for the cross are shown in Fig. 4.12.

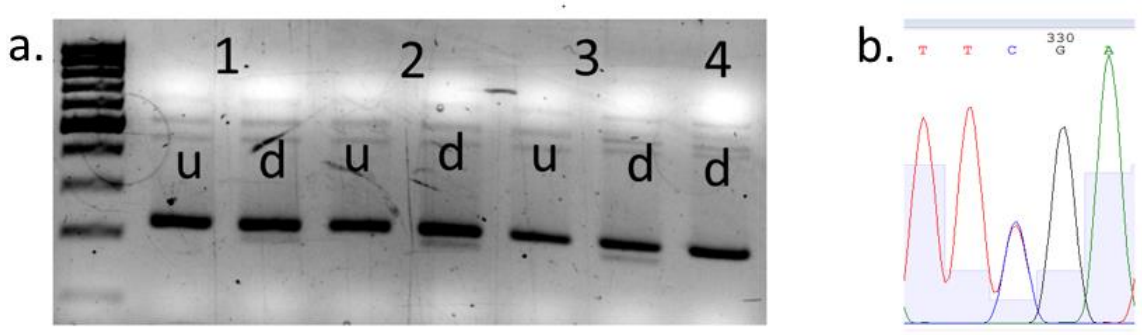

Figure 4.12. Genotyping of *Brprt6.2-12* and *Brprt6.3-1* lines. a. dCAPS assay to identify the *prt6.2-12* SNP. Nested PCR was carried out using the BM93 + BM94 primers for the external PCR and BM97 + BM98 for the internal PCR. Samples were digested with BclI for 6 hours at 55°C. Wild-type plants are expected to be undigested (219 bp), while mutants will be cleaved to 199 bp + 30 bp. u = undigested control, d = digested. Plants #1, 2 and 3 carry the *Brprt6.2-12* SNP (as heterozygotes), while #4 appears to be wild-type. Plant #3 was used as the parent for double cross with *prt6.3-1*. **b.** Sanger sequencing chromatogram of the *Brprt6.3-1* SNP region after PCR with BM36 + BM37. A heterozygous C>T mutation is visible, resulting in the substitution of an Arginine (CGA) for a premature stop codon.

A heterozygotic double mutant was identified in the F1 generation and self-fertilized. 80 plants in the resulting F2 population were then screened for homozygous *prt6.2-12* and *prt6.3-1* mutations using DMAS-qPCR. Two candidate double homozygous mutants were isolated and confirmed by Sanger sequencing – *Brprt6.2prt6.3* #68 and #80 (Fig. 4.13). F3 seeds were collected from each of these lines. I also collected seeds from plant #67, which was genotyped as wild-type for both SNPs by DMAS-qPCR (Fig. A12 – Appendix A). As mentioned earlier,

'wild-type' plants re-isolated from the TILLING collection can serve as appropriate controls for the presence of persisting background mutations. It should be noted however, that the exact profile of segregating background mutations will likely differ in any two plants from the population. Unlike *Brate1ate2* mutant plants (shown in Fig. 4.11), the *Brprt6.2prt6.3* mutant lines exhibited a wild-type-like ontogeny (Fig. A13 - Appendix A), indicating their suitability for further characterisation, including via the transient expression protocol devised earlier (Fig 4.2).

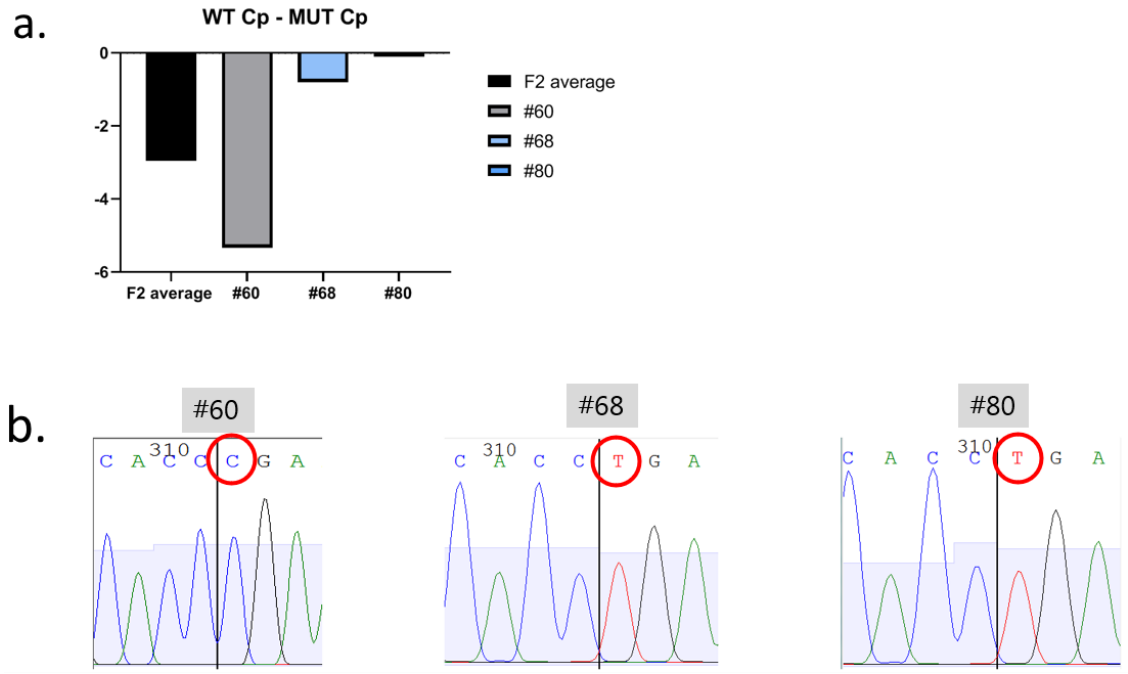

Figure 4.13. Genotyping of *prt6.2-12* in the *Brprt6.2prt6.3* F2 population. a. DMAS-qPCR genotyping results showing the difference in Cp values obtained from the wild-type and mutant specific qPCRs. The average difference for the F2 population is shown in the black column. A predicted 'wild-type' plant #60 and two candidate homozygous double mutants #68 and #80 are shown. Primer pairs used for the wild-type and mutant specific qPCRs were qBM247 + qBM246 and qBM248 + qBM246 respectively. **b.** Sanger sequencing chromatograms for the *prt6.2-12* SNP site. As predicted based on DMAS-qPCR, #60 contains the wild-type arginine codon (CGA) while an early stop codon (TGA) is present in #68 and #80.

4.4 Validating loss-of-function in *B. rapa* N-degron pathway mutants

4.4.1 Destabilizing X-LUC reporters are stabilized in *Brprt6.2prt6.3*

To validate that the N-degron pathway was indeed disrupted in the *Brprt6.2prt6.3* double mutants, I employed the agroinfiltration method developed earlier to assess whether the stability of the X-LUC N-degron pathway reporters was altered. The canonically stable Met-LUC and the destabilizing Asp-LUC and Arg-LUC reporters were transiently expressed in *Brprt6.2prt6.3* lines #68 and #80 alongside an R-o-18 wild-type control and the #67 wild-type line re-isolated from the TILLING collection. LUC enzymatic activity was quantified (Fig. 4.14a) and normalized to *LUC* transgene expression (Fig. 4.14b). A clear increase in Arg-LUC and Asp-LUC stability was observed in the *Brprt6.2prt6.3* mutants (Fig. 4.14c), while Met-LUC stability was unchanged.

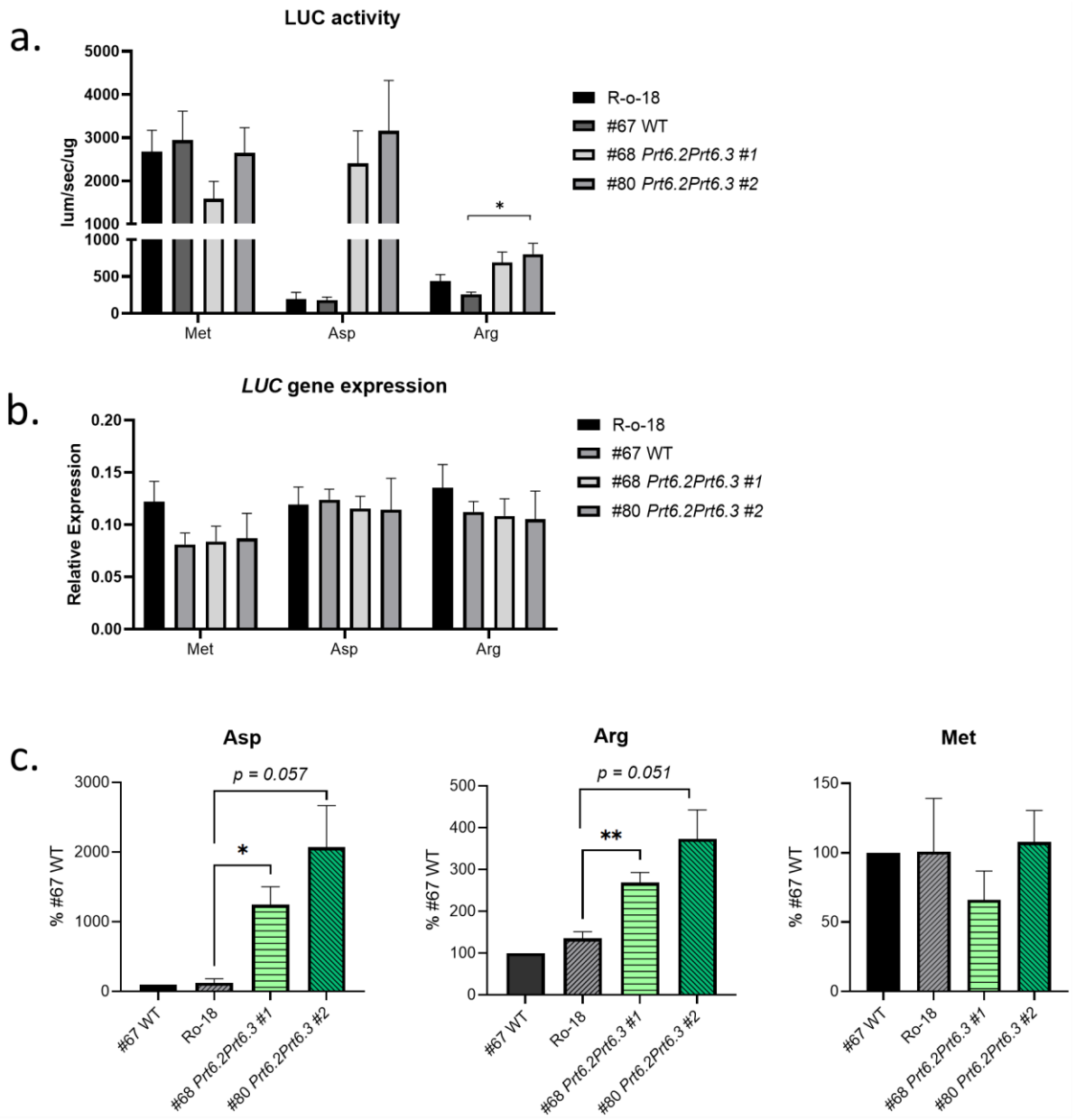

Figure 4.14. Stabilization of N-terminal Asp and Arg in *BrPrt6.2Prt6.3*. The indicated X-LUC reporters were transiently expressed in *B. rapa* plants as described earlier. All columns in **a-c** represent the means +/- SEMs of 5 independent biological replicates, except for R-o-18 Asp-LUC where 3 independent replicates were performed. **a.** Met-LUC, Asp-LUC and Arg-LUC enzymatic activity values (un-normalized) in each genotype. The activity of each construct was compared between genotypes by one-way ANOVA. Asterisk indicates statistical significance ($p<0.05$). **b.** Expression of the *LUC* transgene relative to *BrGAPDH*. **c.** Normalized LUC stability (LUC activity / *LUC* relative expression) expressed as a % of the value obtained for #67 wild-type (WT) per replicate. Asterisks indicate statistical significance ($p<0.05$) after one-way ANOVA repeated comparison to the R-o-18 wild-type. No statistically significant difference was observed among plants infiltrated with the Met-LUC construct.

As PRT6 also directly recognizes N-terminal lysine (Lys) and histidine (His) (Fig. 1.2), I next investigated whether these X-LUC reporters were stabilized in the *Brprt6.2prt6.3* lines (Fig. 4.15). Both Lys-LUC and His-LUC appeared to be stabilized in #68 *Brprt6.2prt6.3* compared to wild-type plants, indicating that the entire cohort of PRT6-recognized N-termini are stabilized in this line. It is unclear why His-LUC does not appear to be stabilized in *Brprt6.2prt6.3* line #80, and additional biological replicates may be necessary to confirm this observation.

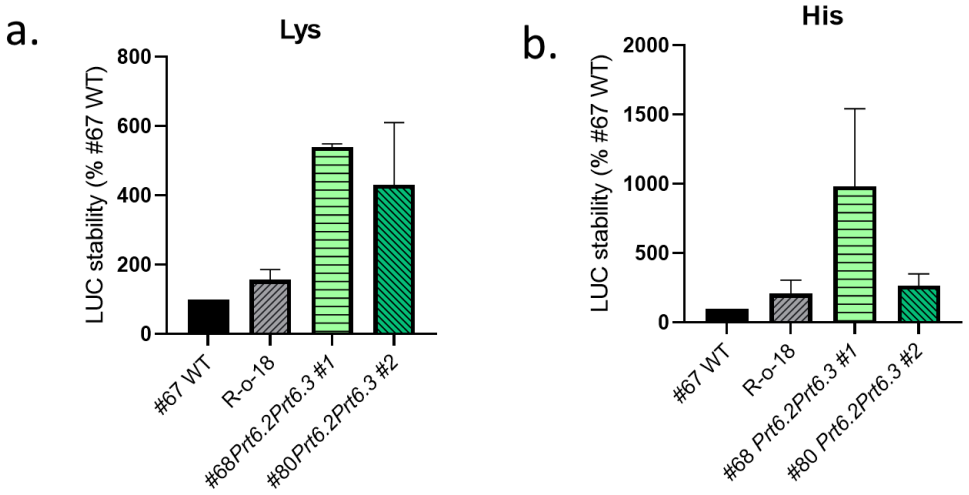

Figure 4.15. Transient expression of Lys and His-LUC in *Brprt6.2prt6.3*. a. Lys-LUC and **b.** His-LUC reporters were transiently expressed in *B. rapa* plants as described earlier. LUC activity values normalized to the relative expression of the *LUC* transgene are shown and expressed as a % of the value obtained for the #67 wild-type line. Columns indicate means + SEM after 2 independent biological replicates.

4.4.2 X-LUC transient expression in *B. rapa* ATE lines

As the transient expression protocol was not feasible in *Brate1ate2* double mutants for the reasons described in section 4.3.4, I instead tested whether LUC reporters bearing destabilizing N-terminal residues were stabilized in the *Brate1 +/- ate2 -/-* mutant which exhibits a wild-type like morphology. No stabilization of the Asp-LUC reporter was observed in this line in a preliminary experiment, suggesting that the presence of a single allele of wild-type *BrATE1* is sufficient for normal N-degron pathway function (Fig. 4.16). This result is similar to previous findings in *Arabidopsis* that have indicated functional redundancy among Arg-transferases (Graciet *et al.*, 2009).

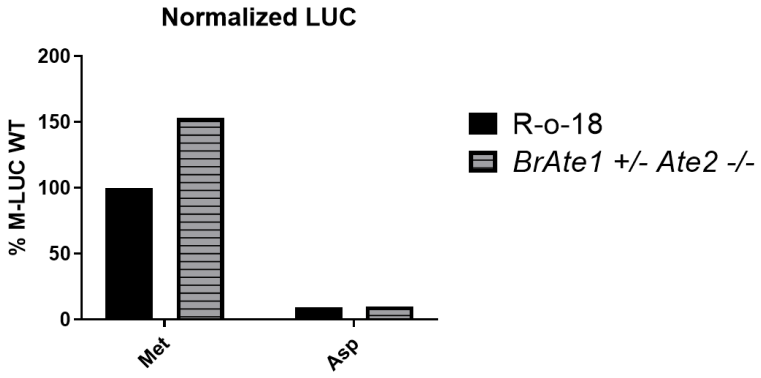

Figure 4.16. Transient expression of X-LUC reporters in *Brate1+/- ate2-/-*. Normalized Met-LUC and Asp-LUC stability transiently expressed in R-o-18 wild-type or *Brate1 +/- ate2 -/-* plants. X-LUC reporters were transiently expressed as described earlier and LUC activity was normalized to activity of the GUS reference protein. Data from one replicate is shown. Un-normalized LUC and GUS activities are shown in Fig. A14 (Appendix A).

4.4.3 Discussion

These results describe the successful isolation of the first *B. rapa* N-degron pathway mutants from a TILLING collection. Interestingly, the *Brate1ate2* double mutant exhibited significantly compromised early plant development, culminating in seedling lethality (Fig. 4.11). *Arabidopsis ATE* genes are known to contribute to shoot and leaf development (Graciet *et al.*, 2009), and a shoot meristem regulator known as LITTLE ZIPPER 2 (ZPR2) is directly targeted for degradation by the N-degron pathway (Weits *et al.*, 2019). However the *B. rapa* phenotype is markedly more severe than that of an *Arabidopsis ate1ate2* mutant. This may suggest the presence of additional *B. rapa* specific N-degron pathway substrates whose removal is required for seedling development to proceed. Further experiments will be necessary to investigate whether this may be the case. For example, proteomic approaches could reveal whether any proteins with known roles in development have altered abundance in *Brate1ate2.*

The early lethality of *Brate1ate2* restricts its experimental utility, and it was not possible to assess the loss of N-degron pathway function via transient expression of the X-LUC N-degron pathway reporters in this line. Notably, the combination of the heterozygous *Brate1* +/- SNP with a homozygous *ate2* mutation resulted in plants with a wild-type like morphology, and a

seemingly functional N-degron pathway (Fig. 4.16), suggesting functional redundancy of the *B. rapa* Arg-transferases (as is the case in *Arabidopsis* (Graciet *et al.*, 2009)). On this basis, detailed characterisation of a *Brate1 +/- ate2 -/-* line is not likely to be a suitable approach to investigate the biological functions of the *B. rapa* N-degron pathway.

In response to these findings, I next generated a *Brprt6.2prt6.3* line, containing early stop codon mutations in the two most strongly expressed *B. rapa* homologs of *PRT6*. *Brprt6.2prt6.3* mutants develop similarly to wild-type plants (Fig. A12) and were compatible with the agroinfiltration-based transient expression protocol. The dramatically increased stability of Asp-LUC and Arg-LUC reporters in both *Brprt6.2prt6.3* lines resoundingly indicates that Arg/N-degron pathway function is impaired by these mutations (Fig. 4.14). Notably, *LUC* transgene expression was very similar among all genotypes and reporter constructs (Fig. 4.14b), indicating that the differential LUC activities observed are attributable to differences at the protein level. Remarkably, the Asp-LUC construct was stabilized to the levels of Met-LUC, while the increase in Arg-LUC stability was less pronounced. This could suggest that the presence of *PRT6.2* and *PRT6.3* promote the arginylation of Nt Asp, which is a pre-requisite for its recognition as a primary destabilizing residue (Fig. 1.2). Importantly, the comparable results obtained for the two wild-type lines (R-o-18 and #67 re-isolated from the TILLING collection) suggest that residual background mutations segregating in the TILLING lines are unlikely to influence the outcomes of these experiments. Lys-LUC also appeared to be stabilized in both *Brprt6.2prt6.3* lines, while His-LUC was stabilized in *Brprt6.2prt6.3* #68 (Fig. 4.15).

Together, this data suggests that all peptides bearing N-terminal residues directly targeted by PRT6 are at least partially stabilized in the *Brprt6.2prt6.3* mutants. Correspondingly, I primarily utilized this line to investigate the physiological roles of the *B. rapa* N-degron pathway in more detail in the forthcoming Chapter 5. The function of the *BrPRT6.1* homolog remains to be investigated and particularly whether its removal from *Brprt6.2prt6.3* lines (i.e. in a *Brprt6.1prt6.2prt6.3* triple mutant) would lead to a further increase in the stabilization of model X-LUC N-degron pathway substrates,or would yield a similar phenotype to the *Brate1ate2* line. However, it is clear from the stabilization of N-terminal Asp, Arg, Lys and His in *Brprt6.2prt6.3* that the retained presence of *BrPRT6.1* alone is not sufficient to operate a functional N-degron pathway.

4.5. *B. rapa* PRT1 mutant lines

The BLASTp analysis shown in Fig. 4.8 revealed two *B. rapa* proteins homologous to the *Arabidopsis* N-recognin PRT1 which is responsible for the degradation of peptides bearing the aromatic residues phenylalanine (Phe), tyrosine (Tyr) and tryptophan (Trp) at the N-terminus (Fig. 1.2; Stary *et al.*, 2003). *BrPRT1.1* and *BrPRT1.2* both appear to be highly expressed across a range of tissues (Fig. 4.8b). I obtained M_3 seeds from the RevGenUK *B. rapa* TILLING collection (Stephenson *et al.*, 2010) containing SNP mutations occurring at splice sites within each gene, which were designated *Brprt1.1-5* and *Brprt1.2-5* respectively. It should be noted that SNPs located at these exon-intron boundaries can lead to modified splicing events that impact translation efficiency (Yang *et al.*, 2009; Faber *et al.*, 2011). Two candidate *Brprt1.1-5* homozygous mutants were identified with DMAS-qPCR. Despite an otherwise wild-type like morphology, neither plant produced any seeds (Fig. A15 – Appendix A).

Homozygous *Brprt1.2-5* mutants were capable of producing seeds, however, no increase in the activity of Phe or Tyr-LUC was observed in this line in a preliminary experiment (Fig. 4.17), likely because of functional redundancy with *BrPRT1.1*. Generation of a *Brprt1.1prt1.2* double mutant should be a priority for future studies to investigate the physiological roles of the PRT1 branch of the *B. rapa* N-degron pathway.

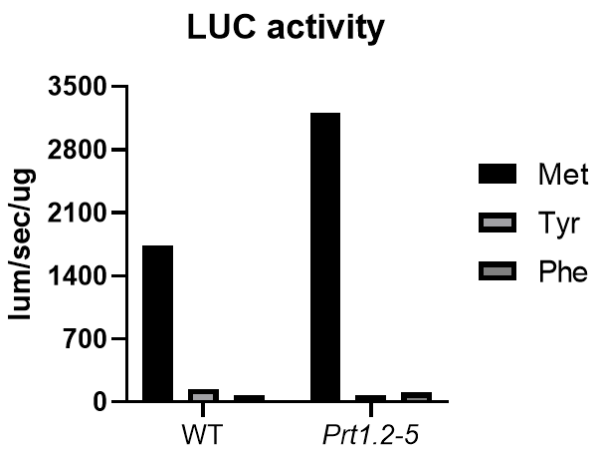

Figure 4.17. Transient expression of X-LUC reporters in *Brprt1.2-5*. X-LUC reporters bearing either Met, Tyr or Phe at the N-terminus were transiently expressed in wild-type or *Brprt1.2-5* mutant plants. Raw LUC activity measurements from a single experiment are shown.

5

The physiological roles of the *B. rapa* N-degron pathway

5.1 Introduction and aims

The previous chapters have described novel roles of the *Arabidopsis* N-degron pathway as a regulator of plant immune responses, the characterisation of the *B. rapa* N-degron pathway and the isolation of the first *B. rapa* N-degron pathway mutants. This final results chapter aims to synthesize the knowledge and tools developed in Chapters 3 and 4 respectively to interrogate the physiological functions of the *B. rapa* N-degron pathway, particularly in the context of its potential contribution to the immune response. As the response to flagellin is well conserved in plants including *Brassica* crops (Lloyd *et al.*, 2013), elicitation of PTI using flg22 is particularly suitable for a direct comparison of the roles of the N-degron pathway during immunity in these species.

Initially, I investigated altered gene expression in the *Brprt6.2prt6.3* double mutant in detail, including via RNA-Seq analysis of its global transcriptomic response to flg22. This is followed by assessment of other PTI hallmarks including flg22-induced ROS assays, MAPK phosphorylation immunoblots and seedling growth inhibition experiments. These findings are used to compare and contrast the roles of the *Arabidopsis* and *B. rapa* N-degron pathways in regulating plant immunity and highlight promising avenues for future research on the potential exploitation of the N-degron pathway for crop development.

5.2 The N-degron pathway regulates hypoxia-response genes in *B. rapa*

Expression levels of selected genes in *Brprt6.2prt6.3* seedlings were compared by RT-qPCR with wild-type plants, as well as *prt6.2-12* and *prt6.3-1* single mutants. Initially, I analysed the expression of *B. rapa* homologs of key hypoxia-response markers (*Hb1*, *PCO2* and *HRE2*) whose constitutive elevation is a characteristic feature of *Arabidopsis* N-degron pathway mutants including *ate1ate2* and *prt6-1*. Both *Brprt6.2prt6.3* double mutant lines (#68 and #80; see section 4.3.5) showed enhanced expression of *BrHb1* (Bra001958), *BrPCO2* (Bra025636) and *BrHRE2* (Bra021401) compared to wild-type R-o-18 or the #67 wild-type line re-isolated from the TILLING collection (Fig. 5.1). Although the average expression level was visibly different between either of the double mutant lines and the two wild-types, differences for *BrPCO2* and *BrHRE2* were not found to be statistically significant due to variation. Notably, single mutation of either *BrPRT6.2* or *BrPRT6.3* did not result in elevated expression of these hypoxia-marker genes. This indicates that the combined disruption of both genes in the *Brprt6.2prt6.3* lines is necessary and sufficient for N-degron pathway malfunction.

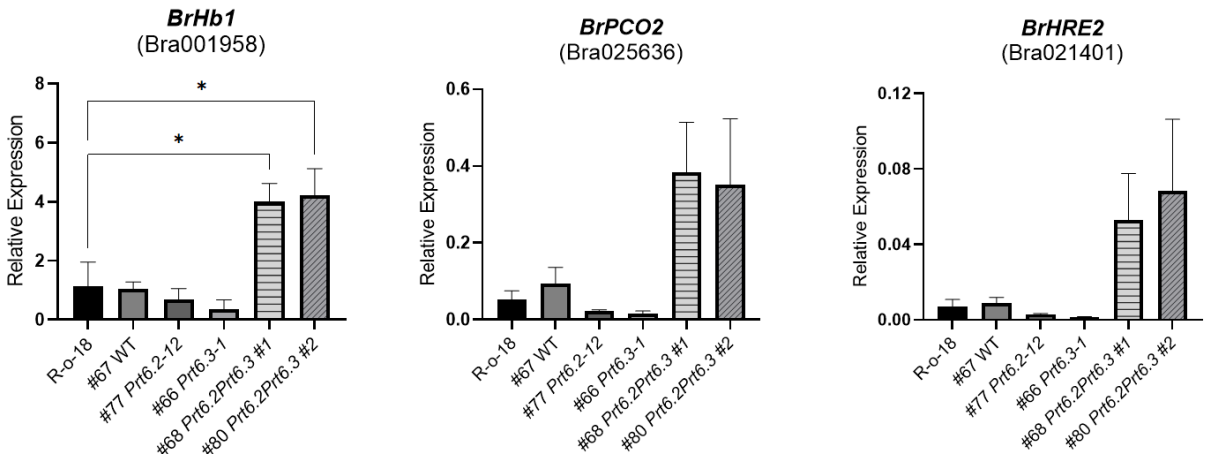

Fig 5.1. Hypoxia-response marker genes are overexpressed in *Brprt6.2prt6.3*. RT-qPCR analysis of orthologs of hypoxia-response genes in 3-day-old *B. rapa* seedlings. *BrGAPDH* (Bra016729) was used as a reference gene. Columns represent means with SEM error bars. Data for R-o-18, #67 WT, #68 *prt6.2prt6.3 #1* and #80 *prt6.2prt6.3 #2* is from 3 independent replicates, while 2 replicates were performed for the single mutants #77 *Prt6.2-12* and #66 *Prt6.3-1*. Asterisks indicate statistical significance ($p<0.05$) after one-way ANOVA comparisons with R-o-18 wild-type seedlings.

5.3 The N-degron pathway regulates some flg22-responsive genes in *B. rapa*

Having validated that *Brprt6.2prt6.3* plants accumulate model N-degron pathway substrates (Figs. 4.13 and 4.14) and display the constitutive hypoxia-response (Fig. 5.1) characteristic of *Arabidopsis* N-degron pathway mutants, I subsequently used these lines to investigate the roles of the *B. rapa* N-degron pathway in response to flg22. Seedlings of R-o-18, #67 wild-type, #68 *prt6.2prt6.3 #1* and #80 *prt6.2prt6.3 #2* were treated with 1 µM flg22 or an equivalent volume of mock solution (dH_2O) for 1 hour, mirroring the experimental procedure used for the *Arabidopsis* RNA-Seq experiment described in section 3.2. Preliminary RT-qPCRs confirmed the activation of key immune genes in all lines after flg22 treatment, confirming the successful activation of PTI in these experimental conditions (Fig. 5.2).

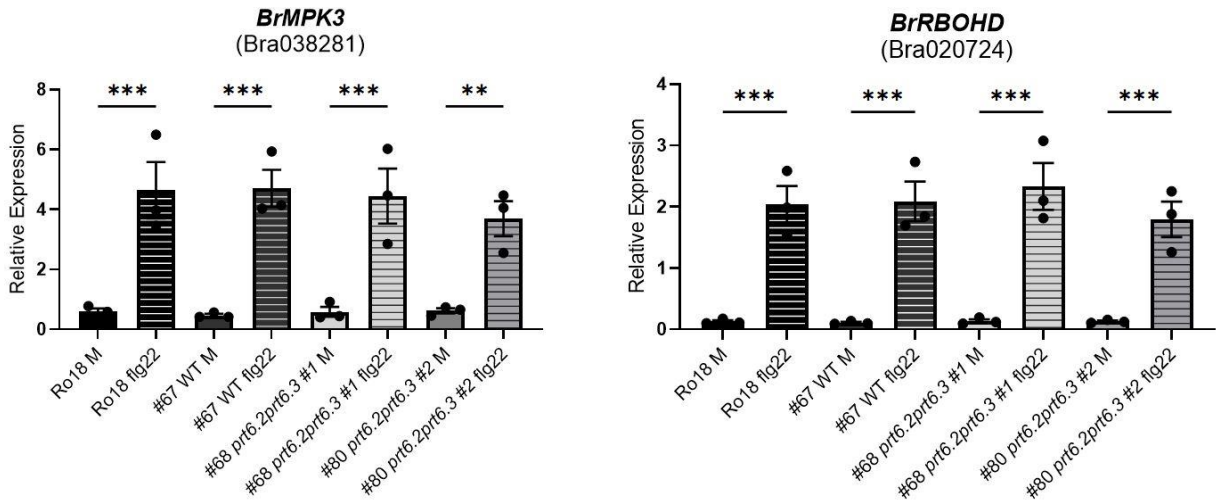

Figure 5.2. Activation of PTI marker genes after flg22 treatment in *B. rapa*. RT-qPCR analysis of *B. rapa* seedlings subjected to 1 µM flg22 or mock (M) treatment for 1 hour. Relative expression of *BrMPK3* and *BrRBOHD* are displayed. *BrGAPDH* was used as a reference gene. Means +/- SEM from 3 independent experiments are shown. Asterisks indicate statistical significance after one-way ANOVA comparisons of mock and flg22-treated samples from each genotype (** = $p \leq 0.01$, *** = $p \leq 0.001$).

RNA samples isolated from the #67 wild-type line and #68 *prt6.2prt6.3* were subsequently sent to BGI Genomics for RNA-Seq analysis (Hong Kong). The #67 wild-type line re-isolated from the TILLING population was chosen as the wild-type control (instead of R-o-18) to mitigate for the potential effects that any remaining background SNPs may have on gene expression.

5.3.1 Flg22-responsive genes

RNA from three independent replicates of wild-type and *Brprt6.2prt6.3* mutant samples treated with water (mock) or 1 µM flg22 were sequenced using the DNBseq™ technology and reads were aligned to the *B. rapa* v3.0 genome (Chiffu-401-42 cultivar) (Zhang *et al.*, 2018). An average of 84.79% of clean reads were mapped to the reference genome (ranging from 83.7-86.6%). A total of 38,933 genes were retrieved in the mRNA population, 37,925 of which had been previously identified.

Cut-off values identical to those used to analyse the *Arabidopsis* dataset (adjusted p-value < 0.05, $|\log_2$ of fold-change$|$ > 0.585) were applied to determine the sets of DEGs (Fig 5.3). In wild-type plants, 5,632 genes were up-regulated in response to flg22, while 3,995 genes were down-regulated. In the *Brprt6.2prt6.3* mutant, a slightly higher figure of 5,964 genes were elicited by flg22, with 4,123 being down-regulated (Fig. 5.3a). Venn diagram analysis revealed 8,136 flg22-responsive genes commonly found in both genotypes, with 1,491 exclusively responding in wild-type plants and 1,951 exclusive to the *Brprt6.2prt6.3* mutants (Fig. 5.3b).

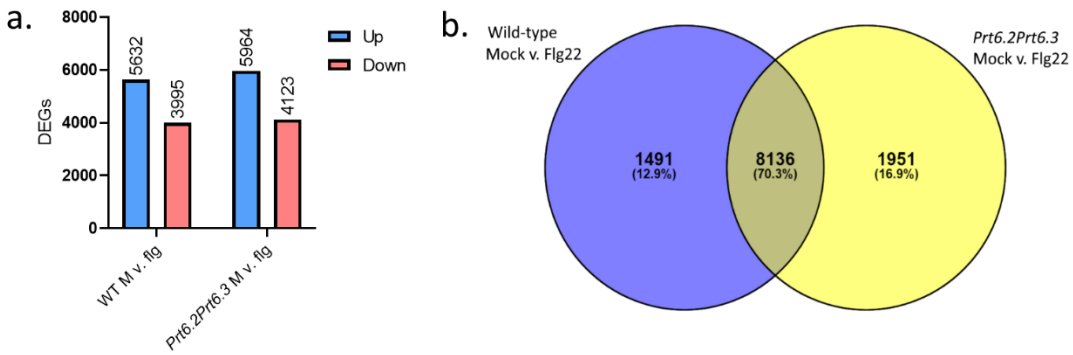

Figure 5.3. Mock v. flg22 DEGs in wild-type and *Brprt6.2prt6.3*. a. Flg22-responsive genes in wild-type and *Brprt6.2prt6.3* mutant seedlings after cut-off values were applied (p<0.05, fold-change >1.5). **b.** Venn diagram showing overlap of flg22-responsive genes in wild-type and *Brprt6.2prt6.3* seedlings. This panel was prepared using Venny 2.1 (https://bioinfogp.cnb.csic.es/tools/venny/ Oliveros, 2007).

5.3.2 GO enrichment analysis

To investigate the biological pathways that were over-represented in each dataset, I performed GO term enrichment analyses. GO analysis can be highly challenging in non-model organisms

like *B. rapa* where knowledge of gene function is limited or poorly annotated (Duarte *et al.*, 2021). To overcome this, I instead performed GO analysis on the *Arabidopsis* homologs of the *B. rapa* DEG datasets. Homologous genes were identified in collaboration with Joseph Beegan and Prof. Frank Wellmer from the Plant Developmental Genetics laboratory at Trinity College Dublin. Briefly, *B. rapa* gene coding sequences were queried against the *Arabidopsis* TAIR10 genome via standard nucleotide BLAST (BLASTn). An E-value threshold of 1e-6 was applied and a maximum of 6 hits per query gene were accepted (see also section 2.2.9). It can be expected that up to three paralogous genes in *B. rapa* may correspond to a single *Arabidopsis* gene (Stephenson *et al.*, 2005) as a result of an ancient chromosome triplication event in *Brassicaceae* which occurred after the *Arabidopsis-Brassicaceae* divergence (Lysak *et* al., 2005).

With these parameters, the orthology analysis identified 7,944 *Arabidopsis* genes corresponding to the 9,627 *B. rapa* genes (Fig. 5.3) differentially expressed in wild-type plants after flg22 treatment. This dataset was then assessed for GO pathway enrichment. As could be expected, categories including 'protein phosphorylation', 'defense response to bacterium' and 'response to salicylic acid' were among the most significantly enriched (Fig. 5.4a). The same analysis was also performed on 8,068 *Arabidopsis* genes considered orthologous to the 10,087 flg22-responsive DEGs in *Brprt6.2prt6.3* (Fig. 5.4b). Similar immunity-related GO categories were also enriched in this dataset, alongside a small number of notable differences (e.g. 'MAPK cascade' and 'response to jasmonic acid' enriched in *Brprt6.2prt6.3*). This overview suggests that although the *Brprt6.2prt6.3* response to flg22 does not appear to be severely compromised, specific genes and pathways may be misregulated.

Considering the results from the overlap analysis shown in Fig. 5.3b, I next investigated the 1,491 DEGs exclusively flg22-responsive in wild-type *B. rapa* to identify pathways enriched specifically in wild-type *B. rapa*. Significantly enriched GO categories among the 1,455 corresponding *Arabidopsis* homologs included multiple photosynthesis-related terms, 'response to salicylic acid' and 'positive regulation of reactive oxygen species' (Fig. 5.4c). The 1,967 *Arabidopsis* genes homologous to the 1,951 DEGs exclusively identified as flg22-responsive in *Brprt6.2prt6.3* were also analysed, with 'protein phosphorylation' and 'regulation of jasmonic acid mediated signaling' among the most strongly enriched GO terms (Fig 5.4d).

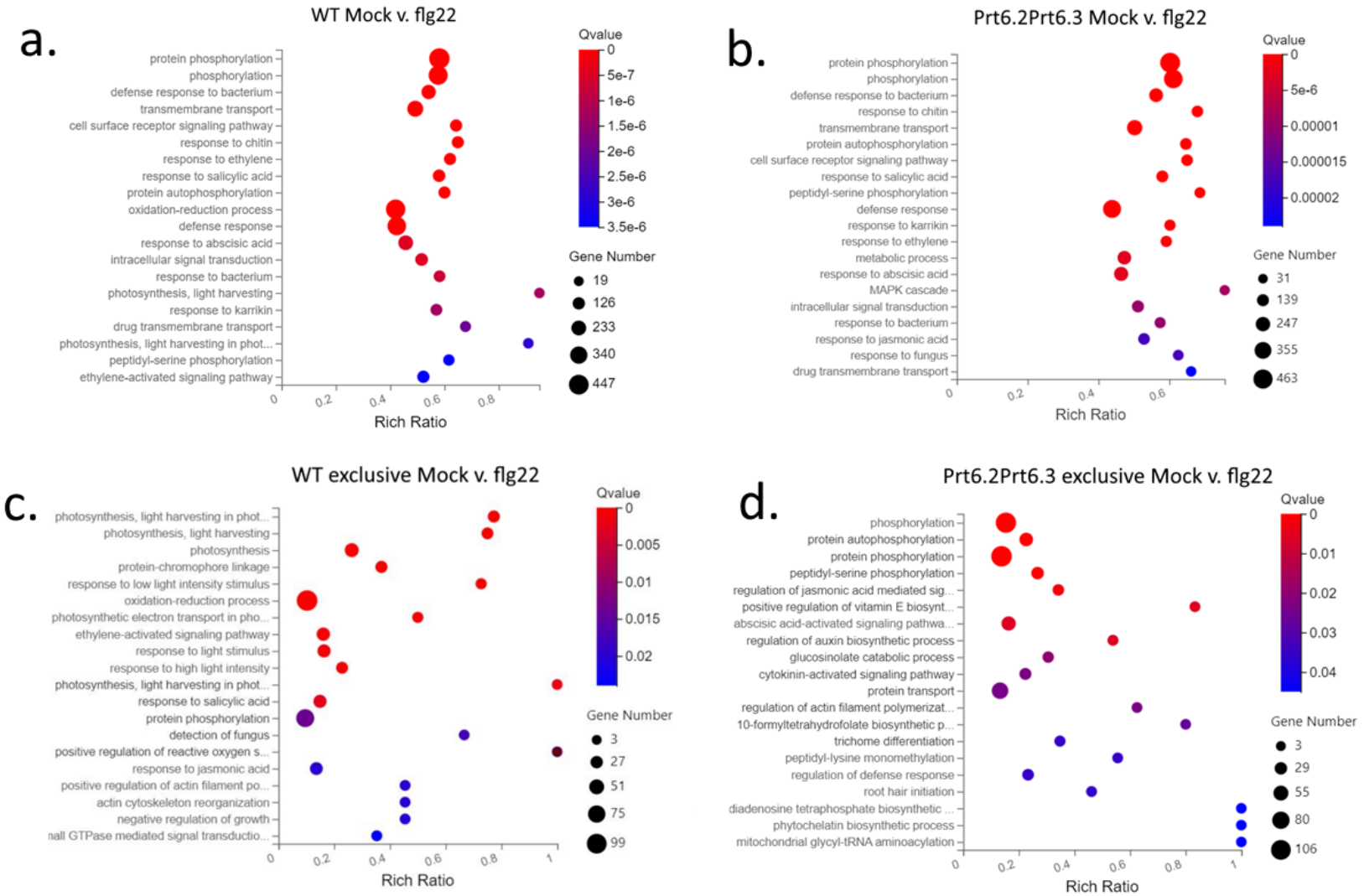

Fig. 5.4. GO enrichment analysis of flg22-responsive DEGs. Graphics displaying the most strongly enriched GO categories among DEGs from indicated comparisons. GO analysis and figures were prepared using the Dr. Tom analysis platform from BGI genomics. **a.** Wild-type mock v. flg22 **b.** *Brprt6.2prt6.3* mock v. flg22 **c.** DEGs exclusively found in wild-type mock v. flg22 dataset and **d.** DEGs exclusively found in *BrPrt6.2Prt6.3* mock v. flg22 dataset.

5.3.3 *Brprt6.2prt6.3* vs. wild-type

The two genotypes were also compared to each other directly after each treatment (Fig. 5.4). This led a smaller subset of genes being called as differentially expressed. In the comparison between mock-treated samples, 30 genes showed increased expression in the *Brprt6.2prt6.3* line compared to the wild-type, while 36 genes exhibited reduced expression (Fig. 5.4a). Flg22 treatment potentiated the differences between genotypes, with the total number of DEGs almost doubling from 66 to 129. Of these, 73 showed elevated expression in the *Prt6.2Prt6.3* mutant and 56 genes had reduced expression (Fig. 5.5a). An overlap analysis of these datasets revealed 24 genes that were differentially expressed in both conditions, with 42 genes only differentially expressed in mock-treated samples and 105 genes detected as differentially expressed only in the flg22-treated comparison (Fig. 5.5b).

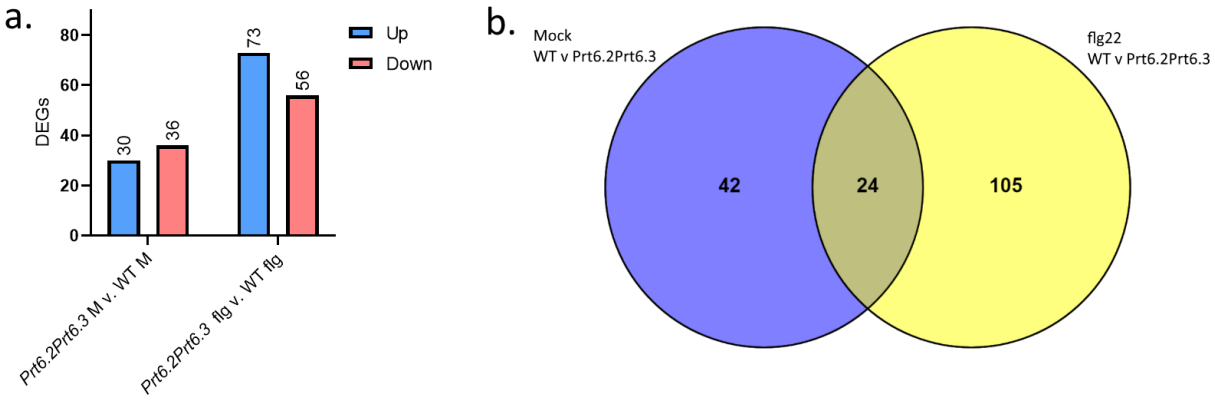

Figure 5.5. *Brprt6.2prt6.3* v. wild-type DEGs after flg22 or mock treatment. a. DEGs in *Brprt6.2prt6.3* versus wild-type seedlings after mock or flg22 treatment (cut-off values: $p<0.05$, fold-change >1.5). **b.** Venn diagram showing overlap of DEGs in the *Brprt6.2prt6.3* vs. wild-type comparison in mock or flg22-treated conditions. Diagram was created using Venny 2.1 (Oliveros, 2007).

GO enrichment analysis was also performed with these two DEG datasets (Fig. 5.6), after retrieving the gene identifiers of *Arabidopsis* homologs, as outlined above. Notably, hypoxia-related terms such as 'detection of hypoxia', 'response to hypoxia' and 'peptidyl-cysteine oxidation' feature in both the mock-treated and flg22-treated comparisons. Together with the data shown in Fig. 5.1, this data strongly indicates that regulation of the hypoxia response is a conserved role of the N-degron pathway in *Arabidopsis* and in *B. rapa.*

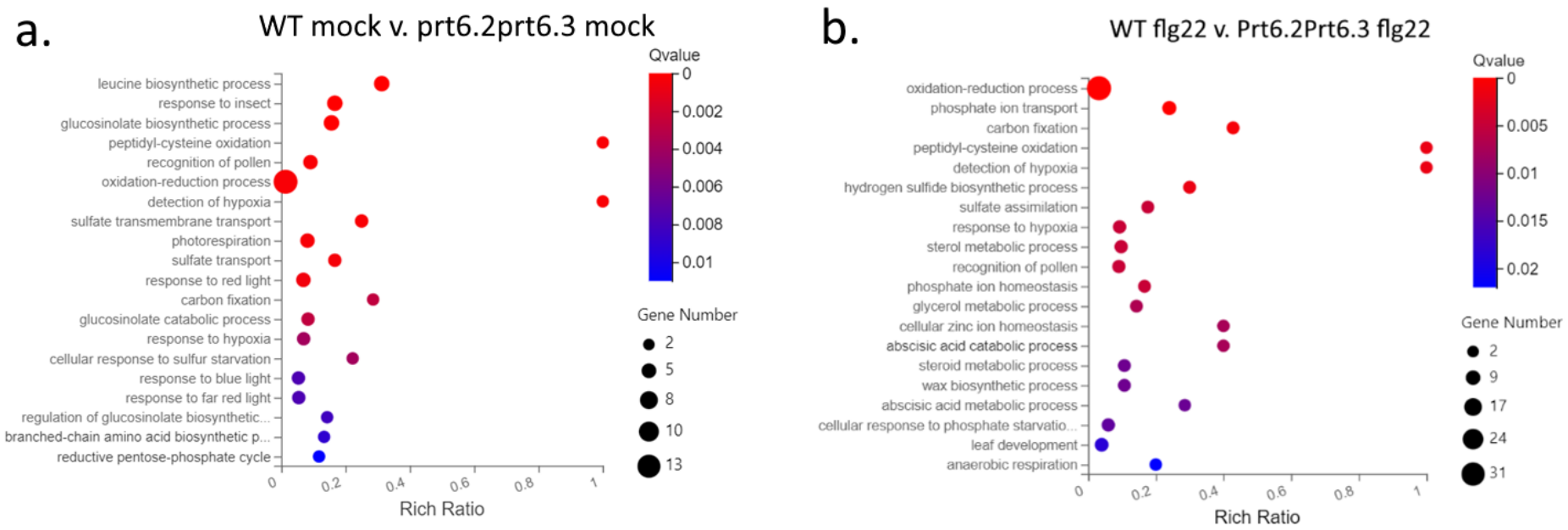

Fig. 5.6. GO enrichment of *Brprt6.2prt6.3* vs. wild-type DEGs after flg22 or mock treatment. Graphics displaying the most strongly enriched GO categories among DEGs from indicated comparisons. GO analysis and figures were prepared using the Dr. Tom analysis platform from BGI genomics. **a.** Wild-type mock v. *Brprt6.2prt6.3* mock **b.** Wild-type flg22 v. *Brprt6.2prt6.3* flg22.

Following the GO enrichment analysis, I screened the DEG datasets for specific genes-of-interest that are misregulated in *Brprt6.2prt6.3.* Complete lists of the DEGs identified in the wild-type vs. *Brprt6.2prt6.3* comparisons after both mock and flg22 treatment are included in Tables B2, B3, B4 and B5 in Appendix B. The 25 genes most strongly upregulated in *Brprt6.2prt6.3* compared to wild-type after flg22 treatment are shown in Table 5.1.

Table 5.1. Genes with highly elevated expression in *Brprt6.2prt6.3* flg22 vs. wild-type flg22. The 25 genes with most strongly enhanced expression in *Brprt6.2prt6.3* compared to wild-type after flg22 treatment. Average expression values (FPKM) indicated were provided by BGI Genomics.

GeneID	WT flg22 Expression	Prt6.2Prt6.3 flg22 Expression	log2FC	Padj	Direction	Description (predicted)
117126611	1.74E-05	63.12965361	21.78861728	4.90E-05	Up	Zeaxanthin epoxidase, chloroplastic
BGI_novel_G000579	0.176975827	82.2583941	8.86046678	1.20E-08	Up	NA
103846440	1.920544822	140.1411972	6.189221682	4.70E-14	Up	Plant cysteine oxidase 1
103838445	1.922858081	102.4238069	5.73515499	8.40E-12	Up	G-type lectin S-receptor-like serine/threonine-protein kinase At1g61390
BGI_novel_G000251	0.946393777	29.31910875	4.953256851	5.10E-03	Up	NA
103828296	29.84108138	906.6209379	4.925127758	4.10E-06	Up	1-aminocyclopropane-1-carboxylate oxidase 1
103846065	144.9443179	3862.511156	4.735968417	4.00E-49	Up	Non-symbiotic hemoglobin 1
103863926	97.41977611	1824.246856	4.226942489	3.70E-72	Up	Plant cysteine oxidase 2
103856111	45.48372219	847.1464426	4.219189156	6.40E-43	Up	Plant cysteine oxidase 1
103843716	23.6189243	371.912861	3.976949473	2.60E-27	Up	ERF71 / HRE2
103843350	87.72213246	1093.873706	3.640361487	9.30E-04	Up	LOB domain-containing protein 41
103858971	7.701071156	78.70640522	3.353350017	1.60E-03	Up	Delta(7)-sterol-C5(6)-desaturase 1
103862549	5.889708486	46.43246235	2.978865656	3.70E-02	Up	Uncharacterized
103872757	36.8011238	196.0934394	2.413719541	1.40E-10	Up	Uncharacterized
103872329	12.31884119	65.55326571	2.411801102	4.50E-03	Up	Uncharacterized
103835054	14.99240305	69.02895094	2.202969916	5.60E-03	Up	DETOXIFICATION 40
103870965	370.3514815	1252.392672	1.757719959	8.40E-12	Up	Hypersensitive-induced response protein 3
103871169	718.0583277	2278.531752	1.665931531	1.10E-04	Up	Stem-specific protein TSJT1
103862836	60.18912377	175.9691658	1.547747936	1.80E-03	Up	(+)-neomenthol dehydrogenase
103832423	56.32761633	157.0883845	1.479662182	3.60E-02	Up	Inosine-5'-monophosphate dehydrogenase 1
103851209	266.9155697	740.1519347	1.471437987	1.70E-03	Up	Stem-specific protein TSJT1
103842451	51.61557114	142.3322532	1.463384359	2.30E-03	Up	Uncharacterized
103863819	233.6679739	626.3231152	1.42244711	3.10E-03	Up	Phenolic glucoside malonyltransferase 1
103837285	95.81155041	255.7610449	1.41652505	6.40E-04	Up	Basic leucine zipper 1
103874000	54.23783216	144.6297048	1.414992469	1.80E-02	Up	Bhlh93

Several genes with notable predicted functions exhibit elevated expression in *Brprt6.2prt6.3* including putative hypoxia-related genes (e.g. *PCO1* – 103846440 and 103856111*, PCO2* - 103863926*, Hemoglobin 1 (Hb1)* - 103846065*, HRE2* - 103843716*, LBD41* – 103843350 and *CYP707A3 / ABA 8'-hydroxylase 3* - 10389129), likely immunity-related genes (e.g. *Hypersensitive-induced response protein 3* – 103870965 and *PR5-like receptor kinase* - 103856198), a calcium signaling-related gene *Calmodulin-like 12* (103860375) and *ACO1*

(103828296), an ortholog of the enzyme responsible for ethylene biosynthesis in *Arabidopsis* (Houben & Van de Poel, 2019). Note that *CYP707A3 / ABA 8'-hydroxylase 3* (10389129), *PR5-like receptor kinase* (103856198) and *Calmodulin-like 12* (103860375) are only visible in Table B5 (Appendix B), as they are not among the most strongly elevated genes shown in Table 5.1.

The average FPKM values for selected flg22-responsive genes with the increased expression in the *Brprt6.2prt6.3* line are displayed in Fig. 5.7.

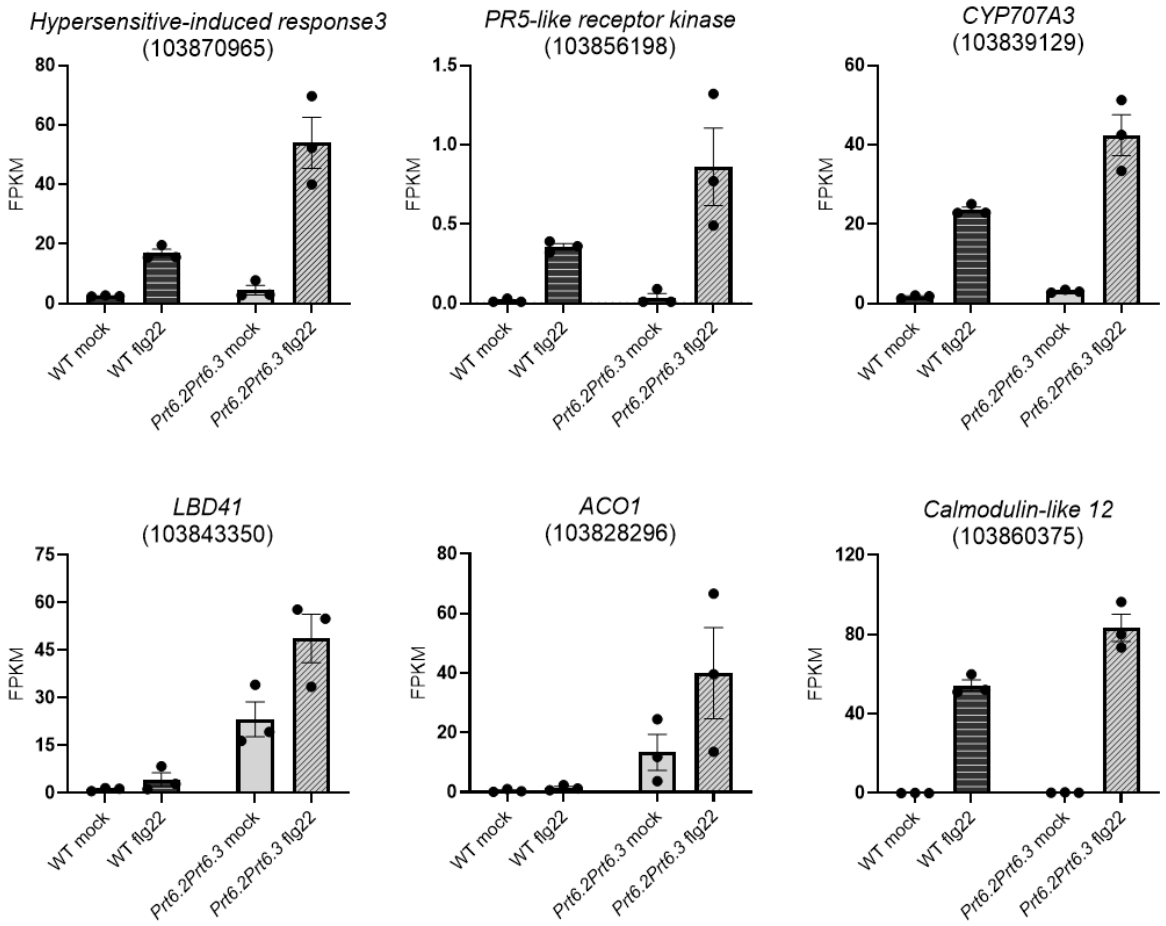

Figure 5.7. Flg22-responsive genes with increased expression in *Brprt6.2prt6.3*. Selected flg22-responsive genes with elevated expression in *Brprt6.2prt6.3* seedlings compared to wild-type after flg22 treatment. Columns represent means of FPKM values from 3 independent replicates +/- SEM.

In contrast, Table 5.2 displays the genes with the most strongly reduced expression in *Brprt6.2prt6.3* compared to wild-type after flg22 treatment. Notable genes in this dataset include the probable immune-related *Nuclear speckle RNA binding protein B / MKS1*

(103872924), three expansins (*EXPA12* – 103869925, *EXPA9* – 103847465 and *EXPA3* - 103867175) and a *GDSL-esterase / lipase* (103857011). *Nuclear speckle RNA binding protein B / MKS1* (103872924) and *EXPA3* (103867175) are not included in Table 5.2, but are visible in Table B4.

Table 5.2. Genes with strongly reduced expression in *Brprt6.2prt6.3* after flg22 treatment. List of the 25 DEGs with the most strongly reduced expression in *Brprt6.2prt6.3* versus wild-type after flg22 treatment. The average expression values shown were provided by BGI Genomics following RNA-Seq.

GeneID	WT flg22 Expression	Prt6.2Prt6.3 flg22 Expression	log2FC	Padj	Direction	Description (predicted)
BGInovelG000021	30.14710431	1.05E-05	-21.4481784	7.20E-05	Down	NA
117133380	31.90683618	0.186432404	-7.41906912	7.20E-05	Down	Non-classical arabinogalactan protein 30-like
103840832	250.3278772	2.040966507	-6.93842265	9.50E-22	Down	Uncharacterized
BGInovelG000587	58.60294056	0.681724509	-6.4256404	7.20E-05	Down	NA
103841255	21.52804018	0.680568002	-4.98333386	4.20E-02	Down	Cytochrome P450 71B8
BGInovelG000533	41.80601557	1.703393945	-4.61722652	3.60E-03	Down	NA
103856520	40.01409434	2.380196713	-4.07135554	1.70E-03	Down	Uncharacterized
117130004	26.00156813	1.70550989	-3.93032361	3.70E-02	Down	Uncharacterized
117131446	52.29771376	4.744493026	-3.46242204	2.50E-04	Down	Uncharacterized
103862179	48.54055586	4.737508308	-3.35699025	3.20E-03	Down	ECERIFERUM 2
117130584	84.23704601	8.819868369	-3.25562582	1.60E-05	Down	Uncharacterized
117130589	169.5252939	22.05852149	-2.94209255	3.30E-12	Down	Uncharacterized
117130799	74.3707849	13.2682991	-2.48675256	6.90E-04	Down	Uncharacterized
103837093	41.86193881	8.491019388	-2.30162946	4.00E-02	Down	BURP domain protein RD22
103869925	88.62085185	18.02219671	-2.29787132	6.80E-04	Down	Expansin-A12
103852947	233.8066238	57.00601483	-2.03612975	2.40E-04	Down	bZIP transcription factor 44
117126780	111.144155	27.55377839	-2.01211001	1.70E-03	Down	Transcription factor HEC1
103855508	378.7437656	95.67559225	-1.98499931	2.40E-07	Down	Probable protein phosphatase 2C 67
103847465	90.22426452	25.8337639	-1.80425762	2.50E-02	Down	Expansin-A9
103861006	149.0809193	45.86480296	-1.70063627	7.80E-03	Down	Uncharacterized
103845164	81.95860584	25.88049195	-1.6630304	3.40E-02	Down	Oxysterol-binding protein-related protein 4C
103836062	191.7495561	63.47500905	-1.59496264	5.10E-03	Down	Transmembrane 9 superfamily member 2
103857011	572.2339928	198.8091587	-1.52522098	3.00E-07	Down	GDSL esterase/lipase At5g55050
103869328	94.35232781	33.34441987	-1.50061276	4.60E-02	Down	NEP1-interacting protein-like 2
103834943	166.4592168	60.53731282	-1.45927221	3.20E-03	Down	Uncharacterized

In *Arabidopsis*, MKS1 (MAP4 kinase substrate 1) bolsters resistance against *P. syringae* by enabling an interaction between MPK4 and the transcription factor WRKY33 (Petersen *et al.*, 2010). Interestingly, several GDSL lipase genes are targets for WRKY33 and have been shown to contribute to resistance against *Botrytis cinerea* (Han *et al.*, 2019). Expansins primarily control cell wall loosening during development but have also been implicated in abiotic stress responses (Marowa *et al.*, 2016). The expression of both *PRT6.2* (103847459) and *PRT6.3* (103850043) also appeared to be reduced in the *Brprt6.2prt6.3* line, potentially indicating a positive feedback loop, where PRT6 proteins promote their own transcription. Notably, the

expression of *PRT6.3* was also repressed following flg22 treatment in both the wild type and the *Brprt6.2prt6.3* double mutant, suggesting a particular role of *PRT6.3* in PTI. The average FPKM values of selected genes with reduced expression in the *Brprt6.2prt6.3* line compared to wild-type after flg22 treatment are shown in Fig. 5.8.

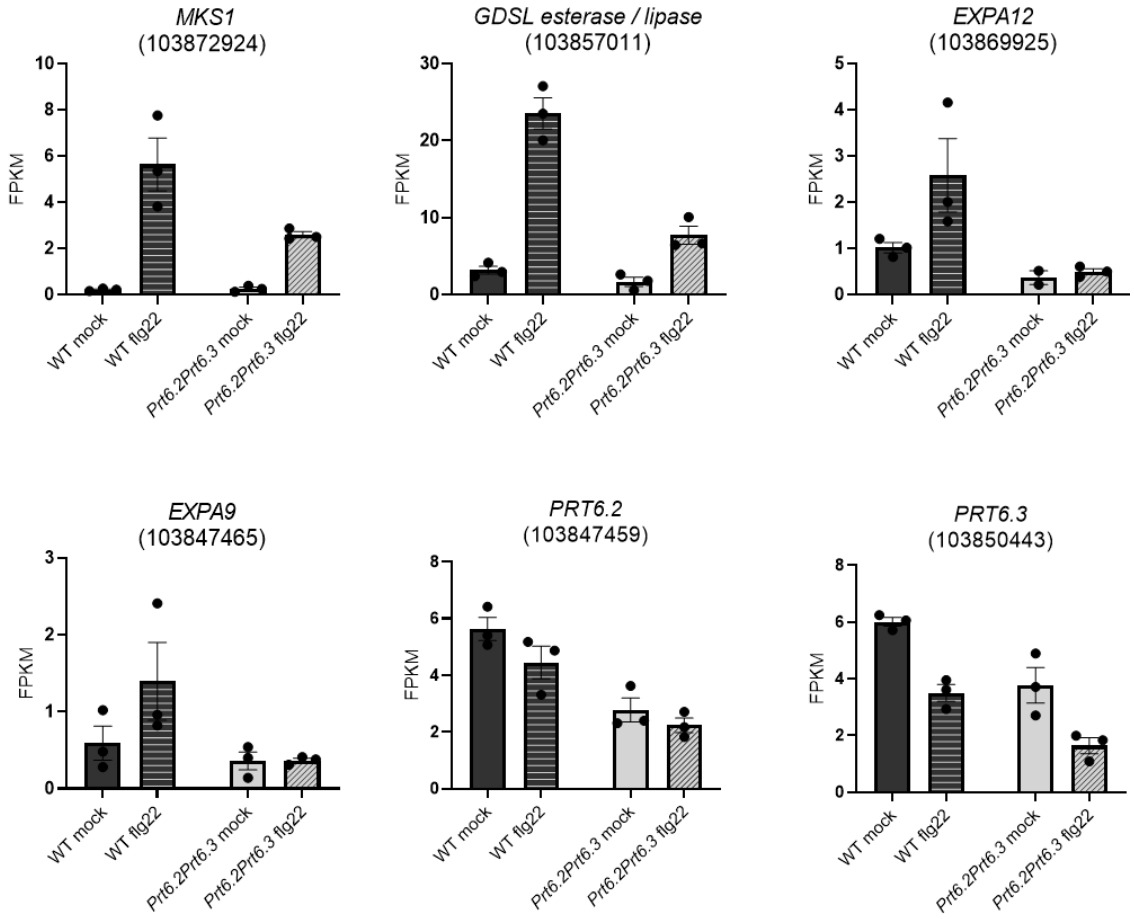

Figure 5.8. Genes with reduced expression in *Brprt6.2prt6.3* compared to wild-type. Selected genes with reduced expression in *Brprt6.2prt6.3* seedlings compared to wild-type after flg22 treatment. Columns represent means of FPKM values from 3 independent replicates +/- SEM.

Follow up RT-qPCRs on two genes of interest (*LBD41* and *GDSL-esterase / lipase*) validated that the transcriptional misregulation detected in the #68 *Brprt6.2prt6.3* line was also apparent in the second *Brprt6.2prt6.3* line #80 (Fig. 5.9), although the differences compared to the wild-type were not found to be statistically significant. Together with the retrieval of expected terms identified during GO analyses (e.g. 'response to hypoxia'), this data supports that the genes

identified as misregulated in the RNA-Seq experiment are indeed regulated by the N-degron pathway in *B. rapa*.

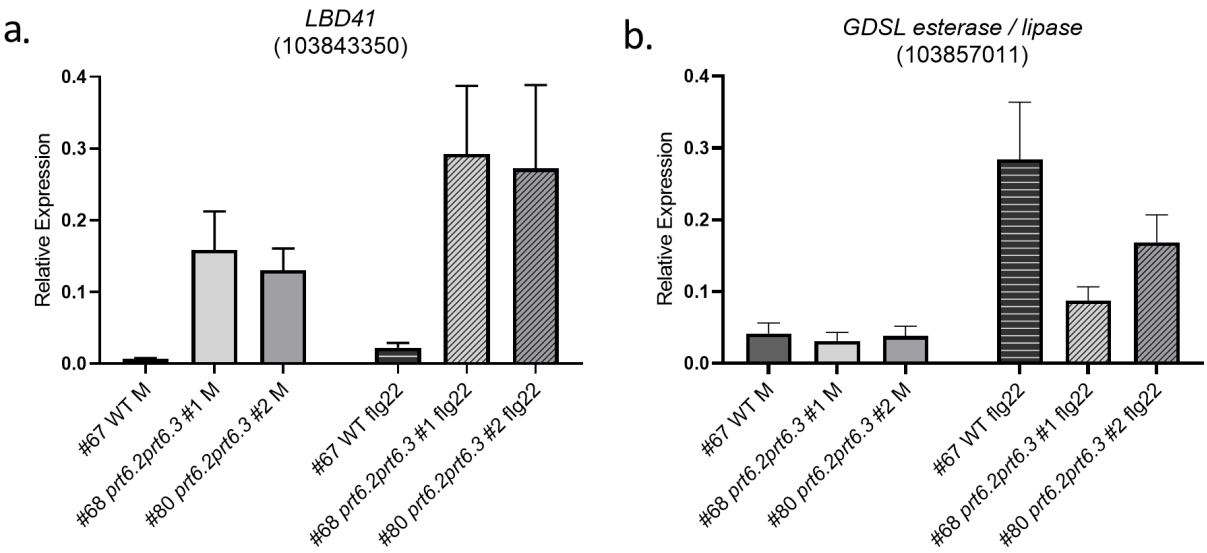

Figure. 5.9. RT-qPCR analysis of DEGs identified in *B. rapa* RNA-Seq experiment. RT-qPCR analysis of two **a.** *BrLBD41* and **b.** *GDSL esterase / lipase* (103857011) in wild-type and *Brprt6.2prt6.3* mutants. Gene expression was calculated relative to the *BrGAPDH* reference gene. Columns represent means of 3 independent replicates +/- SEM error bars. Differences between genotypes were not statistically significant after one-way ANOVA comparisons.

5.4 Comparing the roles of the N-degron pathway as a transcriptional regulator in *Arabidopsis* and *B. rapa*

5.4.1 Comparing the flg22 responses of wild-type *B. rapa* and *Arabidopsis*

The data shown in section 5.3 reveals positive and negative misregulation of numerous PTI-responsive genes in the *B. rapa* N-degron pathway mutant. To investigate whether the regulation of specific immune response pathways is a conserved role of the N-degron pathway in *Brassicaceae*, I sought to compare the transcriptomic datasets obtained from the *Arabidopsis* and *B. rapa* RNA-Seq experiments. To facilitate direct comparisons, the *Arabidopsis* genes homologous to the *B. rapa* DEG lists were first retrieved using BLAST as described previously in section 5.3.2.

Initially, I compared the flg22-responsive genes in wild-type *Arabidopsis* and wild-type *B. rapa* to assess the common features of PTI-induced transcriptional reprogramming (Fig. 5.10). In this case, 7,944 *Arabidopsis* homologs of the 9,627 *B. rapa* genes with altered expression after flg22 treatment were compared with the 4,250 flg22-responsive genes observed in Col-0. Over 60% of the differentially expressed genes identified in the *Arabidopsis* RNA-Seq experiment were also found in the converted *B. rapa* dataset (2,556/4,250 genes), indicating that the responses to flg22 in wild-type *Arabidopsis* and *B. rapa* are largely conserved and are thus suitable for direct comparisons. In agreement with this assertion, over 73% (637/868 genes) of so-called '*Brassicaceae* core' flg22-responsive genes (Winkelmuller *et al.*, 2021) were commonly found in both of my datasets (Fig. 5.10). This gene set comprises 868 genes that show altered expression in response to flg22 in several diverse species from the *Brassicaceae* family (specifically *C. rubella*, *C. hirsuta* and *E. salsugineum*) (Winkelmuller *et al.*, 2021).

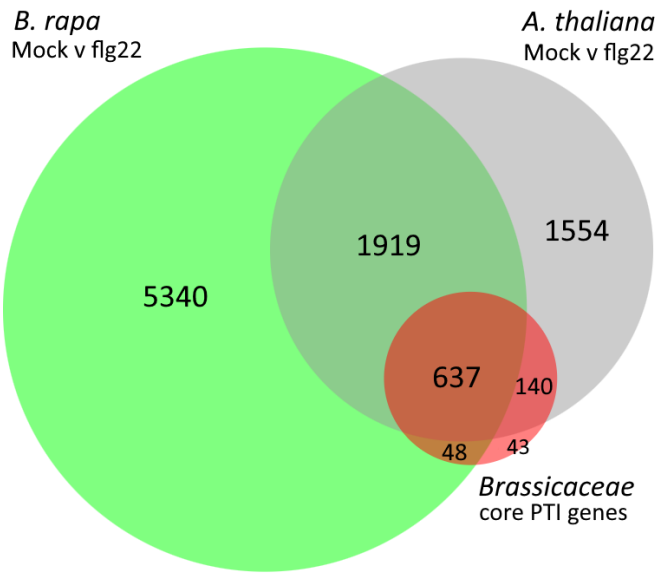

Figure. 5.10. Flg22-responsive genes in wild-type *B. rapa* and *A. thaliana*. Overlap of the flg22-responsive genes in wild-type *B. rapa* (green), *Arabidopsis* (grey) and the *Brassicaceae* 'core' dataset generated by Winkelmuller *et al.* (2021) (red). *B. rapa* genes were first converted to their corresponding *Arabidopsis* orthologs as described previously to enable this comparison. The area-proportional Venn diagram figure as created using BioVenn (Hulsen et al., 2008).

Interestingly, species-specific flg22-responsive genes were also identified, with a far greater number (5,340) of exclusive, species-specific DEGs detected in the *B. rapa* dataset (Fig. 5.10). It should be noted that this analysis is limited to *B. rapa* genes for which an *Arabidopsis* homolog could be identified, and thus an additional cohort of flg22-responsive and *B. rapa* specific genes are not accounted for in this comparison.

5.4.2 Comparing N-degron pathway regulated genes in *B. rapa* and *Arabidopsis*

To explore whether N-degron pathway regulation of transcription is conserved between these species, I sought to compare genes misregulated in *Arabidopsis ate1ate2* with those misregulated in *B. rapa Brprt6.2prt6.3* mutants. One potential challenge with these comparisons is that the *Arabidopsis* and *B. rapa* lines contain mutations in different enzymatic components of the N-degron pathway. Indeed, PRT6 can target for degradation proteins that are not previously modified by Arg-transferase (e.g. substrates with Nt His or Lys for example). Hence, it is possible that transcriptomic differences between *Arabidopsis ate1ate2* and *B. rapa prt6.2prt6.3* mutant plants do not originate only from species-specific differences, but also from the use of mutants affected for different enzymatic components whose activity is not entirely overlapping. At the same time, all Arg-transferase substrates are expected to be ubiquitylated in a PRT6-dependent manner, so one would expect the transcriptomes of *ate1ate2* and *prt6* mutant lines to be nevertheless very similar. This outlook is consistent with the fact that *Arabidopsis ate1ate2* and *prt6* mutants have very similar phenotypes, including at the whole-transcriptome level (Gibbs *et al.*, 2011), even though certain defects tend to be stronger in *ate1ate2* plants (Gibbs *et al.*, 2011; de Marchi *et al.*, 2016). The disruption of different enzymatic components in *Arabidopsis ate1ate2* and *B. rapa prt6.2prt6.3* may in fact bolster confidence that any commonly misregulated genes detected are indeed subject to *bona fide* regulation by the N-degron pathway.

Firstly, I compared the 65 *Arabidopsis* homologs of the DEGs misregulated in *Brprt6.2prt6.3* after mock-treatment, with the 104 genes misregulated in *Arabidopsis ate1ate2* under the same conditions (Fig. 5.11). Only 11 genes were found to be present in both datasets, with the remainder of DEGs specifically misregulated in either the *Arabidopsis* or *B. rapa* N-degron pathway mutants.

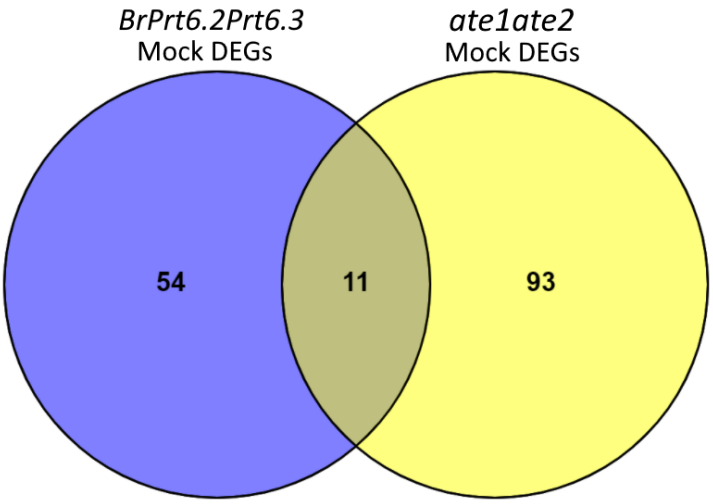

Figure 5.11. Overlap of DEGs misregulated in *ate1ate2* and *Brprt6.2prt6.3* compared to wild-type after mock treatment. Venn diagram comparison of the DEGs identified in mock-treated *Brprt6.2prt6.3* (blue) and *Arabidopsis ate1ate2* (yellow) relative to the respective wild-type control in dual RNA-Seq experiments. This figure was generated using Venny (Oliveros, 2007).

The 11 common genes are listed in Table 5.3. The directionality of the gene expression differences relative to the respective wild-type controls are the same in N-degron pathway mutants across both species. As expected, among the common up-regulated genes, several hypoxia-response genes are present, such as *PCO1*, *LBD41*, *Hb1* and *HRE2*. The expression of these genes depends on the ERF-VII transcription factors, whose degradation under normoxia requires the sequential activity of Arg-transferases and PRT6. Importantly, the N-terminal Met-Cys peptide sequence that renders *Arabidopsis* ERF-VII proteins eligible for N-degron pathway mediated degradation is conserved in *B. rapa* (Fig. A16 – Appendix A).

Table 5.3. List of common genes misregulated in *ate1ate2* and *Brprt6.2prt6.3* compared to wild-type after mock treatment. Log_2(fold-change) values are taken from the respective RNA-Seq experiments. Pink = higher expression in N-degron pathway mutant, green = reduced expression.

Locus (AGI)	B. rapa gene ID	Gene name	LOG2(fold-change)		Description
			a1a2 / Col-0	*BrPrt6* / WT	
AT5G15120	103856111, 103846440	*PCO1*	5.22137	4.82, 7.37	Plant cysteine oxidase 1
AT4G10265	103840073	*WIP3*	4.25098	2.92405	wound-induced polyptide 3
AT4G10270	103840073	*WIP4*	4.22425	2.92405	wound-induced polypeptide 4
AT5G39890	103863926	*PCO2*	3.78607	5.35449	Plant cysteine oxidase 2
AT3G02550	103843350	*LBD41*	3.72478	4.33188	LOB-domain containing 41
AT2G16060	103846065	*Hb1*	3.54593	5.11726	Hemoglobin 1
AT2G47520	103843716	*ERF71 / HRE2*	3.23384	3.58742	Hypoxia resopnsive ERF
AT2G19590	103828296	*ACO1*	2.56414	4.89190	Ethylene biosynthesis
AT5G65640	103874000	*bHLH093*	1.32315	1.48611	Bhlh transcription factor
AT5G25980	103833480	*TGG2*	-0.82499	-1.36734	glucosinolate metabolism
AT4G11650	103853512	*OSM34*	-1.50470	-2.90739	Osmotin-like protein, defence

Venn diagram analysis was also employed to compare the 87 genes misregulated in the *ate1ate2* mutant compared to wild-type after flg22 elicitation with the 129 DEGs misregulated in *Brprt6.2prt6.3* (corresponding to 144 *Arabidopsis* orthologs) after the same treatment. In this case, only 10 genes were found to co-occur in both datasets (Fig. 5.12) with the remainder being specifically misregulated in either *Arabidopsis* or *B. rapa* N-degron pathway mutants after flg22 treatment. Altogether, these comparisons of the respective mutant transcriptomes suggest that a sizeable portion of N-degron pathway mediated-regulation of gene expression may in fact be species-specific. However, as discussed above, there remains the possibility that some differences may be partially due to the contribution of PRT6-specific substrates that do not require modification by Arg-transferases.

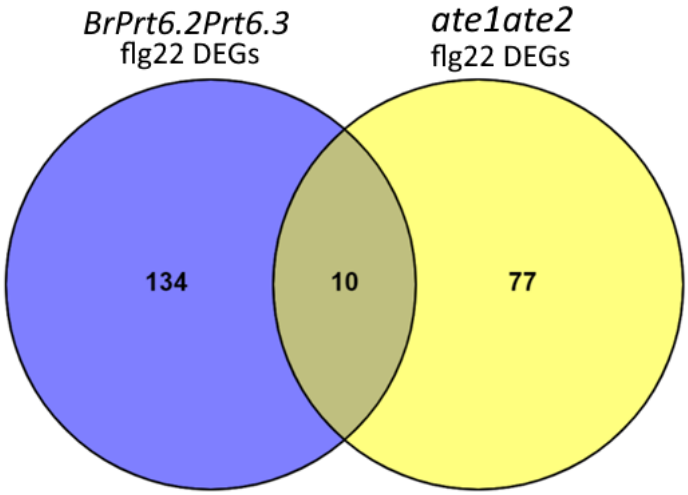

Figure 5.12. Overlap of DEGs misregulated in *ate1ate2* and *Brprt6.2prt6.3* compared to wild-type after flg22 treatment. Venn diagram comparison of the DEGs identified in *Brprt6.2prt6.3* (blue) and *Arabidopsis ate1ate2* (yellow) after flg22 treatment relative to the respective wild-type control in dual RNA-Seq experiments. This figure was generated using Venny (Oliveros, 2007).

The genes in the overlap of the flg22-treated datasets are displayed in Table 5.4. Interestingly, 9 of the 10 genes commonly regulated by N-degron pathway components in both species are expressed at higher levels in the mutant lines, with only the *Arabidopsis* ortholog of *APS4* (ATP sulfurylase 4) expressed at lower levels in *ate1ate2* compared to the wild type after flg22 treatment. Notably, the majority of these genes have been previously implicated in the response to hypoxia and/or have been identified as targets of the ERF-VII transcription factors that are subjected to N-degron pathway mediated degradation. These include *PCO1*, *PCO2*, *ADH1*, *Hb1*, *ACO1*, *HRE2*, *LBD41*, and *CYP707A3* (Licausi *et al.*, 2010, Licausi *et al.*, 2011). Aside from *ADH1* and *CYP707A3*, all of these genes were also retrieved in the overlap of DEGs found in mock-treated *Brprt6.2prt6.3* and *ate1ate2* (Table 5.3). This strongly suggests that the role of the N-degron pathway as a regulator of ERF-VII transcription factors is conserved in *Arabidopsis* and *B. rapa*.

Table 5.4. List of common genes misregulated in *ate1ate2* and *Brprt6.2prt6.3* compared to wild-type after flg22 treatment. LOG_2(fold-change) values are taken from the respective RNA-Seq experiments. Pink = higher expression in N-degron pathway mutant, green = reduced expression.

Locus (AGI)	B. rapa gene ID	Gene name	LOG2(fold-change)		Description
			a1a2 / Col-0	*BrPrt6* / WT	
AT5G15120	103856111	*PCO1*	5.63115	4.21919	Plant cysteine oxidase 1
AT5G39890	103863926	*PCO2*	3.91995	4.22694	Plant cysteine oxidase 2
AT1G77120	103832166	*ADH1*	3.28329	1.34434	Alcohol Dehydrogenase 1
AT2G16060	103846065	*Hb1*	3.26010	4.73597	Hemoglobin 1
AT2G19590	103828296	*ACO1*	2.32865	4.92513	Ethylene biosynthesis
AT2G47520	103843716	*ERF71 / HRE2*	2.14709	3.97695	Hypoxia responsive ERF
AT3G02550	103843350	*LBD41*	2.10995	3.64036	LOB-domain containing 41
AT5G65640	103874000	*bHLH093*	1.22687	1.41499	bHLH transcription factor
AT5G45340	103839129	*CYP707A3*	0.66619	0.91891	Involved in ABA catabolism
AT5G43780	103827954	*APS4*	-1.02463	0.83669	Sulfate adenylyltransferase

5.4.3 Discussion

Overall, the comparison of the RNA-Seq datasets revealed both conserved and species-specific features of transcriptional regulation by the N-degron pathway in *Arabidopsis* and *B. rapa*. The genes commonly misregulated in N-degron pathway mutants of both species predominantly appear to be under the control of ERF-VII transcription factors, while the species-specific genes may be regulated by as-yet-unidentified N-degron pathway substrates exclusive to either *Arabidopsis* or *B. rapa*. Examples of different sets of genes are shown in Figure 5.13, which provides a side-by-side comparison of transcript abundance for selected homologous flg22-inducible genes. The hypoxia-responsive and flg22-inducible gene *CYP707A3* is shown to be overexpressed in both *ate1ate2* and *Brprt6.2prt6.3* compared to wild-type, likely as a result of ERF-VII accumulation (Licausi *et al.*, 2011) (Fig.5.13a). In contrast, the chitinase gene *ChiA* shows reduced expression in *ate1ate2* while no obvious difference is apparent in *Brprt6.2prt6.3* (Fig. 5.13b). Finally, the NAC transcription factor *NAC036* exhibits normal expression levels in *ate1ate2* but appears to be N-degron pathway regulated in *B. rapa* (Fig. 5.13c). NACs constitute one of the largest plant-specific transcription factor families and have been implicated in various roles in plant immunity (Yuan *et al.*, 2019), although a specific role of NAC036 in immunity has not been described. Future investigations into the upstream transcriptional regulators of genes like *ChiA* and *BrNAC036* could lead to the identification of novel N-degron pathway substrates in *Arabidopsis* or *B. rapa*, respectively.

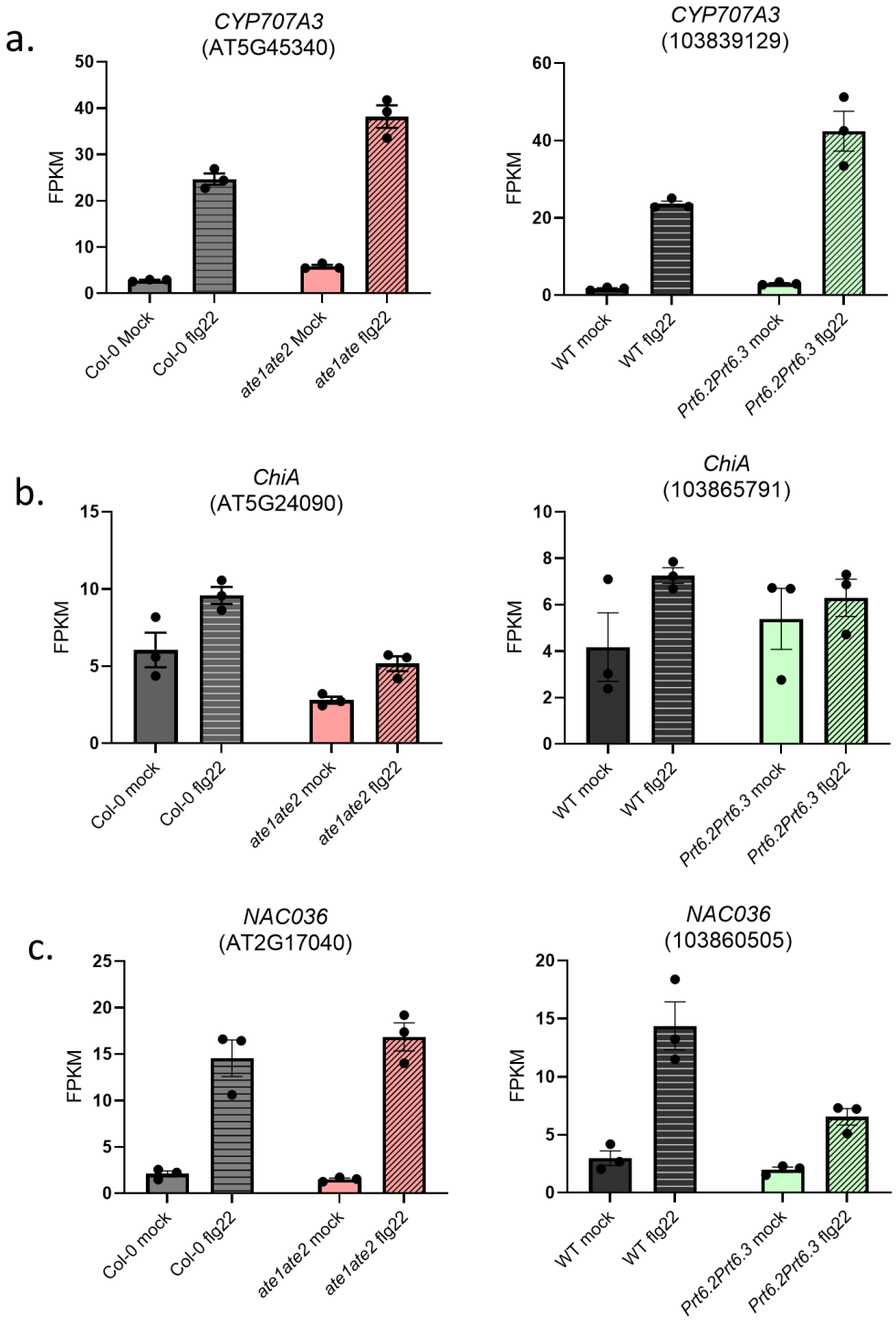

Figure 5.13. Flg22-inducible genes misregulated in N-degron pathway mutants of *Arabidopsis* and/or *B. rapa*. Comparison of transcript abundance as detected by RNA-Seq showing misregulation of flg22-inducible genes in N-degron pathway mutants. Left = *Arabidopsis* gene, right = *B. rapa* gene. FPKM = Fragments Per Kilobase of transcript per Million mapped reads. **a.** Common elevation of *CYP707A3* in *ate1ate2* and *Brprt6.2prt6.3*. **b.** *Arabidopsis*-specific misregulation of *ChiA* in *ate1ate2*. **c.** *B. rapa* specific misregulation of *NAC036* in *Brprt6.2prt6.3*. Columns indicate means of 3 replicates +/- SEM error bars.

5.4.4 CIR gene expression in *Brprt6.2prt6.3*

The *Arabidopsis* RNA-Seq experiment revealed that the *ate1ate2* mutant exhibits reduced expression of some 'core immune response' (CIR) genes compared to wild-type seedlings after flg22 treatment (Fig. 3.4). To investigate whether a similar trend would be apparent in *Brprt6.2prt6.3*, I assessed the expression of *B. rapa* CIR gene homologs after flg22 treatment (Fig. 5.14). The 75 *B. rapa* orthologs to the set of 38 *Arabidopsis* CIR genes were identified using the OrthoDB database (available at orthodb.org) and are listed in Table B6 (Appendix B).

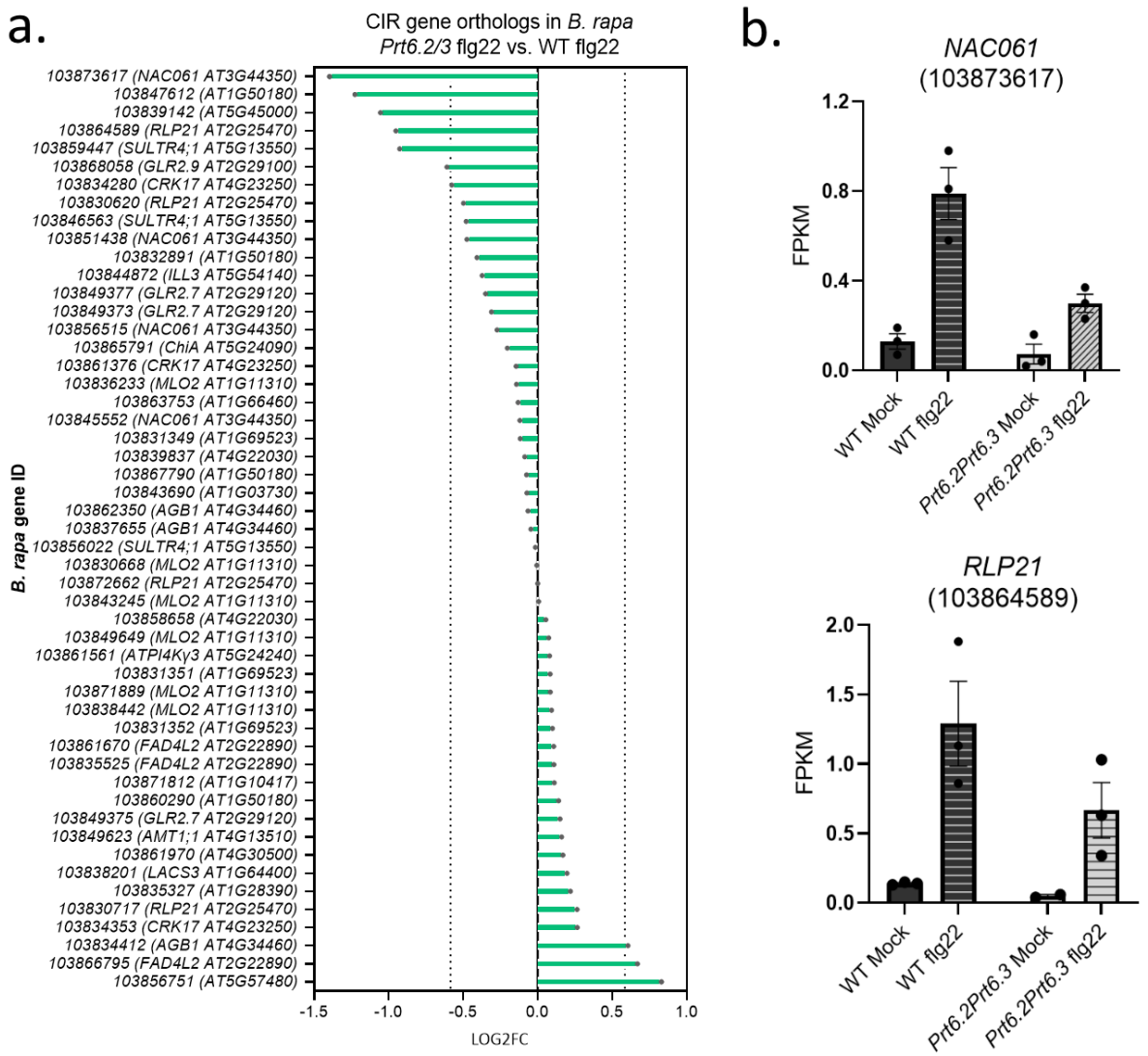

Figure 5.14. CIR gene homolog expression in *Brprt6.2prt6.3*. Expression of *B. rapa* orthologs of CIR genes (defined by Bjornson *et al.*, 2021) in *Brprt6.2prt6.3* flg22 vs. wild-type flg22 as detected by RNA-Seq. Dotted line on x-axis indicates fold-change greater than 1.5 (i.e. $|\log_2(\text{fold-change})| \geq 0.585$) **b.** FPKM values for selected genes *NAC061* (103873617) and *RLP21* (103864589).

Interestingly, the specific identities of the misregulated CIR genes differed in *Arabidopsis* and *B. rapa*. For example, the *B. rapa NAC061* ortholog (gene ID 103873617) exhibits strongly reduced expression in *Brprt6.2prt6.3*, while the *Arabidopsis NAC061* (AT3G44350) is unchanged in *ate1ate2* compared to wild-type (Fig. 3.4). The reduced expression of *NAC061* in *Brprt6.2prt6.3* is particularly notable considering the potential species-specific N-degron pathway mediated regulation of *NAC036* highlighted in Fig. 5.13c. By contrast, the *Arabidopsis* CIR *ChiA* is dampened in *ate1ate2*, while the homologous *B. rapa* gene (103865791) behaves similarly in wild-type and *Brprt6.2prt6.3* mutants. This suggests that although certain essential PTI genes appear to be partly regulated by the N-degron pathway in both *B. rapa* and *Arabidopsis*, the specific mechanisms underpinning this activity may not be conserved.

5.5 PTI-induced ROS production in *Brprt6.2prt6.3*

Characterisation of PTI responses in *Arabidopsis* revealed that *ate1ate2* appears to accumulate less ROS after flg22 elicitation compared to wild-type Col-0 (Fig. 3.10). Using the same luminol-based assay, I investigated whether the *Brprt6.2prt6.3* would also exhibit altered ROS production (Fig. 5.15).

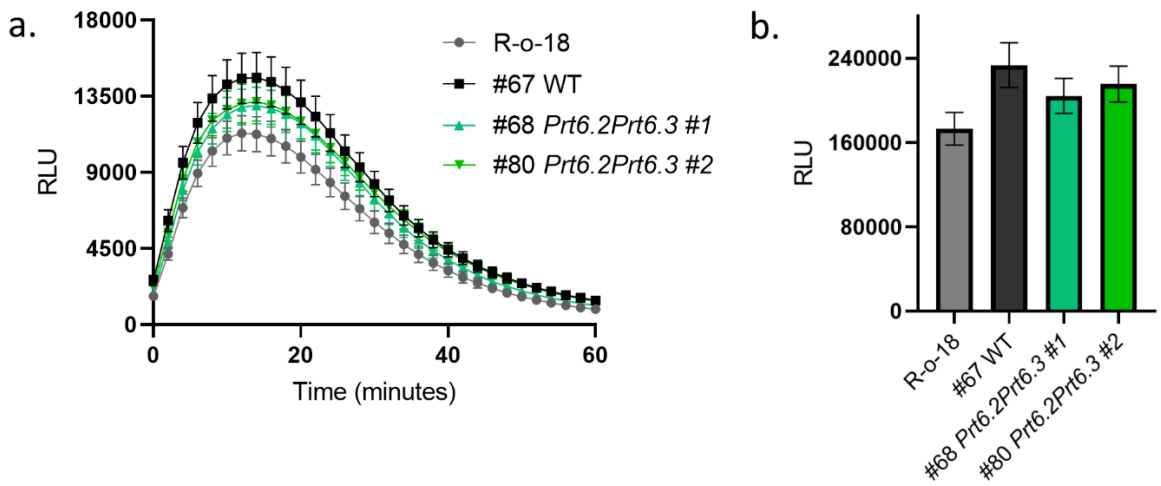

Figure 5.15. Flg22-induced ROS production in *Brprt6.2prt6.3*. a. ROS production in 4-week-old *B. rapa* after elicitation with 100 nM flg22. ROS were detected every 2 minutes for 1 hour after the addition of flg22. Datapoints represent means of 72 readings (leaf-disc quarters) taken from 18 leaf discs over 3 independent replicates. Error bars indicate SEM. RLU = Relative Light Units. **b.** Cumulative RLU detected from 0-60 minutes. Error bars indicate SEM.

The dynamic production of flg22-induced ROS is shown in Fig. 5.15a, while the cumulative RLU over the course of 60 minutes is shown in Fig. 5.15b. Both *Brprt6.2prt6.3* lines behaved very similarly, producing slightly less ROS than the #67 wild-type line isolated from the TILLING population (Fig. 5.15). This marginal reduction in peak ROS production is reminiscent of the mild diminished ROS phenotype observed in the *ate1ate2* mutant (Fig.3.10).

However, all 3 TILLING lines exhibited greater ROS production than the R-o-18 wild-type, suggesting that remnant background SNPs in these lines may influence the outcome of this assay. Additionally, no statistically significant differences between genotypes were observed when the cumulative ROS production was compared by one-way ANOVA (Fig. 5.15b). As such, it is difficult to make conclusive interpretations based on the existing data, and further replicate experiments are warranted to confirm this potential phenotype.

5.6 Flg22-induced growth inhibition in *Brprt6.2prt6.3*

Next, I investigated growth inhibition induced by flg22 treatment of *Brprt6.2prt6.3* seedlings. 3-day-old seedlings of wild-type and two *Brprt6.2prt6.3* lines were incubated in liquid medium supplemented with 100 nM flg22 or a dH_2O (mock) for 7 days. No obvious differences were observed between the three genotypes in these conditions (Fig. 5.16). In fact, seedlings of *Brprt6.2prt6.3* line #68 grew almost identically to wild-type seedlings irrespective of treatment. In both cases, flg22-treated seedlings grew to ~74% the size of those subjected to the mock treatment. The second *Brprt6.2prt6.3* mutant line #80 exhibited a marginal reduction in growth compared to wild-type and *Brprt6.2prt6.3* line #68 after either mock or flg22 treatment. Taken together, this data indicates that N-degron pathway impairment induced by disruption of BrPRT6.2 and BrPRT6.3 does not severely compromise the sum PTI response in *B. rapa*.

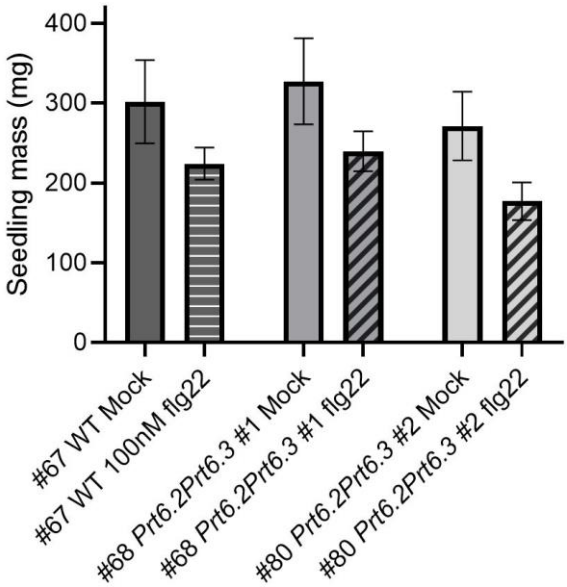

Figure 5.16. Flg22-induced growth inhibition in *Brprt6.2prt6.3* seedlings. *B. rapa* seedlings were grown for 3 days on agar plates before transfer to liquid media containing 100 nM flg22 or dH_2O (mock) for a further 7 days of growth. Columns indicate means +/- SEM of 3 independent replicates with the masses of 3 seedlings measured per condition per replicate.

5.7 MAPK activation in *Brprt6.2prt6.3*

The activation of MAPK cascades after flg22 elicitation was also assessed in *Brprt6.2prt6.3*. Seedlings were incubated with 1 µM flg22 for 15 minutes prior to tissue collection and protein extraction for immunoblot. Although a preliminary experiment indicated a flg22-induced elevation in the phosphorylation of MAPKs MPK3 and MPK6 in *Brprt6.2prt6.3* compared to wild-type (Fig. 5.17), this phenotype was not observed in a replicate experiment (Fig. A18 – Appendix A). On this basis, it is not appropriate to draw conclusions on the contribution of the *B. rapa* N-degron pathway to the regulation of flg22-induced MAPK cascade activation from the data obtained..

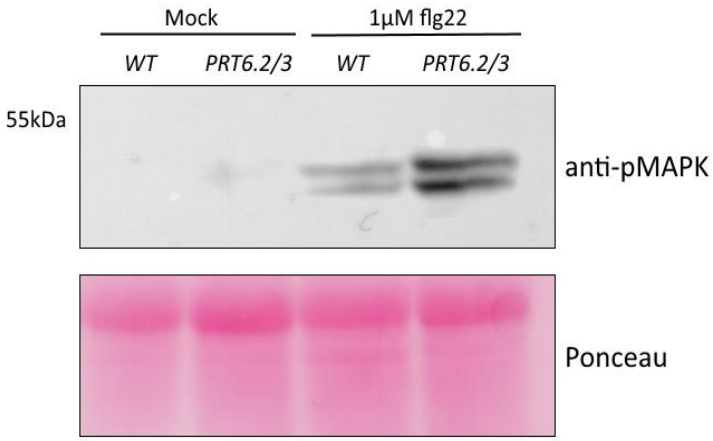

Figure 5.17. Flg22-induced MAPK phosphorylation in *Brprt6.2prt6.3*. Wild-type and *Brprt6.2prt6.3 B. rapa* seedlings were incubated with 1 µM flg22 or dH_2O (mock) for 15 minutes. 50 µg of protein was loaded per well of an SDS-PAGE gel as indicated. After protein transfer, phosphorylated MAPK proteins were detected with 1:1,000 dilution of anti-Phospho-p44/42 MAPK antibody. Bands corresponding to phosphorylated MPK6 (upper) and MPK3 (lower) were visible.Ponceau staining of PVDF membrane indicates equal protein transfer (lower panel). Uncropped images are included in Appendix A (Fig. A17). A replicate experiment is shown in Fig. A18.

5.8 Discussion

Characterisation of the PTI responses of the *Brprt6.2prt6.3* mutant revealed novel understanding of the physiological roles of the *B. rapa* N-degron pathway. Firstly, RNA-Seq analysis conducted following treatment with flg22 revealed numerous PTI-responsive genes that appear to be subject to N-degron pathway regulation. Importantly, the roles of the *B. rapa* N-degron pathway during PTI appear to include both positive and negative regulation of transcriptional changes, demonstrated by reduced expression of some flg22-inducible genes in *Brprt6.2prt6.3* seedlings (e.g. *Nuclear speckle RNA binding protein B / MKS1* (Fig. 5.8)), and increased expression of others (e.g. *Hypersensitive-induced response protein 3* (Fig. 5.7)). This phenotype is reminiscent of the transcriptomic response of the *Arabidopsis ate1ate2* mutant to flg22 described in section 3.2.

To further investigate the similarities between the roles of the N-degron pathway in *B. rapa* and *Arabidopsis*, the RNA-Seq datasets obtained in each species were compared directly. Importantly, the response of wild-type *Arabidopsis* and *B. rapa* plants to flg22 showed

considerable overlap (Fig. 5.10), and included the vast majority of previously published *Brassicaceae* core PTI genes (Winkelmuller *et al.*, 2021). Only 11 and 10 genes were commonly misregulated in *ate1ate2* and *Brprt6.2prt6.3* after mock or flg22 treatment, respectively, while a larger subset of genes were exclusively misregulated in the N-degron pathway mutant of only one species (e.g. *ChiA* in *Arabidopsis* and *NAC036* in *B. rapa*) (5.13). Interestingly, most genes that appear to be commonly misregulated in N-degron pathway mutants of *Arabidopsis* and *B. rapa* are likely regulated by the ERF-VII transcription factors (Tables 5.3 and 5.3). Together with the conservation of their N-terminal Met-Cys sequence (Fig. A16 – Appendix A), this strongly indicates the conservation of their N-degron pathway mediated degradation in *Brassicaceae*, as well as highlighting the contribution of these genes to PTI responses. One interesting possibility is that some ERF-VII regulated genes primarily associated with the hypoxia response have been co-opted to contribute to immunity in *Brassicaceae*. This would explain the flg22-inducible expression of certain ERF-VII regulated genes e.g. *LBD41* in both species. Like their *Arabidopsis ate1ate2* counterparts, *Brprt6.2prt6.3* seedlings also exhibit a general trend towards reduced expression of some CIR gene homologs (Fig. 5.14), highlighting that the observed transcriptional misregulation extends to genes with likely important functions in immunity.

A wider assessment of core PTI responses was conducted to explore additional roles of the *B. rapa* N-degron pathway in the regulation of PTI. Quantification of ROS production following elicitation with flg22 revealed a potential reduction in the peak ROS burst in two *Brprt6.2prt6.3* mutant lines relative to the wild-type line re-isolated from the TILLING population (Fig. 5.15). This mildly diminished ROS phenotype is consistent with the characterisation of the *Arabidopsis ate1ate2* mutant, suggesting a potentially conserved role for the N-degron pathway as a positive regulator of flg22-induced ROS. However, further experiments will be required to validate this phenotype and identify the molecular mechanisms underlying this observation. Interestingly, a preliminary experiment suggested that MAPK cascade phosphorylation may be enhanced in *Brprt6.2prt6.3* (Fig. 5.17). Although this phenotype was not reproduced in a replicate experiment, follow-up experiments may be warranted to substantiate this finding.

Taken together, these experiments revealed the first physiological functions of the *B. rapa* N-degron pathway and particularly its contribution to the regulation of PTI. The knowledge

generated here also provides novel insights into the conservation and divergence of the roles of the N-degron pathway in the *Arabidopsis* and its close relative *B. rapa*. The latter serves as a reminder of the importance of validating knowledge derived in *Arabidopsis* directly in model crops prior to application for crop development.

6

Conclusions

6.1 Introduction

Previous studies have described the response of N-degron pathway mutants to a range of pathogens including bacteria, fungi and protists with different lifestyles (i.e. biotrophs, necrotrophs and hemi-biotrophs) (de Marchi *et al.*, 2016; Gravot *et al.*, 2016; Vicente *et al.*, 2018). These reports suggested both positive and negative regulatory roles of the N-degron pathway during plant immunity and included some contradictory observations. The altered response of N-degron pathway mutants in different plant species (e.g. *Arabidopsis* and *H. vulgare*) to diverse sets of pathogens further suggests potential misregulation of fundamental immune response programmes such as PTI, the first line of plant defences triggered in response to highly conserved pathogen molecules. PTI can be selectively activated by treating plants with purified PAMP molecules such as flg22, enabling dissection of immunity-related regulatory mechanisms in the absence of the confounding factors like pathogen effectors, effector-triggered immunity and mitigating the impact of environmental differences that may affect pathogen virulence.

The experiments undertaken here sought to elucidate the molecular mechanisms underpinning the apparent roles of the N-degron pathway in plant immunity with a particular focus on PTI, to clarify previous observations and generate new knowledge that could be used to direct crop improvement strategies. The data obtained during this project yielded novel insights into the roles of the N-degron pathway in the immune responses of *Arabidopsis thaliana* and the related, economically important crop *Brassica rapa*.

6.2 The N-degron pathway regulates PTI responses in *Arabidopsis*

Transcriptomic analyses by RNA-Seq and RT-qPCR in Chapter 3 revealed certain flg22-induced transcriptional changes that appear to be subject to N-degron pathway regulation in *Arabidopsis.* Specifically, numerous genes with known roles in immunity exhibit altered expression in the *ate1ate2* mutant. This includes, for example, *ChiA*, a member of the recently described set of 'core immunity response' genes that are responsive to multiple PAMPs (Winkelmuller *et al.*, 2021). Subsequent investigation of the expression of all 38 CIR genes after flg22 treatment revealed several with reduced expression in *ate1ate2* compared to wild-type plants after flg22 treatment. Failure to induce expression of flg22-responsive genes to the levels required for effective resistance could potentially contribute to the previously reported increased susceptibility of *ate1ate2* to bacterial pathogens (de Marchi *et al.*, 2016).

Conversely, a cohort of flg22-inducible genes also appear to exhibit increased expression in *ate1ate2*, such as *LBD41*. These apparently opposing roles of the Arg transferases *ATE1* and *ATE2* as regulators of transcriptional change during PTI highlight the complexity of the contribution of the N-degron pathway to the regulation of immunity. Notably, many of the flg22-responsive genes with increased expression in *ate1ate2* after flg22 treatment, including *LBD41*, appear to be regulated by the ERF-VII transcription factors that primarily govern the response to hypoxia. Predicting the impact of the increased expression of these genes on pathogen susceptibility phenotypes is quite challenging, as constitutive elevation of hypoxia-responsive genes has been associated with increased susceptibility to pathogens in some cases, such as the response to *Plasmodiophora brassicae* (Gravot *et al.*, 2016). Presumably, in alternative plant-pathogen species contexts, these genes may contribute to increased host resistance, thus accounting for their flg22-induced activation. Thus, the bilateral misregulation of PTI-responsive genes in *ate1ate2* may partially explain the discrepancy concerning the role of the N-degron pathway as both a positive and negative regulator of defence responses against pathogens.

Detailed assessment of PTI responses in the *ate1ate2* mutant revealed additional outputs, such as flg22-triggered ROS production, that appear to be mildly impaired. Subsequent experiments to identify genetic interactions between the N-degron pathway and known regulators of the ROS burst suggested that the observed positive regulation by the Arg

transferases may depend on CPK28, which promotes the activity of RBOHD via BIK1. This proposed role would be distinct from the previously reported positive regulation of *RBOHD* by RAP2.12, whose stabilization in N-degron pathway mutants may have been expected to lead to enhanced ROS production. Further experiments will be required to validate these roles of the N-degron pathway in regulating the PTI-associated ROS burst.

As mentioned above, a previous study by de Marchi *et al.* (2016) has described increased susceptibility of *ate1ate2* and *prt6-1* to *Pst* DC3000, while Vicente *et al.* (2018) conflictingly reported increased resistance of *prt6-1* to the same pathogen. Here, inoculations with *Pst* DC3000 revealed that plant age appears to be an important determinant of the outcome of *Pst* infection assays with N-degron pathway mutants. Specifically, *ate1ate2* appears to be compromised in the onset of age-related resistance, presenting as reduced or increased pathogen susceptibility relative to wild-type plants dependent on plant age. Identifying the molecular mechanisms underlying the contribution of the N-degron pathway to ARR should be a priority for future studies.

Taken together, the experiments detailed in Chapter 3 shed new light on the roles of the N-degron pathway in the regulation of immune responses in *Arabidopsis* and the knowledge generated here could have implications for efforts to exploit the N-degron pathway to develop crop varieties with improved agronomic traits, particularly considering the well-established roles of the N-degron pathway-targeted ERF-VIIs as mediators of the response to hypoxia-related stresses (Gibbs *et al.*, 2011). For example, impairment of the N-degron pathway in *Arabidopsis* has been associated with greater tolerance to abiotic stresses such as submergence (Gibbs *et al.*, 2011), as well as drought, salt and heat stress (Vicente *et al.,* 2017). Accordingly, barley mutant plants for *HvPRT6* have been shown to be more resistant to waterlogging (Mendiondo *et al.*, 2016). However, the complex phenotypes observed in response to pathogens, together with the results obtained in Chapter 3 indicate that these benefits must be carefully weighed against the costs associated with the aberrant regulation of certain immune responses.

6.3 The roles of the N-degron pathway in *B. rapa*

Despite the insights gained from the experiments conducted in *Arabidopsis*, sole reliance on this model plant to investigate the roles of the N-degron pathway naturally limits the acquisition and implementation of new knowledge suitable for model-to-crop translation. To address this, I also aimed to investigate the roles of the N-degron pathway in the important crop species *Brassica rapa*. As well as being a species of economic and societal value, (section 1.X), *B. rapa* is closely related to *Arabidopsis* as well as *Brassica napus* (oilseed rape), a staple crop of global importance. The development of an EMS-mutagenized TILLING population in the last decade (Stephenson *et al.*, 2010) has enabled reverse genetics approaches in this species. Availing of this collection, I describe here the isolation of the first N-degron pathway mutants of *B. rapa*, harbouring truncated versions of the BrATE (*Brate1ate2)* and BrPRT6 proteins (*Brprt6.2prt6.3*) respectively. In contrast to the mild developmental defects of an *Arabidopsis ate1ate2* mutant, *B. rapa ate1ate2* mutants exhibited a striking seedling-lethality phenotype, rendering cultivation and experimental characterisation of these plants highly challenging. To overcome this problem and avoid provoking a similar phenotype in *Brprt6* lines, I instead generated a *Brprt6.2prt6.3* double mutant, bearing mutations in the two most strongly expressed *BrPRT6* orthologs (*BrPRT6.2* and *BrPRT6.3*), while retaining the functionality of the lesser-expressed *BrPRT6.1*. These plants exhibited a wild-type like development and were compatible with an agroinfiltration-based transient expression system which I adapted for use in *B. rapa*. Model 'X-LUC' N-degron pathway reporters were significantly stabilized in *Brprt6.2prt6.3* lines, clearly highlighting that substrates of PRT6 accumulate in this double mutant. In addition, these mutant plants showed a constitutive up-regulation of hypoxia-response genes, a hallmark of *Arabidopsis* N-degron pathway mutants due to their stabilization of the ERF-VII transcription factors. Hence, *Brprt6.2prt6.3* lines are a suitable tool to study the physiological impacts of N-degron pathway interruption in *B. rapa*, and thus reveal its potential applications for the improvement of *Brassica* crops.

The strategy employed to investigate the physiological roles of the N-degron pathway during immunity in *B. rapa* was guided by the earlier findings in *Arabidopsis*. Most notably, transcriptomic analysis after flg22 treatment identified PTI-inducible genes that appear to be misregulated in *Brprt6.2prt6.3*, again suggesting a potential role of the arginylation branch of the N-degron pathway in the regulation of PTI. Direct comparison of the results of RNA-Seq

analyses in *Arabidopsis* and *B. rapa* revealed two distinct sets of N-degron pathway genes, i.e. those that are exclusively N-degron pathway regulated in either *Arabidopsis* or *B. rapa*, and those commonly regulated by the N-degron pathway in both of these *Brassicaceae* species (Fig. 6.1). The latter category is mostly comprised of targets of the ERF-VII transcription factors, highlighting their conserved contribution to immunity in *B. rapa* and *Arabidopsis*, and reiterating the complex and the partially overlapping interactions between the responses to hypoxia and immunity. One potential limitation of the comparison between the *Arabidopsis* and *B. rapa* RNA-seq datasets is that the N-degron pathway mutants in each species are disrupted for different enzymatic components of the pathway. This problem arose because of the finding later in my PhD project that *B. rapa ate1ate2* double mutants were seedling lethal, which prevented their use for detailed PTI assessment. Nevertheless, to date, phenotypic comparisons of *Arabidopsis ate1ate2* and *prt6* mutants have not revealed any significant differences, aside from somewhat milder phenotypes in *prt6* mutants. Hence, until PRT6-specific substrates (i.e. PRT6 substrates that do not undergo arginylation first) are discovered, and their function is understood, current knowledge of the pathway suggests that *ate1ate2* and *prt6* mutants accumulate similar sets of substrates.

The N-degron pathway also appears to positively regulate ROS production during PTI in *B. rapa.* Although the exact mechanism underpinning this activity remains to be elucidated, this phenotype is likely not attributable to the stabilization of ERF-VII transcription factors (see section 3.3), and thus may indicate the presence of conserved, hitherto unknown N-degron pathway substrates that inhibit the ROS burst.

The results from the comparative analyses performed in this project reinforce the need to validate knowledge gained in model systems via direct experimentation in crop species. For example, the species-specific functions of the N-degron pathway identified here suggest a partial divergence of the physiological roles of the N-degron pathway since the split of *Arabidopsis* from *Brassicas* 43 million years ago (Yu *et al.*, 2017). As the N-degron pathway components and structure appear to be well-conserved (Figs. 4.5 and 4.7), this likely reflects variability in the substrate repertoire in each species. Such differences could be driven by direct selective pressures at N-termini (e.g. gain or loss of a destabilizing N-terminal residue), or by species-specific proteases that may generate destabilizing neo-N-termini after cleavage. Proteome-wide comparisons of N-terminal sequences could be used to identify novel species-

specific N-degron pathway substrates, alongside further phenotypic comparisons of *Arabidopsis* N-degron pathway mutants with the *B. rapa* lines isolated in this study.

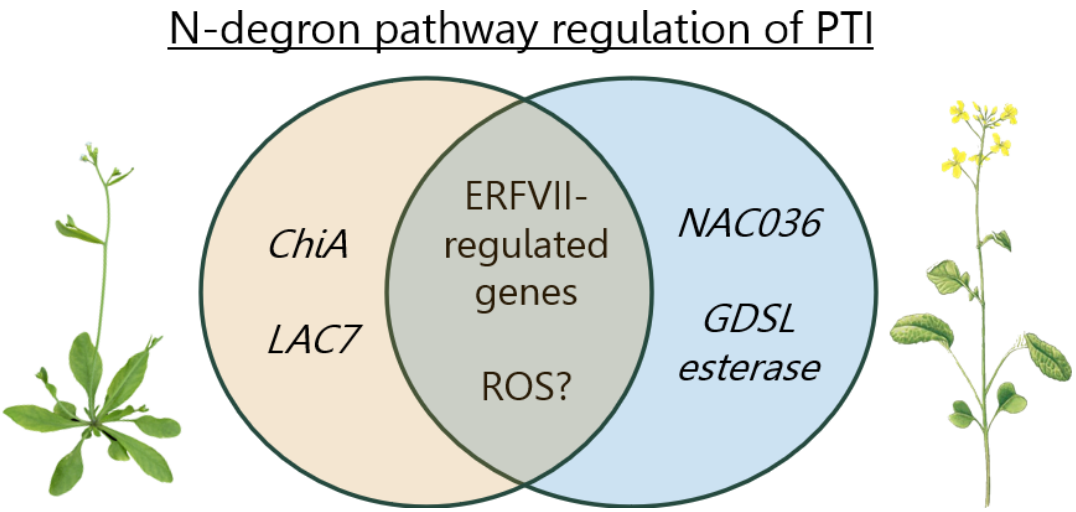

Figure 6.1. Model of N-degron pathway regulation of PTI responses in *Arabidopsis* and *B. rapa*. Examples of *Arabidopsis*-specific genes regulated by the N-degron pathway are shown on the left (orange circle) while *B. rapa* specific roles are shown on the right (blue circle). Features common features are indicated in the overlap.

6.4 Future directions

The future identification of novel substrates will be paramount to gain enhanced understanding of N-degron pathway functions in immunity and beyond. Previous approaches to substrate identification have centred on candidate proteins bearing N-terminal Met-Cys sequences (e.g. ERF-VII transcription factors, VRN2 and ZPR2 (Gibbs *et al.*, 2011; Gibbs *et al.*, 2018) Weits *et al.*, 2019)), whose initiator Met residues are readily cleaved by Met aminopeptidases thus exposing Cys at the N-terminus. Alternatively, detailed knowledge of protease cleavage events that result in fragments bearing destabilizing neo-N-termini has also been used to identify candidates for N-degron pathway mediated degradation (e.g. the NOI protein fragments released after cleavage by the effector protease AvrRpt2 (Goslin *et al.*, 2019)). Attempts to identify N-degron pathway substrates via unbiased proteomics approaches, such as comparison of N-degron pathway mutant proteomes with those of wild-type plants, have so far proved highly challenging (Zhang *et al.*, 2015). Potential explanations

for these difficulties include: (i) substrates may only accumulate to low abundance; (ii) substrates may also be degraded by alternative mechanisms and (iii) substrates may only be generated under specific environmental conditions (e.g. after a specific cleaveage event or upon perception of an immune stimulus). However, assuming the sensitivity of proteomics techniques continues to improve, the importance of these approaches in the N-degron pathway field will only increase.

During my PhD, I isolated proteomes from *ate1ate2* mutants following elicitation with flg22, with the aim of identifying candidate substrate proteins with immune functions (in collaboration with Prof. Pitter Huesgen based at Forschungszentrum Jülich, Germany). Analysis of these datasets is ongoing and could not be included here. In tandem with the RNA-Seq data shown in Chapter 3, these experiments could yet reveal substrates that may explain the PTI-related phenotypes observed in N-degron pathway mutant plants.

7

References

Abbas, M., Berckhan, S., Rooney, D. J., Gibbs, D. J., Vicente Conde, J., Sousa Correia, C., Bassel, G. W., Marín-de la Rosa, N., León, J., Alabadí, D., Blázquez, M. A., & Holdsworth, M. J. (2015). Oxygen sensing coordinates photomorphogenesis to facilitate seedling survival. *Current biology : CB*, **25**(11), 1483–1488. https://doi.org/10.1016/j.cub.2015.03.060

Adams, J. (2003) The proteasome: structure, function, and role in the cell. *Cancer Treat Rev.*, **29**, 3-9. doi: 10.1016/s0305-7372(03)00081-1.

Adams, E. H. G. & Spoel, S. H. (2018) The ubiquitin-proteasome system as a transcriptional regulator of plant immunity. *J. Exp. Bot.,* **69(19)**, 4529-4537.

Akhter, S., Uddin, M. N., Jeong, I. S., Kim, D. W., Liu, X. M., & Bahk, J. D. (2016). Role of Arabidopsis AtPI4Kγ3, a type II phosphoinositide 4-kinase, in abiotic stress responses and floral transition. *Plant biotechnology journal*, *14*(1), 215–230. https://doi.org/10.1111/pbi.12376

Aung, K., Jiang, Y., & He, S. Y. (2018). The role of water in plant-microbe interactions. *The Plant Journal*, **93**(4), 771–780. https://doi.org/10.1111/tpj.13795

Bachmair, A., Finley, D. & Varshavsky, A. (1986) *In vivo* half-life of a protein is a function of its amino-terminal residue. *Science*, **234**, 179-186.

Baker, R.T. and Varshavsky, A. (1995) Yeast N-terminal amidase. A new enzyme and component of the N-end rule pathway. *J. Biol. Chem.* **270**, 12065–12074.

Balint-Kurti P. (2019). The plant hypersensitive response: concepts, control and consequences. *Molecular plant pathology*, **20**(8), 1163–1178.

Belkhadir, Y., Nimchuk, Z., Hubert, D. A., Mackey, D., & Dangl, J. L. (2004). Arabidopsis RIN4 negatively regulates disease resistance mediated by RPS2 and RPM1 downstream or independent of the NDR1 signal modulator and is not required for the virulence functions of bacterial type III effectors AvrRpt2 or AvrRpm1. *The Plant Cell*, **16**(10), 2822–2835. https://doi.org/10.1105/tpc.104.024117

Bigeard, J., Colcombet, J. & Hirt, H. (2015) Signaling Mechanisms in Pattern-Triggered Immunity (PTI). *Molecular Plant*, **8(4)**, 521-539.

Bigeard, J. & Hirt, H. (2018) Nuclear Signaling of Plant MAPKs. *Front. Plant Sci*. https://doi.org/10.3389/fpls.2018.00469.

Birkenbihl, R. P., Diezel, C., & Somssich, I. E. (2012). Arabidopsis WRKY33 is a key transcriptional regulator of hormonal and metabolic responses toward Botrytis cinerea infection. *Plant physiology*, **159(1)**, 266–285. https://doi.org/10.1104/pp.111.192641

Birkenbihl, R. P., Kracher, B., Roccaro, M., & Somssich, I. E. (2017). Induced Genome-Wide Binding of Three Arabidopsis WRKY Transcription Factors during Early MAMP-Triggered Immunity. *The Plant cell*, **29(1)**, 20–38. https://doi.org/10.1105/tpc.16.00681

Bisgrove, S. R., Simonich, M. T., Smith, N. M., Sattler, A., & Innes, R. W. (1994). A disease resistance gene in Arabidopsis with specificity for two different pathogen avirulence genes. *The Plant Cell*, **6**(7), 927–933. https://doi.org/10.1105/tpc.6.7.927

Bjornson, M., Pimprikar, P., Nürnberger, T., & Zipfel, C. (2021). The transcriptional landscape of Arabidopsis thaliana pattern-triggered immunity. *Nature plants*, **7**(5), 579–586. https://doi.org/10.1038/s41477-021-00874-5

Boller, T. & Felix, G. (2009) A Renaissance of Elicitors: Perception of Microbe-Associated Molecular Patterns and Danger Signals by Pattern-Recognition Receptors. *Annual Review of Plant Biology*, **60**, 379-406. https://doi.org/10.1146/annurev.arplant.57.032905.105346.

Book, A. J., Smalle, J., Lee, K. H., Yang, P., Walker, J. M., Casper, S., Holmes, J. H., Russo, L. A., Buzzinotti, Z. W., Jenik, P. D., & Vierstra, R. D. (2009). The RPN5 subunit of the 26s proteasome is essential for gametogenesis, sporophyte development, and complex assembly in Arabidopsis. *The Plant Cell*, **21(2),** 460–478. https://doi.org/10.1105/tpc.108.064444

Bradford, M. M. (1976) A rapid and sensitive method for the quantiation of microgam quantities of protein utilizing the principle of protein-dye binding. *Analytical Biochemistry*, **72**, 248-56.

Brower, C. S., & Varshavsky, A. (2009). Ablation of arginylation in the mouse N-end rule pathway: loss of fat, higher metabolic rate, damaged spermatogenesis, and neurological perturbations. *PloS one*, **4**(11), e7757. https://doi.org/10.1371/journal.pone.0007757

Büttner, D. & He, S. Y. (2009) Type III Protein Secretion in Plant Pathogenic Bacteria. *Plant Physiology*, **150**, 1656-1664. https://doi.org/10.1104/pp.109.139089

Camejo, D., Guzmán-Cedeño, Á. and Moreno, A., 2016. Reactive oxygen species, essential molecules, during plant–pathogen interactions. *Plant Physiology and Biochemistry*, **103**, pp.10-23.

Cao, Y., Liang, Y., Tanaka, K., Nguyen, C. T., Jedrzejczak, R. B., Joachimiak, A. & Stacey, G. (2014) The kinase LYK5 is a major chitin receptor in *Arabidopsis* and forms a chitin-induced complex with related kinase CERK1. *eLife 2014*, 3:e03766. DOI: 10.7554/eLife.03766

Cartea, M. E., De Haro-Bailón, A., Padilla, G., Obregón-Cano, S., Del Rio-Celestino, M., & Ordás, A. (2019). Seed Oil Quality of *Brassica napus* and *Brassica rapa* Germplasm from Northwestern Spain. *Foods (Basel, Switzerland)*, **8**(8), 292. doi.org/10.3390/foods8080292

Cartea, M. E., Camara-Martos, F., Oregon, S., Badenes-Perez, F. R. & De Haro, A. (2021) Advances in Breeding in Vegetable *Brassica rapa* Crops. *Brassica reeding and Biotechnology*. DOI: 10.5772/intechopen.95769

Chang, X., Seo, M., Takebayashi, Y., Kamiya, Y., Riemann, M., & Nick, P. (2017). Jasmonates are induced by the PAMP flg22 but not the cell death-inducing elicitor Harpin in Vitis rupestris. *Protoplasma*, **254(1)**, 271–283. https://doi.org/10.1007/s00709-016-0941-7

Chen, J., Shen, C., Yeh, C., Fang, B., Huang, T. Liu, C. (2011) N-Acetyl Glucosamine Obtained from Chitin by Chitin Degrading Factors in *Chitinbacter tainanesis*. *Int J Mol Sci.*, **12(2)**, 1187-1195. doi: 10.3390/ijms12021187

Chen, X., Li, C., Wang, H. *et al.* WRKY transcription factors: evolution, binding, and action. *Phytopathol Res* **1,** 13 (2019). https://doi.org/10.1186/s42483-019-0022-x

Chen, S., Ding, Y., Tian, H., Wang, S., & Zhang, Y. (2021). WRKY54 and WRKY70 positively regulate SARD1 and CBP60g expression in plant immunity. *Plant signaling & behavior*, **16**(10), 1932142. https://doi.org/10.1080/15592324.2021.1932142

Cheng, Y. T., Li, Y., Huang, S., Huang, Y., Dong, X., Zhang, Y. & Li, X. 2011. Stability of plant immune-receptor resistance proteins is controlled by SKP1-CULLIN1-F-box (SCF)-mediated protein degradation. Proc Natl Acad Sci U S A, **108**, 14694-9.

Chisholm ST, Dahlbeck D, Krishnamurthy N, Day B, Sjolander K, Staskawicz BJ (2005) Molecular characterization of proteolytic cleavage sites of the Pseudomonas syringae effector AvrRpt2. *Proc Natl Acad Sci USA* **102**: 2087–2092

Chisholm, S. T, Coaker, G., Day, B., Staskawicz, B. J. (2006) Host-Microbe Interactions: Shaping the Evolution of the Plant Immune Response. *Cell*, **124 (4)**, 803-814.

Ciechanover, A., Elias, S., Heller, H., and Hershko, A. 1982. "Covalent affinity" purification of ubiquitin-activating enzyme. *J. Biol. Chem.* **257**: 2537– 2542.

Ciechanover, A. (2010) The Ubiquitin System: historical perspective. *Proceedings of the American Thoracic Society*, **7 (1)**, 11-12, doi: 10.1513/pats.200908-095JS.

Cho, S. K., Ryu, M. Y., Kim, J. H., Hong, J. S., Oh, T. R., Kim, W. T. & Yan, S. W. (2017) RING E3 ligases: key regulatory elements are involved in abiotic stress responses in plants. *BMB Rep*, **50(8)**, 393-400.

Cui, H., Tsuda, K. & Parker, J. E. (2014) Effector-Triggered Immunity: From Pathogen Perception to Robust Defence. *Annu. Rev. Plant Biol.*, **66**, 6.1-6.25. 10.1146/annurev-arplant-050213-040012.

Das, M., Naiya, H., Marik, A., Mukherjee, G., & Seal, A. (2019). A protocol for functional study of genes in Brassica juncea by Agrobacterium-mediated transient expression: Applicability in other Brassicaceae. *Journal of Plant Biochemistry and Biotechnology*, 1–12. https://doi.org/10.1007/s13562-019-00543-x

De Araújo, A. C., De Assis Fonseca, F. C., Cotta, M. G., Alvesm G. S. C. & Miller, R. N. G. (2020) Plant NLR receptor proteins and their potential in the development of durable genetic resistance to biotic stresses. *Biotechnology Research and Innovation*, https://doi.org/10.1016/j.biori.2020.01.002.

De Block, M., De Brouwer, D. and Tenning, P. (1989) Transformation of Brassica napus and Brassica oleracea Using Agrobacterium tumefaciens and the Expression of the bar and neo Genes in the Transgenic Plants. *Plant Physiol.*, **91**, 694-701.

De Duve, C., Gianetto, R., Appelmans, F., Wattiaux R. (1953) Enzymic content of the mitochondria fraction. *Nature*, **172**, 1143–1144.

De Marchi, R., Sorel, M., Mooney, B., Fudal, I., Goslin, K., Kwasniewska, K., Ryan, P. T., Pfalz, M., Kroymann, J., Pollmann, S., Feechan, A., Wellmer, F., Rivas, S. & Graciet, E. (2016) The N-end rule pathway regulates pathogen responses in plants. *Scientific Reports*, **6**, 26020.

Denoux, C., Galletti, R., Mammarella, N., Gopalan, S., Werck, D., De Lorenzo, G., Ferrari, S., Ausubel, F. M., & Dewdney, J. (2008). Activation of defense response pathways by OGs and Flg22 elicitors in Arabidopsis seedlings. *Molecular plant*, **1**(3), 423–445. https://doi.org/10.1093/mp/ssn019

Dissmeyer, N. (2019) Conditional Protein Function via N-Degron Pathway-Mediated Proteostasis in Stress Physiology. *Annu Rev Plant Biol.*, **70**, 83-117. doi: 10.1146/annurev-arplant-050718-095937.

Ding, Y., Sun, T., Ao, K., Peng, Y., Zhang, Y., Li, X., & Zhang, Y. (2018). Opposite Roles of Salicylic Acid Receptors NPR1 and NPR3/NPR4 in Transcriptional Regulation of Plant Immunity. *Cell*, **173**(**6)**, 1454–1467.e15. https://doi.org/10.1016/j.cell.2018.03.044

Dong, H., Dumenil, J., Lu, F. H., Na, L., Vanhaeren, H., Naumann, C., Klecker, M., Prior, R., Smith, C., McKenzie, N., Saalbach, G., Chen, L., Xia, T., Gonzalez, N., Seguela, M., Inze, D., Dissmeyer, N., Li, Y., & Bevan, M. W. (2017). Ubiquitylation activates a peptidase that promotes cleavage and destabilization of its activating E3 ligases and diverse growth regulatory proteins to limit cell proliferation in *Arabidopsis*. *Genes & development*, **31(2)**, 197–208. https://doi.org/10.1101/gad.292235.116

Doroodian, P. & Hua, Z. (2021) The Ubiquitin Switch in Plant Stress Response. *Plants*, **10**(2), 246.

Duarte, G. T., Volkova, P. Y., & Geras'kin, S. A. (2021). A Pipeline for Non-model Organisms for *de novo* Transcriptome Assembly, Annotation, and Gene Ontology Analysis Using Open Tools: Case Study with Scots Pine. *Bio-protocol*, **11**(3), e3912. https://doi.org/10.21769/BioProtoc.3912

Dubiella, U., Seybold, H., Durian, G., Komander, E., Lassig, R., Witte, C.P., Schulze, W.X. and Romeis, T., 2013. Calcium-dependent protein kinase/NADPH oxidase activation circuit is required for rapid defence signal propagation. *Proceedings of the National Academy of Sciences*, *110*(21), pp.8744-8749.

Dreher, K. & Callis, J. (2007) Ubiquitin, hormones and biotic stress in plants. *Ann Bot.*, **99(5)**, 787-822.

Edwards, K., Johnstone, C., Thompson, C. (1991) A simple and rapid method for the preparation of plant genomic DNA for PCR analysis. *Nucleic Acids Res.*, **19(6)**, 1349. doi:10.1093/nar/19.6.1349

Ellinger, D., & Voigt, C. A. (2014). Callose biosynthesis in Arabidopsis with a focus on pathogen response: what we have learned within the last decade. *Annals of botany*, **114(6)**, 1349–1358. https://doi.org/10.1093/aob/mcu120

Etlinger, J. D. & Goldberg, A. L. (1977) A soluble ATP-dependent proteolytic system responsible for the degradation of abnormal proteins in reticulocytes. *Proc Natl Acad Sci U S A*, **74**(1), 54-58.

Faber, K., Glatting, KH., Mueller, P.J. *et al.* (2011) Genome-wide prediction of splice-modifying SNPs in human genes using a new analysis pipeline called AASsites. *BMC Bioinformatics* **12,** S2. https://doi.org/10.1186/1471-2105-12-S4-S2

Fatima, U. & Senthil-Kumar, M. (2015) Plant and pathogen nutrient acquisition strategies. *Front. Plant Sci.*, https://doi.org/10.3389/fpls.2015.00750.

Felix, G., Regenass, M. & Boller, T. (1993) Specific perception of subnanomolar concentrations of chitin fragments by tomato cells: induction of extracellular alkalinization, changes in protein phosphorylation, and establishment of a refractory state. *Plant J.* **4(2)**:307–316.

Felix, G., Duran, J. D., Volko, S. & Boller, T. (1999) Plants Have a Sensitive Perception System for the Most Conserved Domain of Bacterial Flagellin. *Plant J.*, **18(3)**, 265-276. doi: 10.1046/j.1365-313x.1999.00265.x.

Figueroa-Macías, J. P., García, Y. C., Núñez, M., Díaz, K., Olea, A. F., & Espinoza, L. (2021). Plant Growth-Defense Trade-Offs: Molecular Processes Leading to Physiological Changes. *International journal of molecular sciences*, **22**(2), 693. https://doi.org/10.3390/ijms22020693

Flor, H. H. (1942) Inheritance of pathogenicity in *Melampsora lini*. *Phytopath.*, **32**, 653-669.

Gao, Y., Wang, Y., Xin, H., Li, S. & Liang, Z. (2017) Involvement of Ubiquitin-Conjugating Enzyme (E2 Gene Family) in Ripening Process and Response to Cold and Heat Stress of *Vitis vinifera*. *Scientific Reports*, **7**, Article number: 13290 (2017).

Garzon, M., Eifler, K., Faust, A., Scheel, H., Hofmann, K., Koncz, C., Yephremov, A. & Bachmair, A. (2007) PRT6/At5g02310 encodes an Arabidopsis ubiquitin ligase of the N-end rule pathway with arginine specificity and is not the CER3 locus. *FEBS Lett*, **581**, 3189–96.

Geilfus C. M. (2017). The pH of the Apoplast: Dynamic Factor with Functional Impact Under Stress. *Molecular plant*, **10**(11), 1371–1386. https://doi.org/10.1016/j.molp.2017.09.018

Geilfus, C., Wang, L., Wu, J. & Xue, C. (2020) The pH of the leaf apoplast is critical for the formation of Pseudomonas syringae-induced lesions on leaves of the common bean

(*Phaseolus vulgaris*). *Plant Science*, **290**, 110328. https://doi.org/10.1016/j.plantsci.2019.110328

Genschik, P., Parmentier, Y., Durr, A., Marbach, J., Criqui, M. C., Jamet, E., et al. (1992). Ubiquitin genes are differentially regulated in protoplast-derived cultures of Nicotiana sylvestris and in response to various stresses. Plant Mol. Biol. 20, 897–910. doi: 10.1007/BF00027161

Gibbs, D. J., Lee, S. C., Isa, N. M., Gramuglia, S., Fukao, T., Bassel, G. W., Correia, C. S., Corbineau, F., Theodoulou, F. L., Bailey-Serres, J. & Holdsworth, M. J. (2011) Homeostatic response to hypoxia is regulated by the N-end rule pathway in plants. *Nature*, **479(7373)**, 415-418, doi: 10.1038/nature10534.

Gibbs DJ, Md Isa N, Movahedi M, Lozano-Juste J, Mendiondo GM, Berckhan S, Marín-de la Rosa N, Vicente Conde J, Sousa Correia C, Pearce SP, Bassel GW, Hamali B, Talloji P, Tomé DF, Coego A, Beynon J, Alabadí D, Bachmair A, León J, Gray JE, Theodoulou FL, Holdsworth MJ (2014) Nitric oxide sensing in plants is mediated by proteolytic control of group VII ERF transcription factors. *Mol. Cell*, **53**, 369–379.

Gibbs, D. J., Tedds, H. M., Labandera, A. M., Bailey, M., White, M. D., Hartman, S., Sprigg, C., Mogg, S. L., Osborne, R., Dambire, CC., Boeckx, T., Paling, Z., Voesenek, L. A. C. J., Flashman, E. & Holdsworth, M. J. (2018) Oxygen-dependent proteolysis regulates the stability of angiosperm polycomb repressive complex 2 subunit VERNALIZATION 2. *Nat Commun*, **9(1)**, 5438. doi: 10.1038/s41467-018-07875-7.

Gigli-Bisceglia. N., Gravino, M., Savatin, D.V. (2015) Luminol-based assay for detection of immunity elicitor-induced hydrogen peroxide production in *Arabidopsis thaliana* leaves. *Bio-protocol*, **5(24):e1685** http://www.bio-protocol.org/e1685

Gil, P., Dewey, E., Friml, J., Zhao, Y., Snowden, K. C., Putterill, J., Palme, K., Estelle, M., & Chory, J. (2001) BIG: a calossin-like protein required for polar auxin transport in Arabidopsis. *Genes & development*, *15*, 1985-1997 https://doi.org/10.1101/gad.905201

Gingerich, D. J., Hanada, K., Shiu, S. H. & Vierstra, R. D. (2007) Large-scale, lineage-specific expansion of a bric-a-brac/tramtrack/broad complex ubiquitin-ligase gene family in rice. *Plant Cell,* **19**, 2329–2348.

Giolai, M., Verweij, W., Lister, A. *et al.* Spatially resolved transcriptomics reveals plant host responses to pathogens. *Plant Methods* **15,** 114 (2019). https://doi.org/10.1186/s13007-019-0498-5

Giuntoli, B., Shukla, V., Maggiorelli, F., Giorgi, F. M., Lombardi, L., Perata, P., & Licausi, F. (2017). Age-dependent regulation of ERF-VII transcription factor activity in Arabidopsis thaliana. *Plant, cell & environment*, *40*(10), 2333–2346. https://doi.org/10.1111/pce.13037

Glazebrook, J. (2005) Contrasting Mechanisms of Defence Against Biotrophic and Necrotrophic Pathogens. *Annu. Rev. Phytopathol.*, **43**, 205-227.

Gomez-Gomez, L., Felix, G. & Bolller, T. (1999) A single locus determines the sensitivity to bacterial flagellin in *Arabidopsis thaliana*. *Plant J*, **18**(3), 277-284. doi: 10.1046/j.1365-313x.1999.00451.x.

Gomez-Gomez, L. & Boller, T. (2000) FLS2: An LRR Receptor–like Kinase Involved in the Perception of the Bacterial Elicitor Flagellin in *Arabidopsis. Molecular Cell*, **5**(6), 1003-1011.

Goslin, K., Eschen-Lippold, L., Naumann, C., Linster, E., Sorel, M., Klecker, M., de Marchi, R., Kind, A., Wirtz, M., Lee, J., Dissmeyer, N. & Graciet, E. (2019) Differential N-end Rule Degradation of RIN4/NOI Fragments Generated by the AvrRpt2 Effector Protease. *Plant Physiology*, **180**, 2272-2289.

Gou, M., Shi, Z., Zhu, Y., Bao, Z., Wang, G. & Hua, J. 2012. The F-box protein CPR1/CPR30 negatively regulates R protein SNC1 accumulation. Plant J, 69, 411-20.

Graciet, E., Walter, F., Maoileidigh, D.O., Pollmann, S., Meyerowitz, E.M., Varshavsky, A. & Wellmer, F. (2009) The N-end rule pathway controls multiple functions during Arabidopsis shoot and leaf development. *Proc. Natl Acad. Sci. USA*, **106**, 13618–13623.

Graciet, E., Mesiti, F. & Wellmer, F. (2010) Structure and evolutionary conservation of the plant N-end rule pathway. *The Plant Journal*, **61**, https://doi.org/10.1111/j.1365-313X.2009.04099.x.

Gravot, A., Richard, G., Lime, T., Lemarié, S., Jubault, M., Lariagon, C., Lemoine, J., Vicente, J., Robert-Seilaniantz, A., Holdsworth, , M. J., Manzanares-Dauleux, M. J. (2016) Hypoxia response in Arabidopsis roots infected by Plasmodiophora brassicae supports the development of clubroot. *BMC Plant Biology*, **16**:251.

Griffey, R.T., and Leach, J.G. (1965). The influence of age on tissue development of bean anthracnose lesions. *Phytopathology*, **55**, 915–918.

Gullner, G., Komives, T., Király, L., & Schröder, P. (2018). Glutathione S-Transferase Enzymes in Plant-Pathogen Interactions. *Frontiers in plant science*, *9*, 1836. https://doi.org/10.3389/fpls.2018.01836

Guo, Q., Zhang, J., Gao, Q., Xing, S., Li, F. & Wang, W. (2008) Drought tolerance through overexpression of monoubiquitin in transgenic tobacco. *J Plant Physiology*, **165(16)**, 1745-55. doi: 10.1016/j.jplph.2007.10.002.

Guo, X., Lu, W., Ma, Y., Qin, Q., & Hou, S. (2013). The BIG gene is required for auxin-mediated organ growth in Arabidopsis. *Planta*, **237**(4), 1135–1147. https://doi.org/10.1007/s00425-012-1834-4

Gupta, P. (2013) Characterization of Genetic Elements of Arabidopsis Thaliana Involved In Defense Responses against Bacterial Pathogen Pseudomonas Syringae. *Biology - Dissertations*. **84**. https://surface.syr.edu/bio_etd/84

Guzel Deger, A., Scherzer, S., Nuhkat, M., Kedzierska, J., Kollist, H., Brosché, M., Unyayar, S., Boudsocq, M., Hedrich, R., & Roelfsema, M. R. (2015). Guard cell SLAC1-type anion channels mediate flagellin-induced stomatal closure. *The New phytologist*, **208**(1), 162–173.

Haas, A. L., Warms, J. V., Hershko, A. & Rose, I. A. (1982) Ubiquitin-activating enzyme. Mechanism and role in protein-ubiquitin conjugation. *J Biol Chem*, **257** (5), 2543-2548.

Han, L., Li, G., Yang, K., Mao, G., Wang, R., Liu, Y. & Zhang, S. (2010) Mitogen-activated Protein Kinase 3 and 6 Regulate Botrytis Cinerea-Induced Ethylene Production in Arabidopsis. *Plant J.*, **64(1)**, 114-127. doi: 10.1111/j.1365-313X.2010.04318.x.

Han, G. (2018) Origin and evolution of the plant immune system. *New Phytologist*, **222**, https://doi.org/10.1111/nph.15596

Han, X., Li, S., Zhang, M., Yang, L., Liu, Y., Xu, J., & Zhang, S. (2019). Regulation of GDSL Lipase Gene Expression by the MPK3/MPK6 Cascade and Its Downstream WRKY Transcription Factors in *Arabidopsis* Immunity. *Molecular plant-microbe interactions : MPMI*, **32**(6), 673–684. https://doi.org/10.1094/MPMI-06-18-0171-R

Hann, Z. S., Cheng, J., Olsen, S. K., Lu, X. Lux, M. C., Tan, D. S. & Lima, C. D. (2019) Structural basis for adenylation and thioester bond formation in the ubiquitin E1

Proceedings of the National Academy of Sciences, **116** (31) 15475-15484; DOI: 10.1073/pnas.1905488116

Havecker, E. R., Wallbridge, L. M., Fedito, P., Hardcastle, T. J., & Baulcombe, D. C. (2012). Metastable differentially methylated regions within Arabidopsis inbred populations are associated with modified expression of non-coding transcripts. *PloS one*, **7**(9), e45242. https://doi.org/10.1371/journal.pone.0045242

He, Z., Ji, R., Havlickova, L. *et al.* Genome structural evolution in *Brassica* crops. *Nat. Plants* **7,** 757–765 (2021). https://doi.org/10.1038/s41477-021-00928-8

Hershko, A., Heller, H., Elias, S., and Ciechanover, A. 1983. Components of ubiquitin–protein ligase system. Resolution, affinity purification, and role in protein breakdown. J. Biol. Chem. 258: 8206– 8214.

Hershko, A. & Ciechanover, A. (1998) The ubiquitin system. *Annual Review of Biochemistry*, **67**, 425-479.

Hershko, A., Ciechanover, A., and Varshavsky, A. (2000) The ubiquitin system. *Nat. Med.* 10: 1073– 1081.

Hickman, R., Van Verk, M. C., Van Dijken, A., Mendes, M. P., Vroegop-Vos, I. A., Caarls, L., Steenbergen, M., Van der Nagel, I., Wesselink, G. J., Jironkin, A., Talbot, A., Rhodes, J., De Vries, M., Schuurink, R. C., Denby, K., Pieterse, C., & Van Wees, S. (2017). Architecture and Dynamics of the Jasmonic Acid Gene Regulatory Network. *The Plant cell*, **29**(9), 2086–2105. https://doi.org/10.1105/tpc.16.00958

Holman T. J., Jones, P. D., Russell, L., Medhurst, A., Ubeda Tomas, S., Talloji, P., Marquez, J., Schmuths, H., Tung, S. A., Taylor, I., Footitt, S., Bachmair, A., Theodoulou, F. L. & Holdsowrth, M. J. (2009) The N-end rule pathway promotes seed germination and establishment through removal of ABA sensitivity in Arabidopsis. *Proc Natl Acad Sci USA*, **10**, 4549–4554.

Hoppe, T. (2005) Multiubiquitylation by E4 enzymes: 'one size' doesn't fit all. *Trends Biochem Sci*, **30 (4)**, 183-187.

Hou, S., Liu, Z., Shen, H. & Wu, D. (2019) Damage-Associated Molecular Pattern-Triggered Immunity in Plants. *Front. Plant. Sci*, https://doi.org/10.3389/fpls.2019.00646

Houben, M., & Van de Poel, B. (2019). 1-Aminocyclopropane-1-Carboxylic Acid Oxidase (ACO): The Enzyme That Makes the Plant Hormone Ethylene. *Frontiers in plant science*, **10**, 695. https://doi.org/10.3389/fpls.2019.00695

Hsu, F. C., & Shih, M. C. (2013). Plant defense after flooding. *Plant signaling & behavior*, **8**(11), e26922. https://doi.org/10.4161/psb.26922

Hu, R. G., Sheng, J., Qi, X., Xu, Z., Takahashi, T. T. & Varshavsky, A. (2005) The N-end rule pathway as a nitric oxide sensor controlling the levels of multiple regulators. *Nature,* **437**, 981–986.

Hulsen, T., de Vlieg, T & Alkema, W. (2008) BioVenn - a web application for the comparison and visualization of biological lists using area-proportional Venn diagrams. BMC Genomics, 9 (1): 488

Huot, B., Yao, J., Montgomery, B. L. & He, S. Y. (2014) Growth-Defence Tradeoffs in Plants: A Balancing Act to Optimize Fitness. *Molecular Plant*, **7**(8), 1267-1287.

Ichinose Y. et al. (2003) Role of Flagella and Flagellin in Plant — *Pseudomonas syringae* Interactions. In: Iacobellis N.S. et al. (eds) Pseudomonas syringae and related pathogens. Springer, Dordrecht. https://doi.org/10.1007/978-94-017-0133-4_33

Igarashi, D., Bethke, G., Xu, Y., Tsuda, K., Glazebrook, J. & Katagiri, F. (2013) Pattern-Triggered Immunity Suppresses Programmed Cell Death Triggered by Fumonisin B1. *PLOS One*, 8(4):e60769. doi: 10.1371/journal.pone.0060769.

Ishiga, Y., Ishiga, T., Uppalapati, S. R., & Mysore, K. S. (2011) *Arabidopsis* seedling flood-inoculation technique: a rapid and reliable assay for studying plant-bacterial interactions. *Plant methods*, **7**, 32. https://doi.org/10.1186/1746-4811-7-32

Jabs, T., Tschöpe, M., Colling, C., Hahlbrock, K. and Scheel, D. (1997) Elicitor-stimulated ion fluxes and O2− from the oxidative burst are essential components in triggering defence gene activation and phytoalexin synthesis in parsley. *Proceedings of the National Academy of Sciences*, **94(9)**, 4800-4805.

Jeworutzki, E., Roelfsema, M. R., Anschultz, U., Krol, E., Elzenga, J. T., Felix, G., Boller, T., Hedrich, R. & Becker, D. (2010) Early signaling through the Arabidopsis pattern recognition receptors FLS2 and EFR involves Ca-associated opening of plasma membrane anion channels. *Plant J.*, **62**, 367-378.

Jingjing, C., Wenxing, P., Bing, C., Chunyu, Z. & Zhongyun, P. (2016) Transcriptome Analysis of Brassica rapa Near-Isogenic Lines Carrying Clubroot-Resistant and –Susceptible Alleles in Response to Plasmodiophora brassicae during Early Infection. *Front. Plant Sci.*, **6**, 1183. https://doi.org/10.3389/fpls.2015.01183

Jones, D.A., and Jones, J.D.G. (1997). The role of leucine-rich repeat proteins in plant defences. In *Advances in Botanical Research Incorporating Advances in Plant Pathology*, **24**, (London: Academic Press), 89–167.

Jones, J. D. G & Dangl, J. L. (2006) The plant immune system. *Nature,* **444,** 323-329.

Kadota, Y., Sklenar, J., Derbyshire, P., Stransfeld, L., Asai, S., Ntoukakis, V., Jones, J.D., Shirasu, K., Menke, F., Jones, A. and Zipfel, C., 2014. Direct regulation of the NADPH oxidase RBOHD by the PRR-associated kinase BIK1 during plant immunity. *Molecular cell*, **54**(1), 43-55.

Kagias, K., Nehammer, C., & Pocock, R. (2012). Neuronal responses to physiological stress. *Frontiers in genetics*, **3**, 222, https://doi.org/10.3389/fgene.2012.00222

Kaku, H., Nishizawa, Y., Ishii-Minami, N., Akimoto-Tomiyama, C., Dohmae, N., Takio, K., Minami, E., & Shibuya, N. (2006). Plant cells recognize chitin fragments for defence signaling through a plasma membrane receptor. Proceedings of the National Academy of Sciences of the United States of America, 103(29), 11086–11091. https://doi.org/10.1073/pnas.0508882103

Kanyuka, K., Praekelt, U., Franklin, K. A., Billingham, O. E., Hooley, R., Whitelam, G. C., & Halliday, K. J. (2003). Mutations in the huge Arabidopsis gene BIG affect a range of hormone and light responses. *The Plant journal : for cell and molecular biology*, *35*(1), 57–70. https://doi.org/10.1046/j.1365-313x.2003.01779.x

Kasajima, I., Ohkama-Ohtsu, N., Ide, Y., Hayashi, H., Yoneyama, T., Suzuki, Y., Naito, S. & Fujiwara, T. (2007) The *BIG* gene is involved in regulation of sulfur deficiency-responsive genes in *Arabidopsis thaliana*. *Physiologia Plantarum*, **129**, 351-363.

Khan, N., Hu, C., Khan, W. A., Naseri, E., Ke, H., Huiji, D. & Hou, X. (2018) Evolution and Expression Divergence of E2 Gene Family under Multiple Abiotic and Phytohormones Stresses in *Brassica rapa*. *Biomed Res Int*., **2018: 5206758,** doi: 10.1155/2018/5206758.

Kim, M. G., da Cunha, L., McFall, A. J., Belkhadir, Y., DebRoy, S., Dangl, J. L., & Mackey, D. (2005). Two Pseudomonas syringae type III effectors inhibit RIN4-regulated basal defense in Arabidopsis. *Cell*, **121**(5), 749–759. https://doi.org/10.1016/j.cell.2005.03.025

Kim, J. G., Shin, H. C., Seo, T., Nawale, L., Han, G., Kim, B. Y., Kim, S. J., & Cha-Molstad, H. (2021). Signaling Pathways Regulated by UBR Box-Containing E3 Ligases. *International journal of molecular sciences*, **22**(15), 8323. https://doi.org/10.3390/ijms22158323

Klassen, A. J., Downey, R. K. & Capcara, J. J. (1986) Westar Summer Rape. *Can. J. Plant Sci*., **67,** 491-493.

Klecker, M., Gasch, P., Peisker, H., Dormann, P., Schlicke, H., Grimm, B. & Mustroph, A. (2014) A shoot-specific hypoxic response of Arabidopsis sheds light on the role of the phosphate-responsive transcription factor PHOSPHATE STARVATION RESPONSE1. *Plant Physiology*, **165**, 774-790.

Koegl, M., Hoppe, T., Schlenker, S., Ulrich, H. D., Mayer, T. U.& Jentsch, S. (1999) A novel ubiquitination factor, E4, is involved in multiubiquitin chain assembly. *Cell*, **96 (5)**, 635-644.

Komander, D. & Rape, M. (2012) The Ubiquitin Code. *Annu. Rev. Biochem.*, **81**, 203-229.

Kopp F, Steiner R, Dahlmann B, Kuehn L, Reinauer H. (1986) Size and shape of the multicatalytic proteinase from rat skeletal muscle". *Biochimica et Biophysica Acta.*, **872 (3),** 253–60.

Koren, I., Timms, R. T., Kula, T., Xu, Q., Li, M. Z. & Elledge, S. J. (2018) The Eukaryotic Proteome is Shaped by E3 Ubiquitin Ligases Targeting C-terminal Degrons. *Cell*, **173 (7)**, 1622-1635.

Kriventseva, E. V., Kuznetsov, D., Tegenfeldt, F., Manni, M., Dias, R., Simão, F. A., & Zdobnov, E. M. (2019). OrthoDB v10: sampling the diversity of animal, plant, fungal, protist, bacterial and viral genomes for evolutionary and functional annotations of orthologs. *Nucleic acids research*, **47**(D1), D807–D811. https://doi.org/10.1093/nar/gky1053

Krysan, P. J. & Colcombet, J. (2018) Cellular Complexity in MAPK Signaling in Plants: Questions and Emerging Tools to Answer Them. *Front. Plant Sci.*, https://doi.org/10.3389/fpls.2018.01674.

Kunze, G., Zipfel, C., Robatzek, S., Niehaus, K., Boller, T. & Felix, G. (2004) The N Terminus of Bacterial Elongation Factor Tu Elicits Innate Immunity in Arabidopsis Plants. *Plant Cell*, **16**(12), 3496-507, doi: 10.1105/tpc.104.026765.

Kus, J. V., Zaton, K., Sarkar, R., & Cameron, R. K. (2002). Age-related resistance in Arabidopsis is a developmentally regulated defense response to Pseudomonas syringae. *The Plant cell*, *14*(2), 479–490. https://doi.org/10.1105/tpc.010481

Kwon, Y.T., Kashina, A.S. and Varshavsky, A. (1999) Alternative splicing results in differential expression, activity, and localization of the two forms of arginyl–tRNA–protein transferase, a component of the N-end rule pathway. *Mol. Cell. Biol.* **19**, 182–193.

Kwon, Y.T., Balogh, S.A., Davydov, I.V., Kashina, A.S., Yoon, J.K., Xie, Y., Gaur, A., Hyde, L., Denenberg, V.H. and Varshavsky, A. (2000) Altered activity, social behavior, and spatial memory in mice lacking the NTAN1p amidase and the asparagine branch of the N-end rule pathway. *Mol. Cell. Biol.* **20**, 4135–4148.

Labandera, A. M., Tedds, H. M., Bailey, M., Sprigg, C., Etherington, R. D., Akintewe, O., Kalleechurn, G., Holdsworth, M. J. & Gibbs, D. J. (2020) The PRT6 N-degron pathway restricts VERNALIZATION 2 to endogenous hypoxic niches to modulate plant development. *New Phytologist*. doi: 10.1111/nph.16477. [Epub ahead of print]

Lam YA, Lawson TG, Velayutham M, Zweier JL, Pickart CM (2002) *Nature*, **416(6882)**, 763-7.

Lang, J., & Colcombet, J. (2020). Sustained Incompatibility between MAPK Signaling and Pathogen Effectors. *International journal of molecular sciences*, **21(**21), 7954 https://doi.org/10.3390/ijms21217954

Lee, J. & Kim, W. T. (2011) Regulation of Abiotic Stress Signal Transduction by E3 Ubiquitin Ligases in Arabidopsis. *Mol Cells*, **31 (3)**, 201-208, doi: 10.1007/s10059-011-0031-9.

Lee, D., Lal, N. K., Lin, Z. D., Ma, S., Liu, J., Castro, B., Toruño, T., Dinesh-Kumar, S. P., & Coaker, G. (2020). Regulation of reactive oxygen species during plant immunity through

phosphorylation and ubiquitination of RBOHD. *Nature communications*, **11**(1), 1838. https://doi.org/10.1038/s41467-020-15601-5

Leestemaker, Y., & Ovaa, H. (2017). Tools to investigate the ubiquitin proteasome system. *Drug discovery today. Technologies*, *26*, 25–31. doi.org/10.1016/j.ddtec.2017.11.006.

Lefever, S., Rihani, A., Van der Meulen, J. *et al.* Cost-effective and robust genotyping using double-mismatch allele-specific quantitative PCR. *Sci Rep* **9,** 2150 (2019). https://doi.org/10.1038/s41598-019-38581-z

Li, L., Li, M., Yu, L., Zhou, Z., Liang, X., Liu, Z., Cai, G., Gao, L., Zhang, X., Wang, Y., Chen, S. & Zhou, J. (2014) The FLS2-associated kinase BIK1 directly phosphorylates the NADPH oxidase RbohD to control plant immunity. *Cell Host Microbe*, **15**, 329-338. https://doi.org/10.1016/j.chom.2014.02.009

Li, J.F. and Nebenfuhr, A**.** (2010) FAST technique for Agrobacterium-mediated transient gene expression in seedlings of Arabidopsis and other plant species. *Cold Spring Harb Protoc*, 2010, pdb prot5428.

Libault, M., Wan, J., Czechowski, T., Udvardi, M., & Stacey, G. (2007) Identification of 118 Arabidopsis transcription factor and 30 ubiquitin-ligase genes responding to chitin, a plant-defence elicitor. *Molecular plant-microbe interactions : MPMI*, **20(8)**, 900–911. https://doi.org/10.1094/MPMI-20-8-0900

Licausi, F., van Dongen, J. T., Giuntoli, B., Novi, G., Santaniello, A., Geigenberger, P., & Perata, P. (2010). HRE1 and HRE2, two hypoxia-inducible ethylene response factors, affect anaerobic responses in Arabidopsis thaliana. *The Plant journal : for cell and molecular biology*, **62**(2), 302–315.

Licausi, F., Weits, D. A., Pant, B. D., Scheible, W. R., Geigenberger, P., & van Dongen, J. T. (2011). Hypoxia responsive gene expression is mediated by various subsets of transcription factors and miRNAs that are determined by the actual oxygen availability. *The New phytologist*, **190**(2), 442–456. https://doi.org/10.1111/j.1469-8137.2010.03451.x

Lin, H. C., Yeh, C. W., Chen, Y. F., Lee, T. T., Hsieh, P. Y., Rusnac, D. V., Lin, S. Y., Elledge, S. J., Zheng, N. & Yen, H. S. (2018) C-Terminal End-Directed Protein Elimination by CRL2 Ubiquitin Ligases. *Mol Cell*, **70(4)**, 602-613.

Lindsey, B. E., 3rd, Rivero, L., Calhoun, C. S., Grotewold, E., & Brkljacic, J. (2017) Standardized Method for High-throughput Sterilization of Arabidopsis Seeds. *Journal of visualized experiments*, (128), 56587. https://doi.org/10.3791/56587

Liu, Y., Maierhofer, T., Rybak, K., Sklenar, J., Breakspear, A., Johnston, M. G., Fliegmann, J., Huang, S., Roelfsema, M., Felix, G., Faulkner, C., Menke, F. L., Geiger, D., Hedrich, R., & Robatzek, S. (2019) Anion channel SLAH3 is a regulatory target of chitin receptor-associated kinase PBL27 in microbial stomatal closure. *eLife*, **8**, e44474. https://doi.org/10.7554/eLife.44474

Liu, X., Grabherr, H. M., Willmann, R., Kolb, D., Brunner, F., Bertsche, U., Kühner, D., Franz-Wachtel, M., Amin, B., Felix, G., Ongena, M., Nürnberger, T., & Gust, A. A. (2014). Host-induced

bacterial cell wall decomposition mediates pattern-triggered immunity in Arabidopsis. *eLife*, **3**, e01990. https://doi.org/10.7554/eLife.01990

Livneh, I., Cohen-Kaplan, V., Cohen-Rosenzweig, C., Avni, N. & Ciechanover, A. (2016) The life cycle of the 26S proteasome: from birth, through regulation and function, and onto its death. Cell Res **26**, 869–885. https://doi.org/10.1038/cr.2016.86

Lloyd, S. R., Schoonbeek, H. J., Trick, M., Zipfel, C., & Ridout, C. J. (2014). Methods to study PAMP-triggered immunity in Brassica species. *Molecular plant-microbe interactions : MPMI*, **27**(3), 286–295. https://doi.org/10.1094/MPMI-05-13-0154-FI

Lysak MA, Koch MA, Pecinka A, Schubert I. (2005) Chromosome triplication found across the tribe Brassiceae. Genome Research15: 516-525. 10.1101/gr.3531105.

Ma, X., Claus, L., Leslie, M. E., Tao, K., Wu, Z., Liu, J., Yu, X., Li, B., Zhou, J., Savatin, D. V., Peng, J., Tyler, B. M., Heese, A., Russinova, E., He, P., & Shan, L. (2020). Ligand-induced monoubiquitination of BIK1 regulates plant immunity. *Nature*, **581**(7807), 199–203. https://doi.org/10.1038/s41586-020-2210-3

Macho, A. P. & Zipfel, C. (2014) Plant PRRs and the Activation of Innate Immune Signaling. *Molecular Cell*, **54**(2), 263-272. https://doi.org/10.1016/j.molcel.2014.03.028

Mackey, D., Holt III, B. F.., Wiig, A. & Dangl, J. L. (2002). RIN4 Interacts with *Pseudomonas syringae* Type III Effector Molecules and Is Required for RPM1-Mediated Resistance in *Arabidopsis. Cell*, **108**(6), 743-754.

Mao, G., Meng, X., Liu, Y., Zheng, Z., Chen, Z., & Zhang, S. (2011). Phosphorylation of a WRKY transcription factor by two pathogen-responsive MAPKs drives phytoalexin biosynthesis in *Arabidopsis*. *The Plant Cell*, *23*(4), 1639–1653. https://doi.org/10.1105/tpc.111.084996

Marowa, P., Ding, A., & Kong, Y. (2016). Expansins: roles in plant growth and potential applications in crop improvement. Plant cell reports, **35**(5), 949–965. https://doi.org/10.1007/s00299-016-1948-4

Matschi, S., Werner, S., Schulze, W.X., Legen, J., Hilger, H.H. and Romeis, T. (2013), Function of calcium-dependent protein kinase CPK28 of *Arabidopsis thaliana* in plant stem elongation and vascular development. *Plant J*, **73**, 883-896. https://doi.org/10.1111/tpj.12090

McBride, K. E., & Summerfelt, K. R. (1990). Improved binary vectors for Agrobacterium-mediated plant transformation. *Plant molecular biology*, *14*(2), 269–276. https://doi.org/10.1007/BF00018567

McDonald, B. A., & Stukenbrock, E. H. (2016). Rapid emergence of pathogens in agro-ecosystems: global threats to agricultural sustainability and food security. *Philosophical transactions of the Royal Society of London. Series B, Biological sciences*, *371*(1709), 20160026. doi.org/10.1098/rstb.2016.0026

McVetty, P. B. E., Lukow, O. M., Hall, L. M., Rajcan, I. & Rahman, H. (2016) Oilseeds in North America. *Food Science*. doi.org/10.1016/B978-0-08-100596-5.00052-4

Melotto, M., Underwood, W., Koczan, J., Nomura, K., & He, S. Y. (2006). Plant stomata function in innate immunity against bacterial invasion. *Cell*, **126**(5), 969–980. https://doi.org/10.1016/j.cell.2006.06.054

Melotto, M., Zhang, L., Oblessuc, P. R., & He, S. Y. (2017). Stomatal Defence a Decade Later. *Plant Physiology*, **174**(2), 561–571. https://doi.org/10.1104/pp.16.01853

Mendiondo, G. M., Gibbs, D. J., Szurman-Zubrzycka, M., Korn, A., Marquez, J., Szarejko, I., Maluszynski, M., King, J., Axcell, B., Smart, K., Corbineau, F., & Holdsworth, M. J. (2016). Enhanced waterlogging tolerance in barley by manipulation of expression of the N-end rule pathway E3 ligase PROTEOLYSIS6. *Plant biotechnology journal*, *14*(1), 40–50. https://doi.org/10.1111/pbi.12334

Meng, X. & Zhang, S. (2013) MAPK Cascades in Plant Disease Resistance Signaling. *Annual Review of Phytopathology*, **51**, 245-266.

Miricescu, A., Goslin, K., & Graciet, E. (2018). Ubiquitylation in plants: signaling hub for the integration of environmental signals. *Journal of experimental botany*, *69*(19), 4511–4527. https://doi.org/10.1093/jxb/ery165

Miricescu, A. (2019) Identification and generation of new germplasms in barley with increased tolerance to waterlogging.

Miya, A., Albert, P., Shinya, T., Desaki, Y., Ichimura, K., Shirasu, K., Narusaka, Y., Kawakami, N., Kaku, H. & Shibuya, N. (2007) CERK1, a LysM receptor kinase, is essential for chitin elicitor signaling in *Arabidopsis*. *Proc Natl Acad Sci U S A*, **104(49)**, 19613-19618. doi: 10.1073/pnas.0705147104

Moeder. W., Urquhart, W., Ung, H. & Yoshioka, K. (2011) The role of cyclic nucleotide-gated ion channels in plant immunity. *Mol. Plant.,* **4(3)**, 442-452. doi: 10.1093/mp/ssr018.

Monaghan, J., Matschi, S., Shorinola, O., Rovenich, H., Matei, A., Segonzac, C., Malinovsky, F. G., Rathjen, J. P., MacLean, D., Romeis, T., & Zipfel, C. (2014). The calcium-dependent protein kinase CPK28 buffers plant immunity and regulates BIK1 turnover. *Cell host & microbe*, **16**(5), 605–615. https://doi.org/10.1016/j.chom.2014.10.007

Monaghan, J. & Zipfel, C. (2012) Plant Pattern Recognition Receptor Complexes at the Plasma Membrane. *Curr Opin Plant Biol.*, **15(4)**, 349-357. doi: 10.1016/j.pbi.2012.05.006.

Mooney, B. C. & Graciet, E. (2020) A simple and efficient Agrobacterium-mediated transient expression system to dissect molecular processes in *Brassica rapa* and *Brassica napus*. *Plant Direct*, **4**, 1-12. https://doi.org/10.1002/pld3.237.

Morcx S Kunz C Choquer Met al. (2013) Disruption of Bcchs4, Bcchs6 or Bcchs7 chitin synthase genes in Botrytis cinerea and the essential role of class VI chitin synthase (Bcchs6). *Fungal Genet Biol* **52** 18.

Mun, JH., Kwon, SJ., Yang, TJ. *et al.* (2009) Genome-wide comparative analysis of the *Brassica rapa* gene space reveals genome shrinkage and differential loss of duplicated genes after

whole genome triplication. *Genome Biol* **10,** R111 https://doi.org/10.1186/gb-2009-10-10-r111

Mustroph A, Zanetti ME, Jang CJH, Holtan HE, Repetti PP, Galbraith DW, Girke T, Bailey-Serres J (2009) Profiling translatomes of discrete cell populations resolves altered cellular priorities during hypoxia in Arabidopsis. *Proc Natl Acad Sci USA*, **106**, 18843–18848.

Nakamura N. (2018). Ubiquitin System. *International journal of molecular sciences*, **19(4)**, 1080. https://doi.org/10.3390/ijms19041080

Navarro, L., Zipfel, C., Rowland, O., Keller, I., Robatzek, S., Boller, T., & Jones, J. D. (2004). The transcriptional innate immune response to flg22. Interplay and overlap with Avr gene-dependent defence responses and bacterial pathogenesis. *Plant physiology*, **135(2)**, 1113–1128. https://doi.org/10.1104/pp.103.036749

Neff, M. M., Neff, J. D., Chory, J. & Pepper, A. E. (1998) dCAPS, a simple technique for the genetic analysis of singlenucleotide polymorphisms: experimental applications in *Arabidopsis thaliana* genetics. *The Plant Journal* **14**(3), 387-392.

Neik, T. X., Barbetti, M. J., & Batley, J. (2017). Current Status and Challenges in Identifying Disease Resistance Genes in *Brassica napus*. *Frontiers in plant science*, **8**, 1788. doi.org/10.3389/fpls.2017.01788

Ngou, B.P.M., Ahn, HK., Ding, P. *et al.* Mutual potentiation of plant immunity by cell-surface and intracellular receptors. *Nature* **592,** 110–115 (2021). https://doi.org/10.1038/s41586-021-03315-7

Oliveros, J.C. (2007-2015) Venny. An interactive tool for comparing lists with Venn's diagrams. https://bioinfogp.cnb.csic.es/tools/venny/index.html

Ó Lochlainn, S., Amoah, S., Graham, N.S. *et al.* High Resolution Melt (HRM) analysis is an efficient tool to genotype EMS mutants in complex crop genomes. *Plant Methods* **7,** 43 (2011). https://doi.org/10.1186/1746-4811-7-43

O'Malley, R. C., Barragan, C. C., & Ecker, J. R. (2015). A user's guide to the Arabidopsis T-DNA insertion mutant collections. *Methods in molecular biology (Clifton, N.J.)*, **1284**, 323–342. https://doi.org/10.1007/978-1-4939-2444-8_16

Padmanabhan, M., Cournoyer, P. & Dinesh-Kumar, S. P. (2009) The Leucine-Rich Repeat Domain in Plant Innate Immunity: A Wealth of Possibilities. *Cell Microbiol.*, **11(2)**, 191-198. doi: 10.1111/j.1462-5822.2008.01260.x.

Petersen, K., Qiu, J. L., Lütje, J., Fiil, B. K., Hansen, S., Mundy, J., & Petersen, M. (2010). Arabidopsis MKS1 is involved in basal immunity and requires an intact N-terminal domain for proper function. *PloS one*, **5**(12), e14364. https://doi.org/10.1371/journal.pone.0014364

Pillitteri, L. J., & Dong, J. (2013). Stomatal development in Arabidopsis. *The Arabidopsis Book*, **11**, e0162. https://doi.org/10.1199/tab.0162

Poirier, B. C., Feldman, M. J., & Lange, B. M. (2018). bHLH093/NFL and bHLH061 are required for apical meristem function in Arabidopsis thaliana. *Plant signaling & behavior*, *13*(7), e1486146. https://doi.org/10.1080/15592324.2018.1486146

Potuschak, T., Stary, S., Schlögelhofer, P., Becker, F., Nejinskaia, V., & Bachmair, A. (1998). PRT1 of Arabidopsis thaliana encodes a component of the plant N-end rule pathway. *Proceedings of the National Academy of Sciences of the United States of America*, **95(14)**, 7904–7908. https://doi.org/10.1073/pnas.95.14.7904

Procko, C., Crenshaw, C. M., Ljung, K., Noel, J. P., Chory, J. (2014) Cotyledon-Generated Auxin Is Required for Shade-Induced Hypocotyl Growth in Brassica rapa, Plant Physiology, Volume **165**, Issue 3, 1285–1301, https://doi.org/10.1104/pp.114.241844

Qi, J., Wang, J., Gong, Z. & Zhou, J. (2017) Apoplastic ROS signaling in plant immunity. *Current Opinion in Plant Biology*, **38**, 92-100.

Ray, R. V., Gevaert, K. & Holdsworth, M. (2018) Distinct branches of the N-end rule pathway modulate the plant immune response. *New Phytologist*, **221**, https://doi.org/10.1111/nph.15387.

Riber, W., Muller, J. T., Visser, E. J., Sasidharan, R., Voesenek, L. A. & Mustroph, A. (2015) The greening after extended darkness1 is an N-end rule pathway mutant with high tolerance to submergence and starvation. *Plant Physiol.*, **167(4)**, 1616-1629. doi: 10.1104/pp.114.253088.

Rossez, Y., Wolfson, E. B., Holmes, A., Gally, D. L. & Holden, N. J. (2015) Bacterial Flagella: Twist and Stick, or Dodge across the Kingdoms. *PLoS Pathog.*, **11**(1): e1004483. doi: 10.1371/journal.ppat.1004483

Rudolf, E. E., Hüther, P., Forné, I., Georgii, E., Han, Y., Hell, R., Wirtz, M., Imhof, A., Becker, C., Durner, J., & Lindermayr, C. (2021). GSNOR Contributes to Demethylation and Expression of Transposable Elements and Stress-Responsive Genes. *Antioxidants (Basel, Switzerland)*, **10**(7), 1128. https://doi.org/10.3390/antiox10071128

Russell, A. R., Ashfield, T. & Innes, R. W. (2015) *Pseudomonas syringae* Effector AvrPphB Suppresses AvrB-Induced Activation of RPM1 but Not AvrRpm1-Induced Activation. *MPMI*, **28**(6), 727-735.

Safaeizadeh, M., Boller, T. & Becker, C. (2021) Transcriptomic profiling uncovers novel players in innate immunity in *Arabidopsis thaliana*. *bioRxiv* 2021.01.02.425067, doi: https://doi.org/10.1101/2021.01.02.425067

Sánchez-Vallet, A., Mesters, J. R. & Thomma, B. P. H. J. (2015) The battle for chitin recognition in plant-microbe interactions. *FEMS Microbiology Reviews*, **39,** 171-183.

Sanimah, S., Sundakar, J.T., Linthorst, H. and Verpoorte, R. (2010) Optimization conditions for *Agrobacterium*-mediated transformation of *Brassica rapa* with a bacterial isochorismate synthase gene. *J. Trop. Agric. and Fd. Sc.*, **38**, 189-202.

Schaffner, W. & Weissmann, C. (1973) A rapid, sensitive, and specific method for the determination of protein in dilute solution. *Analytical Biochemistry*, **56**, 502-514.

Schmitz, R. J., Schultz, M. D., Lewsey, M. G., O'Malley, R. C., Urich, M. A., Libiger, O., Schork, N. J., & Ecker, J. R. (2011). Transgenerational epigenetic instability is a source of novel methylation variants. Science, **334** (6054), 369–373. https://doi.org/10.1126/science.1212959

Schuessele, C., Hoernstein, S. N. W., Mueller, S. J., Rodriguez-Franco, M., Lorenz, T., Lang, D., Igloi, G. L. & Reski, R. (2015) Spatio-temporal patterning of arginyl-tRNA protein transferase (ATE) contributes to gametophytic development in a moss. *New Phytologist*, **209 (3)**, https://doi.org/10.1111/nph.13656

Sega G. A. (1984). A review of the genetic effects of ethyl methanesulfonate. *Mutation research*, **134**(2-3), 113–142. https://doi.org/10.1016/0165-1110(84)90007-1

Seybold, H., Trempel, F., Ranf, S., Scheel, D., Romeis, T. & Lee, J. (2014) Ca2+ signalling in plant immune response: from pattern recognition receptors to Ca2+ decoding mechanisms. *New Phytologist*, **204(4)**. https://doi.org/10.1111/nph.13031

Seyfferth, C., & Tsuda, K. (2014). Salicylic acid signal transduction: the initiation of biosynthesis, perception and transcriptional reprogramming. *Frontiers in plant science*, **5**, 697. https://doi.org/10.3389/fpls.2014.00697

Sharma, B., Joshi, D., Yadav, P. K., Gupta, A. K. & Bhatt, T. K. (2016) Role of Ubiquitin-Mediated Degradation in Plant Biology. *Front Plant Sci*, **7**: **806**, doi: 10.3389/fpls.2016.00806

Shetty, N. P., Mehrabi, R., Lutken, H., Haldrup, A., Kema, G. H., Collinge, D. B. Jørgensen, H. J. (2007) Role of hydrogen peroxide during the interaction between the hemibiotrophic fungal pathogen Septoria tritici and wheat. *New Phytologist*,**174(3)**, 637-647. DOI: 10.1111/j.1469-8137.2007.02026.x

Smith J.M., Heese, A. (2014) Rapid bioassay to measure early reactive oxygen species production in Arabidopsis leave tissue in response to living *Pseudomonas syringae*. *Plant Methods*, **10**, 6. doi:10.1186/1746-4811-10-6

Song, W. Y., Wang, G. L., Chen, L. L., Kim, H. S., Pi, L. Y., Holsten, T., Gardner, J., Wang, B., Zhai, W. X., Zhu, L. H., Fauquet, C. & Ronald, P. (1995) A receptor kinase-like protein encoded by the rice disease resistance gene, Xa21. *Science*, **270**, 1804-1806.

Sorel, M., Mooney, B., de Marchi, R. and Graciet, E. (2019). Ubiquitin/Proteasome System in Plant Pathogen Responses. *Annual Plant Reviews online*, J.A. Roberts (Ed.). doi:10.1002/9781119312994.apr0665

Soulie MC Piffeteau A Choquer Met al. (2003) Disruption of Botrytis cinerea class I chitin synthase gene Bcchs1 results in cell wall weakening and reduced virulence *Fungal Genet Biol.* **40** 3846.

Soulie, M. C., Perino, C., Piffeteau Aet al. (2006) *Botrytis cinerea* virulence is drastically reduced after disruption of chitin synthase class III gene (Bcchs3a) *Cell Microbiol* 8 131021.

Sparrow, P.A., Dale, P.J. and Irwin, J.A**.** (2006) Brassica oleracea. *Methods Mol Biol*, **343**, 417-426.

Stary, S., Yin, X.J., Potuschak, T., Schlogelhofer, P., Nizhynska, V. and Bachmair, A. (2003) PRT1 of Arabidopsis is a ubiquitin protein ligase of the plant N-end rule pathway with specificity for aromatic amino-terminal residues. *Plant Physiol.*, **133**, 1360–1366.

Stephenson, P., Baker, D., Girin, T., Perez, A., Amoah, S., King, G.J. and Ostergaard, L. (2010) A rich TILLING resource for studying gene function in Brassica rapa. *BMC Plant Biol.*, **10**, 62.

Stephenson, P., Stacey, N., Brüser, M., Pullen, N., Ilyas, M., O'Neill, C., Wells, R., & Østergaard, L. (2019). The power of model-to-crop translation illustrated by reducing seed loss from pod shatter in oilseed rape. *Plant reproduction*, **32(**4), 331–340. https://doi.org/10.1007/s00497-019-00374-9

Stone, S. L. & Callis, J. (2007) Ubiquitin ligases mediate growth and development by promoting protein death. *Curr Opin Plant Biol.*, **10 (6)**, 624-632.

Stone, S. L. (2014) The role of ubiquitin and the 26S proteasome in plant abiotic stress signaling. *Front. Plant Sci.*, https://doi.org/10.3389/fpls.2014.00135

Strodtkötter, I., Padmasree, K., Dinakar, C., Speth, B., Niazi, P. S., Wojtera, J., Voss, I., Do, P. T., Nunes-Nesi, A., Fernie, A. R., Linke, V., Raghavendra, A. S., & Scheibe, R. (2009). Induction of the AOX1D isoform of alternative oxidase in A. thaliana T-DNA insertion lines lacking isoform AOX1A is insufficient to optimize photosynthesis when treated with antimycin A. *Molecular plant*, **2**(2), 284–297. https://doi.org/10.1093/mp/ssn089

Sun, Y., Li, L., Macho, A. P., Han, Z., Hu, Z., Zipfel, C., Zhou, J. & Chai, J. (2013) Structural Basis for flg22-induced Activation of the Arabidopsis FLS2-BAK1 Immune Complex. *Science*, **342**(6158):624-628. doi: 10.1126/science.1243825.

Suzuki, N., Miller, G., Morales, J., Shulaev, V., Torres, M.A. and Mittler, R., 2011. Respiratory burst oxidases: the engines of ROS signaling. *Current opinion in plant biology*, **14(6)**, 691-699.

Swatek, K. N. & Komander, D. (2016) Ubiquitin modifications. *Cell Research*,**26,** 399-422, https://doi.org/10.1038/cr.2016.39.

Takemoto D, Jones DA (2005) Membrane release and destabilization of Arabidopsis RIN4 following cleavage by Pseudomonas syringae AvrRpt2. *Mol Plant Microbe Interact,* 18, 1258–1268.

Tasaki, T., Mulder, L.C., Iwamatsu, A., Lee, M.J., Davydov, I.V., Varshavsky, A., Muesing, M. and Kwon, Y.T. (2005) A family of mammalian E3 ubiquitin ligases that contain the UBR box motif and recognize N-degrons. *Mol. Cell. Biol.* **25**, 7120–7136.

The Brassica rapa Genome Sequencing Project Consortium., Wang, X., Wang, H. *et al.* The genome of the mesopolyploid crop species *Brassica rapa*. *Nat Genet* **43,** 1035–1039 (2011). https://doi.org/10.1038/ng.919

Thrower, J. S., Hoffman, L., Rechsteiner, M. & Pickart, C. M. (2000) Recognition of the polyubiquitin proteolytic signal. *EMBO J*, **19(1),** 94-102.

Tian, W., Hou, C., Ren, Z., Wang, C., Zhao, F., Dahlbeck, D., Hu, S., Zhang, L., Niu, Q., Li, L., Staskawicz, B. J. & Luan, S. (2019) A calmodulin-gated calcium channel links pathogen patterns to plant immunity. *Nature*, **572,** 131–135.

Till, C. J., Vicente, J., Zhang, H., Oszvald, M., Deery, M. J., Pastor, V., Lilley, K. S., Ray, R. V., Theodoulou, F. L. & Holdsworth, M. J. (2019) The *Arabidopsis thaliana* N-recognin E3 ligase PROTEOLYSIS1 influences the immune response. *Plant Direct*, **3**, https://doi.org/10.1002/pld3.194.

Tong, C., Wang, X., Yu, J., Wu, J., Li, W., Huang, J., Dong, C., Hua, W. & Liu, S. (2013) Comprehensive analysis of RNA-seq data reveals the complexity of the transcriptome in Brassica rapa. *BMC Genomics*, **14**, 689.

Torres, M. A, Dangl, J. L. & Jones, J. D. G. (2002) *Arabidopsis* gp91^{phox} homologues *AtrbohD* and *AtrbohF* are required for accumulation of reactive oxygen intermediates in the plant defence response. *Proceedings of the National Academy of Sciences*, **99** (1), 517-522, https://doi.org/10.1073/pnas.012452499

Trick M, Kwon S-J, Choi SR, Fraser F, Soumpourou E, Drou N, Wang Z, Lee SY, Yang T-J, Mun J-H, et al: Complexity of genome evolution by segmental rearrangement in *Brassica rapa* revealed by sequence-level analysis. BMC Genomics. 2009, 10: 539-10.1186/1471-2164-10-539.

Tsuda, K., Sato, M., Glazebrook, J., Cohen, J. D., & Katagiri, F. (2008). Interplay between MAMP-triggered and SA-mediated defence responses. *The Plant journal : for cell and molecular biology*, **53(5)**, 763–775. https://doi.org/10.1111/j.1365-313X.2007.03369.x

Tsuda, K. & Somssih, I. E. (2015) Transcriptional Networks in Plant Immunity. *New Phytol.*, **206(3)**, 932-947. doi: 10.1111/nph.13286

Valeri, M. C., Novi, G., Weits, D. A., Mensuali, A., Perata, P., & Loreti, E. (2021). Botrytis cinerea induces local hypoxia in Arabidopsis leaves. *The New phytologist*, *229*(1), 173–185. https://doi.org/10.1111/nph.16513

Van Nocker S, Deveraux Q, Rechsteiner M, Vierstra RD (1996) *Proc Natl Acad Sci U S A,* **93(2),**856-60.

Varshavsky, A. (1996) The N-end rule: functions, mysteries, uses. *Proc. Natl Acad. Sci. USA*, **93**, 12142–12149.

Varshavsky A. Discovery of cellular regulation by protein degradation. *J Biol Chem*. 2008;283(50):34469–34489. doi:10.1074/jbc.X800009200

Varshavsky, A. (2006) The early history of the ubiquitin field. *Protein science*, **15**(3), https://doi.org/10.1110/ps.052012306

Varshavsky, A. (2019) N-degron and C-degron pathways of protein degradation. *PNAS*, **116**(2), 358-366, https://doi.org/10.1073/pnas.1816596116.

Vicente J, Mendiondo GM, Movahedi M, Peirats-Llobet M, Juan YT, Shen YY, Dambire C, Smart K, Rodriguez PL, Charng YY, Gray JE, Holdsworth MJ (2017) The Cys-Arg/N-End Rule Pathway Is a General Sensor of Abiotic Stress in Flowering Plants. *Curr Biol.*, **27(20)**, 3183-3190.

Vicente, J., Mendiondo, G. M., Pauwels, J., Pastor, V., Izquierdo, Y., Naumann, C., Movahedi, M., Rooney, D., Gibbs, D. J., Smart, K., Bachmair, A., Gray, J. E., Dissmeyer, N., Castersana, C.,

Vierstra R. D. (2009). The ubiquitin–26S proteasome system at the nexus of plant biology. *Nat. Rev. Mol. Cell Biol.*, **10**, 385–397.

Voges, D., Zwickl, P & Baumeister, W. (1999) The 26S proteasome: a molecular machine designed for controlled proteolysis. *Annu Rev Biochem*, **68**, 1015-1068.

Walter, F. (2010). Identification and characterization of N-recognins in Arabidopsis. (Trinity College Dublin).

Wang, L., Tsuda, K., Truman, W., Sato, M., Nguyen, l., Katagiri, F., & Glazebrook, J. (2011). CBP60g and SARD1 play partially redundant critical roles in salicylic acid signaling. *The Plant journal : for cell and molecular biology*, *67*(6), 1029–1041. https://doi.org/10.1111/j.1365-

Warmerdam, S., Sterken, M.G., Sukarta, O.C.A. et al. (2020) The TIR-NB-LRR pair DSC1 and WRKY19 contributes to basal immunity of Arabidopsis to the root-knot nematode Meloidogyne incognita. *BMC Plant Biol* **20**, 73. https://doi.org/10.1186/s12870-020-2285-x

Weits, D. A., Giuntoli, B., Kosmacz, M., Parlanti, S., Hubberten, H., Riegler, H., Hoefgen, R., Perata, P., van Dongen, J. T. & Licausi, F. (2014) Plant cysteine oxidases control the oxygen-dependent branch of the N-end-rule pathway. *Nat Commun*, **5**, 3425.

Weits, D. A., Kunkowska, A. B., Kamps, N. C. W., Portz, K. M. S., Packbier, N. K., Venza, Z. N., Gaillochet, C., Lohmann, J. U., Pedersen, O., van Dongen, J. T. & Licausi, F. (2019) An apical hypoxic niche sets the pace of shoot meristem activity. *Nature*, **569**, 714-717.

Weng, S., Demir, F., Ergin, E. K., Dirnberger, S., Uzozie, A., Tuscher, D., Nierves, L., Tsui, J., Huesgen, P. F., & Lange, P. F. (2019). Sensitive Determination of Proteolytic Proteoforms in Limited Microscale Proteome Samples. *Molecular & cellular proteomics : MCP*, **18**(11), 2335–2347. https://doi.org/10.1074/mcp.TIR119.001560

White, M.D., Klecker, M., Hopkinson, R.J., Weits, D.A., Mueller, C., Naumann, C., O'Neill, R., Wickens, J., Yang, J., Brooks-Bartlett, J.C., Garman, E.F., Grossmann, T.N., Dissmeyer, N. and Flashman, E**.** (2017) Plant cysteine oxidases are dioxygenases that directly enable arginyl transferase-catalysed arginylation of N-end rule targets. *Nat Commun*, **8**, 14690.

White, M. D., Kamps, J. J. A. G., East, S., Taylor Kearney, L. J. & Flashman, E. (2018) The plant cysteine oxidases from Arabidopsis thaliana are kinetically tailored to act as oxygen sensors. *Journal of Biological Chemistry*, **293**, 11786-11795, doi: 10.1074/jbc.RA118.003496.

Wilkinson, K. D., Urban, M. K. & Haas, A. L. (1980) Ubiquitin is the ATP-dependent proteolytic factor of rabbit reticulocytes. *J. Biol. Chem.* **255**, 7529-7532.

Williamson, B., Tudzynski, B., Tudzynski, P. & van Kan, J. A. L. (2007) Botrytis Cinerea: The Cause of Grey Mould Disease. *Mol Plant Pathol.*, **8(5)**:561-580. doi: 10.1111/j.1364-3703.2007.00417.x.

Winkelmüller, T. M., Entila, F., Anver, S., Piasecka, A., Song, B., Dahms, E., Sakakibara, H., Gan, X., Kułak, K., Sawikowska, A., Krajewski, P., Tsiantis, M., Garrido-Oter, R., Fukushima, K., Schulze-Lefert, P., Laurent, S., Bednarek, P., & Tsuda, K. (2021). Gene expression evolution in pattern-triggered immunity within Arabidopsis thaliana and across Brassicaceae species. *The Plant cell*, **33**(6), 1863–1887. Advance online publication. https://doi.org/10.1093/plcell/koab073

Worley, C.K., Ling, R. and Callis, J. (1998) Engineering in vivo instability of firefly luciferase and Escherichia coli beta-glucuronidase in higher plants using recognition elements from the ubiquitin pathway. *Plant Mol. Biol.,* **37**, 337–347.

Wu, H.Y., Liu, K.H., Wang, Y.C., Wu, J.F., Chiu, W.L., Chen, C.Y., Wu, S.H., Sheen, J. and Lai, E.M**.** (2014) AGROBEST: an efficient Agrobacterium-mediated transient expression method for versatile gene function analyses in Arabidopsis seedlings. *Plant Methods*, **10**, 19.

Yamada, K., Yamaguchi, K., Shirakawa, T., Nakagami, H., Mine, A., Ishikawa, K., Fujiwara, M., Narusaka, M., Narusaka, Y., Ichimura, K., Kobayashi, Y., Matsui, H., Nomura, Y., Nomoto, M., Tada, Y., Fukao, Y., Fukamizo, T., Tsuda, K., Shirasu, K., Shibuya, N., Kawasaki, T. (2016). The *Arabidopsis* CERK1-associated kinase PBL27 connects chitin perception to MAPK activation. *The EMBO journal*, **35(22)**, 2468–2483. https://doi.org/10.15252/embj.201694248

Yamaguchi, Y. & Huffaker, A. (2011) Endogenous peptide elicitors in higher plants. *Curr. Opin. Plant Biol.*, **14**, 351-357.

Yang, J. O., Kim, W. Y., & Bhak, J. (2009). ssSNPTarget: genome-wide splice-site Single Nucleotide Polymorphism database. *Human mutation*, **30**(12), E1010–E1020. https://doi.org/10.1002/humu.21128

Yao, Y., He, R. J., Xie, Q. L., Zhao, X. H., Deng, X. M., He, J. B., Song, L., He, J., Marchant, A., Chen, X. Y., & Wu, A. M. (2017). ETHYLENE RESPONSE FACTOR 74 (ERF74) plays an essential role in controlling a respiratory burst oxidase homolog D (RbohD)-dependent mechanism in response to different stresses in Arabidopsis. *The New phytologist*, **213**(4), 1667–1681. https://doi.org/10.1111/nph.14278

Yau, R. & Rape, M. (2016) The increasing complexity of the ubiquitin code. *Nat Cell Biol*, **18 (6)**, 579-586.

Ye, J., Zha, J., Shi, Y., Li, Y., Yuan, D., Chen, Q., Lin, F., Fang, Z., Yu, Y., Dai, Y., & Xu, B. (2019). Co-inhibition of HDAC and MLL-Menin interaction targets MLL-rearranged acute myeloid leukemia cells via disruption of DNA damage checkpoint and DNA repair. *Clinical epigenetics*, **11** (1), 137. https://doi.org/10.1186/s13148-019-0723-0

Yi, S. Y., & Kwon, S. Y. (2014). How does SA signaling link the Flg22 responses? *Plant signaling & behavior*, **9(11)**, e972806. https://doi.org/10.4161/15592316.2014.972806

Yoshida, S., Ito, M., Callis, J., Nishida, I. and Watanabe, A. (2002) A delayed leaf senescence mutant is defective in arginyl–tRNA:protein arginyltransferase, a component of the N-end rule pathway in Arabidopsis. *Plant J.*, **32**, 129–137.

Yu, D., Chen, C., & Chen, Z. (2001). Evidence for an important role of WRKY DNA binding proteins in the regulation of NPR1 gene expression. *The Plant cell*, *13*(7), 1527–1540. https://doi.org/10.1105/tpc.010115

Yu, J., Tehrim, S., Wang, L. *et al.* Evolutionary history and functional divergence of the cytochrome P450 gene superfamily between *Arabidopsis thaliana* and *Brassica* species uncover effects of whole genome and tandem duplications. *BMC Genomics* **18,** 733 (2017). https://doi.org/10.1186/s12864-017-4094-7

Yuan, X., Wang, H., Cai, J. et al. NAC transcription factors in plant immunity. (2019). *Phytopathol* Res **1**, 3 https://doi.org/10.1186/s42483-018-0008-0

Yuan, M., Jiang, Z., Bi, G. *et al.* (2021) Pattern-recognition receptors are required for NLR-mediated plant immunity. *Nature* **592,** 105–109 https://doi.org/10.1038/s41586-021-03316-6

Zhang, S.Q. & Outlaw, W.H., JR (2001) Abscisic acid introduced into the transpiration stream accumulates in the guard-cell apoplast and causes stomatal closure. *Plant, Cell & Environment*, **24**: 1045-1054. doi:10.1046/j.1365-3040.2001.00755.x

Zhang, Y., Xu, S., Ding, P., Wang, D., Cheng, Y. T., He, J., Gao, M., Xu, F., Li, Y., Zhu, Z., Li, X. & Zhang, Y. (2010) Control of salicylic acid synthesis and systemic acquired resistance by two members of a plant-specific family of transcription factors. Proc. Natl Acad. Sci. USA, **107**, 18220-18225.

Zhang, H., Deery, M. J., Gannon, L., Powers, S. J., Lilley, K. S., & Theodoulou, F. L. (2015). Quantitative proteomics analysis of the Arg/N-end rule pathway of targeted degradation in Arabidopsis roots. *Proteomics*, **15**(14), 2447–2457. https://doi.org/10.1002/pmic.201400530

Zhang, H., Gannon, L., Jones, P.D. *et al.* Genetic interactions between ABA signalling and the Arg/N-end rule pathway during Arabidopsis seedling establishment. *Sci Rep* **8,** 15192 (2018). https://doi.org/10.1038/s41598-018-33630-5

Zhang, L., Cai, X., Wu, J. *et al.* Improved *Brassica rapa* reference genome by single-molecule sequencing and chromosome conformation capture technologies. *Hortic Res* **5,** 50 (2018). https://doi.org/10.1038/s41438-018-0071-9

Zhao, Q., Nakashima, J., Chen, F., Yin, Y., Fu, C., Yun, J., Shao, H., Wang, X., Wang, Z. Y., & Dixon, R. A. (2013). Laccase is necessary and nonredundant with peroxidase for lignin polymerization during vascular development in Arabidopsis. *The Plant cell*, *25*(10), 3976–3987. https://doi.org/10.1105/tpc.113.117770

Zhong, L., Zhang, Y., Liu, H. *et al. Agrobacterium*-mediated transient expression via root absorption in flowering Chinese cabbage. *SpringerPlus* **5,** 1825 (2016). https://doi.org/10.1186/s40064-016-3518-1

Zhou, J., Wang, X., He, Y., Sang, T., Wang, P., Dai, S., Zhang, S. & Meng, X. (2020) Differential Phosphorylation of the Transcription Factor WRKY33 by the Protein Kinases CPK5/CPK6 and MPK3/MPK6 Cooperatively Regulates Camalexin Biosynthesis in Arabidopsis. *Plant Cell*, https://doi.org/10.1105/tpc.19.00971.

Zhuo, T., Wang, X., Chen, Z., Cui, H., Zeng, Y., Chen, Y., Fan, X., Hu, X., & Zou, H. (2020). The Ralstonia solanacearum effector RipI induces a defence reaction by interacting with the bHLH93 transcription factor in Nicotiana benthamiana. *Molecular plant pathology*, *21*(7), 999–1004. https://doi.org/10.1111/mpp.12937

Zipfel C, Robatzek S, Navarro L, Oakeley EJ, Jones JD, Felix G, Boller T (2004) Bacterial disease resistance in Arabidopsis through flagellin perception. *Nature*, **428**, 764–767.

Zipfel, C. & Felix, G. (2005) Plants and Animals: A Different Taste for Microbes? *Curr Opin Plant Biol.*, **8**(4), 353-360. doi: 10.1016/j.pbi.2005.05.004.

Appendix A. Supplementary Figures

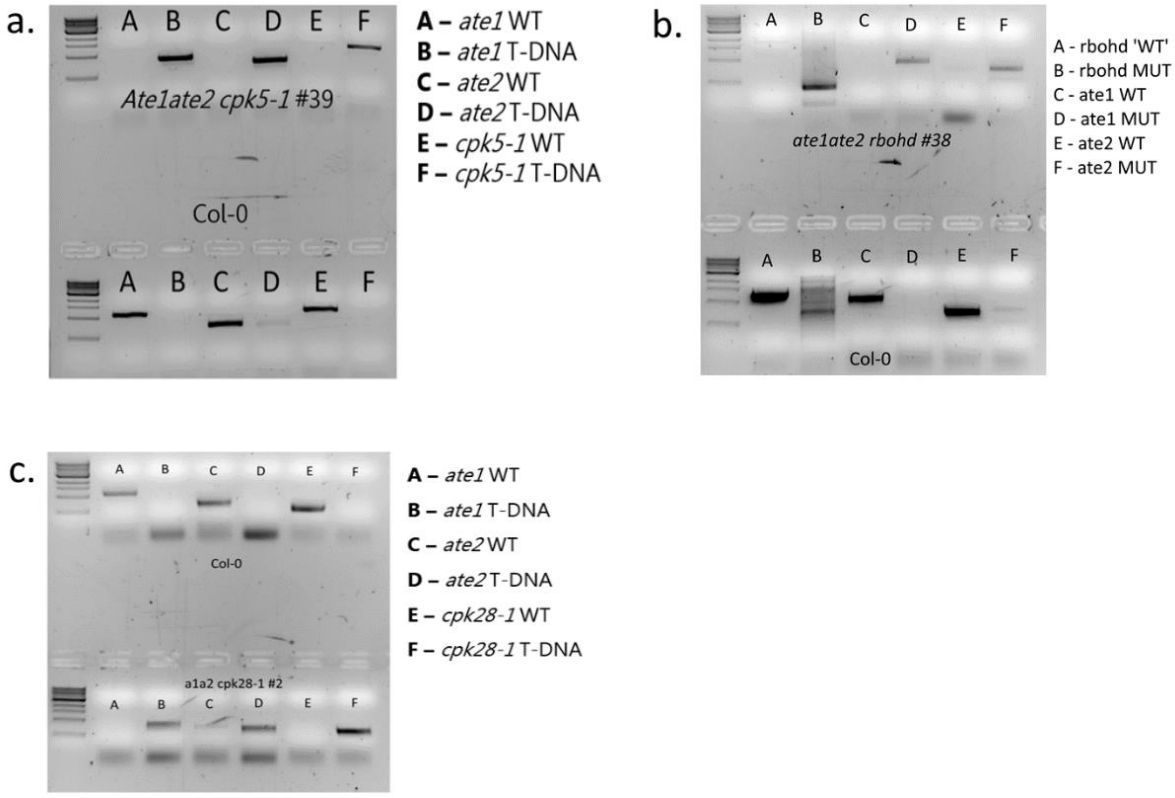

Figure A1. Genotyping of *ate1ate2* x ROS regulator mutants. a-c. 'Wild-type' and 'mutant' only genotyping PCRs after gel electrophoresis showing isolation of *ate1ate2 cpk5-1*, *ate1ate2 rbohd* and *ate1ate2 cpk28-1* respectively. DNA from Col-0 wild-type plants was used as a control where indicated.

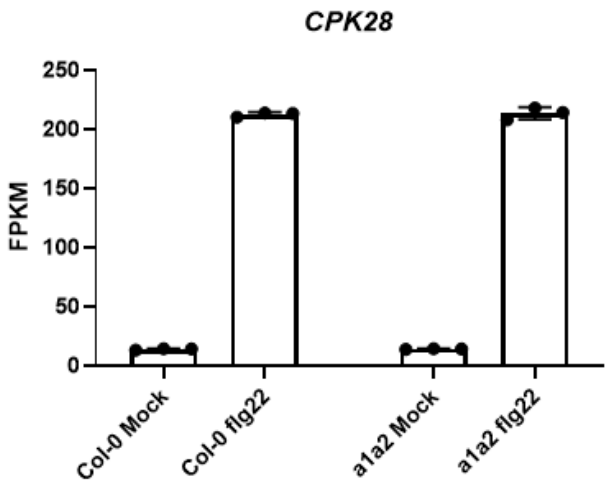

Figure A2. Expression of *CPK28* in *ate1ate2*. Transcript abundance of *CPK28* in Col-0 and *ate1ate2* after mock or 1 µM flg22 treatment as detected by RNA-Seq.

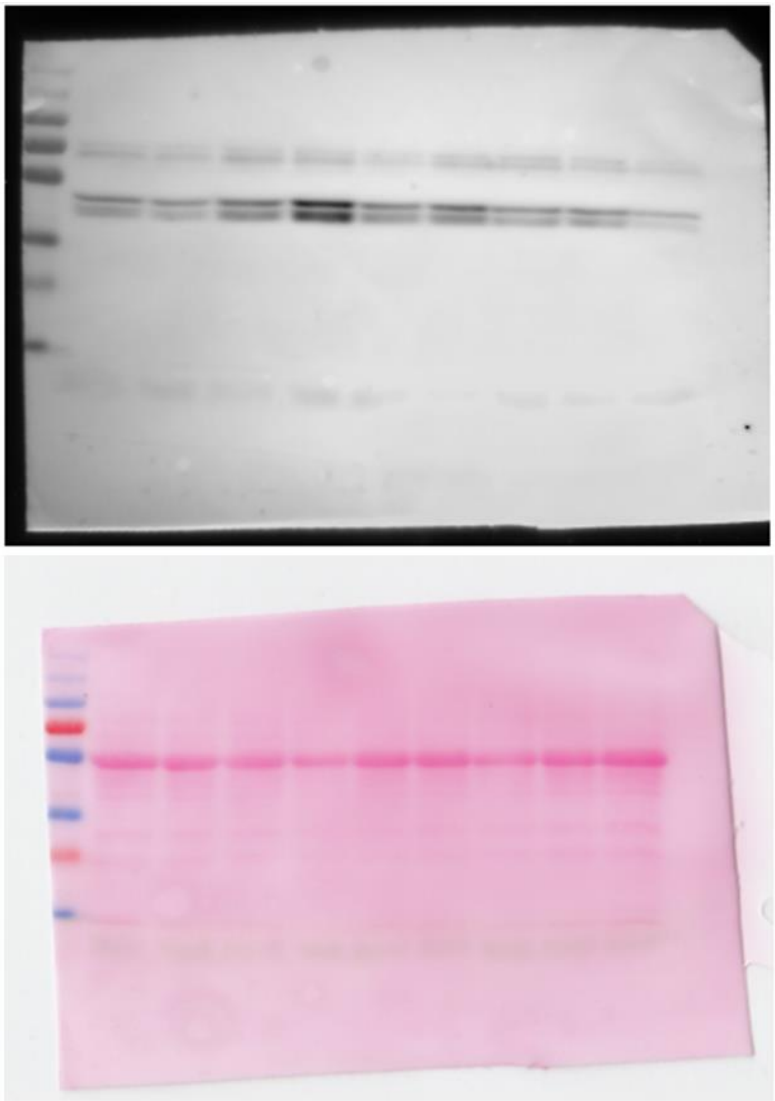

Figure A3. pMAPK immunoblot. Ponceau scan (top) and full membrane (bottom) for blot shown in Fig. 3.17.

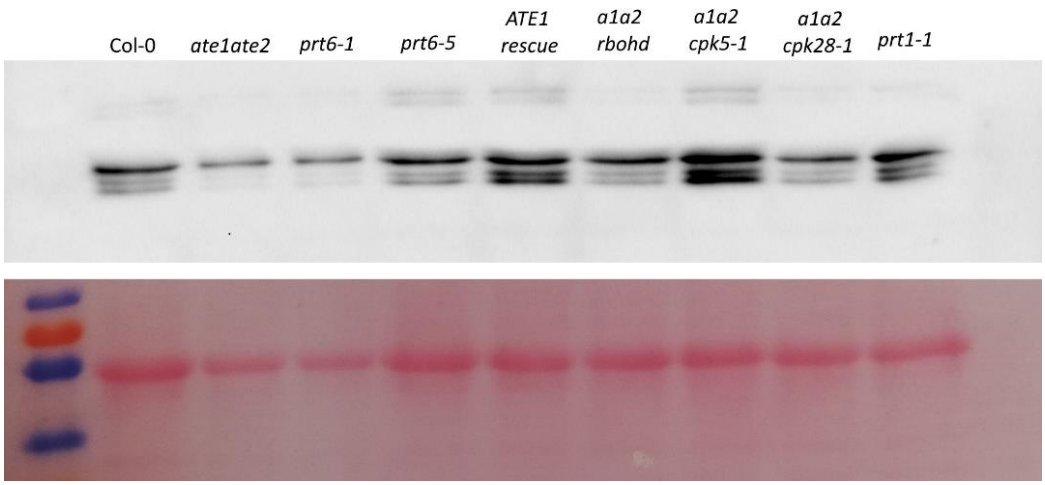

Figure A4. pMAPK immunoblot in N-degron pathway mutants. This is an independent replicate of the experiment shown in Fig. 3.17.

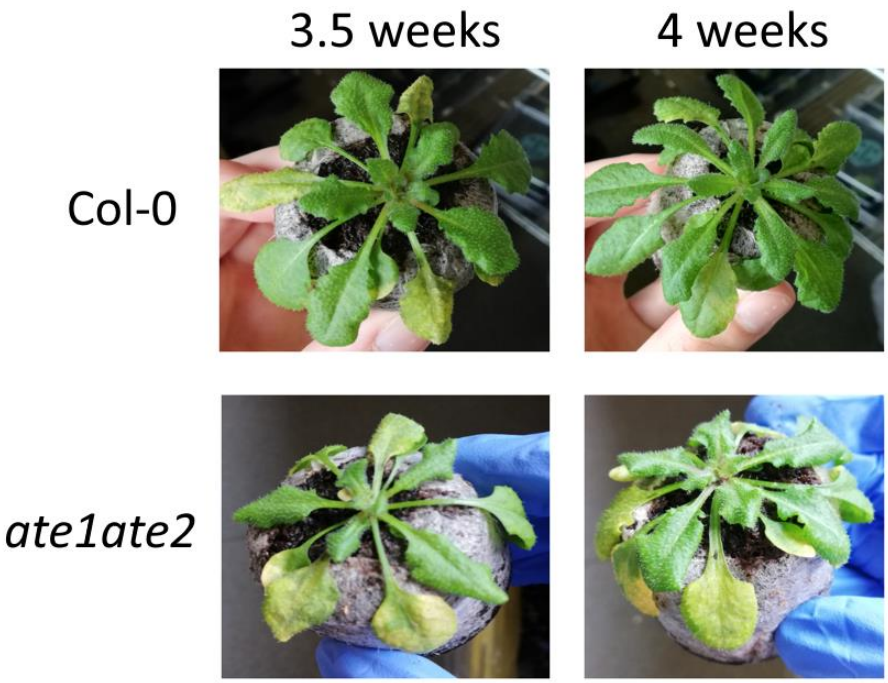

Figure A5. Investigating ARR in *ate1ate2*. Images of Col-0 and *ate1ate2* plants 3 days post-inoculation with *Pst* DC3000 (5 x 10^5 cfu/mL).

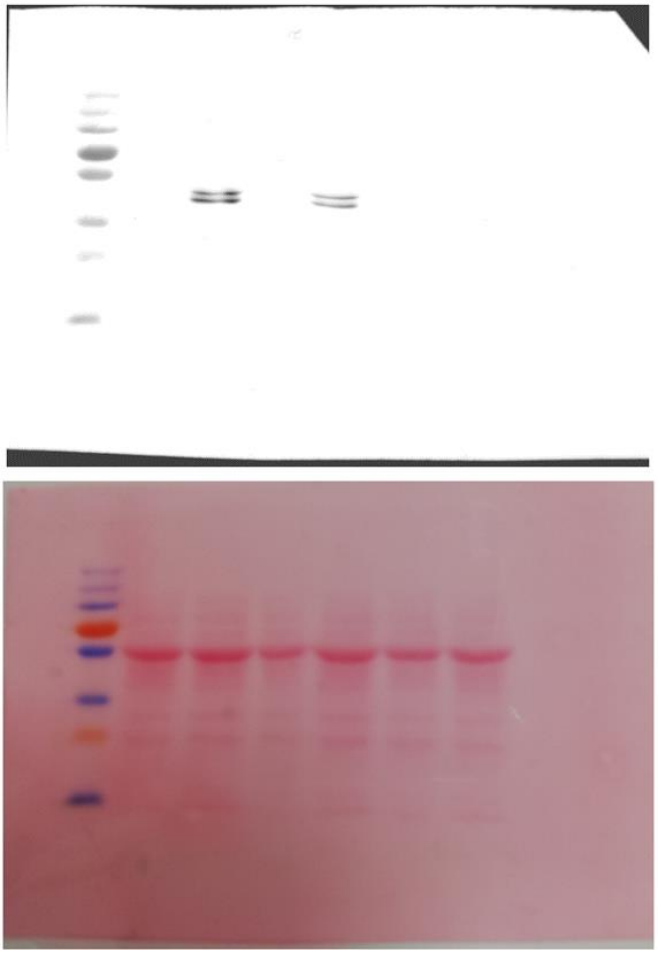

Figure A6. pMAPK immunoblot. Uncropped membrane (upper panel) and Ponceau stain (lower panel) for blot shown in Fig. 3.21b.

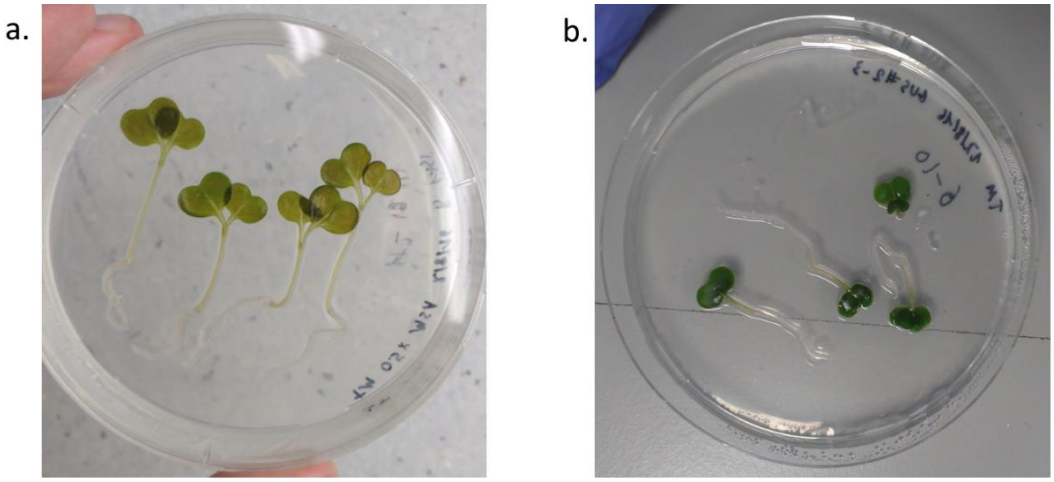

Figure A7. 3-day-old *B. rapa* seedlings during recovery period after **a.** 48-hour co-cultivation in medium containing 0.005% Silwet or **b.** 30-hour co-cultivation in medium containing 0.001% Silwet.

Figure A8. Representative images of the morphology of *B. rapa* (upper panels) and *B. napus* (lower) at the time of agroinfiltration.

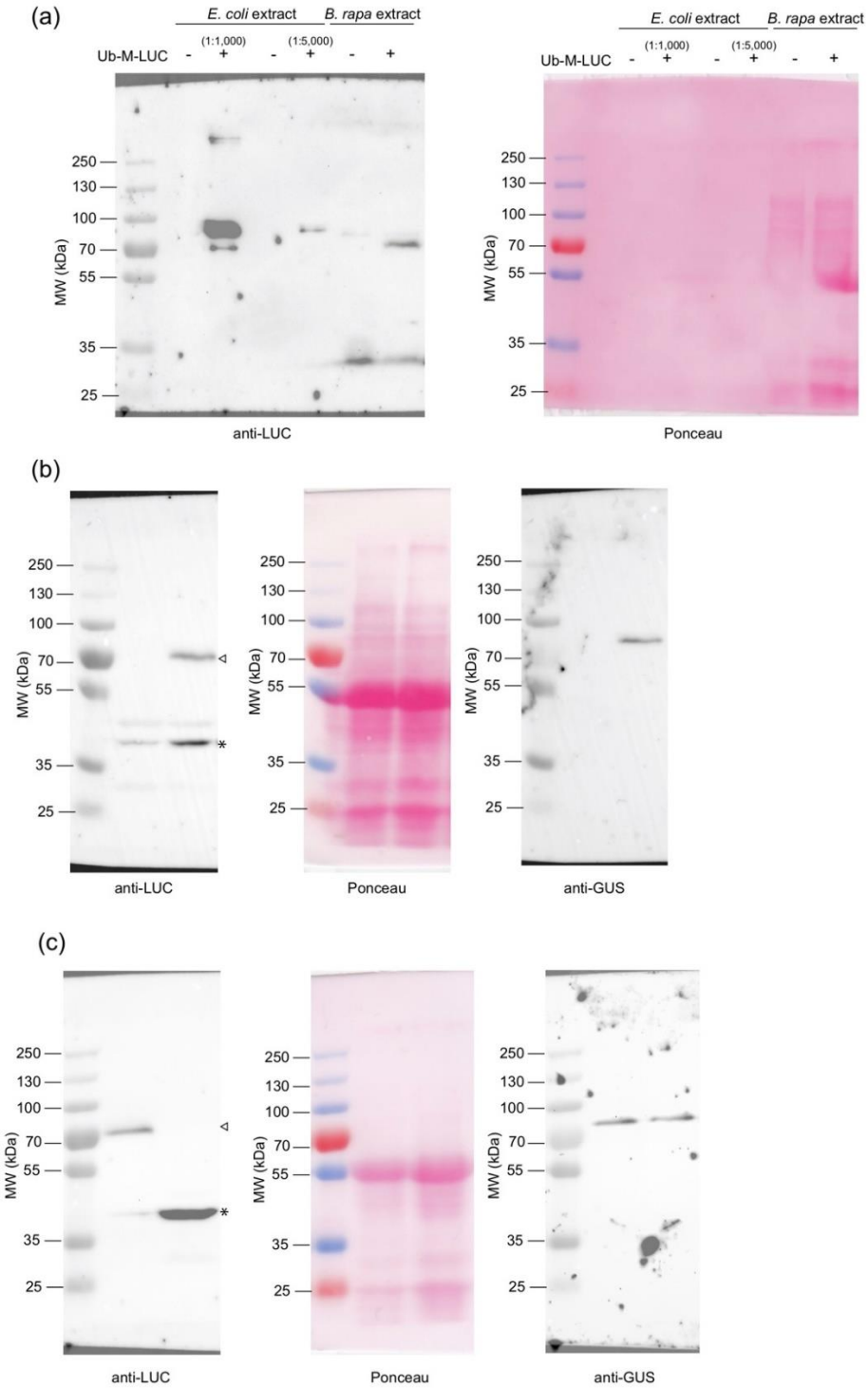

Figure A9. Full blot images from section 4.2. a. *In vivo* deubiquitylation of Ub-Met-LUC. A polyhistidine-tagged His_6-Ub-Met-LUC was expressed in *E. coli* to serve as a control for a non-deubiquitylated N-degron reporter. Different dilutions of the crude *E. coli* protein extract were loaded (1:1,000 and 1:5,000) to ensure that the signal for the LUC fusion would be comparable to that obtained for expression of Ub-Met-LUC in *B. rapa*. Because of the dilution factor for *E. coli* extract, no proteins are visible on the Ponceau stain of the membrane. Expected molecular weights: His_6-Ub-Met-LUC: 72 kDa; Ub-Met-LUC: 71 kDa; Met-LUC: 62 kDa. Black arrowhead indicates His_6-Ub-Met-LUC; open arrowhead indicates Met-LUC. Molecular weight (MW) of the ladder proteins are indicated (PageRuler Plus pre-stained). **b.** Immunoblot analysis of LUC and GUS protein levels for N-terminal Met.

Approximately equal protein amounts were loaded to determine potential cross-reacting proteins in *B. rapa* infiltrated with *Agrobacterium* transformed with an empty vector (e.v.) or pEG356 (coding for UBQ3$_{pro}$:Ub-Met-LUC 35S$_{pro}$:GUS). Ponceau staining was performed before immunoblotting with anti-LUC. The membranes were then stripped and incubated with an GUS-specific antibody. Open arrowhead: Met-LUC; asterisk: cross-reacting protein. **c.** Comparison of Met-LUC and Arg-LUC with equal GUS levels after infiltration with *Agrobacterium* transformed with pEG356 (UBQ3$_{pro}$:Ub-Met-LUC 35S$_{pro}$:GUS) or pEG368 (UBQ3$_{pro}$:Ub-Arg-LUC 35S$_{pro}$:GUS). Ponceau staining was performed before immunoblotting with anti-LUC. The membranes were then stripped and incubated with an GUS-specific antibody. Open arrowhead: X-LUC; asterisk: cross-reacting protein.

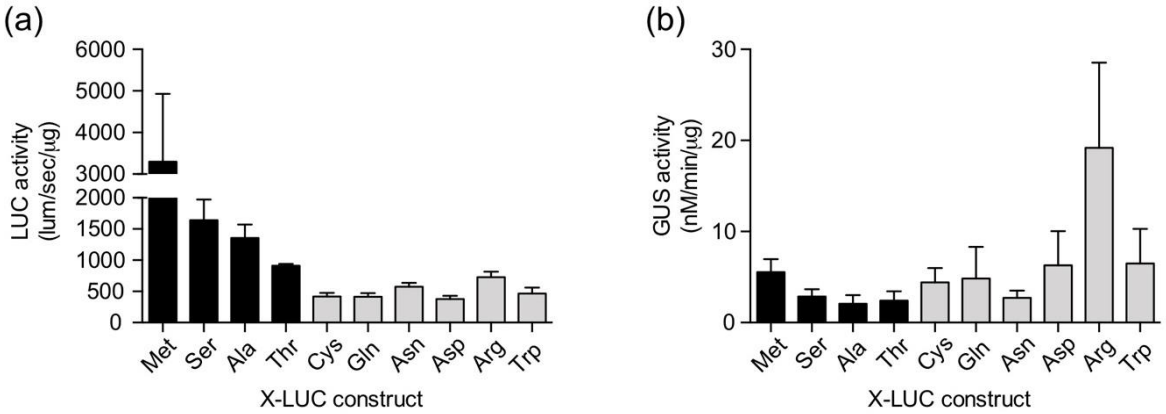

Figure A10. Uncorrected LUC and GUS activities. a. Average non-normalized LUC activities expressed in lumin. Error bars represent standard errors of 4 independent replicates, except for Asn, for which two independent relicates were conducted. Black and grey bars correspond to stabilizing and destabilizing N-terminal residues, respectively. **b.** Average GUS activities for each of the constructs indicated. Error bars represent standard errors of 4 independent replicates, except for Asn, for which two independent replicates were conducted. Black and grey bars correspond to stabilizing and destabilizing N-terminal residues, respectively.

Figure A11. Images of M3 *B. rapa* plants from the TILLING collection. Various morphological abnormalities are visible, highlighting the mutation load present in the M_3 TILLING generation.

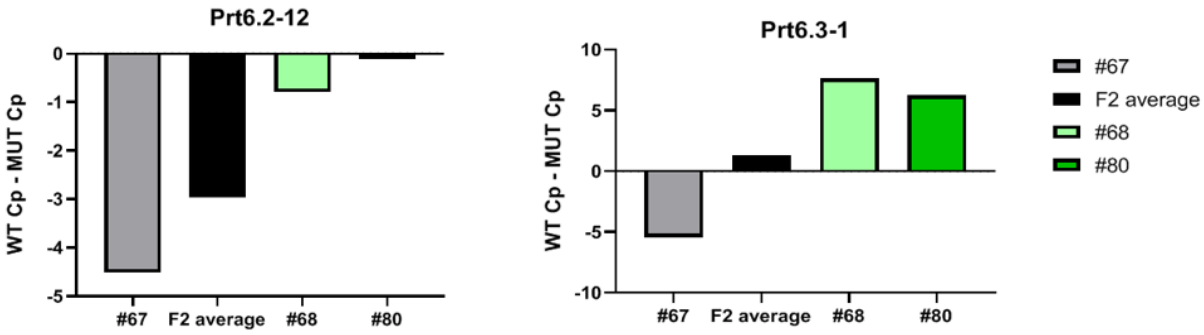

Figure A12. DMAS-qPCR genotyping results for selected plants from the *Brprt6.2prt6.3* F2 population. Genotyping of *prt6.2-12* SNP (left), *prt6.3-1* genotyping (right). Based on these results, #67 appears to be wild-type at both SNP sites, while, #68 and #80 are double mutants.

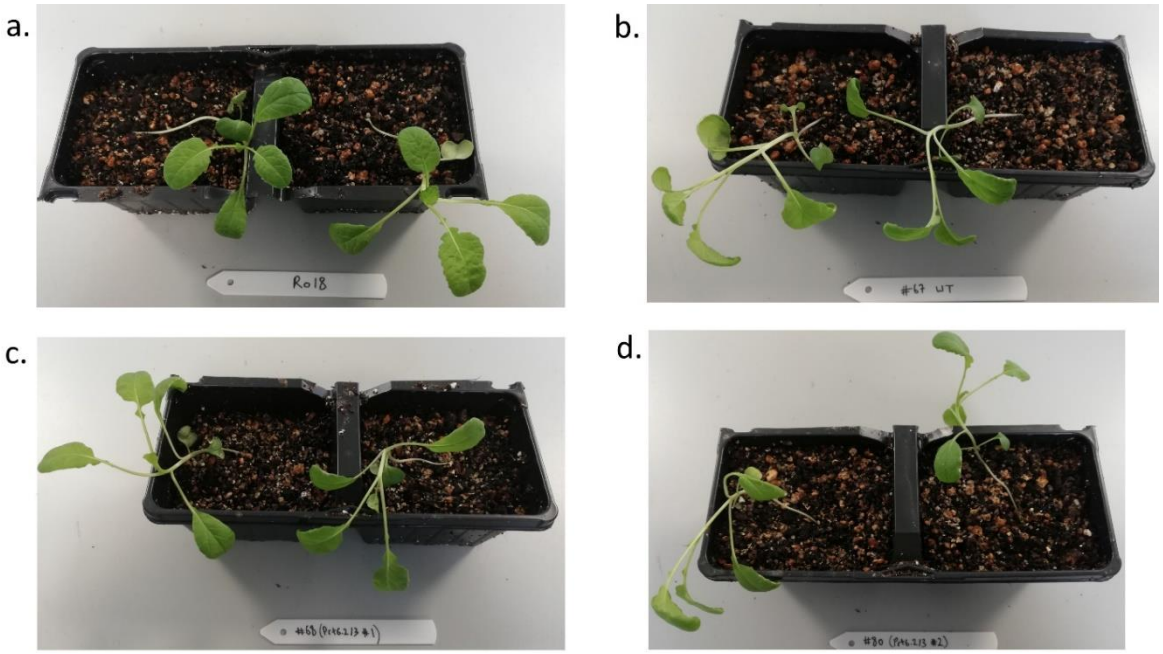

Figure A13. *Brprt6.2prt6.3* morphology at 4-weeks old. Representative images of 4-week-old plants of **a.** R-o-18 wild-type **b.** #67 wild-type **c.** *Brprt6.2prt6.3* #68 and **d.** *Brprt6.2Prt6.3* #80.

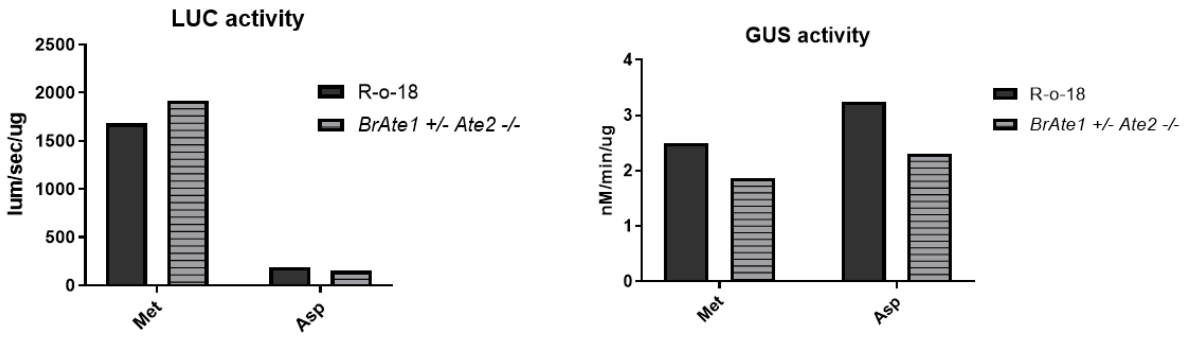

Figure A14. LUC and GUS activities after transient expression in *Brate1 +/- ate2 -/-*. Raw LUC (left) and GUS (right) activity measurements after transient expression of N-degron pathway reporter constructs in R-o-18 wild-type or *Brate1* +/- *ate2* -/- plants.

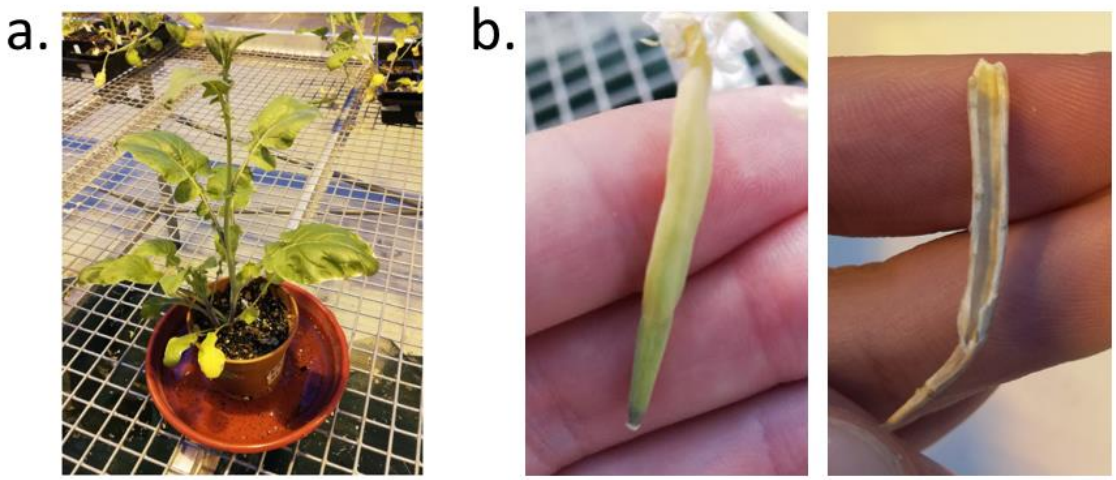

Figure A15. Morphology of *Brprt1.1-5* mutant. a. 8-week old *Brprt1.1-5* homozygous mutant. **b.** Close up images of dried silique before and after detachment from *Brprt1.1-5*. No seeds were obtained.

```
>XP_009105895.1 ethylene-responsive transcription factor ERF073 / HRE1
[Brassica rapa]
MCGGAVISDYIAPRAGKPSWRRDDVVDLTLDDLEGDSQYYPWLGMKREDGTRRKKKTNKSSSSEYRGIRR
RPWGRWAAEIRDPIKGVRVWLGTFNTAEDAARAYDFEAKRLRGVKAKLNFPNESPASSSRKRKASSPPPT
QRPQVRKIEEKREDVDVLGGGCFDFLWEENNNADTSQVDTQWLEDVIIMGDDAEKRQKGYYDCEGNVDEL
LSFQNETECFLQTPFMEGGNCGFSTSLTSLLDEVNVMDLWS

>XP_009118731.1 ethylene-responsive transcription factor ERF071/HRE2
[Brassica rapa]
MCGGAVISDFIWSLRRASFAEAEPSQVGYEGCVSIEKRVCSGSVGGEKRKEKKKEGKNKRERKNMYRGIR
QRPWGKWAAEIRDPRKGVRVWLGTFKTAEEAARAYDSAAIRIRGGKAKLNFPNDDSSSTRRNCIIKKNKE
VCGGDHLMNACDQSPPPTDDTENQQVKQLSEELMAYEDYMGFYQIPYLDGQSSTEDVPQLSLIGNLWSFQ
DNV

>XP_009146390.1 ethylene-responsive transcription factor RAP2-2 [Brassica
rapa]
MCGGAIISEFIPPSRSRRVTSEHLWPDLKNKGKASKKKRSGFIDLDDEFEADFQGFKDDASFDCEDEFDV
DDDVFADVKPFVFAAGAKPVASPPAAFASTGSVSGKKTIESGGQAEKSAKRKRKNQYRGIRQRPWGKWAA
EIRDPRKGSREWLGTFDTAEEAARAYDAAARRIRGNKAKVNFPEEMVPSVSQKRPSAKKAVAKPNQSPAS
VQQPTHVSQYCNNSFDNMGHDSSFGDVSFMEEKPQMYNNQFFDVGGNNGYQYFSSDQGSNSLDCSEFGWS
DQTPKTPEISSMLVNNNQAPFIEETNPAKKLKTSSEDGTSNNDSSDDLMAYLNNALWESPLEVEAMFGGD
AATMTQEEGNPMDLWSLDDINSMLDGGVF

>XP_009114507.1 ethylene-responsive transcription factor RAP2-3 [Brassica
rapa]
MCGGAIISDFAPNVTKAKGRKLTAEELWSELDASAADDFWGFHSTSKTQSTNQQVTLKEEAAEKEKEKEP
VTEKRRKRKNVYRGIRKRPWGKWASEIRDPRKGARVWLGTFNTAEEAAMAYDVAAKRIRGDKAKLNFPDL
LHHPPRSPATPLASSPVSEVQPPAKKHCVVSQSELTQPSFPVECSGFGSGDEFQLDYDLKQQISSLESFL
ELDGDTVEQPSRLDESVSEVDMWMIDDVIASYQ

>XP_009106954.1 ethylene-responsive transcription factor RAP2-12 [Brassica
rapa]
MCGGAIISDFIPPPRSRRVTSEFLWPDLKKSSKKRSSFFDLDDEFEADFQGFKDDSSIDCDDAKPFVFAG
ARKPAVSAATADSVIGKKVADGEGERSAKRKRKSQYRGIRQRPWGKWAAEIRDPREGSRVWLGTFKTAEE
AARAYDAAARRIRGSKAKVNFPEEKENPPAKKVAPNPSPVLAQNLDNSFDNMCFMEEKHQVNNNSNQFGG
NGYHQYFSSDQGSNSFGCSEFGWNDQAPITPEISSAFINNNSATFAEEADPAKQLKVMDFETTYNSTEWD
SSLDFFSGDAVATQDNGANPMELWSIDEIDSMIGGVF
```

Figure A16. *B. rapa* ERF-VII amino acid sequences. FASTA sequences of *B. rapa* homologs of ERF-VII transcription factors HRE1, HRE2, RAP2.2, RAP2.3 and RAP2.12. Conserved N-termini are highlighted in yellow.

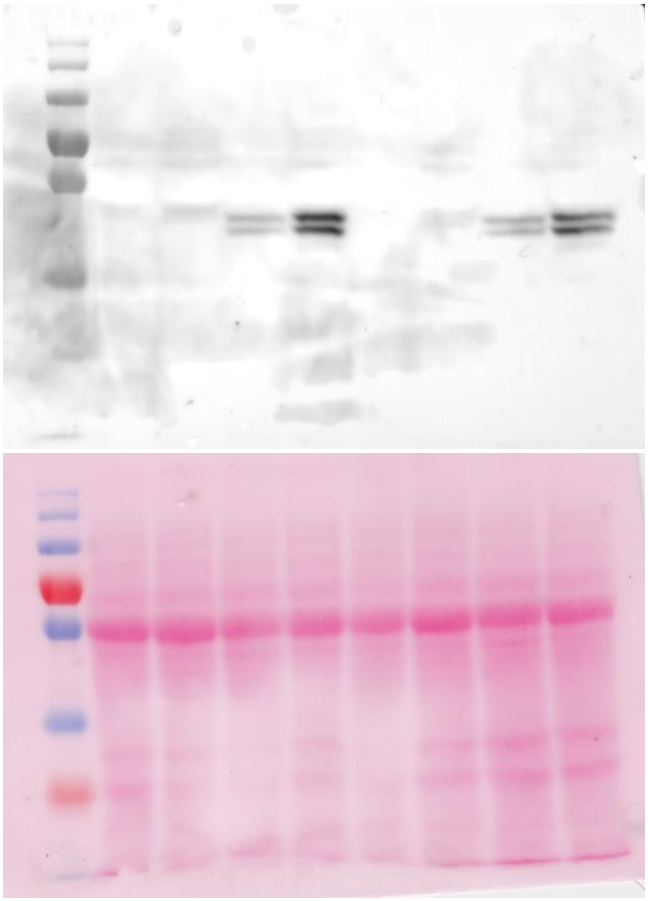

Figure A17. Uncropped immunoblot and Ponceau staining images of *B. rapa* wild-type and *Bprt6.2prt6.3* seedlings probed with anti-pMAPK antibody.

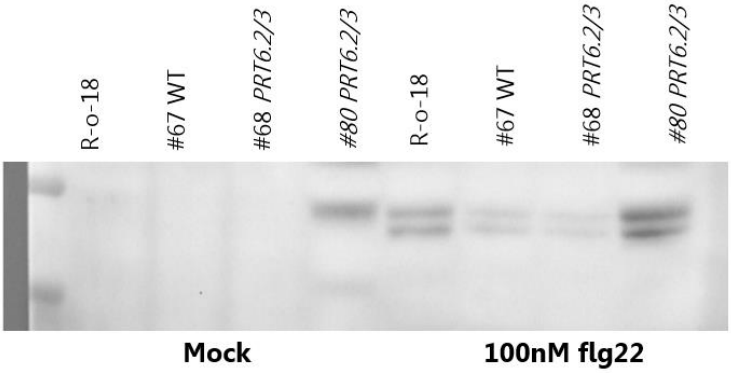

Figure A18. Replicate anti-pMAPK blot in wild-type and *Brprt6.2prt6.3* after mock or 100 nM flg22 treatment.

Appendix B. Supplementary Tables

Gene ID	Gene Symbol	log2 (a1a2_Mock / Col-0_Mock)	Qvalue
820295	'ATE2'	-3.921777338	4.03E-26
830454	'ATE1'	-3.100152725	3.89E-63
827042	'AT4G14060'	-2.901197858	0.040786604
832491	'AT5G24240'	-2.820536962	9.35E-13
826958	'TPS12'	-2.533937488	7.75E-05
842069	'MYB72'	-2.493193235	7.47E-04
825841	'AT4G04990'	-2.339423314	0.002432829
835707	'NAS2'	-2.148660426	0.034899958
826959	'CYP71A19'	-2.097045866	3.63E-06
837912	'AT1G13520'	-1.788020499	0.035478093
819331	'GolS1'	-1.770634466	1.18E-10
826734	'AT4G11320'	-1.671068229	2.83E-25
830293	'BHLH101'	-1.65847559	0.042495566
834057	'AT5G40590'	-1.536374201	0.046768641
838478	'GLP4'	-1.516707363	0.00699178
826770	'OSM34'	-1.504697549	0.014842693
818961	'AT2G43590'	-1.421831165	2.54E-08
816011	'AT2G15220'	-1.332900835	0.042495566
843668	'DR4'	-1.31780908	8.66E-06
821135	'DOX1'	-1.311665012	0.004949785
815093	'GRP9'	-1.300362385	1.38E-06
843192	'AT1G68620'	-1.245750395	0.042495566
828296	'WRKY31'	-1.224154136	0.006666587
832750	'CBP60G'	-1.110342918	0.011890207
833659	'THI2.2'	-1.088292884	2.70E-04
828919	'UMAMIT33'	-1.06855982	0.030949839
819288	'GulLO2'	-1.044906182	0.027460033
822455	'AT14A'	-0.932970773	0.040661064
822457	'AT14A'	-0.932970773	0.040661064
838052	'PCR2'	-0.915973634	9.41E-05
834400	'APS4'	-0.912528605	1.39E-07
818736	'AT2G41380'	-0.891280833	6.97E-04
842880	'AT1G65690'	-0.87986921	0.006369418
832667	'TGG2'	-0.824986597	0.001655863
824592	'AT3G54250'	-0.79707855	0.012333241
841550	'AT1G51270'	-0.788575268	0.005263637
844013	'IGMT5'	-0.77630434	1.52E-04
825024	'AT3G58550'	-0.764064189	0.004952635
816256	'AT2G17500'	-0.696232836	0.009114855
830882	'SULTR2;1'	-0.613824065	0.018642813

Table B1. List of genes downregulated in *ate1ate2* mock vs. Col-0 mock as determined by RNA-Seq.

Gene ID	Gene Symbol	log2 (a1a2_Mock / Col-0_Mock)	Qvalue
822700	AT3G29970'	8.73145953	1.42E-07
816295	AT2G17850'	8.690971604	1.92E-10
816294	AT2G17845'	6.862832896	7.47E-04
2745749	'AT1G12805'	6.336059712	0.006408066
821726	'ICL'	6.003663054	3.70E-49
840977	'FTM1'	5.723078434	4.13E-06
834435	'CRA1'	5.275753129	0.008147251
831364	PCO1'	5.221372037	2.07E-70
830411	'EXPA2'	4.872437468	0.009884232
843030	'LBD40'	4.587285647	0.027277037
815907	'AGL44'	4.457735923	1.36E-04
826618	'AT4G10265'	4.250984528	0.004252071
826619	'AT4G10270'	4.224252195	1.09E-14
840201	'AT1G33055'	3.846788129	1.21E-09
833986	PCO2'	3.786074386	1.45E-34
821112	'LBD41'	3.724777553	6.21E-18
28718918	'AT3G06435'	3.707847662	1.93E-22
821303	'AT3G03270'	3.591817464	1.82E-16
823393	'SUS4'	3.557597997	2.04E-27
816103	'HB1'	3.545926782	4.79E-15
820152	'IPS1'	3.518345596	1.42E-06
28717429	'AT1G75945'	3.492999959	1.11E-19
829444	'AT4G33070'	3.45521089	1.26E-13
844047	'ADH1'	3.235626463	4.63E-09
819365	'ERF71'	3.233840638	9.22E-07
828854	'AT4G27450'	3.200187138	0.004952635
828511	'AT4G24110'	2.949256128	9.41E-05
834484	'AT5G44570'	2.622310249	0.003791474
829495	'AT4G33560'	2.566502215	3.38E-08
816478	'ACO1'	2.564144747	1.20E-30
819053	'BGLU28'	2.42802573	1.26E-07
822341	'AT3G27220'	2.407397291	1.42E-10
827157	'AT4G14980'	2.281637873	8.51E-05
822807	'QQS'	2.189646866	2.02E-10
820165	'AT3G10040'	2.180691833	4.78E-07
838347	'PEPC1'	2.143939107	0.03037973
838919	'AT1G23110'	1.922797621	0.009694216
836833	'AT5G66985'	1.914566402	7.00E-06
844051	'AT1G77145'	1.828406737	1.21E-06
839784	'AT1G29090'	1.6443661	0.03993523
834943	'ATSDI1'	1.624156032	6.86E-05
829841	'CP1'	1.504542248	0.007873911
830122	'AT4G39675'	1.423489421	1.15E-05
827185	'BAM5'	1.41760824	0.027748848
820737	'AT3G02620'	1.415211583	2.06E-12
817435	'CYP710A4'	1.375151502	0.03993523
836690	'bHLH093'	1.323150792	3.70E-06
832206	'SUS1'	1.294038363	7.29E-04
832691	'AT5G26220'	1.254294835	0.004949785
836638	'TPPJ'	1.176043163	0.006714128
821047	'PAP17'	1.174087484	2.00E-04
835246	'NEET'	1.129016344	7.76E-05
834570	'CYP707A3'	1.072501602	3.38E-05
824119	'LSU3'	1.068173226	0.038683729
819369	'AT2G47560'	1.039186734	1.54E-05
821175	'SRG3'	1.027744395	0.035478093
819704	'AT3G05400'	0.986952826	1.24E-05
818261	'AT2G36885'	0.931833087	0.034415177
837701	'PMEPCRA'	0.885744349	4.78E-07
834195	'AT5G41900'	0.885641607	0.014629604
829440	'SQD1'	0.781191406	0.006049544
824787	'AT3G56210'	0.721381918	2.29E-05
842514	'APR2'	0.616946221	6.88E-04
839418	'AT1G04770'	0.589252471	0.001918664

Table B2. List of genes upregulated in *ate1ate2* mock vs. Col-0 mock as determined by RNA-Seq.

Gene ID	Gene Symbol	log2 (a1a2_flg22 / Col-0_flg22)	Qvalue
832491	'AT5G24240'	-4.820507733	1.00E-44
820295	'ATE2'	-4.368133373	1.63E-17
842201	'AT1G58320'	-3.504776903	0.009248299
830454	'ATE1'	-2.969063479	3.30E-27
818785	'PGAZAT'	-2.889330915	0.002272497
835707	'NAS2'	-2.860628805	4.35E-08
827042	'AT4G14060'	-2.857521219	6.83E-08
839649	'AT1G27580'	-2.729091661	0.048441131
841827	'AT1G53890'	-2.617283934	0.013840919
823710	'AT3G45680'	-2.516251846	7.21E-04
814743	'PDF2.1'	-2.406795561	2.69E-06
825841	'AT4G04990'	-2.232167924	4.81E-07
826770	'OSM34'	-2.210519365	1.13E-04
819331	'GolS1'	-1.993817699	1.44E-14
817373	'AT2G28270'	-1.987411983	0.019586065
826959	'CYP71A19'	-1.962064833	1.26E-04
840127	'AOX1D'	-1.959224987	0.002434821
832547	'VSP1'	-1.958169798	0.001957343
838478	'GLP4'	-1.946522725	1.02E-05
842767	'AT1G64590'	-1.774565951	0.008862267
826734	'AT4G11320'	-1.684220869	2.23E-09
821135	'DOX1'	-1.542568889	5.55E-18
830293	'BHLH101'	-1.457285517	2.47E-04
843668	'DR4'	-1.363496659	1.14E-09
819562	'NAC047'	-1.245715291	0.001700702
843799	'GSTU10'	-1.203769886	0.046307169
828296	'WRKY31'	-1.101774509	0.002369646
819288	'GulLO2'	-1.059878351	1.72E-06
834400	'APS4'	-1.024633161	3.81E-04
841611	'AT1G51840'	-1.000013375	0.042348971
825868	'CRK25'	-0.985591782	0.008540364
824571	'AT3G54040'	-0.965291379	0.003848455
844013	'IGMT5'	-0.866740568	0.003477462
832474	'CHIA'	-0.860897468	0.00286386
821794	'AT3G22240'	-0.822914277	9.20E-06
832667	'TGG2'	-0.756587739	0.00605054
820078	'LAC7'	-0.753053251	0.001899251
834794	'TIP2;3'	-0.737661388	0.032510307
836246	'GUS1'	-0.736959154	0.041957415
842554	'FMO GS-OX4'	-0.697664002	0.04996214
829861	'PLP1'	-0.687130671	0.003023757
816256	'AT2G17500'	-0.682363557	0.00286386

Table B3. List of genes downregulated in *ate1ate2* flg22 vs. Col-0 flg22 as determined by RNA-Seq.

Gene ID	Gene Symbol	log2 (a1a2_flg22 / Col-0_flg22)	Qvalue
816295	'AT2G17850'	9.609343966	2.92E-11
822700	'AT3G29970'	7.827637209	1.28E-08
2745749	'AT1G12805'	6.831067764	3.38E-07
843030	'LBD40'	6.071139147	0.00371346
840977	'FTM1'	5.770276297	7.37E-37
831364	'AT5G15120'	5.63115115	9.66E-97
821726	'ICL'	5.151765032	2.32E-36
826619	'AT4G10270'	4.825429651	1.29E-14
815907	'AGL44'	4.64019894	3.41E-05
823393	'SUS4'	4.038895628	5.13E-31
833986	'AT5G39890'	3.919954165	2.06E-46
834672	'AT5G46295'	3.883192019	7.81E-40
28718918	'AT3G06435'	3.790569302	5.80E-30
840201	'AT1G33055'	3.654507494	3.06E-13
821303	'AT3G03270'	3.291732942	1.70E-17
844047	'ADH1'	3.283294493	2.36E-08
816103	'HB1'	3.260100996	4.25E-27
28717429	'AT1G75945'	3.168427268	3.28E-21
828854	'AT4G27450'	3.15299198	5.81E-08
829495	'AT4G33560'	2.923568494	1.45E-14
829444	'AT4G33070'	2.770765979	2.25E-14
820165	'AT3G10040'	2.720694407	5.86E-14
819053	'BGLU28'	2.526895164	2.47E-04
818002	'NIP2;1'	2.41142463	0.00236965
816478	'ACO1'	2.328651856	3.03E-17
822807	'QQS'	2.219095074	6.07E-07
819365	'ERF71'	2.147084771	9.50E-06
821112	'LBD41'	2.109948032	3.43E-05
827157	'AT4G14980'	1.872705149	0.0041658
822341	'AT3G27220'	1.829254506	3.35E-08
832206	'SUS1'	1.551520388	3.51E-04
844051	'AT1G77145'	1.544548377	0.00286386
836833	'AT5G66985'	1.406224321	0.00409853
830122	'AT4G39675'	1.362564955	0.00924691
819369	'AT2G47560'	1.24779979	0.01133888
836690	'bHLH093'	1.22686921	3.63E-09
835246	'NEET'	1.210634813	0.02765243
818261	'AT2G36885'	1.036646055	2.17E-05
837701	'PMEPCRA'	0.900670201	0.01384814
832075	'ASP2'	0.870681572	0.01918499
829404	'GLB3'	0.782640207	0.0089373
840017	'AGO3'	0.77838912	0.0321665
824787	'AT3G56210'	0.750050653	0.0015748
821660	'AT3G21080'	0.682353082	0.04044469
834570	'CYP707A3'	0.666184568	0.03857634

Table B4. List of genes upregulated in *ate1ate2* flg22 vs. Col-0 flg22 as determined by RNA-Seq.

GeneID	WT Mock Expression	Prt6.2Prt6.3 Mock expression	log2FC(Prt6.2 Prt6.3/WT)	Padj	Up/Down	Description (predicted)
BGI_novel_G000372	45.06256254	1.07E-05	-22.0101196	3.17E-05	Down	NA
BGI_novel_G000602	36.42633217	1.05E-05	-21.7220082	4.64E-05	Down	NA
117130584	134.6513491	0.18479535	-9.50908452	7.50E-10	Down	Uncharacterized
103874843	41.03619084	0.360410885	-6.83111043	0.000881	Down	65-kDa microtubule-associated protein 9
117130360	43.6637338	1.324073602	-5.04338028	0.001644	Down	Uncharacterized
103840832	160.5419942	5.366640002	-4.9027878	1.55E-16	Down	Uncharacterized
117130589	366.9488308	23.83522362	-3.94441183	0.021679	Down	Uncharacterized
103872297	84.11489334	6.635599034	-3.66406265	0.001644	Down	Auxin-responsive protein IAA34
117130649	25.92607947	2.692265068	-3.2675117	0.044768	Down	Uncharacterized
117131002	25.92607947	2.692265068	-3.2675117	0.044768	Down	Uncharacterized
BGI_novel_G000724	96.77466636	10.49120732	-3.20544872	0.000881	Down	NA
117130799	135.5183193	16.16527069	-3.06751832	3.85E-06	Down	Uncharacterized
103836605	273.6968105	33.70070203	-3.02172807	1.60E-08	Down	Zinc finger CCCH domain-containing protein 2
103853512	62.80196232	8.370676601	-2.90739349	0.000337	Down	Osmotin-like protein OSM34
117127346	117.4070406	16.45301004	-2.83509548	0.000337	Down	Uncharacterized
103829664	54.83440648	9.392812087	-2.54545236	0.042166	Down	Uncharacterized
103874162	56.91611011	9.763550951	-2.54335922	0.005887	Down	Two-component response regulator ARR5
117130544	193.5027407	37.39765856	-2.37133415	0.000463	Down	Uncharacterized
103846849	78.2965819	19.0835088	-2.03662287	0.000622	Down	Cytochrome P450 78A7
103854373	271.4969431	68.88299397	-1.9787162	0.013495	Down	Uncharacterized
103852372	80.5987692	22.16936308	-1.86219049	0.044248	Down	Ribulose bisphosphate carboxylase small chain 1B, chloroplastic
103852245	80.87130944	22.82981121	-1.82470904	0.001332	Down	Uncharacterized
103830091	177.7963486	54.00682379	-1.71901209	0.00088	Down	Probable glucan endo-1,3-beta-glucosidase BG3
103861112	1821.648212	601.8532751	-1.59776066	0.000349	Down	Methylthioalkylmalate synthase 2, chloroplastic
103831078	647.7154375	230.167248	-1.49267757	0.000122	Down	Peroxiredoxin-2B
103854915	1311.000239	490.4876956	-1.4183791	0.000319	Down	Methylthioalkylmalate synthase 1, chloroplastic
103872429	1317.833466	493.5205425	-1.41698603	0.000881	Down	Dihomomethionine N-hydroxylase
103858722	268.3034014	102.0552342	-1.39451517	0.008773	Down	Probable 2-oxoglutarate-dependent dioxygenase AOP1 (AOP2-1)
103833480	123.9805697	48.055555	-1.36733892	0.01335	Down	Myrosinase MA1
103842609	87.77862064	34.92859941	-1.32946081	0.048563	Down	Eukaryotic translation initiation factor 5B
103833778	1328.128285	555.8673299	-1.25658201	0.006003	Down	Selenium-binding protein 2
103870590	458.8817067	199.0294878	-1.2051401	0.001692	Down	Non-specific lipid-transfer protein 6
103853103	657.3243065	291.9904341	-1.17068423	0.000167	Down	Sulfate transporter 1.2
103847571	254.3242534	116.3735741	-1.12790556	0.032462	Down	Transcription factor MYB29
103847107	536.5560834	255.6650059	-1.06947427	0.009592	Down	Formin-like protein 20
103847459	659.5639979	335.1406639	-0.97674591	0.045158	Down	PRT6

Table B2. Genes with reduced expression in *Brprt6.2prt6.3* vs. wild-type after mock treatment.

GeneID	Length	WT-Mock-Expression	Prt6-2-3-Mock-Expression	log2FC(Prt6.2 Prt6.3/WT)	Padj	Up/Down	Description (predicted)
108870470	2283	1.72E-05	29.57087256	20.71699736	0.00017	Up	SCAI homolog
103872774	3052	0.17893606	85.52255553	8.900717034	3.05E-09	Up	Pentatricopeptide repeat-containing protein At1g19720
103838445	5306	0.34905609	68.73434745	7.621428514	5.28E-06	Up	G-type lectin S-receptor-like serine/threonine-protein kinase At1g61390
103846440	3373	2.26628458	375.9746829	7.374162676	2.39E-27	Up	Plant cysteine oxidase 1
103863926	1172	35.7011095	1460.646715	5.354494558	5.24E-72	Up	Plant cysteine oxidase 2
103846065	2868	156.176299	5420.812569	5.117261689	2.63E-62	Up	Non-symbiotic hemoglobin 1
103828296	1257	10.1615296	301.6938568	4.891895836	0.00697	Up	1-aminocyclopropane-1-carboxylate oxidase 1
103856111	1240	30.4588676	857.9502249	4.815959739	1.31E-50	Up	Plant cysteine oxidase 1
BGI_novel_G000534	1112	2.29173756	52.28647686	4.511924116	0.00036	Up	NA
103843350	1228	25.412577	511.7699441	4.331880833	5.62E-26	Up	LOB domain-containing protein 41
103858971	2077	8.38634716	126.1062887	3.910453859	3.66E-10	Up	Delta(7)-sterol-C5(6)-desaturase 1
103858968	1199	13.9552828	182.5962432	3.709773814	2.78E-12	Up	LOB domain-containing protein 41
103843716	1005	12.2547442	147.3074559	3.587418182	4.03E-10	Up	Ethylene-responsive transcription factor ERF071
103873216	434	8.63489531	96.65577206	3.484605297	3.26E-07	Up	Uncharacterized
103840073	707	36.7626941	279.0191409	2.924049695	1.51E-09	Up	Uncharacterized
BGI_novel_G000379	2864	10.9332151	81.39418747	2.896208062	0.02998	Up	NA
103832423	1776	69.1709259	309.7309283	2.162777779	1.88E-06	Up	Inosine-5'-monophosphate dehydrogenase 1
BGI_novel_G000145	1587	22.3054775	87.37453161	1.969814784	0.0408	Up	NA
103842451	4696	51.4358553	199.9780617	1.958995439	6.71E-08	Up	Uncharacterized
103830464	808	785.958505	2397.46346	1.608983775	4.03E-10	Up	Chaperone protein dnaJ 8
103874000	1500	380.854016	1066.893765	1.486106512	8.85E-07	Up	Transcription factor Bhlh93
103859336	2492	294.850356	677.693377	1.200649735	0.00017	Up	Putative zinc transporter At3g08650
103831751	816	646.967839	1461.95664	1.176134621	0.00088	Up	Auxin-responsive protein SAUR78
103863379	1814	1044.82826	2195.497713	1.071282213	0.01491	Up	Protochlorophyllide-dependent translocon component 52, chloroplastic
103832473	1474	163.174799	328.0706778	1.007588391	0.01552	Up	3-isopropylmalate dehydrogenase, chloroplastic
103852206	2559	449.084862	812.0644105	0.85460607	0.00877	Up	Ethylene-responsive transcription factor ERF060
103859414	1541	366.118267	659.8982864	0.849933914	0.0324	Up	Amino acid transporter ANT1
103837843	1277	1970.85799	3412.129818	0.791848711	0.00087	Up	bZIP transcription factor 2
103859462	1543	835.664355	1446.72647	0.791796676	0.01273	Up	Aspartic proteinase NANA
103827734	2464	299.498171	516.2033994	0.785392448	0.04614	Up	CTD small phosphatase-like protein 2

Table B3. Genes with increased expression in *Brprt6.2prt6.3* vs. wild-type after mock treatment.

GeneID	WT flg22 Expression	Prt6.2Prt6.3 flg22 Expression	log2FC(Prt6.2 Prt6.3/WT)	Padj	Direction	Description (predicted)
BGInovelG000021	30.14710431	1.05E-05	-21.4481784	7.20E-05	Down	NA
117133380	31.90683618	0.186432404	-7.41906912	7.20E-05	Down	Non-classical arabinogalactan protein 30-like
103840832	250.3278772	2.040966507	-6.93842265	9.50E-22	Down	Uncharacterized
BGInovelG000587	58.60294056	0.681724509	-6.4256404	7.20E-05	Down	NA
103841255	21.52804018	0.680568002	-4.98333386	4.20E-02	Down	Cytochrome P450 71B8
BGInovelG000533	41.80601557	1.703393945	-4.61722652	3.60E-03	Down	NA
103856520	40.01409434	2.380196713	-4.07135554	1.70E-03	Down	Uncharacterized
117130004	26.00156813	1.70550989	-3.93032361	3.70E-02	Down	Uncharacterized
117131446	52.29771376	4.744493026	-3.46242204	2.50E-04	Down	Uncharacterized
103862179	48.54055586	4.737508308	-3.35699025	3.20E-03	Down	ECERIFERUM 2
117130584	84.23704601	8.819868369	-3.25562582	1.60E-05	Down	Uncharacterized
117130589	169.5252939	22.05852149	-2.94209255	3.30E-12	Down	Uncharacterized
117130799	74.3707849	13.2682991	-2.48675256	6.90E-04	Down	Uncharacterized
103837093	41.86193881	8.491019388	-2.30162946	4.00E-02	Down	BURP domain protein RD22
103869925	88.62085185	18.02219671	-2.29787132	6.80E-04	Down	Expansin-A12
103852947	233.8066238	57.00601483	-2.03612975	2.40E-04	Down	bZIP transcription factor 44
117126780	111.144155	27.55377839	-2.01211001	1.70E-03	Down	Transcription factor HEC1
103855508	378.7437656	95.67559225	-1.98499931	2.40E-07	Down	Probable protein phosphatase 2C 67
103847465	90.22426452	25.8337639	-1.80425762	2.50E-02	Down	Expansin-A9
103861006	149.0809193	45.86480296	-1.70063627	7.80E-03	Down	Uncharacterized
103845164	81.95860584	25.88049195	-1.6630304	3.40E-02	Down	Oxysterol-binding protein-related protein 4C
103836062	191.7495561	63.47500905	-1.59496264	5.10E-03	Down	Transmembrane 9 superfamily member 2
103857011	572.2339928	198.8091587	-1.52522098	3.00E-07	Down	GDSL esterase/lipase At5g55050
103869328	94.35232781	33.34441987	-1.50061276	4.60E-02	Down	NEP1-interacting protein-like 2
103834943	166.4592168	60.53731282	-1.45927221	3.20E-03	Down	Uncharacterized
103859699	160.5578077	59.84845804	-1.42370684	1.40E-02	Down	Uncharacterized
103852424	186.6198066	72.53708677	-1.3633114	9.20E-03	Down	Probable pectate lyase 5
103869972	276.6525315	110.3436603	-1.32607138	1.80E-03	Down	Phosphoenolpyruvate carboxylase 3
103831449	135.3382855	55.44091602	-1.28754702	3.40E-02	Down	Histone-lysine N-methyltransferase, H3 lysine-9 specific SUVH3
103872429	350.5948771	143.9855223	-1.28388116	2.70E-02	Down	Dihomomethionine N-hydroxylase
103830964	1623.075743	680.6568377	-1.25373079	1.00E-02	Down	Alpha-xylosidase 1
103863415	315.0888321	137.8929495	-1.19220993	2.00E-02	Down	Uncharacterized
103870590	349.4198284	155.5134234	-1.16792236	1.00E-03	Down	Non-specific lipid-transfer protein 6
103850912	2826.333148	1261.924184	-1.16330629	2.70E-04	Down	Uncharacterized
103850977	1100.336251	508.7707247	-1.1128569	2.70E-02	Down	Gibberellin-regulated protein 4
103828058	425.5135356	197.5953598	-1.10665596	2.20E-02	Down	Glucose-1-phosphate adenylyltransferase large subunit 3, chloroplastic
103870618	1656.297709	774.3889502	-1.09683174	6.30E-03	Down	Uncharacterized
103843834	689.8413925	325.268236	-1.08463475	2.00E-02	Down	Very-long-chain aldehyde decarbonylase CER1
103860505	317.4270273	152.5902674	-1.05676203	2.50E-02	Down	NAC domain-containing protein 22
103859599	255.5115696	123.0823921	-1.05376423	1.70E-02	Down	Phosphoenolpyruvate carboxylase 3
103872924	677.8511544	326.7229929	-1.05290053	2.30E-02	Down	Nuclear speckle RNA-binding protein B
103838202	907.5055809	437.5607457	-1.0524232	1.70E-03	Down	Endoglucanase 6
103867175	382.3517214	184.8594543	-1.04847154	2.50E-02	Down	Expansin-A3 (EXPA3)
103869117	12466.74878	6134.055776	-1.02317208	5.70E-03	Down	36.4 kDa proline-rich protein
103850443	412.2177727	203.4611144	-1.01865362	2.70E-02	Down	E3 ubiquitin-protein ligase PRT6
103836343	1974.967004	978.2895287	-1.01349515	4.20E-02	Down	Putative FBD-associated F-box protein At1g05080
103854751	5039.674768	2557.059406	-0.97884496	2.70E-04	Down	Uncharacterized
103840914	235.9466164	119.7539165	-0.97838764	2.50E-02	Down	LOB domain-containing protein 38
103830993	4186.038606	2126.118152	-0.97736385	4.40E-02	Down	Lipoxygenase 2, chloroplastic-like
103832980	273.2245964	140.630466	-0.95817819	4.80E-02	Down	F-box/kelch-repeat protein At3g27150-like
103838161	2628.654153	1359.297089	-0.95146354	4.50E-03	Down	Endoglucanase 6
103847459	511.4978866	272.0511777	-0.91085021	3.80E-02	Down	E3 ubiquitin-protein ligase PRT6
103867130	1737.975117	975.6494881	-0.83297258	4.40E-02	Down	Vacuolar cation/proton exchanger 1
103850771	1157.458193	685.8658378	-0.75496178	4.70E-03	Down	Uncharacterized
103837722	2746.185528	1640.661945	-0.74315109	9.00E-03	Down	L-ascorbate oxidase homolog
103859705	10322.1977	6584.911351	-0.64851424	2.00E-02	Down	L-ascorbate oxidase homolog

Table B4. Genes with reduced expression in *Brprt6.2prt6.3* vs. wild-type after flg22 treatment.

GeneID	WT flg22 Expression	Prt6.2Prt6.3 flg22 Expression	log2FC	Padj	Direction	Description (predicted)
117126611	1.74E-05	63.12965361	21.788617	4.90E-05	Up	Zeaxanthin epoxidase, chloroplastic
BGInovelG000579	0.176975827	82.2583941	8.8604668	1.20E-08	Up	NA
103846440	1.920544822	140.1411972	6.1892217	4.70E-14	Up	Plant cysteine oxidase 1
103838445	1.922858081	102.4238069	5.735155	8.40E-12	Up	G-type lectin S-receptor-like serine/threonine-protein kinase At1g61390
BGInovelG000251	0.946393777	29.31910875	4.9532569	5.10E-03	Up	NA
103828296	29.84108138	906.6209379	4.9251278	4.10E-06	Up	1-aminocyclopropane-1-carboxylate oxidase 1
103846065	144.9443179	3862.511156	4.7359684	4.00E-49	Up	Non-symbiotic hemoglobin 1
103863926	97.41977611	1824.246856	4.2269425	3.70E-72	Up	Plant cysteine oxidase 2
103856111	45.48372219	847.1464426	4.2191892	6.40E-43	Up	Plant cysteine oxidase 1
103843716	23.6189243	371.912861	3.9769495	2.60E-27	Up	ERF71 / HRE2
103843350	87.72213246	1093.873706	3.6403615	9.30E-04	Up	LOB domain-containing protein 41
103858971	7.701071156	78.70640522	3.35335	1.60E-03	Up	Delta(7)-sterol-C5(6)-desaturase 1
103862549	5.889708486	46.43246235	2.9788657	3.70E-02	Up	Uncharacterized
103872757	36.8011238	196.0934394	2.4137195	1.40E-10	Up	Uncharacterized
103872329	12.31884119	65.55326571	2.4118011	4.50E-03	Up	Uncharacterized
103835054	14.99240305	69.02895094	2.2029699	5.60E-03	Up	DETOXIFICATION 40
103870965	370.3514815	1252.392672	1.75772	8.40E-12	Up	Hypersensitive-induced response protein 3
103871169	718.0583277	2278.531752	1.6659315	1.10E-04	Up	Stem-specific protein TSJT1
103862836	60.18912377	175.9691658	1.5477479	1.80E-03	Up	(+)-neomenthol dehydrogenase
103832423	56.32761633	157.0883845	1.4796622	3.60E-02	Up	Inosine-5'-monophosphate dehydrogenase 1
103851209	266.9155697	740.1519347	1.471438	1.70E-03	Up	Stem-specific protein TSJT1
103842451	51.61557114	142.3322532	1.4633844	2.30E-03	Up	Uncharacterized
103863819	233.6679739	626.3231152	1.4224471	3.10E-03	Up	Phenolic glucoside malonyltransferase 1
103837285	95.81155041	255.7610449	1.4165251	6.40E-04	Up	Basic leucine zipper 1
103874000	54.23783216	144.6297048	1.4149925	1.80E-02	Up	Bhlh93
103866480	111.7599111	296.9531324	1.4098325	3.20E-02	Up	Uncharacterized
103875050	875.8201524	2292.03608	1.3879232	5.00E-03	Up	Proline dehydrogenase 1, mitochondrial
103843361	122.9588571	314.0103586	1.3526365	1.30E-04	Up	Uncharacterized
103856198	93.98572292	239.9629649	1.3522982	2.00E-02	Up	PR5-like receptor kinase
103839244	62.90234589	159.7858974	1.3449544	2.70E-02	Up	Probable inorganic phosphate transporter 1-3
103832166	475.5781285	1207.558772	1.3443391	2.30E-03	Up	Alcohol dehydrogenase class-P
103862396	59.56863749	150.0546213	1.3328629	4.00E-02	Up	Lysine histidine transporter-like 7
103843922	303.9601342	750.5651852	1.3040953	2.90E-07	Up	Hexokinase-like 1 protein
103860785	220.8900752	536.7732928	1.2809843	3.20E-03	Up	Pyruvate, phosphate dikinase 1, chloroplastic
103846560	67.83734599	160.6389332	1.24367	1.70E-02	Up	ABC transporter G family member 6
103863379	521.7075579	1228.581379	1.2356802	1.90E-05	Up	Protochlorophyllide-dependent translocon component 52, chloroplastic
103854374	63.83211955	150.1750395	1.2342906	2.00E-02	Up	Cytochrome P450 71B4
103864052	218.876993	508.0305043	1.2147948	8.80E-04	Up	Glycerophosphodiester phosphodiesterase GDPD2
103873743	1801.427832	4136.749156	1.1993566	6.80E-03	Up	Senescence-associated protein DIN1
103830464	353.2909144	808.4829465	1.1943607	3.60E-05	Up	Chaperone protein dnaJ 8, chloroplastic
103867449	219.5653063	493.1618175	1.167411	9.60E-03	Up	Cytochrome P450 710A1
103832483	923.4021157	2071.272404	1.1654864	3.70E-02	Up	Pyrophosphate-energized vacuolar membrane proton pump 1-like (AVP1-2)
103840759	894.5739167	1988.756425	1.152594	2.60E-02	Up	Stem-specific protein TSJT1
103845694	2304.318236	5073.286269	1.1385806	1.40E-02	Up	Probable galactinol--sucrose galactosyltransferase 6
103839828	1135.373834	2454.138158	1.1120491	1.60E-02	Up	Putative cysteine-rich receptor-like protein kinase 39
103870831	3581.445868	7739.725556	1.1117403	2.00E-02	Up	Pyruvate, phosphate dikinase 1, chloroplastic
103868159	449.7440954	971.9218046	1.1117359	5.90E-03	Up	Putative cysteine-rich receptor-like protein kinase 39
103868065	342.297678	731.8905601	1.0963764	2.50E-02	Up	Uncharacterized
103865652	99.74723998	212.1976363	1.0890598	2.00E-02	Up	Glycerol-3-phosphate 2-O-acyltransferase 6
103835241	251.477527	532.8981045	1.0834302	3.30E-04	Up	Gibberellin 2-beta-dioxygenase 2
103861948	193.1615583	406.8486017	1.074684	1.00E-02	Up	Xyloglucan endotransglucosylase/hydrolase protein 24
103850184	3642.629332	7555.715518	1.0525882	3.40E-04	Up	Uncharacterized
103867663	314.240622	648.4470584	1.0451191	1.90E-02	Up	Uncharacterized
103843375	79.97281761	162.9395678	1.0267554	4.80E-02	Up	Uncharacterized
103842587	316.5788941	630.0658689	0.9929376	2.00E-02	Up	Uncharacterized
103828156	299.7071716	595.2226085	0.9898757	2.50E-02	Up	Uncharacterized
103861558	407.4482045	795.9314473	0.9660275	2.00E-02	Up	UDP-glucose 4-epimerase 2
103830281	430.2485535	825.8133231	0.9406454	3.20E-03	Up	Protein-ribulosamine 3-kinase, chloroplastic
103850206	414.1849385	792.815763	0.9367106	2.00E-02	Up	Glycerophosphodiester phosphodiesterase GDPD2
103871394	228.9453925	438.2108384	0.9366216	2.50E-02	Up	Cytochrome P450 72A15-like
103839129	814.9918005	1540.895673	0.9189117	3.20E-03	Up	Abscisic acid 8'-hydroxylase 3
103859462	213.3608749	396.8808089	0.8954102	5.10E-03	Up	Aspartic proteinase NANA, chloroplast
103872215	1962.501627	3577.689388	0.8663343	4.80E-02	Up	Phosphate transporter PHO1 homolog 3
103837843	2161.737956	3909.050637	0.8546266	5.10E-03	Up	bZIP transcription factor 2
103827954	1698.757822	3033.895181	0.836691	1.80E-03	Up	ATP sulfurylase 4, chloroplastic
103831159	245.6450749	438.6195349	0.8363948	2.00E-02	Up	Beta-glucosidase 46-like
103854672	720.8373768	1268.399434	0.8152634	1.80E-03	Up	Uncharacterized
103853207	959.8971176	1647.471179	0.7793015	4.80E-02	Up	Chaperone protein dnaJ 8, chloroplastic
103869653	485.3009886	827.7096372	0.770245	2.50E-02	Up	Putative 3,4-dihydroxy-2-butanone kinase
103874006	927.8332351	1578.41924	0.766543	3.20E-03	Up	Phosphoenolpyruvate carboxykinase (ATP)
103859336	475.4272311	807.9290161	0.765004	3.70E-02	Up	Putative zinc transporter At3g08650
103865848	357.5880504	598.249472	0.7424487	3.20E-02	Up	Cytochrome P450 98A3
103860375	2513.145771	4055.50282	0.6903864	2.50E-02	Up	Calmodulin-like protein 12

Table B5. Genes with increased expression in *Brprt6.2prt6.3* vs. wild-type after flg22 treatment.

At gene name	*At* gene ID	*B. rapa* orthologous gene(s) ID (OrthoDB)										
GLR2.9	*AT2G29100*	*103849373*	*103849377*	*103849375*	*103849376*	*103868058*						
	AT1G36640											
AMT1;1	*AT4G13510*	*103849623*										
	AT1G66460	*103831106*	*103863753*									
ACD6	*AT4G14400*											
	AT4G19520											
CRK17	*AT4G23250*	*103834353*	*103861377*	*103834280*	*103861376*							
IST1-LIKE 12	*AT1G51900*											
	AT5G45000	*103839142*										
NAC061	*AT3G44350*	*103873617*	*103856515*	*103873643*	*103851438*	*103845552*						
	AT2G20150											
EXPA2	*AT5G05290*	*103846882*	*103850578*									
	AT1G10417	*103871812*										
MLO2	*AT1G11310*	*103849649*	*103836233*	*103838442*	*103843245*	*103871889*	*103830668*					
ATPI4Kγ3	*AT5G24240*	*103861561*	*103874293*	*103841208*	*103829830*							
	AT5G57480	*103856751*	*103845184*									
LACS3	*AT1G64400*	*103838201*										
A/N-InvF	*AT1G72000*	*103831714*										
AGB1	*AT4G34460*	*103862350*	*103834412*	*103837655*								
	AT1G28390	*103835327*										
MYB97	*AT4G26930*											
WAKL10	*AT4G00955*											
FAD4L2	*AT2G22890*	*103861670*	*103835525*	*103866795*	*103834822*							
	AT1G50180	*103867790*	*103847612*	*103832891*	*103860290*							
GLR2.7	*AT2G29120*	*103849373*	*103849377*	*103849375*	*103849376*	*103868058*						
SULTR4;1	*AT5G13550*	*103856022*	*103859447*	*103846563*								
	AT1G69523	*103831352*	*103831349*	*103831351*								
ILL3	*AT5G54140*	*103844872*										
	AT1G03730	*103843690*										
	AT5G48550											
	AT4G22030	*103858658*	*103839837*									
	AT3G57210											
	AT4G30500	*103861970*	*103852632*									
	AT5G40910	*103850388*										
ADT6	*AT1G08250*											
HAK5	*AT4G13420*	*103829994*										
CHIA	*AT5G24090*	*103865791*	*103874278*									
RLP21	*AT2G25470*	*103831891*	*103829918*	*103830714*	*103830620*	*103864589*	*103868842*	*103852890*	*103831892*	*103872662*	*103830717*	*103872664*

Table B6. *B. rapa* orthologs to *Arabidopsis* 'core immune response' (CIR) genes. CIR genes were defined by Bjornson *et al*. (2021). *B. rapa* orthologs were identified using the OrthoDB database.